MHD Instabilities In Simple Plasma Configuration

ELECTED

AUG 2 9 1984

A

NAVAL RESEARCH LABORATORY
Washington, D.C.

84 08 29 108

MHD Instabilities in Simple Plasma Configuration

WALLACE M. MANHEIMER

Plasma Physics Division
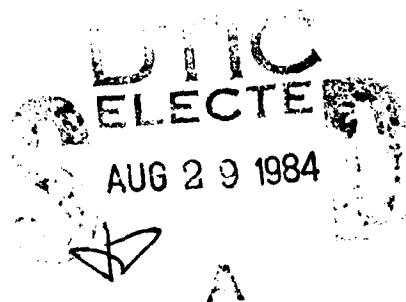*Naval Research Laboratory*
Washington, D.C.

CHRIS LASHMORE-DAVIES

Theory Division
*Culham Laboratory*
Abingdon, Oxon, England

1984

NAVAL RESEARCH LABORATORY
Washington, D.C.

i

On the Front Cover:

A picture of flux surfaces for an $n = m = 1$ MHD insta-
bility taken from the simulations of R. B. White, D. A. Monti-
cello, M. N. Rosenbluth and B. V. Waddell, Plasma Physics
and Controlled Fusion Research 1976, Vol. 1, p. 569, Interna-
tional Atomic Energy Agency, Vienna, 1977. In the unper-
turbed state the flux surfaces are nested circles. Notice the
island formation due to field line breaking and reconnection.
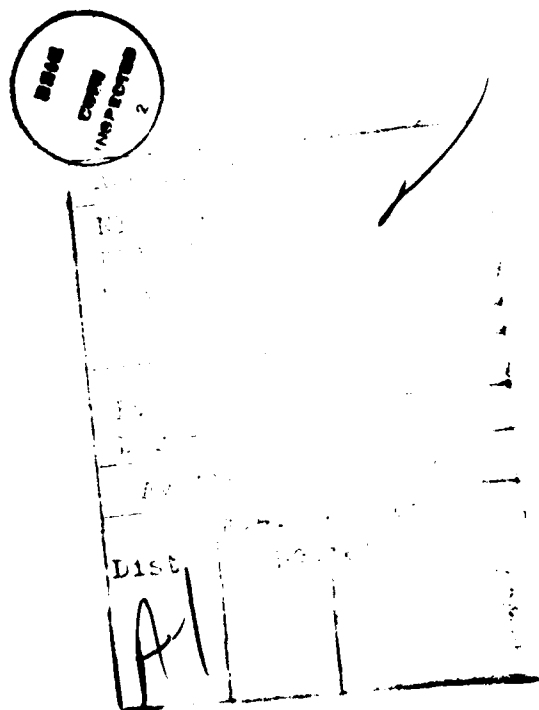
FOREWORD

This work provides what we hope is a relatively simple, self contained description of MHD instabilities in plasmas with simple configurations. This work is partially the result of a one year sabbatical (Sept. 77 - Sept. 78) one of us (WMM) spent at Culham Laboratory in Abingdon, England. During the year there, the two of us worked very closely, and we each received a tremendous amount of help from Dr. John Wesson, also of Culham.

By simple configuration, we mean a plasma in which all quantities vary in only one spatial direction. We deal with such plasmas here because we want to emphasize the basic physics of MHD instabilities. In more complicated configurations, this is often very difficult to discern because the mathematical description is so much more involved. Usually one has to first define a new coordinate system in which the magnetic field corresponds to one coordinate, and then solve a two or three dimensional problem in this system. Although some fusion devices (for instance Elmo Bumpy Torus, tandem mirror, and spheromak) are inherently two or three dimensional in nature, there are others, specifically tokamaks and reversed field pinches which are, to good approximation, one dimensional. Also, these devices both display a wealth of complex MHD activity which can be fruitfully discussed here. We hope that a good description of the physics of instabilities in simple configurations is both interesting in its own right, and also will provide a useful stepping stone to a study of instabilities in more complex configurations.

One deceptive aspect of MHD instabilities is that the simplest ones are extremely easy to understand. For instance the instabilities of a Z pinch to sausage and kink displacements have been described in such standard texts as Jackson's *Classical Electrodynamics*. However more complicated instabilities, for instance in a plasma where both an axial and azimuthal field are present are much more difficult to visualize; but they are also much more interesting. $\Rightarrow \left(T_0 \, p \, V \right)$

Although, as we will see, there is a tremendous variety of MHD instabilities, all those which we will study are driven by one of two

mechanisms. First of all there may be a gravity (or something equivalent to a gravitational force) which is opposite to the density gradient. This can drive Rayleigh-Taylor type instabilities. This is the fundamental driving force behind both ideal and resistive pressure driven modes in a reversed field pinch, ballooning modes in a tokamak, rotationally driven modes in a θ pinch and the mirror instability in a magnetic mirror whose field lines bulge outward away from the plasma. Second, a plasma which carries a current is potentially unstable because current elements traveling in the same direction attract each other and would like to all clump up together. Of course this is not so simple because the current flows through a conducting fluid and, as will be amply demonstrated, this imposes all sorts of constraints. Nevertheless, this mutual attraction of like current elements is the basic mechanism which drives free surface modes in a cylindrical or toroidal plasma; tearing modes in plane, cylindrical and tokamak geometry, and the internal $m = 1$ kink tearing mode in cylindrical or tokamak geometry.

There are other views we have on this area which affected the material we chose to cover. First of all, we de-emphasized both the energy principle and also modes in a plasma with a free surface. At least for one dimensional configurations which we emphasize, it is really no simpler to utilize the energy principle than it is to solve for the eigenfunction and eigenvalue. This is especially true now, where second order ordinary differential equations can be so easily solved numerically. Also, to discuss the nonlinear evolution of MHD unstable plasmas, it is necessary to know not only whether or not a plasma is stable, but also to have some idea of growth rates and eigenfunctions.

As far as free surfaces are concerned, first of all it is rare that plasmas have free surfaces; usually experimental plots of, say, density or temperature profile usually show them going smoothly to zero with radius, at least in tokamak and reversed field pinch plasmas. (For plasmas with more complicated configurations however, a free surface may be a good model if there is a magnetic separatrix in the plasma.) Secondly, free surfaces are not particularly difficult to understand, but applying boundary conditions across them in their unperturbed and perturbed state can involve a great deal of mathematical complexity. Therefore, they do not seem to be worth expending a great deal of effort on in a manuscript like ours which attempts to emphasize physical principle, not mathematical detail. Hence we deal with free surfaces in only one chapter in which we drive some fundamental stability requirements for tokamak plasmas.

One thing which we attempt to emphasize however is magnetic reconnection. As we will see shortly, in ideal MHD, each magnetic field line maintains its integrity and behaves rather like a string which threads the fluid and cannot break. However there are flow patterns which force two magnetic field lines together. Often nonideal effects, for instance resistivity, can cause the field lines to break and reconnect.

This work is divided into two parts. Chapters II-IX describe linear theory and Chapters X-XV describe the nonlinear theory. The latter part is naturally much more speculative than the former because less is known about nonlinear theory. The mathematical details in any non-linear theory can rapidly mushroom out of all proportion. For this reason much work in nonlinear MHD theory is done by numerical simulation. However there still are some relatively simple nonlinear calculations which can be done analytically, as well as some fairly simple physical insights which can be gotten. These are emphasized in Chapters X-XV. Preceding both sections is Chapter I which discusses experimental evidence for MHD instabilities in tokamaks and reversed field pinches. As we proceed through the book we will show what light theory can shed on these experimental results.

We would also like to thank the Americal Physical Society for permission to use the figures which were taken from the Physical Review Letters.

CONTENTS

Chapter I

EXPERIMENTAL EVIDENCE FOR
MHD INSTABILITIES

The subject of MHD stability has been studied for many years. The motivation for this research has come from astrophysics (e.g., solar flare theory), space physics (e.g., the physics of the magnetosphere), controlled thermonuclear fusion, other geomagnetism and many other fields. Controlled thermonuclear fusion has been pursued very actively over the last decade in view of its energy potential. As a result this field has probably provided the most detailed and reliable experimental data on MHD instabilities in plasmas. Within the field of magnetic confinement of high temperature plasmas, the tokamak device is currently the most successful. This device originated in the Kurchatov Laboratory in Moscow where the first one was built around 1956-57.[1] More recently, tokamaks have been built and studied in all countries actively pursuing the goal of fusion (e.g., USSR, USA, Europe, Japan, and Australia). Since the performance of tokamaks is presently limited by an effect known as the disruptive instability and since this manifests a number of phenomena typical of MHD instability, we shall discuss, in this chapter, the experimental evidence for MHD instabilities coming from studies of the tokamak device. Also, we look at experimental evidence for MHD instabilities in reversed field pinches, another relatively simple device which exhibits MHD activity.

First we will give a brief description of a tokamak. A tokamak is a toroidal device in which a strong toroidal magnetic field is created by external currents—the toroidal field coils. A weaker poloidal magnetic field is created by a current flowing through the plasma in the toroidal direction. This current is induced by means of a transformer which produces a large change in magnetic flux through the hole in the torus thus exciting a current in the plasma which forms the secondary circuit of the transformer. The transformer usually has an iron core although for high toroidal field devices an air core is used. The toroidal vacuum vessel (or liner, as it is called) is made of stainless steel whose thickness is typically 0.2-0.3 mm and the interaction of the plasma with the

stainless steel wall is reduced by means of a limiter (or diaphragm)
which is a single loop of tungsten or molybdenum whose inner radius is
a few centimeters less than that of the stainless steel liner. Although
the effect of the limiter is not fully understood it is an indispensable
part of the tokamak apparatus. Finally, the plasma can be maintained
in equilibrium, against major radius expansion, by eddy currents which
flow in a thick (of the order of 2 cm) copper shell enclosing the liner,
or by a vertical magnetic field (parallel to the major axis of the torus)
generated by external windings. The main features of the tokamak
described above are illustrated in Figs. (I-1a, b).

(a) GENERAL ARRANGEMENT

(b) MERIDIONAL CROSS-SECTION
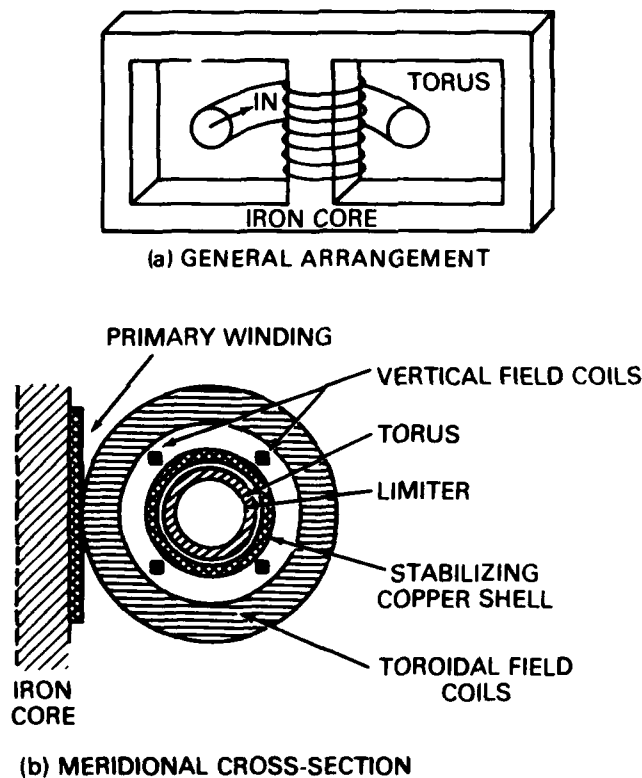
Fig. I-1 — Standard Tokamak

We will now describe the most important experimental results
relating to MHD instabilities obtained from measurements made on a
number of tokamaks in various parts of the world. The detection and
interpretation of the fluctuations occurring in a tokamak plasma is a
very difficult problem for plasma diagnostics. To date, the information
on these fluctuations has come mainly from the measurement of oscil-
lating magnetic fields detected with coils situated outside the plasma

(the Mirnov oscillations) and the analysis of soft x-ray signals coming from the plasma interior. Analysis of these x-ray signals led to the discovery of sawtooth oscillations. Let us now describe the experimental observation of (a) Mirnov oscillations, (b) sawtooth oscillations and (c) the disruptive instability.

(a) Mirnov Oscillations

Mirnov[2] oscillations are fluctuations in the magnetic field of the discharge current (particularly the current near the plasma boundary) which can be detected outside the plasma ring. A concept which has proved to be of great significance for the stability of a plasma in a toroidal magnetic field is that of resonant oscillations. These are oscillations where the helix of the perturbation exactly matches the helix of the confining magnetic field. The equilibrium helix is described by the quantity $q(r)$ (often called the safety factor) where

$$q(r) \equiv \frac{r\, B_{zo}(r)}{R\, B_{\theta o}(r)} \qquad (\text{I-1})$$

where $B_{zo}(r)$ is the applied toroidal magnetic field, $B_{\theta o}(r)$ the poloidal field due to the discharge current, r is the coordinate in the direction of the minor radius and R is the major radius of the torus. The physical significance of q is that it is the number of times a field line circles the major axis in making one transit round the minor axis. The perturbed helix is described by the poloidal and toroidal mode numbers m and n. The theory of MHD stability (see Chapters IV and VIII) now states that the plasma will be unstable to surface or bulk modes when

$$q(a) = m/n \qquad (\text{I-2})$$

where a' is the minor radius of the plasma. Mirnov and Semenov[2] have made a systematic study of the magnetic fluctuations of the discharge current in the tokamak T-3. The parameters of T-3 were as follows: major radius 100 cm, liner radius 20 cm, limiter radius 15-17.5 cm, toroidal magnetic field in the range 17.5 to 26 kG, discharge current from 50 to 150 kA and a plasma density of $1-2 \times 10^{13}$ cm^{-3}. The duration of the current pulse was 70 milliseconds and a hydrogen plasma was used.[2] Mirnov and Semenov employed a system of 18 magnetic probes located on the surface of the discharge liner. The probes were positioned around the torus covering a range of both the poloidal angle θ and the toroidal angle ϕ. Signals from these probes were transmitted to a correlation receiver. The input signals from two probes were first subtracted and then integrated giving a quantity proportional to the difference of the magnetic fields at two points in space.

This quantity was finally squared and time averaged for a period of the order of one millisecond before input to the oscillograph. By measuring the spatial structure of the magnetic field fluctuations in this way the mode numbers m and n were identified.

In order to investigate the prediction of instability when $q(a) = m/n$, Mirnov and Semenov[2] applied a current pulse of the form shown in Fig. (I-2a). In contrast to the usual flat top current, the pulse shown in Fig. (I-2a) had a slowly increasing part thus enabling the stability factor at the boundary, $q(a)$, to be progressively reduced. Figures (I-2b), c show the oscillogram $W(t)$ and the corresponding quantity as a function of the poloidal angle θ. These curves were obtained at three instants in time such that the amplitudes of the fluctuations had clearly formed maxima. It can be seen from these curves that the $m = 6, 5, 4$ perturbations develop successively as the discharge current rises. The toroidal mode number for these perturbations was $n = 1$ and since the values of q in the vicinity of the boundary practically coincided with the corresponding m-numbers, it was concluded that these perturbations were resonance oscillations.
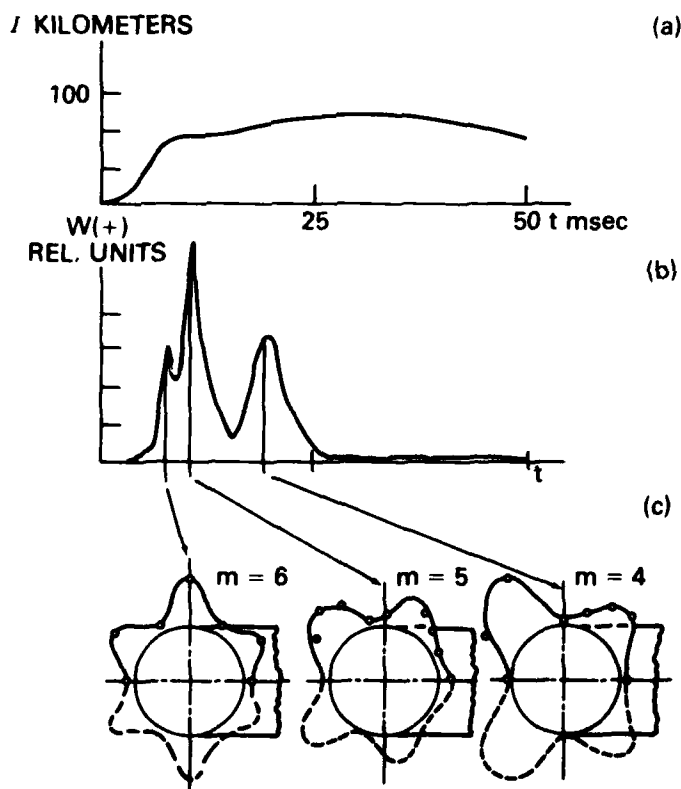

Fig. I-2 — Development of perturbations during
the initial stage of discharge

Perturbations with toroidal mode numbers $n = 2$–4 were also observed in T-3. However, it was found that these oscillations were generally small compared to the fundamental $n = 1$ perturbations. It was therefore concluded that for resonance perturbations one should expect their mode number m to be close to the value of q on the boundary of the plasma.

It should be noted that the magnetic field oscillations detected by Mirnov and Semenov[2] had the character of waves propagating in the poloidal direction with a frequency in the range 4-10 kHz. This was attributed to the effect of a poloidal rotation of a non-uniformly distributed current density $J(\theta)$ in the vicinity of the boundary. It was assumed that the effect of this rotation on the theory of resonance oscillations (Chapter IV) was a simple Doppler shift of the zero frequency instability to a finite frequency.

For larger values of the discharge current Mirnov and Semenov[2] also observed resonance oscillations $m = 3$, 2 as q at the boundary was reduced to these mode numbers. It was noted that the $m = 4$ and higher mode numbers were suppressed with a quasi-stationary discharge current whereas this was not the case for the $m = 3$ and 2 modes. It appeared that the $m = 3$ and 2 modes exerted a marked influence on the macroscopic properties of the discharge. If the safety factor $q(a)$ was decreased through the value of 3 by a sufficiently rapid rise of the current, the $m = 3$ mode could be suppressed. However, Mirnov and Semenov were unable to stabilize the $m = 2$ mode in this way. We shall return to the influence of the $m = 2$ and 3 modes on the discharge when we come to discuss the disruptive instability. The importance of resonance oscillations for the stability of a tokamak is shown in Fig. (I-3) where the unstable regions of T-3A[3] as a function of $1/q(a)$ are shown shaded.

(b) Sawtooth Oscillations

Information concerning fluctuation in the interior of a Tokamak plasma can be obtained from a study of the continuous soft x-ray emission from the discharge. This radiation is produced by the thermal part of the plasma electrons and consists mainly of the recombination radiation of partly ionized impurities. The radiation intensity will therefore depend on the electron density and temperature and on the concentration of impurities. In particular, fluctuations in the electron density or temperature will produce a corresponding fluctuation in the x-ray signal.
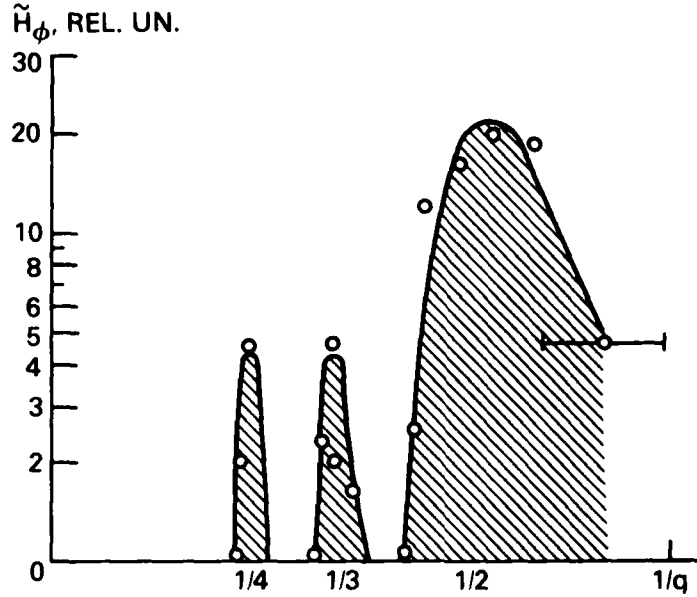
Fig. I-3 — Dependence of $\tilde{H}_\phi$ on the parameter $1/q$

Von Goeler, Stodiek and Sauthoff[4] at the Princeton Plasma Physics Laboratory carried out a study of the soft x-ray emission from the ST-Tokamak. A sketch of their apparatus is shown in Fig. (I-4a). The x-ray detectors were sensitive between 3 and 13 keV and the spatial resolution at the plasma center was about 2 mm. An oscillogram for a high density discharge in the ST Tokamak, shown in Fig. (I-4b) exhibits the characteristic sawtooth oscillation discovered by von Goeler, Stodiek and Sauthoff.[4] The oscillation was interpreted as being due predominantly to temperature fluctuations. It was noted that the trace taken a small distance away from the center of the column ($r = 3.9$ cm.) showed a fast rise and slow exponential drop which was the exact inverse of the trace taken from the center ($r = 0$). This phase change of the sawtooth oscillation is believed to occur at $q = 1$ surface and evidence for this is given below. Similar sawtooth oscillations have been observed in TFR.[5] The sawtooth oscillation consists of two parts: a sinusoidal oscillation $\Delta\tilde{A}$ superimposed on the main sawtooth relaxation $\Delta\bar{A}$. This is illustrated in Fig. (I-5) taken from the TFR work. Using various diagnostic techniques (e.g., Thomson scattering, spectroscopic methods HF coupling studies), the TFR group have shown[5] that th variation in the x-ray signal is due chiefly to the variation in T_e i.e., typical ratios $(\Delta T_e/T_e)$ $r = 0 \sim 10\%$, $(\Delta n_e/n_e)$ $r = 0$ ~ 1 to 2% were found.

In order to elucidate the inversion of the sawtooth oscillation signal between $r = 0$ and $r = 3.9$ von Goeler et al.[4] made an estimate of

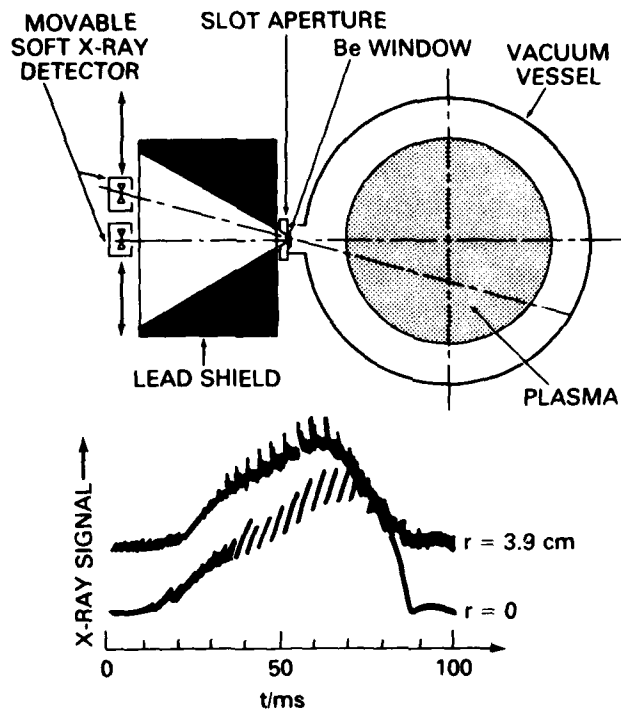Fig. I-4 — Experimental arrangement of x-ray detectors.
The x-ray traces exhibit internal disruptions.

a) $n_0 - 10^{14}$ cm^{-3}
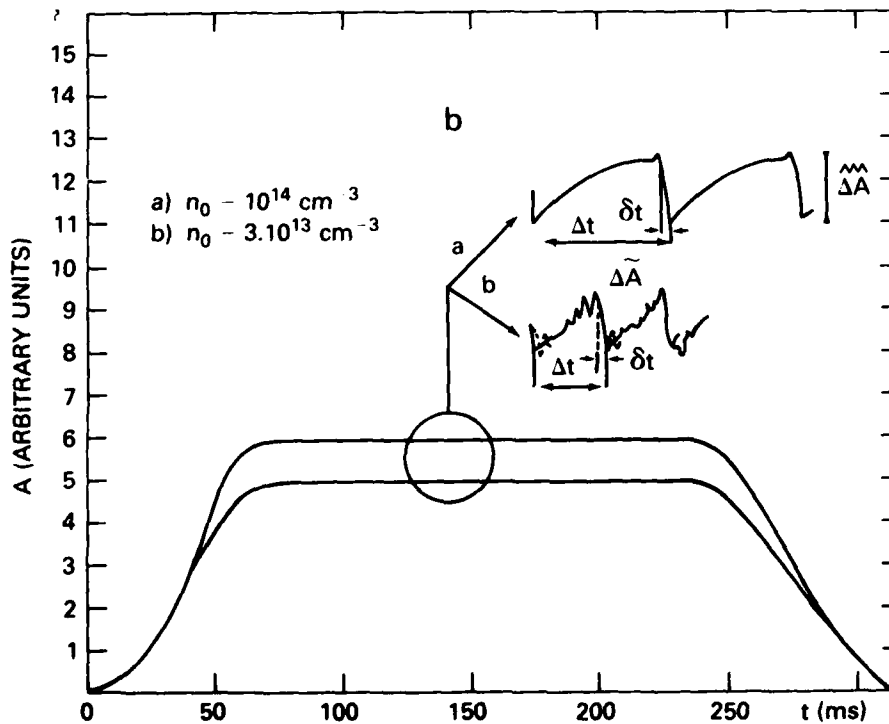b) $n_0 - 3.10^{13}$ cm^{-3}

Fig. I-5 — Typical form of the signal A from soft x-rays
and observed relaxations

the profile $q(r)$. The electron density and temperature profiles were obtained from Thomson scattering and assuming a nearly stationary discharge and a uniform impurity concentration across the discharge, q was found to be roughly 0.8 at the center of the plasma reaching a value of 1.0 at $r \simeq 2$ cm. These measured and estimated profiles are shown in Fig. (I-6a, b). Figure (I-6c) shows the sawtooth relaxation $\Delta A/A$ which has a node at the $q = 1$ point. Outside this node, the sawtooth is "inverted." For radii larger that $r = 4$ cm. the amplitude was very small. Simultaneous measurement of the sawtooth at different radii and at different positions around the torus identified it as an $m = 0$, $n = 0$ mode i.e., an expansion in minor radius of the central region of the plasma column or "internal disruption." Finally, the amplitude of the high frequency oscillation ΔA, superimposed on the sawtooth relaxation, was measured as a function of the radius. The amplitude was small at the center, had a maximum close to the $q = 1$ surface and vanished abruptly outside this surface. This is illustrated in Fig. (I-6d). Such a perturbation is characteristic of the $m = 1$ kink mode (see Chapter VIII) and in fact the oscillation was diagnosed as an $m = 1$, $n = 1$ mode.[4] The mode propagated in the direction of the electron diamagnetic drift and its frequency was close to $\nu^* = (1/2\pi r)$ $(kT_e/eB)p^{-1} \, dp/dr$ evaluated at the $q = 1$ surface.

The rise in the central x-ray signal over the long time scale (see Fig. (I-5)) Δt is consistent with the ohmic heating rate there. This then suggests the following interpretation of the oscillations. Ohmic heating of the plasma inside the $q = 1$ surface and cooling of the plasma (by radiation and other losses) outside this surface causes a further sharpening of the temperature and current profile and q to drop still lower. The $m = 1$, $n = 1$ kink mode is then able to grow to some critical level when the sawtooth break occurs on the fast time scale δt (Fig. (I-5)). The energy is then rapidly redistributed producing a flattening of the temperature and current profiles. The whole process then repeats itself. This picture is supported by the fact that sawtooth oscillations are not seen,[6] when, from the temperature profile and the $J \alpha T_e^{3/2}$ assumption, $q(o) > 1$.

The series of phenomena associated with the sawtooth oscillations are usually referred to as a minor disruption in contrast to a major disruption where the whole plasma column is involved (not just the plasma around the $q = 1$ surface) and where the discharge current may be abruptly terminated. There are also minor disruptions at other m values (for instance $m = 2$), but these generally do not involve a relaxation oscillation. Let us now describe the phenomena observed during a major disruption.
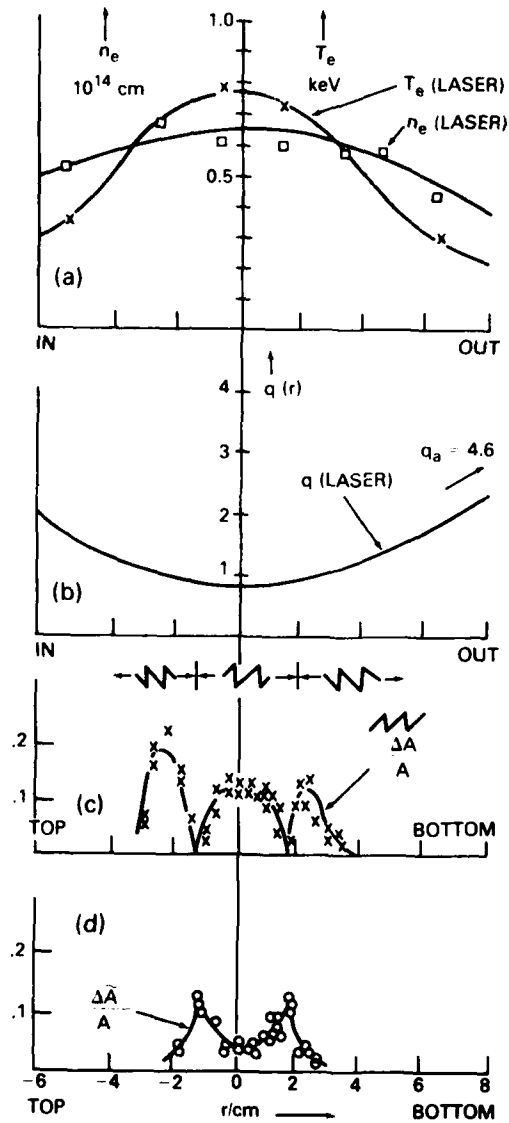
Fig. I-6 — Radial profiles of (a) electron temperature and density from laser data, (b) the safety factor $q(r)$ from laser data, (c) amplitude $\Delta\tilde{A}$ of the internal disruption (sawtooth), and (d) amplitude $\Delta\tilde{A}$ of the sinusoidal $m = 1$ oscillations preceding the step

(c) The Disruptive Instability

The disruptive instability determines the range within which stable discharge conditions exist. For an economic fusion reactor the parameters β, $(\beta \equiv 4\pi \bar{P}/B^2)$ where $\bar{P}$ is the average pressure and B the magnetic field, is required to be in the range 5% to 10% which is much larger than the value attained in present tokamaks. Since $\beta \propto 1/q^2$,[7] it is therefore desirable to operate tokamaks with $q(a)$ close to 1 as possible $(q(a) > 1$ is the Krustal-Shafranov stability requirement of Chapter IV). However, this value cannot be approached in present tokamaks because the disruptive instability limits q to larger values. The disruptive instability is still not understood although a great deal has been learned concerning its external manifestations.[8-10] These are a large negative spike on the loop voltage of the plasma (the loop voltage is a measure of the induced e.m.f which drives the discharge current round the tokamak), a sudden decrease in the major radius of the plasma ring, a significant loss of plasma energy and particles (from the core of the plasma) and a decrease in the current. This decrease can range from a few percent to a complete extinction of the discharge current in a few milliseconds. The instability is almost always preceded by strong helical modes of oscillation (usually $m = 2, 3$) in the outer regions of the plasma. These oscillations (which are often referred to as the precursors) are of the resonance type where $m = q(a)$. As a result of the disruptive instability almost all favorable tokamak results i.e., high temperature and long confinement time, have been obtained when $q(a) > 3$ or even $q(a) > 4$. As we have seen in the previous two sections, both internal and external fluctuations can now be measured. Using these techniques, studies of the phenomena just before and just after a disruption have been made on the Pulsator[8, 9] T-4[10] PLT[11] tokamaks. We shall now describe some of these results.

The Pulsator device is a conventional tokamak with the following parameters ($R = 70$ cm, $a = 12$ cm, $B_{zo} = 28$ kG (max.), $I = 95$ kA for $q = 3$ and $B_{zo} = 28$ kG, a copper shell and an iron core transformer. In addition, the device has a vertical field winding and the unusual feature of an $m = 2$, $n = 1$ helical winding. This winding was particularly advantageous for a study of the disruptive instability as will be seen in a moment. Due to the presence of these other windings, there is an unusually large gap between the plasma and the copper shell. This made the plasmas in the Pulsator device particularly susceptible to the disruptive instability if the plasma column was not well centered. Nevertheless, a minimum value of $q(a) = 2.2$ was attained by careful centering under very different conditions i.e., at high and low currents

and corresponding magnetic fields and for electron densities between 10^{13} and 10^{14} cm^{-3}.

The centering of the plasma column by current programming was achieved by trial and error and became more difficult as $q(a)$ decreased. A disruption sometimes resulted from mis-programming and it was found that if the plasma was displaced inwards too much the resulting intability was a hard disruption (i.e., the discharge current was terminated) whereas if the plasma was displaced too much outwards only a soft disruption occurred (i.e., the current increased after the instability). The observed difference between "hard" and "soft" disruptions can be ascribed to an enhanced interaction between the plasma and the limiter caused by the instability. Evidence for this enhancement is an increase in the release of impurities shown by an increase in the emission of impurity lines, Eq. 0 III, 0 VI, Mo XIII, starting at the appearance of the negative voltage spike. It was also suggested by the Pulsator group that some kind of enhanced interaction of the plasma with the limiter may be a starting mechanism for disruption. This view was examined in a beautiful series of experiments using the helical windings.[8]

It was found that for given plasma parameters a certain critical current I_{hel}^{+} in the helical windings produced a disruptive instability which exhibited all the characteristic features of a spontaneous disruption other than the $n = 2/m = 1$ precursor activity. Disruptions were only produced when the helix of the superimposed field was in the same sense as that of the tokamak magnetic field. It was clear that this effect was not a result of any change in q since $\delta q/q$ due to the critical helical current was negligibly small (of the order 10^{-4} or 10^{-5}). The effect was evidently due to a geometric resonance between the tokamak magnetic field at the $q = 2$ magnetic surface and the superimposed $m = 2$, $n = 1$ helical field. This resonance was shown computationally to lead to the formation of magnetic islands, which will be discussed more fully in Chapter 7, but can be visualized in Fig. (I-7) which shows the magnetic island structure produced by a superposition of the tokamak and helical magnetic fields. The islands originate on the $q = 2$ surface and are of width proportional to $(I_{hel}/B_{zo})^{1/2}$. It was shown experimentally that the macroscopic plasma parameters changed very little for helical currents only slightly smaller than the critical value I_{hel}^{+}.

Another interesting experimental result concerned the rate of change of the helical current or the plasma current. The same value of

$B_0 = 3T$

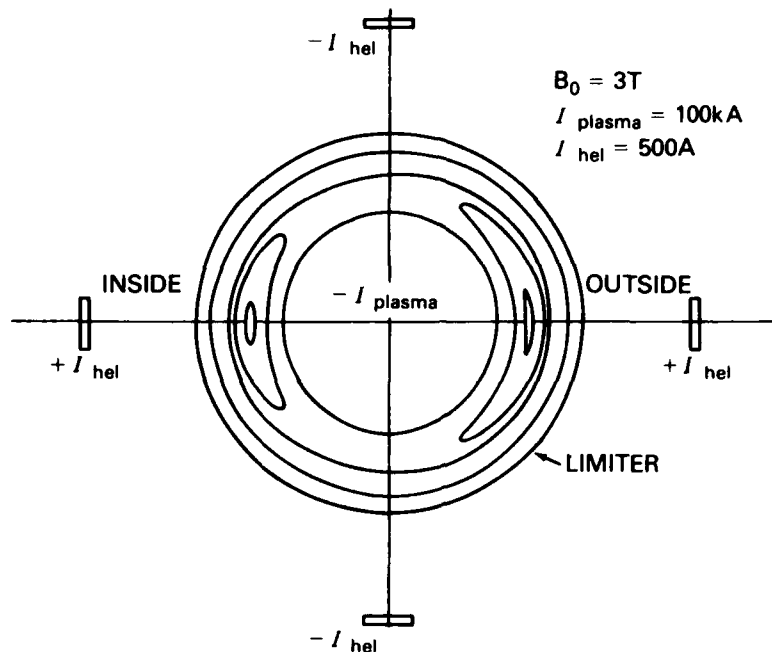$I_{plasma} = 100kA$

$I_{hel} = 500A$

Fig. I-7 — Island structure at the $q = 2$ surface produced by $I = 2$ helical windings for Pulsator-I parameters

I_{hel} was found to lead to disruption whether I_{hel} was increased at constant $q(a)$ or I_{hel} was held constant and $q(a)$ decreased by increasing the plasma current *provided* the time scale for the increase in the currents was large compared to a millisecond. On the other hand, stable, a.c operation was possible above the d.c value of I_{hel}^+ for frequencies of the order 1 kH_z. Since the skin time of the plasma was of the order of 1 millisecond this behavior was attributed to penetration effects.

The case of a slowly increasing I_{hel} (or slowly decreasing $q(a)$) is illustrated in Fig. (I-8). It can be seen that the disruption is preceded by a period of reduced MHD mode activity. The stability of the plasma was improved by a helical field below the critical value. A disruption which occured reproducibly for given plasma parameters could be avoided by the superposition of a helical field leading to an extension of the plasma current duration. However, since the improvement in stability was greater the closer I_{hel} was to the critical value I_{hel}^+ this effect could not be used to extend the stable regime very significantly.

Since the production of disruptions by the helical currents was believed to be related to the formation of magnetic islands, measurements were made to discover the dependence of the critical island size (proportional to $(I_{hel}^+/B_{zo})^{1/2}$) on the plasma parameters. In order to do
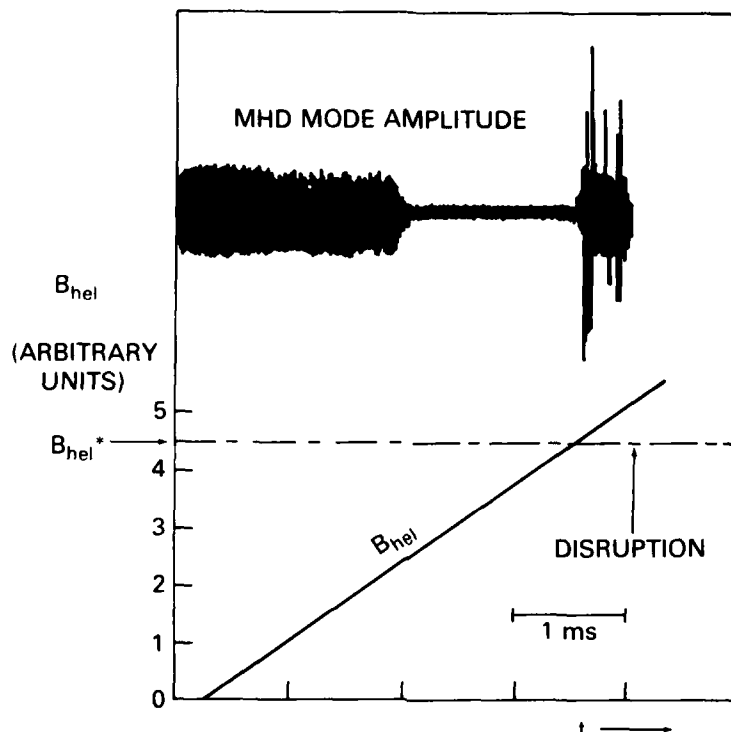
Fig. I-8 — *Decrease of mode amplitude due to*
helical currents below the critical value

this the toroidal magnetic field B_{zo} was varied from 10 to 30 kG and the plasma current from 10 to 120 kA thus covering the range $2 < q(a) < 9$. The results are shown in Fig. (I-9) where it is clear that $(I_{hel}^+/B_{zo})^{1/2}$ is a monotonically increasing function of $q(a)$. On the basis of these results and those on the positioning of the plasma by programmed vertical fields, the hypothesis was put forward that disruption occurred when I_{hel}^+ was such that the islands originating on the $q = 2$ surface touched the limiter. For increasing $q(a)$ the resonant $q = 2$ surface moves inward so that the island size must increase in order to make contact with the limiter. This hypothesis was also supported by the experimental observation[8] that the critical current I_{hel}^+ was larger for an asymmetric racetrack limiter for the case where the islands originating on the $q = 2$ surface were positioned on the major axis compared to the case when they were positioned on the minor axis.

In order to elucidate further the origin of the disruption instability, the Pulsator group have made a detailed study[9] of the phenomena just prior to the occurrence of the negative voltage spike. Signals from the external poloidal probes, the soft x-ray detectors, the loop voltage and the discharge current were measures on a fast time scale with the
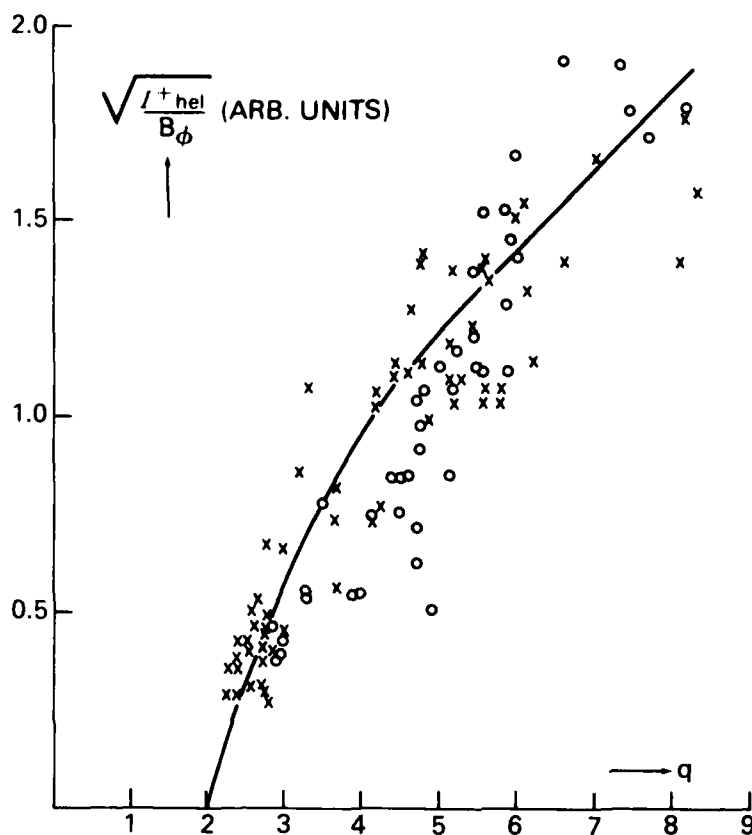
Fig. I-9 — Dependence of critical island size $\sqrt{J_{hel}^+/B_\phi}$
on the safety factor $q(a)$

aid of a 16-channel transient recorder. The $m = 2$, $n = 1$ oscillation, which was measured by the external poloidal field coils (and also with the aid of the helical windings) had a very low amplitude, until, approximately 10 milliseconds before the disruption, it started to grow both in amplitude and cycle duration. A few milliseconds before disruption it imposed its frequency on the $m = 1$, $n = 1$ mode (measured by means of soft x-ray detectors). After coupling, the amplitudes of the oscillation grew faster and the frequency continued to decrease until immediately before the negative voltage spike. At this time the signals of the x-ray detectors showed the superposition of an $m = 1$ mode in the interior of the plasma with a phase-locked $m = 2$ mode further out. The temperature maxima of this $m = 2$ mode coincided with the current maxima as measured by the poloidal field coils. The signals are most easily described as a uniform toroidal rotation of a rigidly coupled system of $m = 1$, $n = 1$ and $m = 2$, $n = 1$ perturbations. The system rotated in the direction of the electron drift resulting from the plasma

current and the coupling was attributed to toroidal effects. Figure (I-10) gives a record of these oscillations and shows the last half millisecond before disruption.

After the perturbations had reached a certain amplitude, immediately before the negative voltage spike, very hard x-rays ($E \geq 1\,\text{MeV}$) were emitted from the limiter. The x-rays were emitted in bursts and were synchronized with the rotation of the helical system, occurring when a given point passed the limiter. After the main burst the temperature in the plasma interior dropped significantly as can be seen from the central trace of the soft x-ray diodes in Fig. (I-10).
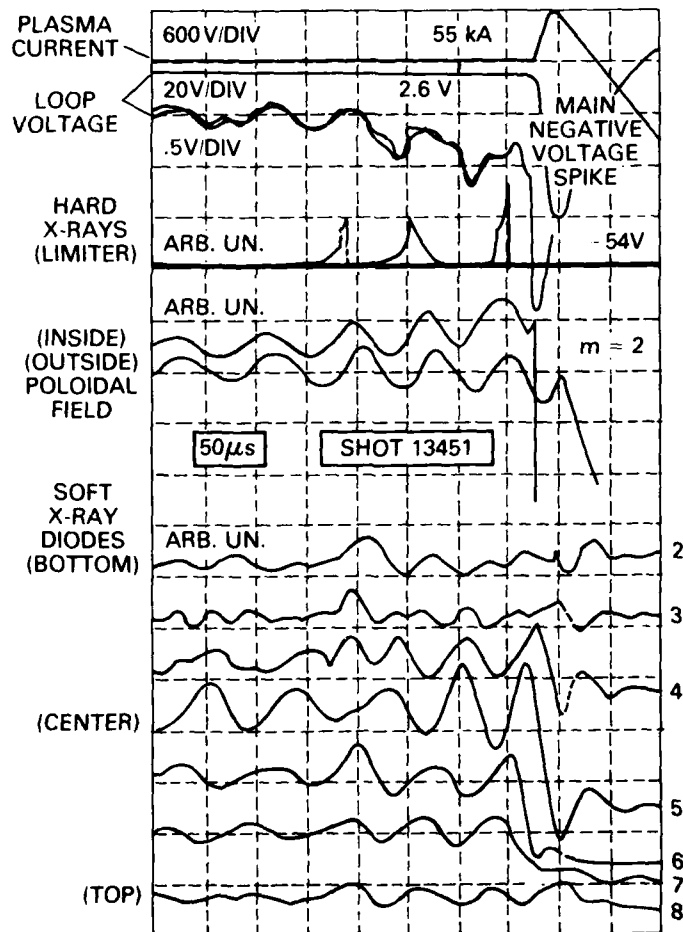
Fig. I-10 — Oscillogram showing approximately the last half millisecond before disruption

In a separate experiment with faster time resolution, it was shown that the temperature drop in the center of the plasma occurred 10-30 microseconds after the beginning of the main burst of hard x-rays and 10-20 microseconds *before* the leading edge of the main negative voltage spike. The negative voltage spike was accompanied by a positive spike in the plasma current (Figs. (I-11a, b)) and a fast inward motion of the plasma column (i.e., a contraction of the major radius). This is shown by Figs. (I-11a, b) by the traces from the poloidal field coils. Figures (I-11a, b) also illustrate the difference between a hard and soft disruption. Disruptions varying from hard to very soft were observed (Figs. (I-11a,b,c)). The intensity of a disruption seems to be determined by the magnitude of the central thermal energy drop effecting the strength of all subsequent processes (rate and magnitude). On the other hand, the strength of the disruption does not seem to depend on the amplitude of the preceding coupled helical oscillations and only weakly on the intensity of the x-ray burst.

The Pulsator group interpreted their results in terms of the following picture. The coupled $m = 1$ and $m = 2$ perturbations impose a growing, rotating helical structure on the drift surfaces of the high energy runaway electrons which have a fixed phase relation to the magnetic island system. The runaways are displaced outward with respect to the magnetic surfaces e.g., 1.5 cm for 6 MeV. Following the growth of the perturbations, deeper and deeper layers of runaways are depleted at each rotation until all the runaways have been dumped on the limiter before the first large negative voltage spike. As the perturbations grow so do the magnetic islands until a large scale ergodisation[12] of the magnetic (i.e., overlap of neighboring magnetic islands of Chapter VIII F and Chapter XII) causes an enhancement of electron heat conduction and therefore a drop in the central temperature. As a result of this drop in the central temperature, the plasma is pushed inwards in major radius by the applied vertical field causing a positive spike on the loop voltage. The calculated and observed inward displacement could at best only explain the magnitude of the first step on the negative voltage spike. One has to assume an additional variation of the plasma inductance corresponding to an expansion of the current channel to account for the full value of the negative voltage spike. Such an expansion is consistent with the increase in the H_α emission and fast neutral particle outflux at the instant of the leading edge of the negative voltage spike.

The Pulsator experiments have demonstrated that the creation of magnetic islands is an essential feature for the onset of the disruptive instability. Moreover, all the results are consistent with the assumption
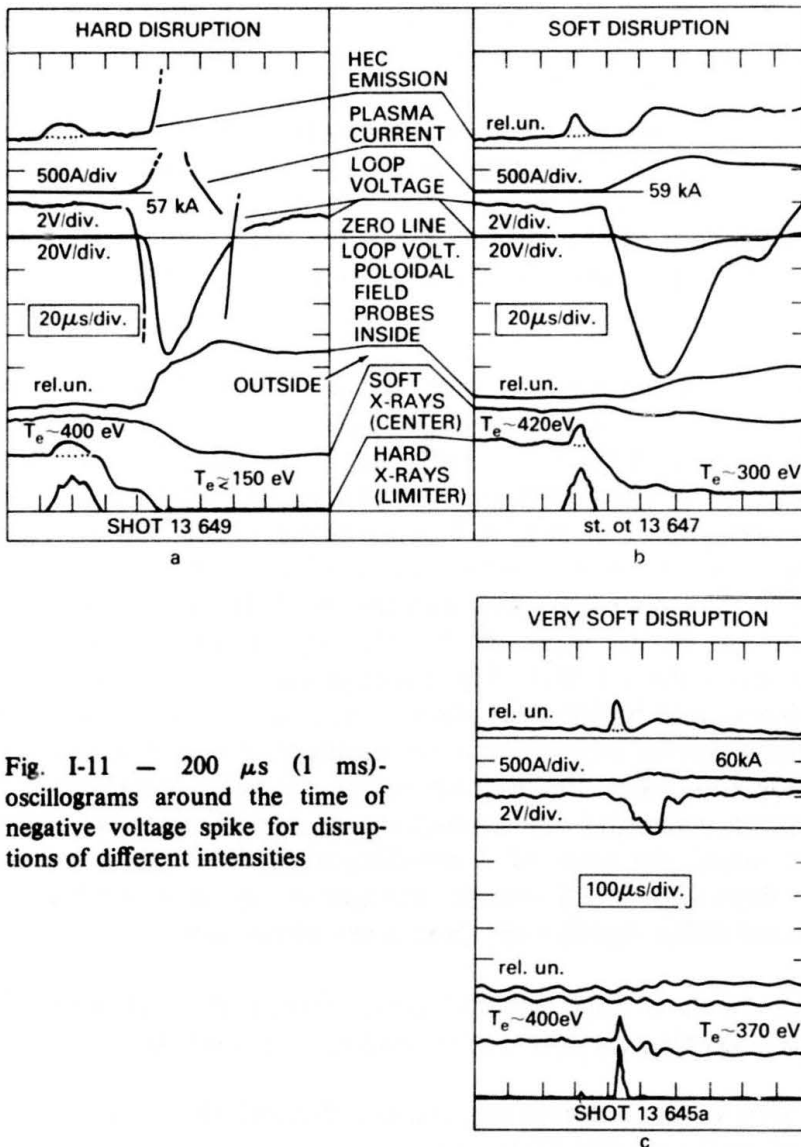
Fig. I-11 — 200 μs (1 ms)-oscillograms around the time of negative voltage spike for disruptions of different intensities

that disruption occurs when the islands come into contact with the limiter.

An important consequence of the Pulsator observations is that the destruction of confinement has occurred <u>before</u> the leading edge of the negative voltage spike so that in order to improve the confinement the discharge must be acted upon before the central temperature drop has taken place.

A similar study of the evolution of the disruptive instability was made on the tokamak T-4. The parameters of T-4 were B_{zo} = 26 kG,

$q(a) \approx 3$ ('a' being the limiter radius) and $n_e = 2 - 3 \times 10^{13} \text{cm}^{-3}$. These T-4 disruptions were produced by a programmed rise in the current. The aim of the T-4 experiments was to study the correlation between the internal and external fluctuations of the plasma column. A similar set of measurements were made as for the Pulsator experiment. These were the discharge current, the loop voltage, the fluctuations in the magnetic field of the current measured with coils located on the outside of the liner and x-radiation from the inner regions of the column.

Mirnov and Semenov[10] observed a complex time structure on T-4 which began with a pre-disruption phase in which a helical $m = 2$ oscillation propagated from the boundary to the interior. This was followed by an $m = 0$ expansion of the central hot plasma and a simultaneous development of an $m = 1$ perturbation at the centre. The final stage was a violent $m = 2$ perturbation which transformed to $m = 3$ and $m = 4$. This transition was thought to be due to a fast expansion of the column to the walls of the discharge chamber resulting in a change of $q(a)$ from 2 to 4. The oscillograms in Fig. (I-12) show the time evolution of a typical disruption. The drop in the central temperature is clearly shown on the soft x-ray oscillograms. The dotted lines in the oscillograms show the corresponding discharge parameters for a pre-disruption which did not develop into a disruption. Also, the vertical line I marks the start of a pre-disruption when the loop voltage begins to drop and line II denotes the instant up to which the disruption does not differ significantly from a pre-disruption.

As a result of their observations, Mirnov and Semenov[10] suggested the following chain of events leading to a disruption:

1. Slow compression of the current channel and ultimate decrease of $q(0)$ to 1 and $q(a)$ to 2.
2. Rapid development of an $m = 2$ perturbation near the boundary with the formation of magnetic islands.
3. Destabilization of an $m = 1$ perturbation near the center due to a deterioration of the stabilizing properties of the periphery or to $q(0) < 1$.
4. Mixing of $m = 1$ and $m = 2$, flattening of the current profile $J(r)$ and increase of $q(0)$ to 1.5.
5. Disruption per se. Non-linear development of the $m = 2$ perturbation in the presence of a flattened distribution $J(r)$. Fully developed turbulence of the plasma column, its expansion to the walls of the discharge chamber with the transformation of the $m = 2$ perturbation in to $m = 3$ and $m = 4$ modes.
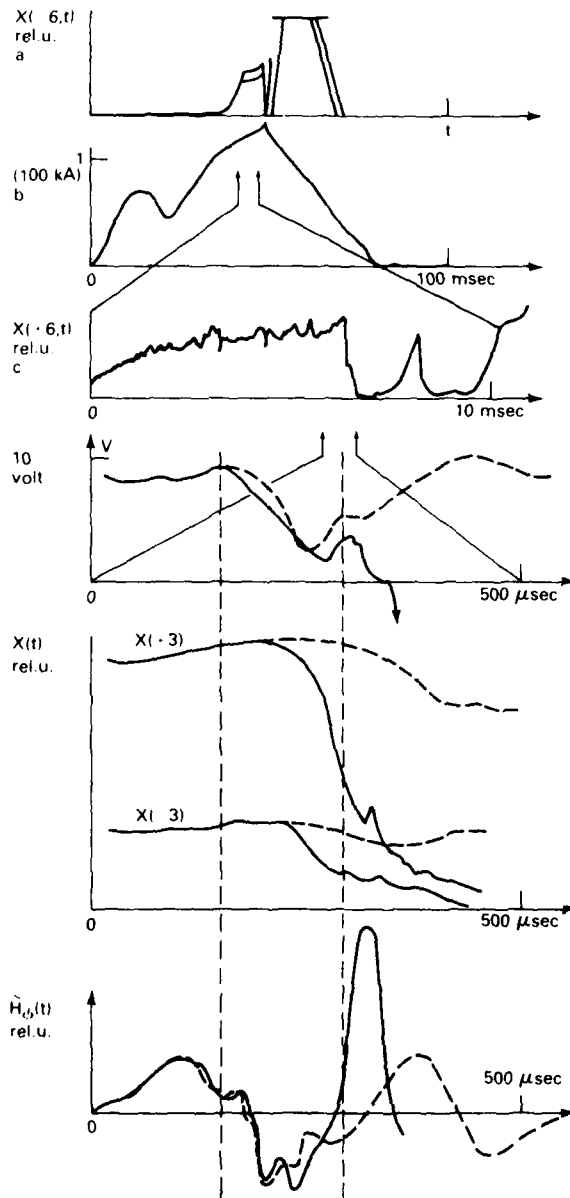
Fig. 1-12 — (a) Oscillations of X-ray radiation $X(-6.a)$ and discharge current $I(t)$ with total scanning time of 100 ms. (b) Oscillations of X-ray signal with scanning time of 10 ms. (c) Fast scans of disruption. Dashed curves show case of pre-disruption not transformed into disruption.

Mirnov and Semenov[10] concluded with an interesting inference concerning the generation of the negative voltage pulse. They noted that from the observed level of the $m = 2$ poloidal magnetic field perturbations the discharge current could be reversed in the outer regions of the plasma. A collapse of these currents could then account for the negative voltage spike. However, owing to the integrating effect of the liner for the short time scales involved they were unable to confirm this experimentally.

In summary both the Pulsator and T-4 groups saw the growth of coupled $m = 1$ and $m = 2$ oscillations, the growth of magnetic islands and a sudden drop in the central temperature following some postulated ergodisation of magnetic field lines. In addition, the T-4 group observed violent $m = 2$ activity in the presence of a flattened $J(r)$.

In conclusion, we emphasize the fact that the disruptive instability limits the current and density at which safe operation of a tokamak is possible. Even an occasional occurrence of the disruptive instability constitutes a serious danger for large tokamak devices since the abrupt termination of the discharge current leads to large currents and forces in the vacuum vessel and the external circuits. Clearly, the incentive to understand and control the disruptive instability is very great.

We now continue with a discussion the reversed field pinch, another fusion device which has a relatively simple configuration and also is characterized by MHD activity. The configuration in fact is the same as a tokamak in that it is a large aspect ratio torus and the plasma carries a toroidal current. It is different in that the longitudinal field B_z is much weaker than in a tokamak. In fact on the average $B_z \sim B_\theta$, and also B_z has a great deal of radial structure. It usually maximizes in the center and reverses sign (thus motivating the name of the device near the wall. A plot of the radial profile of B_z and B_θ, taken from HBTX at Culham is shown in Fig. (I-13). As a model of the reversed field pinch let us consider a toroidal plasma in a conducting shell with an initial uniform bias field B_i. Because the shell is perfectly conducting, no toroidal flux can go in or out, so the toroidal flux, $\pi a^2 B_i$ is constant. However let us imagine there is a poloidal slit in the shell. At time $t = 0$, a voltage V is pulsed across the slit and is kept on for a time δt, after which the slit is short circuited. The voltage pulse will induce toroidal current (and poloidal field) in the plasma and will also trigger complicated plasma motion until the system comes to rest in a steady state. There are other modes of operation of a reversed field pinch in which both toroidal and poloidal fields are programmed, but we will not consider this additional complication here.
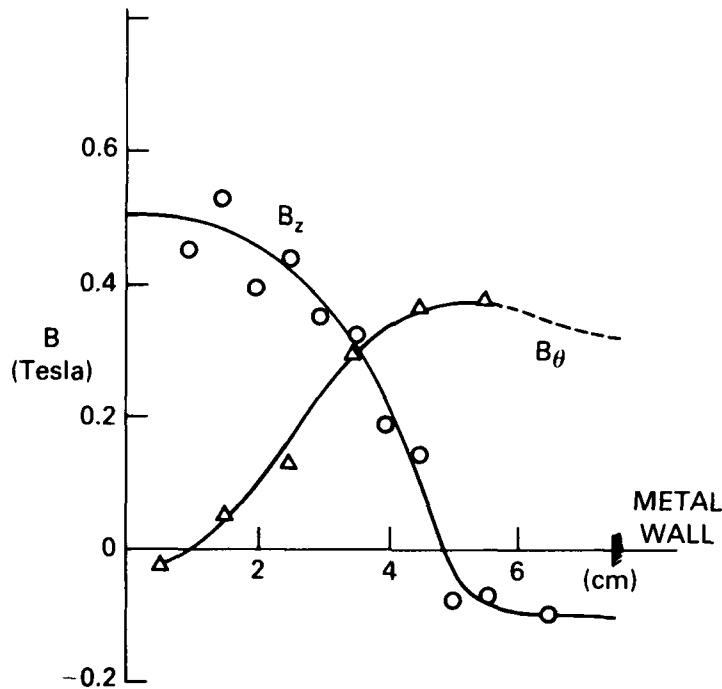
Fig. I-13 — Radial dependence of toroidal and
poloidal field in HBTX

There are three remarkable experimental feature of reversed field
pinches. First, as the voltage applied to the poloidal slit increases, the
toroidal field at the wall decreases until it goes through zero to negative
values. That is the toroidal field at the outer edge of the plasma spon-
taneously reverses. A useful parameter in studies of reversed field
pinches in the pinch parameter

$$\theta = B_\theta(\text{wall})/B_i \qquad \text{(I-3)}$$

which is proportional to plasma current. Experimental plots of

$$F = \frac{B_z(\text{wall})}{B_i} \qquad \text{(I-4)}$$

versus θ for both zeta also at Culham and HBTX as shown in Fig. (I-
14). The toroidal field at the wall reverses for $\theta \geq 1.2$.

Secondly, as the voltage is increased, the current does not remain
a monotonically increasing function of voltage. For low voltage the
steady state current does increase with voltage. However as the voltage
is further increased, the current no longer increases, but saturates at a
pinch parameter of about $\theta \approx 1.8$. For instance, in Fig. (I-15) is
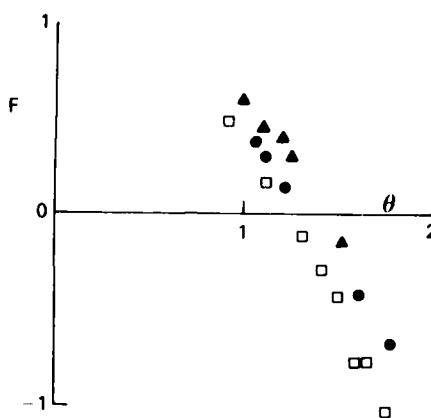shown the time dependence of θ in HBTX for a strongly driven

Fig. I-14 — Plots of F versus θ for
HBTX and ZETA
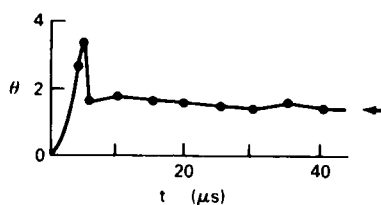
Fig. I-15 — Plot of θ versus time
in HBTX for a strongly driven
discharge

discharge. At first, θ increases to almost 4, but then it drops abruptly
to its equilibrium value of about 1.8 and stays there.

Thirdly, after the initial turbulent evolution of the plasma, it
reaches a quasi-steady state in which the plasma slowly heats up and the
current slowly decays. This quasi-steady state has been seen in both
zeta and in $\eta\beta$II in Padua. For instance the time dependence of density
and temperature during the quiescent phase of zeta is shown in Fig. (I-
16). This quiescent phase generally seems to last until field reversal is
lost on the outer wall. For a field as shown in Fig. (I-13), magnetic
diffusion tends to transport high toroidal field from inside to outside
and thereby tends to reduce and ultimately eliminate the field reversal.
However the magnetic diffusion time in a large, hot device like zeta is
much longer than the millisecond or so quiescent period, so that some-
thing gives rise to anomalously fast magnetic diffusion. In Chapters
XII and XIV we will discuss these experimental results further and see
how knowledge of MHD instabilities can shed light on them.

Fig. I-16 — Plot of density and temperature versus
time during the quiescent phase of zeta
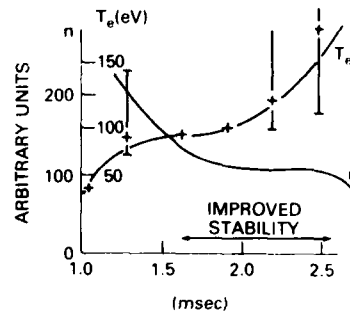
References

[1] Bezbatchenko, A.L. Yolovin, I.N., Koslov, R.I., Strelkov, V.S.,
and Yavlinskii, N.A., 1960 Rev. Plasma Phys., **4**, 135.

[2] Mirnov, S.V., and Semenov, I.B., "Investigation of Instabilities of
Plasma Column in 'Tokamak-3' Device by Correlation Tech-
niques," At. Energ. (USSR), Vol. 30, No. 1, 20-7 (1971).

[3] Mirnov, S.V., and Semenov, I.B., 1971 Sov. Phys. JETP, **33**,
1134.

[4] von Goeler, S., Stodiek, W., and Sauthoff, N., 1974, Phys. Rev.
Letts., **33**, 1201.

[5] Equipe, T.F.R. 1976 Proc. 6th Int. Conf. Plasma Physics and Con-
trolled Nuclear Fusion Research, Berchtesgaden CN-35/A8.

[6] Bickerton, R.J., 1977 Proc. Course "Theory of Magnetically
Confined Plasmas," Varenna, CEC Pergamon Press. p. 423.

[7] Wesson, J.A., 1978 Nucl. Fusion, **18**, 87.

[8] Kluber, O., "Investigation on the Disruptive Instability in Pulsa-
tor," Max-Planck-Inst. fur Plasmaphys., Garching, Germany, 7th
Eur. Conf. Controlled Fusion and Plasma Physics, 50-9 (1975).

[9] Karger, F., Lackner, K., Fussman, G., Cannici, B., Engelhardt,
W., Gernhardt, J., Glock, E., Groening, D.E., Kluber, O.,
Lisitano, G., Mayer, H.M., Meisel, D., Morandi, P., Sesnic, S.,
Wagner, F., Zehrfeld, H.P., "On the Origin of the Disruptive In-
stability in the Pulsator 1 Tokamak," Max-Planck-Inst. fur Plasma-
phys., Garching, Germany, Proc. 6th Int. Conf. Plasma Physics

and Controlled Nuclear Fusion Research, Berchtesgaden, Germany, Vol. 1, Oct. 6-13, 1976.

[10] Mirnov, S.V. and Semenov, I.B., "Observation of Disruptive-Instability Fine Structure in a Tokamak," I.V. Kurchatov Inst. of Atomic Energy, Moscow, USSR, Proc. 6th Int. Conf. Plasma Physics and Controlled Nuclear Fusion Research, Berchtesgaden, Germany, Vol. 1, Oct. 6-13, 1976.

[11] N.R. Sauthoff, S. von Goeler and W. Stodiek, Princeton Matt report 1379 (Jan. 1978).

[12] Stix, T.H., 1976 Phys. Rev. Letts. **36**, 521.

Experimental Reverse Field Pinch work can be found in:

E. Butt, et al. Plasma Physics and Controlled Thermonuclear Fusion Research, 1974, Vol. 3, p. 417 (IAEA Vienna, 1975), D.C. Robinson and R.E. King, Plasma Physics and Controlled Thermonuclear Fusion Research, 1968, Vol. 1, p. 263 (IAEA Vienna, 1969).

Chapter II

INTRODUCTION TO MHD

The Magnetohydrodynamic equations, which form the subject of this work are taken as

$$\frac{\partial \rho}{\partial t} + \nabla \cdot \rho \, \mathbf{V} = 0 \qquad \text{(II-1)}$$

(mass conservation),

$$\rho \frac{\partial \mathbf{V}}{\partial t} + \rho (\mathbf{V} \cdot \nabla) \mathbf{V} = -\nabla p + \frac{1}{c} \mathbf{J} \times \mathbf{B} \qquad \text{(II-2)}$$

(momentum conservation assuming scalar pressure)

$$\frac{1}{c} \frac{\partial \mathbf{B}}{\partial t} = -\nabla \times E \qquad \text{(a)}$$

$$\nabla \cdot \mathbf{B} = 0 \qquad \text{(b)} \qquad \text{(II-3)}$$

$$\nabla \times \mathbf{B} = \frac{4\pi}{c} \mathbf{J} \qquad \text{(c)}$$

(Maxwells equations). In Maxwell's equations, the displacement current is neglected; instead the electric field is related to the current through Ohms law

$$E + \frac{\mathbf{V}}{c} \times B = \eta \, \mathbf{J} \qquad \text{(II-4)}$$

where $E + \dfrac{\mathbf{V}}{c} \times \mathbf{B}$ is the electric field in the reference frame moving with the (nonrelativistic) fluid velocity and η is the resistivity. The only other quantity needed is the pressure. We will assume an adiabadic law

$$\left[\frac{\partial}{\partial t} + \mathbf{V} \cdot \nabla \right] \left[\frac{p}{\rho^{\gamma}} \right] \equiv \frac{d}{dt} \left[\frac{p}{\rho^{\gamma}} \right] = 0. \qquad \text{(II-5)}$$

Equations (II-1) through (II-5) constitute a complete description of the system. The unknowns are density, pressure and the three components

of magnetic field, electric field, current density and fluid velocity, fourteen in all. Equations (II-1 and 5) are two scalar equations for ρ and p, Equations (II-2, 3c and 4) are three vector equations for the three components of V, J and E, and finally Eqs. (II-3 and b) are equations for the solenoidal and irrotational parts of B.

Usually, it is convenient to eliminate E and J directly by using Eqs. (II-3c and 4). Doing so, the momentum equation and Maxwell's equation become

$$\rho\frac{dV}{dt} = -\nabla p + \frac{1}{4\pi}(\nabla \times B) \times B \qquad \text{(II-6)}$$

and

$$\frac{\partial B}{\partial t} = \nabla \times (V \times B) - \frac{\eta c^2}{4\pi}\nabla \times (\nabla \times B) \qquad \text{(II-7)}$$

Much of our discussion will concern perfectly conducting fluids ($\eta = 0$) so that Eq. (II-7) is

$$\frac{\partial B}{\partial t} = \nabla \times (V \times B) \qquad \text{(II-8)}$$

Equations (II-1, 5, 6 and 7 or 8) form a complete description of the magnetized conducting fluid. Derivations of these equations as well as discussions of their validity and possible extensions (for instance including tensor pressure, thermal conduction, finite Larmor radius, etc.) have been discussed in many textbooks on plasma physics. We simply assume these equations describe the plasma and investigate their consequences; particularly we focus on how the magnetic field couples to the fluid motion.

Before doing this, it is worthwhile to quickly review what magnetic field lines and flux tubes are. Any vector field has streamlines. For the magnetic field, these are the solution of

$$\frac{dx}{B_x} = \frac{dy}{B_y} = \frac{dz}{B_z} \qquad \text{(II-9)}$$

The field lines are then everywhere parallel to the magnetic field. Let us now imagine an element of area δA which is parallel to a field line at some point s on the field line. If the magnetic field at this point has strength $B(s)$, the flux through this element of area is $\delta\phi = B(s)$ $\delta A \equiv B(s) \cdot \delta A$. One can then imagine a tube of constant flux around the field line. If the flux is $d\phi$, the area of the flux tube as a function of distance along the field line is given by

$$\delta A(s) = \frac{\delta\phi}{B(s)} \qquad \text{(II-10)}$$

The amazing thing about a flux tube is that in a perfectly conducting plasma ($\eta = 0$), which we will refer to as ideal MHD, a flux tube is convected with the flow. It is a simple matter to prove this from Eq. (II-7). Integrating Eq. (II-7) over a fixed area δA, we find

$$d(\delta\phi) = dt \oint d\mathbf{s} \cdot (\mathbf{V} \times \mathbf{B}) = \oint (d\mathbf{s} \times \mathbf{V}\, dt) \cdot \mathbf{B} \qquad \text{(II-11)}$$

where $\oint ds$ is an integral around the closed line bounding $\delta\phi$. However $d\mathbf{s} \times \mathbf{V}\, dt$ is the area swept out by an element ds of the periphery of the flux loop. The term on the right hand side of Eq. (II-11) is then negative the flux swept out by the circumference in its trajectory. Therefore, the total flux through a surface area moving with the fluid does not change time, or

$$\frac{d\phi}{dt} = 0 \qquad \text{(II-12)}$$

Perhaps a more direct way to see this is to note that if $\eta = 0$, Ohms law Eq. (II-4), simply says that $E = 0$ as one moves with the fluid. However in the inertial frame locally moving with the fluid, Maxwells equation says that the rate of change of the enclosed flux is minus the loop voltage, that is zero.

While the magnetic lines of force are well defined by Eq. (II-9), in general there is no unique way to define the motion of lines of **B** in a changing medium. However in a perfectly conducting fluid, the flux is frozen into the flow. Since the flux tubes can be regarded as bundles of field lines, one can equally look upon the field lines themselves as being carried along with the flow. We will now examine just what this means. Since $\nabla \cdot \mathbf{B} = 0$, the field lines have no start or finish, but either close on themselves or else have infinite length. Since they are frozen into the flow, the field lines cannot reconnect, or in other words, the topological properties of the field is maintained. That is, the field line can stretch and bend, but it cannot change its topology.

Let us illustrate this for two dimensional motion. Say the field line initially is the dotted circle shown in Fig. (II-1a). Since the velocity field is a single valued function of **r** for all time, there is no way that two fluid elements initially far from each other can ever occupy the same point; to do so would mean the fluid elements pass through each other, implying a double valued velocity field. Therefore, while a complicated flow pattern can greatly contort the field line, to for instance the solid line in Fig. (II-1a), the field line can never cross itself, it always has a single inside and outside. Thus the topological properties of the field line are maintained. Once possible flow pattern could distort two nearby field lines to a pattern shown in Fig. (II-1b). While the
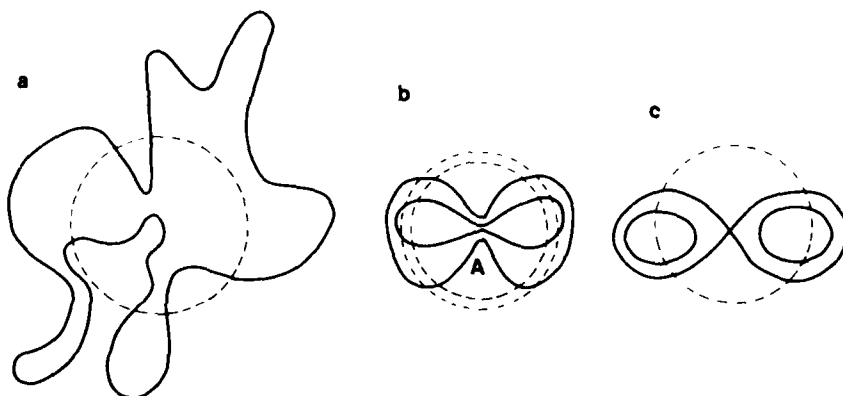
Fig. II-1(a) — A possible contortion of a field in two dimensions which preserve the topological constraint, (b) another motion which also preserves the topology by showing how field lines can be forced together, and (c) a field line pattern similar to 2(b), but where reconnection is allowed

two points near A can be arbitrarily close, the field line still must maintain its integrity. However as we will see in later chapters, the presence of non ideal effects, for instance resistivity, can relax the topological constraint so that the field line can break and reconnect, forming that pattern in Fig. (II-1c). Clearly the topology has changed from a simple closed curve topology to a figure eight. That is there are two inner regions instead of one and two sets of closed field lines.

As another example the topological constraints on the field line motion, we will consider an example in three dimensions. Consider two field lines which are initially parallel to each other shown in Fig. (II-2a). (In order to distinguish which field line is in front of the other, each line is shown with finite width and different shading). Imagine a flow pattern which distorts the field line, but which renders this field line periodic in space with periodicity length L, and which has $V = 0$ along the dark field line.

Since the lighter field line is frozen into the flow, it cannot wind around the dark field line between $Z = 0$ and $Z = L$. For instance, if the fluid winds around the inner field line at say $Z = L/2$, but does not move at $Z = 0$ and $Z = L$, the shaded line winds around the dark line as shown in Fig. (II-2b). Between $Z = 0$ and $Z = L/2$, the shaded line winds around the dark line, but between $Z = L/2$ and $Z = L$ it unwinds. The total winding number of the shaded line around the dark, between $0 < Z < L$, is preserved at zero.

However another type of fluid motion might give rise to the field lines shown in Fig. (II-2c). The topology of the shaded line is the same

Z = 0   Z = L   Z = 2L
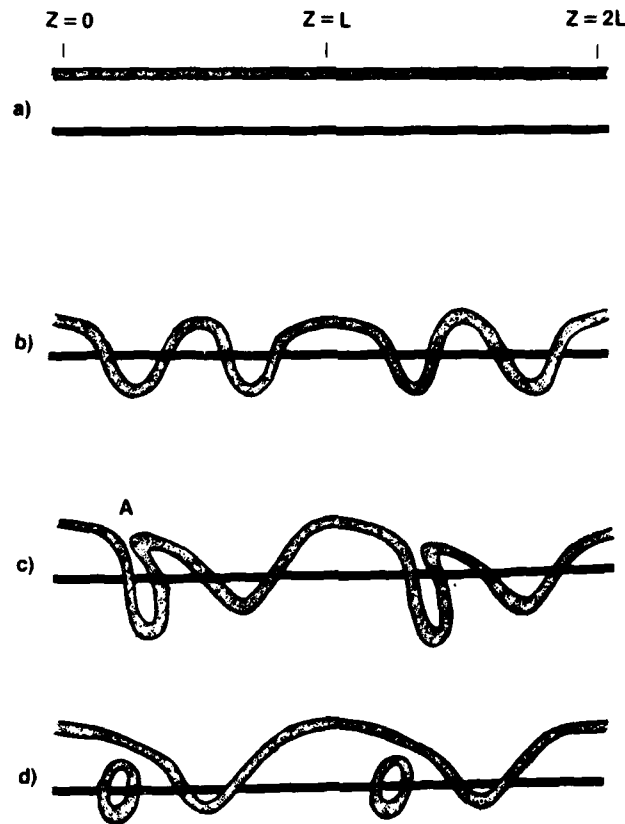
Fig. II-2 — (a) Two neighboring field lines, (b) distortion of one field line which preserves winding number, (c) distortion which preserves winding number but which forces field lines together, (d) field pattern similar to 2(d), but which allows reconnection. Note that winding number is no longer conserved, but dotted field line winds around dark one.

as shown in Fig. (II-2a and b). That is, if one pulled the field line at $Z = 0$ and $Z = L$, it would snap back to that shape in Fig. (II-2a). Notice though that near the point marked A, two parts of the field line are forced close together. Again, the presence of non-ideal effects could cause the field line there to break and reconnect as shown in Fig. (II-2d) where now two sets of field lines are produced, the main field line which now loops around the axis, and an additional circle which also loops the axis. Thus, in ideal MHD if a field line does not wind around another initially, it never does. However if non-ideal effects (for instance resistivity) are allowed, the field lines may break and reconnect and then wind around another field line which it did not initially encircle. In other words, new magnetic axes can be generated.

To summarize, the field lines in a magnetized fluid can be regarded as strings which thread the fluid and go wherever the fluid goes. They can stretch and bend but cannot break or reconnect in ideal MHD. However if non-ideal effects are allowed, the field lines can break and reconnect. Obviously, however, since div $\cdot B = 0$, a field line cannot break unless it reconnects instantaneously with another part of the field line (or with a different field line). As we will see, there are types of fluid motion which tend to force different portions of field lines together, as shown at points A in Fig. (II-1b) and II-2c). In this case, often a very small amount of resistivity can cause reconnection at these points. In other words, given a choice between evolving toward a very complicated structure with the same topology, or a simple structure with different topology, a field line in a real plasma will often choose the latter.

We now turn to a study of the magnetic forces exerted on the plasma. The magnetic force per unit volume is given by

$$F_m = \frac{1}{c} \, J \times B \qquad (II\text{-}13)$$

which is clearly always perpendicular to both B and J. A more convenient form for F_m is

$$F_m = \frac{1}{4\pi} (\nabla \times B) \times B = - \frac{1}{8\pi} \nabla B^2 + \frac{1}{4\pi} (B \cdot \nabla) B \quad (a)$$

$$= - \frac{1}{8\pi} \nabla_\perp B^2 + \frac{B^2}{4\pi} (i_b \cdot \nabla) i_b \qquad (b) \quad (II\text{-}14)$$

In Eq. (II-14b) above $\nabla_\perp$ means the portion of the gradient which is perpendicular to B and i_b is a unit vector in the direction of B.

The two terms in Eq. (II-14b) have simple interpretation. The first term shows that the magnitude of B^2 acts like a pressure in a direction perpendicular to B. That is a gradient in B^2 exerts a force which pushes the plasma toward regions of lower B^2. To interpret the second term, note that $(i_b \cdot \nabla) i_b = i_{R/R}$ where R is the radius of curvature of the field line and i_R is a unit vector pointing toward the center of curvature. Thus if the field lines are bent, there is a force exerted on the plasma of magnitude $\dfrac{B^2}{4\pi R}$ and directed toward the center of curvature. This latter force acts rather as if the field line were a rubber band. If a stretched rubber band is bent, a force is exerted which tends to snap it back to a straight line. This then corresponds to the way a magnetic field line acts. The main difference is, of course, that a stretched bent

rubber band exerts a strong force along its length as well as perpendicular to itself; the bent magnetic field line only exerts this force perpendicular to itself but not along its length. Figure (II-3) illustrates the force exerted on the plasma by the two terms in Eq. (II-14b).

B
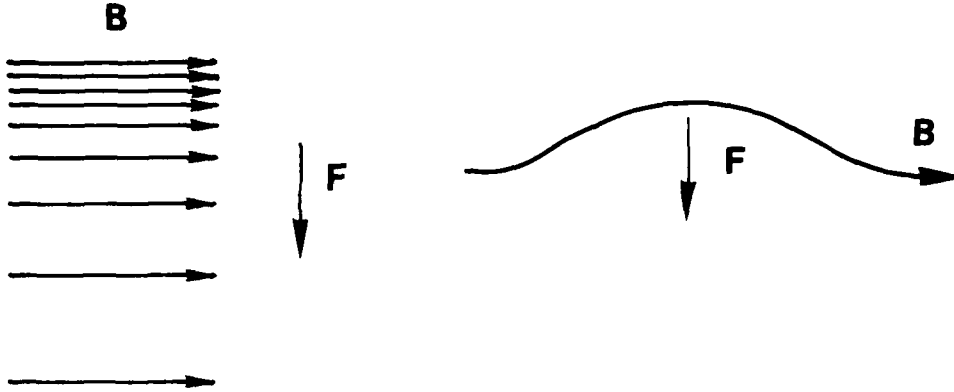
Fig. II-3 — Illustration of the force, a gradient in $B_\perp$, and the
force a curved field line exerts on a plasma

Clearly, before we can concern ourselves with MHD instabilities, a first step is an examination of MHD equilibria. In equilibrium, with $V = \dfrac{\partial}{\partial t} = 0$, the momentum conservation equation is

$$\nabla p = \frac{1}{c} \, \mathbf{J} \times \mathbf{B} = - \frac{1}{8\pi} \, \nabla B^2 + \frac{1}{4\pi} (\mathbf{B} \cdot \nabla)\mathbf{B}. \qquad \text{(II-15)}$$

There are several immediate consequences of Eq. (II-15). First of all, it is easy to show that the pressure must be constant along a field line; simply take dot product of Eq. (II-15) with $\mathbf{i}_b$ and get the result

$$(\mathbf{i}_b \cdot \nabla)p = 0 \qquad \text{(II-16)}$$

so the pressure is constant along a field line. Therefore any open ended device, for instance a magnetic mirror, where field lines end on walls, cannot be in MHD equilibrium, at least for scalar pressure. It is for this reason that the research on open ended devices usually concerns itself principally with Vlasov equilibria and stability or else with tensor pressure.

For the remainder of this chapter we will concern ourselves with devices with enclosed field lines, for instance tokamaks, reversed field pinches, or infinitely long cylinders. As a field line goes around a toroidal machine, there are three possibilities; first, it may close on itself after one or more transits; second, it may trace out a surface, and third, it may ergodically fill a volume, which may be either the entire

volume of the torus or a portion of it. In MHD equilibrium, the pressure is constant along each magnetic line, surface or volume, whatever the case may be. Clearly, if the field lines fill the volume of the device, no MHD equilibrium is possible.

In the case of reverse field pinches or tokamaks, the field lines form surfaces. From Eq. (II-15), it is possible to show that the current lines are also in the flux surfaces. To do so, take the dot product with **J** which shows that $P = $ constant along the lines of **J**. However if P varies from one flux surface to the next, then lines of **J** must also lie in the surfaces of constant P that is the flux surfaces.

In a general axi-symmetric toroidal equilibrium, it is usually convenient to choose as one co-ordinate surface, the flux surface. For our purposes here, we only write the pressure balance equation in cylindrical geometry with variation only in r. These are

$$B_r = 0$$

$$0 = \frac{d}{dr}\left(p + \frac{B_z^2}{8\pi} + \frac{B_\theta^2}{8\pi}\right) + \frac{1}{4\pi}\frac{B_\theta^2}{r}. \qquad \text{(II-17)}$$

Once p and B_z are given, Eq. (II-17) can be solved for the appropriate B_θ for equilibrium.

Having discussed the steady state equilibrium, we now proceed to a discussion of the dynamics by examining what sort of wave motion is allowed in a uniform, magnetized, current free conducting fluid. Denoting an unperturbed (equilibrium) quantity with a subscript zero and a perturbed quantity with no subscript, the linearized equations of motion are

$$\rho_o \frac{\partial V}{\partial t} = -\frac{\gamma p_o}{\rho_o}\nabla\rho + \frac{1}{4\pi}(\nabla \times B) \times B_o \qquad \text{(a)}$$

$$\frac{\partial \rho}{\partial t} + \rho_o \nabla \cdot V = 0 \qquad \text{(b)} \qquad \text{(II-18)}$$

$$\frac{\partial B}{\partial t} = \nabla \times V \times B_o \qquad \text{(c)}$$

where we have made use of the adiabatic relation between ρ and p. Taking $\frac{\partial}{\partial t}$ of Eq. (II-18a) and substituting from Eq. (II-18 b and c), we find a single vector equation for **V**. Assuming $\nabla = i\mathbf{k}$ and $\frac{\partial}{\partial t} = -i\omega$, it is

$$-\omega^2 \mathbf{V} = -c_s^2 \mathbf{k}(\mathbf{k} \cdot \mathbf{V}) + V_A^2 \mathbf{i}_z \times [\mathbf{k} \times \{\mathbf{k} \times (\mathbf{V} \times \mathbf{i}_z)\}] \qquad \text{(II-19)}$$

where c_s is the sound speed, $c_s = \left(\dfrac{\gamma p_0}{\rho_0}\right)^{1/2}$ and V_A is the Alfven speed

$V_A = \dfrac{B_0}{\sqrt{4\pi\rho_0}}$. Also $\mathbf{B}_0$ is assumed to be in the z direction. Since the plasma is isotropic in the $x-y$ plane, we may take $\mathbf{k}$ to be in the yz plane without loss of generality. Then taking the component forms of Eq. (II-19), gives

$$\omega^2 V_x = k_z^2 V_A^2 V_x \qquad \text{(a)}$$

$$\omega^2 V_y = k_y c_s^2 (k_y V_y + k_z V_z) + (k_y^2 + k_z^2) V_A^2 V_y \qquad \text{(b)} \qquad \text{(II-20)}$$

$$\omega^2 V_z = k_z c_s^2 (k_y V_y + k_z V_z). \qquad \text{(c)}$$

As is clear from Eq. (II-20a), the x velocity decouples and this is the shear Alfven wave with dispersion relation

$$\omega^2 = k_z^2 V_A^2 = k^2 V_A^2 \cos^2\theta \qquad \text{(II-21)}$$

k being the magnitude of $\mathbf{k}$ and θ being the angle between $\mathbf{B}$ and $\mathbf{k}$. The other modes involve the coupled y and z motion. A straightforward calculation from Eqs. (II-20 b and c) gives the result

$$\frac{\omega^2}{k^2} = \frac{(V_A^2 + c_s^2) \pm ((V_A^2 - c_s^2)^2 + 4 c_s^2 V_A^2 \sin^2\theta)^{1/2}}{2}. \qquad \text{(II-22)}$$

For $\theta = 0$, the two roots are $\omega^2/k^2 = c_s^2$ and V_A^2, while for $\theta \approx \dfrac{\pi}{2}$, the

two roots are $\dfrac{\omega^2}{k^2} \approx c_s^2 + V_A^2$ and $\dfrac{\omega^2}{k^2} \approx c_s^2 \cos^2\theta / \left(1 + \dfrac{c_s^2}{V_A^2}\right) \approx 0$. A

polar plot $\dfrac{\omega}{kV_A}$ for the three roots is shown in Fig. (II-4) for the case of $V_A = 3c_s$. Figure (II-4) shows that waves in a magnetized fluid have some interesting properties. Since the shear Alfven wave (Eq. (II-21)) has $V_y = V_z = 0$, it does not compress the plasma. At $\theta = 0$, the sound wave does compress the plasma, but by following this root around to $\theta = \dfrac{\pi}{2}$ where $\omega = 0$, one can show that there is no plasma compression there. On the other hand, at $\theta = 0$, the wave which has $\dfrac{\omega}{k} = V_A$ does not compress the plasma; however following the root around to $\theta = \dfrac{\pi}{2}$, where $\dfrac{\omega^2}{k^2} = V_A^2 + c_s^2$, we see that the plasma is compressed. Thus if $V_A > c_s$, there is no such thing as a pure sound wave. What starts out as a compressional wave at $\theta = 0$ ends up as a

shear wave at $\theta = \dfrac{\pi}{2}$, and visa versa. However if $c_s > V_A$, the sound wave is compressional at all angles.

We now give simple physical pictures first for the shear Alfven wave for $\theta = 0$ and then for the compressional Alfven (magnetosonic) wave at $\theta = \dfrac{\pi}{2}$. Imagine that each fluid element is displaced in the x direction an amount

$$x = x_o \cos kz. \tag{II-23}$$

Since the field line is frozen into the flow, Eq. (II-23) above is also the equation for a field line. The perturbed field $B_x \mathbf{i}_x$ is perpendicular to the equilibrium field, $B_o \mathbf{i}_z$, so there is no first order change in the magnitude of $\mathbf{B}$. Hence the only force on the fluid arises from the bending of the field line, as discussed after Eq. (II-14). If terms of order x_o^2 are neglected, the reciprocal of the radius of curvature of the field line is

$$\mathbf{R}^{-1} = - k^2 x_o \cos kz \, \mathbf{i}_x. \tag{II-24}$$

Therefore the force per unit volume on each fluid element is

$$\mathbf{F}_m = - \frac{B_o^2 k^2}{4\pi} \, \mathbf{i}_x x_o \cos kz \tag{II-25}$$

which is just minus a constant times the displacement of the fluid element. That is, each fluid element performs simple harmonic oscillation with frequency given by $\omega^2 = k^2 B_o^2 / 4\pi\rho_o$ perpendicular to the equilibrium magnetic field. The phase speed of this wave is the Alfven speed.

One can picture this oscillation in terms of the magnetic field lines constituting a series of strings which permeate the plasma. Imagine pulling on these strings with a tension of $\dfrac{B^2}{4\pi}$ per unit area. Then if the strings are bent, they will tend to snap back and oscillate about their equilibrium position with frequency $k^2 B^2 / 4\pi\rho$. Therefore as far forces perpendicular to themselves are concerned, the magnetic field lines are like strings with tension $\dfrac{B^2}{4\pi}$ per unit area. They are different however, in that unlike a stretched string there is no force along a magnetic field line.

We now turn to an examination of wave motion across a magnetic field. Say that B_o is in the z direction and the displacement and wave number are both in the y direction. In this case, the field lines remain straight and do not bend. Therefore, according to Eq. (II-14b), the

force density on the plasma is minus the gradient of the scalar magnetic pressure. This perturbed magnetic pressure is

$$P_M = \frac{B_o B_z}{4\pi} = \frac{B_o^2}{8\pi} 2\frac{B_z}{B_o} = \frac{2P_{Mo}}{\rho_o}\rho \qquad \text{(II-26)}$$

where we have used the fact that the field is frozen into the plasma so $\frac{\rho}{\rho_o} = \frac{B_z}{B_{zo}}$. (Also this can be easily verified from Eqs. (II-18b and c).) Hence the magnetic scalar pressure acts like a fluid with $\gamma = 2$. The perturbed fluid pressure is of course $\left(\frac{\gamma p_o}{\rho_o}\right)\rho$ so that the perturbed total pressure in the plasma is given by

$$P_{ToT} = \left(\frac{\gamma p_o}{\rho_o} + 2\frac{P_{Mo}}{\rho_o}\right)\rho. \qquad \text{(II-27)}$$

Now it is clear that perpendicular to the field, waves propagate like sound waves, except that the magnetic field adds an extra 'springiness' to the plasma.

We conclude this chapter with a discussion of what sort of plasma motion an MHD instability is likely to generate. The modes we have discussed all have $\omega^2 > 0$. However for instability, obviously $\omega^2 < 0$. Now imagine that there is some physical effect which perturbs the system so as to drive the plasma toward instability. Clearly this effect will manifest itself by lowering ω^2. However if ω^2 is large to begin with, instability, in general, will not result, but instead just a lowering of the frequency. Clearly, the most likely place for instability is where $\omega^2 = 0$, or for incompressible flow with $\mathbf{k} \cdot \mathbf{B} = 0$, according to Fig. (II-4) and
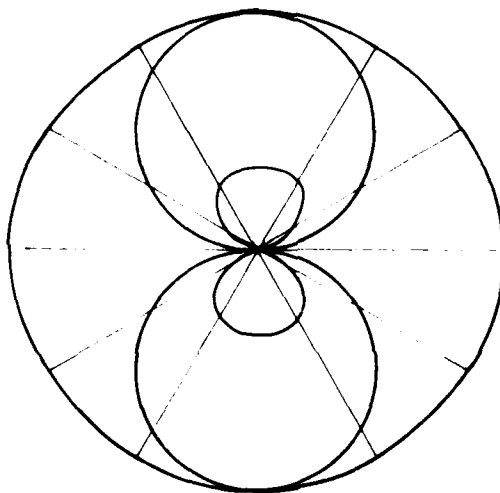

Fig. II-4 — A polar plot of phase velocity versus angle to the magnetic field for the three branches of MHD oscillation

the discussion following Eq. (II-22). In other words, if $\mathbf{k} \cdot \mathbf{B} \neq 0$, the instable flow will couple to shear Alfven waves, which is a stabilizing effect; and if $\nabla \cdot \mathbf{V} \neq 0$, it will couple to sound or magnetosonic waves, which is also stabilizing. In most of the rest of this book, we focus on perturbed plasma motion which is incompressible. This does not mean, of course, that the plasma is impossible to compress, but rather that the motions we consider have phase speed much less than the magnetosonic speed and are therefore decoupled from compressional motion.

Listing relevant previous work in MHD in a complete and fair way is an enormously difficult job because of the tremendous amount of research spanning about a quarter of a century. Our own choice comes generally from the papers that most influenced us, but we have included others dealing with topics not directly covered in this book. Also the papers listed reflect our own experience in magnetic fusion. There are many other papers in astrophysical, solar and magnetospheric research which we are not as familiar with.

We start with a list of recent review articles in this field:

Plasma Equilibrium in a Magnetic Field, V.D. Shafranov in Reviews of Plasma Physics, Vol. 2, Consultants Bureau, New York, 1966, Ed., M.A. Leontovich, p. 103.

Hydromagnetic Stability of a Plasma, B.B. Kadomtsev in Reviews of Plasma Physics, Vol. 2, Consultants Bureau, New York, 1966, Ed., M.A. Leontovich, p. 153.

Plasma Confinement in Closed Magnetic Systems, L.S. Solovév and V.D. Shafranov, In Reviews of Plasma Physics, Vol. 2, Consultants Bureau, New York, 1970, Ed., M.A. Leontovich, p. 1.

Plasma Equilibria in a Tokamak, V.S. Mukhovatov and V.D. Shafranov, Nuclear Fusion, 11, 605 (1971).

Tokamak Devices, L.A. Artsimovich, Nuclear Fusion, 12, 215 (1972).

Tokamak Research, H.P. Furth, Nuclear Fusion, 15, 487 (1975).

Hydromagnetic Stability of Tokamaks, J.A. Wesson, Nuclear Fusion, 18, 87 (1978).

Experimental Studies of Plasma Confinement in Toroidal Systems, H.A. Bodin and B.E. Keen, Europhysics Journal, **40**, 1415 (Dec. 1977).

A paper describing the concept of magnetic field lines in a magnetized fluid is:

Motion of Magnetic Lines of Force, W.A. Newcomb, Ann. Phys. **2**, 362 (1958).

Several papers describing MHD equilibria are:

Equilibrium of Magnetically Confined Plasma in a Toroid, M.D. Kruskal and R.M. Kulsrud, Phys. Fluids, **1**, 265 (1958).

Hydromagnetic Equilibria and Force Free Fields, H. Grad and H. Rubin, IAEA Geneva Conf., **31**, 190 (1958).

On Magnetohydrodynamical Equilibrium Configurations, V.D. Shafranov, Sov. Phys. JETP, **6**, 545 (1958).

Toroidal Containment of a Plasma, H. Grad, Phys. Fluids, **10**, 137 (1967).

Helical Equilibrium of a Current Carrying Plasma, S. Yoshikawa, Phys. Rev. Lett., **27**, 1772 (1971).

MHD Equilibria in Sharply Curved Axisymmetric Devices, J.D. Callen and R.A. Dory, Phys. Fluids, **15**, 1523 (1972).

High Pressure Flux Conserving Tokamak Equilibrium, J.F. Clarke and D.J. Sigmar, Phys. Rev. Lett., **38**, 70 (1977).

Chapter III

THE ENERGY PRINCIPLE

A complete solution of the linear stability of a plasma for a given magnetic field configuration requires the determination of eigen-functions and eigenvalues of the linearized equations. For all but the simplest geometries this proves to be a problem of considerable complexity. It is therefore desirable to have a procedure for deciding the question of stability which does not require the determination of the eigenvalues (or characteristic frequencies). For the problem of the MHD stability of a perfectly conducting plasma in the absence of an equilibrium flow, the Energy Principle provides just such a method.

The original derivation of the Energy Principle by Bernstein et al., assumed that the eigen-functions of the linearized equations formed a complete set. However, it was pointed out by Laval et al., that this assumption is not always valid so that it became necessary to find a proof of the Energy Principle which did not rely on the completeness property. Laval et al., in a very elegant analysis, provided this proof assuming only that the linear operator was self-adjoint. Here we shall give an alternative proof of the Energy Principle which assumes neither completeness nor self-adjointness but instead we shall demonstrate the conservation of small signal energy directly from the linearized ideal MHD equations.

Before giving this proof let us say a few words about the small signal energy mentioned above. The small signal energy is defined entirely in terms of the fields of the linear theory and is not the same as the physical energy. It was Sturrock who first drew attention to the significance of the small signal energy (or "pseudo-energy" as he called it) for the problem of linear stability. It is not obvious that this small signal energy will be conserved in a conservative system simply because the physical energy is conserved since the exact fields have been expanded in a series and truncated at the first order.

We shall now derive a generalization of the Poynting theorem from the linearized MHD equations and from this obtain the conservation of small signal energy. The proof of the Energy Principle is then completed using the arguments given by Laval et al.

Let us consider a plasma in which the pressure is isotropic and which is bounded by a rigid, perfectly conducting wall, where the boundary conditions are the following

$$\hat{n} \cdot \mathbf{V} = 0; \quad \hat{n} \times \mathbf{E} = 0; \quad \hat{n} \frac{\partial \mathbf{B}}{\partial t} = 0$$

when $\hat{n}$ is the unit normal to the boundary. The analysis is easily generalized to other boundary conditions (e.g., plasma-vacuum boundary). The linearized equations of the ideal MHD model are

$$\rho_o \frac{\partial \mathbf{V}}{\partial t} = - \nabla p + \frac{1}{c} \mathbf{J} \times \mathbf{B}_o + \frac{1}{c} \mathbf{J}_o \times \mathbf{B} \qquad \text{(III-1)}$$

$$\frac{\partial \rho}{\partial t} + \nabla \cdot (\rho_o \mathbf{V}) = 0 \qquad \text{(III-2)}$$

$$\mathbf{E} + \frac{1}{c} \mathbf{V} \times B_o = 0 \qquad \text{(III-3)}$$

$$\frac{\partial p}{\partial t} + (\mathbf{V} \cdot \nabla)p = \frac{\gamma p_0}{\rho_o} \left[\frac{\partial \rho}{\partial t} + \mathbf{V} \cdot \nabla \rho_o \right] \qquad \text{(III-4)}$$

$$\nabla \times \mathbf{E} = - \frac{1}{c} \frac{\partial \mathbf{B}}{\partial t} \qquad \text{(III-5)}$$

$$\nabla \times \mathbf{B} = \frac{4\pi}{c} \mathbf{J} \qquad \text{(III-6)}$$

$$\nabla \cdot \mathbf{B} = 0 \qquad \text{(III-7)}$$

where fields with subscript zero are equilibrium quantities and the linearized variables are written without subscripts. As already mentioned there is no equilibrium flow of the plasma. We now scalar multiply Eq. (III-1) by $\mathbf{V}$ to obtain

$$\rho_o \mathbf{V} \cdot \frac{\partial \mathbf{V}}{\partial t} = - \mathbf{V} \cdot \nabla p + \frac{\mathbf{V}}{c} \times (\mathbf{J} \times \mathbf{B}_o) + \frac{\mathbf{V}}{c} (\mathbf{J}_o \times \mathbf{B}) \qquad \text{(III-8)}$$

using the relation

$$\nabla \cdot (p\mathbf{V}) = p\nabla \cdot \mathbf{V} + \mathbf{V} \cdot \nabla p$$

Eq. (III-8) can be written in the form

$$\frac{\partial}{\partial t}\left[\frac{\rho_o \mathbf{V} \cdot \mathbf{V}}{2}\right] = -\nabla \cdot (p\mathbf{V}) + p\nabla \cdot \mathbf{V} + \frac{\mathbf{V}}{c} \cdot (\mathbf{J} \times \mathbf{B}_o)$$

$$+ \frac{\mathbf{V}}{c}(\mathbf{J}_o \times \mathbf{B}). \qquad \text{(III-9)}$$

Next, scalar multiple Eq. (III-6) by $\frac{c}{4\pi}\mathbf{E}$, Eq. (III.5) by $\frac{c\mathbf{B}}{4\pi}$ to obtain

$$\frac{c}{4\pi} \mathbf{E} \cdot \nabla \times \mathbf{B} - \frac{c}{4\pi}\mathbf{B} \cdot \nabla \times \mathbf{E} = \frac{\partial}{\partial t}\left[\frac{\mathbf{B} \cdot \mathbf{B}}{8\pi}\right] + \mathbf{J} \cdot \mathbf{E}.$$

This can be written as

$$\frac{\partial}{\partial t}\left[\frac{\mathbf{B} \cdot \mathbf{B}}{8\pi}\right] + \nabla \cdot \left[\frac{c\mathbf{E} \times \mathbf{B}}{4\pi}\right] + \mathbf{J} \cdot \mathbf{E} = 0 \qquad \text{(III-10)}$$

Substituting for $\mathbf{E}$ from Eq. (III-3) into the term $\mathbf{J} \cdot \mathbf{E}$ Eq. (III-10) becomes

$$\frac{\partial}{\partial t}\left[\frac{\mathbf{B} \cdot \mathbf{B}}{8\pi}\right] + \nabla \cdot \left[\frac{c\mathbf{E} \times \mathbf{B}}{4\pi}\right] = -\mathbf{V} \cdot (\mathbf{J} \times \mathbf{B}_o) \qquad \text{(III-11)}$$

where we have made use of the vector identity $\mathbf{J} \cdot (\mathbf{V} \times \mathbf{B}_o) = \mathbf{V} \cdot (\mathbf{B}_o \times \mathbf{J})$. Adding Eqs. (III-9) and (III-11), we obtain

$$\frac{\partial}{\partial t}\left[\frac{1}{2}\rho_o \mathbf{V} \cdot \mathbf{V} + \frac{B^2}{8\pi}\right] + \nabla \cdot \left[\frac{c\mathbf{E} \times \mathbf{B}}{4\pi} + p\mathbf{V}\right]$$

$$= p\nabla \cdot \mathbf{V} + \mathbf{V} \cdot (\mathbf{J}_o \times \mathbf{B}). \qquad \text{(III-12)}$$

Now consider the term $p\nabla \cdot \mathbf{V}$. With the aid of Eqs. (III-2) and (III-4), we find

$$\nabla \cdot \mathbf{V} = -\left\{\frac{1}{\gamma p_o}\frac{\partial p}{\partial t} + \frac{1}{\gamma p_o}(\mathbf{V} \cdot \nabla)p_o\right\}. \qquad \text{(III-13)}$$

Substituting Eq. (III-13) into (III-12) we have

$$\frac{\partial}{\partial t}\left[\frac{1}{2}\rho_o\mathbf{V} \cdot \mathbf{V} + \frac{\mathbf{B} \cdot \mathbf{B}}{8\pi} + \frac{1}{2}\frac{p^2}{\gamma p_o}\right] + \nabla \cdot \left[\frac{c}{4\pi}\mathbf{E} \times \mathbf{B} + p\mathbf{V}\right]$$

$$= \mathbf{V} \cdot (\mathbf{J}_o \times B) - \frac{p}{\gamma p_o}(\mathbf{V} \cdot \nabla)p_o. \qquad \text{(III-14)}$$

In order to obtain the final form of the conservation equation we must introduce the linear displacement vector $\boldsymbol{\xi}$ defined by

$$\frac{\partial \boldsymbol{\xi}}{\partial t} = \mathbf{V}. \qquad \text{(III-15)}$$

Notice that this is not the actual displacement, which is defined by $\frac{d\xi^{ac}}{dt} = \left[\frac{\partial}{\partial t} + V \cdot \nabla\right] \xi^{ac} = V$. However since ξ and bold V are both small, the two are the same in linear theory. This enables us to integrate Eq. (III-5) in time to obtain **B** in terms of ξ thus

$$B = \nabla \times (\xi \times B_o) \qquad \text{(III-16)}$$

where we have, of course, made use of Eq. (III-3). We can also obtain p in terms of ξ by integrating Eq. (III-13) in time to obtain

$$p = -(\xi \cdot \nabla) p_o - \gamma p_o (\nabla \cdot \xi). \qquad \text{(III-17)}$$

Now consider the two terms on the right hand side of Eq. (III-14). First,

$$V \cdot (J_o \times B) = -J_o \cdot \left[\frac{\partial \xi}{\partial t} \times B\right].$$

Since **B** depends linearly on ξ and J_o is independent of time we may write

$$J_o \cdot \left[\frac{\partial \xi}{\partial t} \times B\right] = \frac{\partial}{\partial t}\left[\frac{1}{2} J_o \cdot [\xi \times B]\right]$$

so that

$$V \cdot (J_o \times B) = \frac{\partial}{\partial t}\left[\frac{1}{2} J_o \cdot [\xi \times B]\right].$$

Next, consider the second term

$$\frac{p}{\gamma p_o}(V \cdot \nabla) p_o = \frac{p}{\gamma p_o}\frac{\partial \xi}{\partial t} \cdot \nabla p_o.$$

Since p depends linearly on ξ through Eq. (III-17) and p_o is independent of time we may again write

$$\frac{p}{\gamma p_o}(V \cdot \nabla) p_o = \frac{\partial}{\partial t}\left[\frac{1}{2}\frac{p}{\gamma p_o} \xi \cdot \nabla p_o\right]. \qquad \text{(III 19)}$$

We may now substitute (III-18) and (III-19) into Eq. (III-14) to obtain

$$\frac{\partial}{\partial t}\left[\frac{1}{2}\rho_o V \cdot V + \frac{B \cdot B}{8\pi} + \frac{1}{2}\frac{p^2}{\gamma p_o} + \frac{1}{2}J_o \cdot (\xi \times B)\right.$$

$$\left. + \frac{1}{2}\frac{p}{\gamma p_o}(\xi \cdot \nabla)p_o\right] + \nabla \cdot \left[\frac{c}{4\pi}E \times B + pV\right] = 0. \quad \text{(III-20)}$$

This is the required energy conservation relation and is the generalized Poynting theorem for linearized ideal MHD. The term inside the first

set of parentheses is the total energy density of the perturbation per unit volume and the second set of parentheses represents the energy flow out of this unit volume. The energy flow terms will be easily recognized as the Poynting vector and the convection of the plasma internal energy by the perturbed plasma motion.

Equation (III-20) is not yet in its most familiar form. Let us combine the pair of terms containing the perturbed pressure

$$\frac{1}{2}\frac{p^2}{\gamma p_o} + \frac{1}{2}\frac{p}{\gamma p_o}\boldsymbol{\xi}\cdot\nabla p_o = \frac{1}{2}\frac{p}{\gamma p_o}(p + \boldsymbol{\xi}\cdot\nabla p_o)$$

Substituting for p from Eq. (III-17) we obtain

$$\frac{1}{2}\frac{p^2}{\gamma p_o} + \frac{1}{2}\frac{p}{\gamma p_o}\boldsymbol{\xi}\cdot\nabla p_o = \frac{1}{2}(\boldsymbol{\xi}\cdot\nabla)p_o + \frac{1}{2}\gamma p_o(\nabla\cdot\boldsymbol{\xi})^2 \quad \text{(III-21)}$$

Substituting (III-21) into (III-20) we obtain the final form for the small signal energy conservation equation

$$\frac{\partial}{\partial t}\left\{\frac{1}{2}\rho_o\mathbf{V}\cdot\mathbf{V} + \frac{\mathbf{B}\cdot\mathbf{B}}{8\pi} + \frac{1}{2}\mathbf{J}_o\cdot(\boldsymbol{\xi}\times\mathbf{B}) + \frac{1}{2}\gamma p_o(\nabla\cdot\boldsymbol{\xi})^2\right.$$
$$\left. + \frac{1}{2}(\boldsymbol{\xi}\cdot\nabla p_o)\nabla\cdot\boldsymbol{\xi}\right\} + \nabla\cdot\left[\frac{c}{4\pi}\mathbf{E}\times\mathbf{B} + p\mathbf{V}\right] = 0 \quad \text{(III-22)}$$

We now integrate this equation over the whole plasma to obtain

$$\frac{\partial}{\partial t}\int\left\{\frac{1}{2}\rho_o\mathbf{V}\cdot\mathbf{V} + \frac{\mathbf{B}\cdot\mathbf{B}}{8\pi} + \frac{1}{2}\mathbf{J}_o\cdot(\boldsymbol{\xi}\times\mathbf{B}) + \frac{1}{2}\gamma p_o(\nabla\cdot\boldsymbol{\xi})^2\right.$$
$$\left. + \frac{1}{2}(\boldsymbol{\xi}\cdot\nabla p_o)\nabla\cdot\boldsymbol{\xi}\right\}d^3\mathbf{r} + \oint\left\{\frac{c}{4n}\mathbf{E}\times\mathbf{B} + p\mathbf{V}\right\}\cdot d\mathbf{S} = 0$$

where $d\mathbf{S}\equiv\hat{n}S$ and S is the surface bounding the volume of integration. Since we have assumed a perfectly conducting, rigid wall in contact with the plasma the boundary conditions ensure that the surface integral vanishes. We are then left with the result that

$$\frac{\partial}{\partial t}(K + \delta W) = 0 \quad \text{(III-23)}$$

where $K \equiv \int\frac{1}{2}\rho_o\mathbf{V}\cdot\mathbf{V}\,dV$ is the total kintic energy of the plasma δW is immediately identified as the potential energy of the perturbation and is given by

$$\delta W = \frac{1}{2} \int \left\{ \frac{\mathbf{B} \cdot \mathbf{B}}{4\pi} + \mathbf{J}_o \cdot (\boldsymbol{\xi} \times \mathbf{B}) + \gamma p_o (\nabla \cdot \boldsymbol{\xi})^2 \right. \qquad \text{(III-24)}$$

$$\left. + (\boldsymbol{\xi} \cdot \nabla) p_o \nabla \cdot \boldsymbol{\xi} \right\} d^3 r.$$

The form of δW given in Eq. (III-24) is in agreement with that first given by Bernstein et al.

We can already draw a number of conclusions at this stage of the analysis with the aid of the equation for the conservation of energy. Since we assumed zero equilibrium flow, it follows that K is always positive definite. Taking as a definition of instability an unbounded increase of K in time, it is clear from Eq. (III-23) that if $\delta W > 0$ the system must be absolutely stable. It is also clear from Eq. (III-23) that in order to have instability $\delta W < 0$ such that $|\delta W|$ grows in time so as to balance exactly the increase in K. To complete the proof of the Energy Principle we now follow the argument given by Laval et al. in order to show that if a $\boldsymbol{\xi}$ and $\mathbf{B} = \nabla \times \boldsymbol{\xi} \times \mathbf{B}_o$ can be found such that $\delta W < 0$ the plasma is unstable.

Equation (III-1) can be written as

$$\rho_o \frac{\partial^2 \boldsymbol{\xi}}{\partial t^2} = \mathbf{F}(\boldsymbol{\xi}) \qquad \text{(III-25)}$$

where

$$\mathbf{F}(\boldsymbol{\xi}) = \nabla (\boldsymbol{\xi} \cdot \nabla p_o) + \nabla (\gamma p_o \nabla \cdot \boldsymbol{\xi}) + \frac{1}{c} \mathbf{J}_o \times \mathbf{B} \qquad \text{(III-26)}$$

$$+ \frac{1}{c} (\nabla \times \mathbf{B}) \times \mathbf{B}_o.$$

The next step is to define the virial $I(\boldsymbol{\xi})$ defined by

$$I(\boldsymbol{\xi}) = \frac{1}{2} \int \rho_o \boldsymbol{\xi} \cdot \boldsymbol{\xi} \; d^3 \mathbf{r}. \qquad \text{(III-27)}$$

Differentiating I twice with respect to time

$$\ddot{I} = \int (\rho_o \dot{\boldsymbol{\xi}} \cdot \dot{\boldsymbol{\xi}} + \rho_o \boldsymbol{\xi} \cdot \ddot{\boldsymbol{\xi}}) d^3 \mathbf{r}. \qquad \text{(III-28)}$$

The first term on the right hand size is twice the kinetic energy and the second term can be written in terms of $F(\boldsymbol{\xi})$ with the aid of Eq. (III-25) giving

$$\ddot{I} = 2K + \int \boldsymbol{\xi} \cdot \mathbf{F}(\boldsymbol{\xi}) d^3 r. \qquad \text{(III-29)}$$

With the aid of some vector algebra it is straightforward to show that

$$\int \boldsymbol{\xi} \cdot \mathbf{F}(\boldsymbol{\xi})\,d^3\mathbf{r} = -2\delta W \qquad \text{(III-30)}$$

where δW is the potential energy defined in Eq. (III-24). The final form of Eq. (III-29) can now be written

$$\ddot{I} = 2K - 2\delta W. \qquad \text{(III-31)}$$

We now assume that there is some displacement η such that $\delta W(\eta) < 0$. We write this explicitly as

$$\delta W(\eta) = -\omega^2 I(\eta) \qquad \text{(III-32)}$$

where $\omega > 0$ and $I(\eta)$, the virial, is, of course, positive definite. The displacement vector $\boldsymbol{\xi}$, which is a solution of Eq. (III-25), is now chosen to satisfy the following initial conditions

$$\boldsymbol{\xi} = \eta, \quad \dot{\boldsymbol{\xi}} = \omega\eta. \qquad \text{(III-33)}$$

Since the total energy Q of the perturbation must be a constant we may calculate its value with the aid of Eq. (III-23). Thus

$$Q = K + \delta W$$
$$= I(\dot{\boldsymbol{\xi}}) + \delta W(\boldsymbol{\xi})$$
$$= \omega^2 I(\eta) + \delta W(\eta)$$

so that $Q = 0$. Using this result we may now eliminate δW from Eq. (III-31) to obtain

$$\ddot{I} = 4K. \qquad \text{(III-34)}$$

We now relate $\ddot{I}$ to I and $\dot{I}$. By the definition of $\dot{I}$,

$$\dot{I}^2 = \left\{\int \rho_o \boldsymbol{\xi} \cdot \dot{\boldsymbol{\xi}}\,d^3\mathbf{r}\right\}^2 = \left\{\int (\rho_o^{1/2}\boldsymbol{\xi}) \cdot (\rho_o^{1/2}\dot{\boldsymbol{\xi}})\,d^3\mathbf{r}\right\}^2.$$

Using Schwarz's inequality, we may write

$$\left\{\int (\rho_o^{1/2}\boldsymbol{\xi}) \cdot (\rho_o^{1/2}\dot{\boldsymbol{\xi}})\,d^3\mathbf{r}\right\}^2 \leqslant \left\{\int \rho_o \boldsymbol{\xi} \cdot \boldsymbol{\xi}\,d^3\mathbf{r}\right\}\left\{\int \rho_o \dot{\boldsymbol{\xi}} \cdot \dot{\boldsymbol{\xi}}\,d^3\mathbf{r}\right\}$$

and therefore $\dot{I}^2 \leqslant 4IK$. With the aid of Eq. (III-34) the inequality becomes

$$\dot{I}^2 < I\ddot{I}. \qquad \text{(III-35)}$$

Now $\dot{I} > 0$ at $t = 0$. Integrating Eq. (III-34) we obtain $\dot{I} = \dot{I}_o + \int_0^t 4K\,dt$ where the subscript zero indicates that the quantity has been evaluated at $t = 0$. We may evaluate the constant I_o with the aid of the initial conditions. Thus

$$\dot{I}_o = \int \rho_o \xi \cdot \dot{\xi} \, d^3\mathbf{r} = \omega \int \rho_o \boldsymbol{\eta} \cdot \boldsymbol{\eta} \, d^3\mathbf{r} = 2\omega \, I_o > 0. \qquad \text{(III-36)}$$

We therefore find that $\dot{I}_o > 0$ so that $\dot{I} > 0$ for $t > 0$. Since $I\dot{I} > 0$ for $t > 0$ we do not alter the sense of inequality (III-35) by dividing throughout by this quantity, so that

$$\frac{\dot{I}}{I} < \frac{\ddot{I}}{\dot{I}}. \qquad \text{(III-37)}$$

Integrating for $t > 0$ we have

$$\ln \frac{I}{I_o} \leqslant \ln \frac{\dot{I}}{\dot{I}_o}. \qquad \text{(III-38)}$$

Using inequality (III-36) we obtain

$$\frac{\dot{I}}{I} > 2\omega. \qquad \text{(III-39)}$$

Again integrating for $t > 0$ we have

$$I \geqslant I_o \exp 2\omega t. \qquad \text{(III-40)}$$

Thus I grows at least as fast as $\exp(2\omega t)$ and since I is quadratic in ξ it follows that the displacement ξ will grow at least as fast as $\exp(\omega t)$. This then completes the proof that for any displacement which makes $\delta W < 0$ instability will always occur.

Actually there are stronger proofs that are possible from the energy principle. One can also prove (although it is more difficult) that if the equation of motion is written as Eq. III-25 then the operator $\underline{F}$ is Hermitian. This means that the eigenfunction ξ is in fact that function which minimizes δW. From this fact, one can draw a number of interesting conclusions. For instance increasing the specific heat ratio γ always makes the plasma more stable. To see this, consider minimizing δW for the case that $\gamma = \gamma_2$. To do so, take for instance a set of possible eigenfunction and minimize δW by varying a set of parameters. Now consider the case of $\gamma = \gamma_1 < \gamma_2$. Using the eigenfunction which minimized δW for $\gamma = \gamma_2$, we can show that the δW for $\gamma = \gamma_1$ is smaller because the only term dependent on γ in δW is $\gamma p_0 (J\nabla \cdot \xi)^2$. Thus increasing γ is a stabilizing effect. Therefore we generally consider the case of $\gamma = \infty$, the incompressible limit. If the plasma is unstable in this limit, it will be unstable at any smaller value of γ also. In the incompressible limit, the perturbed pressure is finite, so according to Eq. III-17, $\gamma\nabla \cdot \xi$ is finite, but $\nabla \cdot \xi$ and $\gamma(\nabla \cdot \xi)^2 \rightarrow$ approach zero.

Let us conclude this chapter by considering, in very simple terms, the physical significance of the potential energy δW defined by equation (III-24). We have seen that the plasma will be stable when $\delta W > 0$. The expression for δW then shows that the energy required to perturb the equilibrium magnetic field (either field line bending or compression) is positive definite and therefore stabilizing. The third term is the expression for δW is also positive definite so that incompressible perturbations may be expected to be the most unstable. The second and fourth terms in the expression for δW are the potentially destabilizing ones. The driving mechanism in the first of these being due to the equilibrium current and is the second to the equilibrium pressure gradient. To apply the energy principle one can do one of two things. First of all, one can try various different displacements and see whether the δW can be made negative. For instance, the well known stability requirement that $\int \frac{dl}{B}$ must decrease as the pressure decreases can be derived by examining the effect of a displacement which interchanges two adjacent flux tubes. Of course this only gives a necessary condition for stability; there may be other untried displacements which give instability. Alternatively one could attempt to minimize δW by applying the variational principle. If the minimum value of $\delta W > 0$, for a displacement normalized in some way, for instance $\int |\xi|^2 d^3 r = 1$, then the plasma is stable, and visa versa. Thus one can derive a necessary and sufficient condition for stability. This is the approach used by Newcomb in analyzing the stability of a diffuse linear pinch. For an illustration of the Energy Principle in a number of simple situations the interested reader may refer to the review of hydromagnetic stability by Kadomtsev.

There are other forms of the energy principle which are also useful. These can be derived from Eq. (III-24) with some algebraic manipulations. There is one other form which we will consider

$$\delta W = \frac{1}{2} \int d^3 r \left\{ \frac{1}{4\pi} |\mathbf{B}_\perp|^2 + 4\pi \left| \frac{\mathbf{B}_{||}}{4\pi} - \frac{\mathbf{B}_o \, \xi \cdot \nabla p_o}{B_o^2} \right|^2 \right.$$

$$\left. + \gamma p_o |\nabla \cdot \xi|^2 + \frac{\mathbf{J}_o \cdot \mathbf{B}_o}{|\mathbf{B}_o|^2} \mathbf{B}_o \times \xi \cdot \mathbf{B} - 2\xi \cdot \nabla p_o \xi \cdot \kappa \right\} \qquad \text{(III-41)}$$

where $\perp$ and $||$ denote components of $\mathbf{B}$ perpendicular to $\mathbf{B}_o$, and κ is the normal field line curvature $\kappa = \hat{\mathbf{B}} \cdot \nabla \hat{\mathbf{B}}$ where $\hat{\mathbf{B}}$ is a normal vector parallel to B_o.

Equation (III-41) is particularly illuminating because each of the five terms in it are from identifiable causes. The first three, which are always positive are the energies associated with the shear alfven, magnetosonic and sound waves. The fourth is the energy driving kink modes and is created by the presence of the plasma current. It can be negative. The fifth term is energy driving interchange modes. It can be negative if the curvature is in the same direction as the pressure gradient. If the pressure gradient is antiparallel to κ, the last term in Eq. (III-41) is always positive. However any angle between ∇p_0 and κ other than $180°$ is potentially unstable. To see this note that if the direction of ξ is along the angle bisector of ∇p_0 and κ, this term is positive.

This last, interchange mode term has exactly the same form as the energy from the displacement of an incompressible plasma in a gravitational field. This gravitational energy released is minus the force dotted into the displacement, or

$$W_G = -\rho \mathbf{g} \cdot \boldsymbol{\xi} \qquad (\text{III-42})$$

where g is the gravitational acceleration. The quantity ρ may be determined in terms of ξ by integrating the mass conservation equation for incompressible plasma,

$$\rho = -\xi \cdot \nabla \rho_0$$

so that

$$W_G = \mathbf{g} \cdot \boldsymbol{\xi} \, \xi \cdot \nabla \rho_0. \qquad (\text{III-43})$$

Thus the gravitational energy is negative if $\mathbf{g}$ and ∇p_0 point in opposite directions. Equation (III-43) for the gravitational energy has exactly the same form as the last term in Eq. (III-41a) if ∇p_0 is replaced with $\nabla \rho_0$ and -2κ is replaced with $\mathbf{g}$. This leads to the conclusion that pressure driven modes can be investigated, qualitatively at least, by studying the much simpler problem of gravity driven modes.

Probably the most cited paper on the energy principle is:

An Energy Principle for Hydromagnetic Stability Problems, I.B. Bernstein, E.A. Frieman, M.D. Kruskal, and R.M. Kulsrud, Proc. Roy. Soc. (London), **A224**, 17 (1958).

Other references are:

Stability of Plasmas Confined by Magnetic Fields, M.N. Rosenbluth and C.L. Longmire, Ann. Phys., **1**, 120 (1957).

Hydromagnetic Equilibria and Stability, J. Greene and J. Johnson in Advances in Theoretical Physics, 1965 (Academic Press, N.Y.).

Sufficient Conditions for Hydrodynamic Stability in a Diffuse Linear Pinch, H.P. Furth, Phys. Fluids, **3**, 977 (1960).

Necessity of the Energy Principles for Magnetostatic Stability, G. Laval, C. Mercier, and R. Pellat, Nuclear Fusion, **5**, 156 (1965).

Some New Variational Principles of Hydromagnetic Equilibria, H. Grad, Phys. Fluids, **5**, 510 (1962).

A new form of the energy principle including kinetic effects is given in:

Variational Principle for low Frequency Stability of Collisionless Plasms, T.M. Antonsen, B. Lane and J.J. Ramos, Phys. Fluids, **24**, 1465 (1981).

Electrostatic Modification of Variational Principles for Anisotropic Plasmas, T.M. Antonsen and Y.C. Lee, Phys. Fluids, **25**, 132 (1982).

A Generalized Kinetic Energy Principle, J.W. Van Dam, M.N. Rosenbluth and Y.C. Lee, Phys. Fluids, **25**, 1349 (1982).

Chapter IV

FREE SURFACE MODES IN A
CYLINDRICAL PLASMA

A very important class of unstable modes occur when the plasma does not extend up to the wall of the metal chamber. In this case, the plasma has a free surface which can undergo unstable helical (or kink) perturbations. In this chapter, we work out the properties of two types of free surface modes, first where the current is carried on the surface, and second where the volume current density J_{oz} is uniform inside the plasma. The former instability is responsible for the famous Kruskal-Shafranov requirement for gross stability $q(a) > 1$ where a is the radius of the free surface. The later instability is responsible for unstable displacements of the free surface wherever $q(a) < \frac{m}{n}$ where m and n are integers. Also $q(r) = rB_z/RB_\theta$, R being the major radius.

We begin with the former type of instability, that is where all the current flows along the free surface. Let us now define our model more precisely. We shall consider an infinitely long cylindrical plasma whose axis is taken to be the z direction. The plasma extends radially from $r = 0$ to $r = a$, beyond which there is a vacuum. For simplicity, assume the vacuum region extends to infinity and that the plasma surface current flows only in the z direction. Then, Maxwell's current equation gives the following boundary conditions for equilibrium magnetic fields

$$(B_{oz}^V - B_{oz})^p|_{r=a} = 0 \qquad (\text{IV-1})$$

$$(B_{o\theta}^V - B_{o\theta}^p)|_{r=a} = \frac{4\pi J_{zo}}{c} \qquad (\text{IV-2})$$

where J_{oz} is the axial surface current and the superscripts V and p denote vacuum and plasma fields respectively. Assuming that $B_r = \frac{\partial}{\partial\theta} = \frac{\partial}{\partial z} = 0$ for the equilibrium we obtain the following equilibrium fields from Maxwell's equations

51

$$B_{oz}^p = B_{oz}^V \equiv B_{oz} \qquad\qquad \text{(IV-3)}$$

$$B_{o\theta}^p = 0 \qquad\qquad \text{(IV-4)}$$

$$B_{o\theta}^V = \frac{4\pi a\, J_{oz}}{rc}. \qquad\qquad \text{(IV-5)}$$

Since the magnetic field is uniform in the plasma, then so must be the pressure. Then equilibrium pressure balance at the plasma vacuum interface is given by

$$p_o(a) = \frac{2\pi J_{oz}^2}{c^2}. \qquad\qquad \text{(IV-6)}$$

Let us now consider perturbations to this equilibrium, which are assumed to vary as $f(r)\ \exp(i\,(kz + m\theta) + \gamma t)$. (To make the transition from cylindrical to toroidal systems, we simply quantize k by taking $k = \dfrac{-n}{R}$ where R is the major radius of the torus.) Here and henceforth we take $B_{\theta o}$, B_{zo}, J_{zo} and $m > 0$. However the sign of k is arbitrary. In general there is only instability for $k < 0$. The linearized equation of motion of the plasma can be written

$$\gamma \rho_o\, \mathbf{V} = \frac{1}{4\pi}\, (\mathbf{B}_o \cdot \nabla)\mathbf{B} - \nabla \tilde{P} \qquad\qquad \text{(IV-7)}$$

where ρ_o is assumed to be uniform and $\tilde{P} = P + \dfrac{\mathbf{B}_o \cdot \mathbf{B}}{4\pi}$. In obtaining (IV-7) we have used the fact that $\mathbf{B}_o$ is uniform in the plasma. Taking the divergence of Eq. (IV-7) we obtain

$$\gamma \rho_o(\nabla \cdot \mathbf{V}) = \frac{ikB_{oz}}{4\pi}\, \nabla \cdot \mathbf{B} - \nabla^2 \tilde{P}. \qquad\qquad \text{(IV-8)}$$

We now assume that the motion is incompressible $\nabla \cdot \mathbf{V} = \nabla \cdot \mathbf{B} = 0$ so Eq. (IV-8) reduces to the simple form

$$\nabla^2 \tilde{P} = 0. \qquad\qquad \text{(IV-9)}$$

The solution of this equation which is bounded at the origin is

$$\tilde{P} = A\ I_m(kr) \qquad\qquad \text{(IV-10)}$$

where A is an arbitrary constant and I_m is the modified Bessel function of the first kind.

We now also need to relate the perturbed velocity $\mathbf{V}$ to $\tilde{P}$. The equation for the perturbed magnetic field is

$$\gamma \mathbf{B} = \nabla \times (\mathbf{V} \times \mathbf{B}_o). \qquad\qquad \text{(IV-11)}$$

Using once more the incompressibility condition for B_o and Maxwell's equations, the above equation reduces to

$$\gamma \mathbf{B} = (\mathbf{B}_o \cdot \nabla) \mathbf{V}. \qquad \text{(IV-12)}$$

Substituting (IV-12) into Eq. (IV-7) we obtain $\mathbf{V}$ in terms of $\tilde{P}$

$$\mathbf{V} = \frac{\gamma \nabla \tilde{P}}{\rho_o (\gamma^2 + k^2 V_A^2)} \qquad \text{(IV-13)}$$

where $V_A^2 = B_{oz}^2/4\pi\rho_o$.

The perturbed field in the vacuum must satisfy $\nabla \cdot B^V = \nabla \times B^V = 0$. Putting $B^V = \nabla\psi$, then ψ satisfies the equation

$$\nabla^2\psi = 0$$

so

$$\psi = C\, K_m(kr) \qquad \text{(IV-14)}$$

where C is a constant and K_m is an arbitrary Bessel function of the second kind. The final step in the analysis is to match the perturbation in the plasma and vacuum. Since we have two arbitrary constants in Eqs. (IV-10 and 14), two boundary conditions are necessary.

The first condition comes from the need to have pressure balance across the interface. Integrating the radial component of the equation of motion across the boundary, we have

$$P + P_o + \frac{(\mathbf{B}_o^p + \mathbf{B}^p) \cdot (\mathbf{B}_o^p + \mathbf{B}^p)}{8\pi} = \frac{(\mathbf{B}_o^V + \mathbf{B}^V) \cdot (\mathbf{B}_o^V + \mathbf{B}^V)}{8\pi}. \qquad \text{(IV-15)}$$

Since we require the linearized form of Eq. (IV-15), we note that the perturbed quantities are to be evaluated at the unperturbed boundary and the equilibrium quantities, at the perturbed boundary, which has been displaced a distance $\xi = \mathbf{V}/\gamma$. We then find the following condition for pressure balance

$$\tilde{P}(a) = \left\{ \frac{\mathbf{B}_o^V \cdot \mathbf{B}^V}{4\pi} + \xi_r \frac{B_{o\theta}}{4\pi} \frac{\partial}{\partial r} B_{o\theta} \right\}_{r=a} \qquad \text{(IV-16)}$$

where we have used the equilibrium pressure balance condition and the fact that equilibrium pressure was assumed uniform.

The second boundary condition results from the following observation. Since the plasma is assumed to have infinite conductivity the electric field moving with the plasma must be identically zero, or

$$\mathbf{E}^p + \frac{\mathbf{V}}{c} \times \mathbf{B}_o^p = 0.$$

If we now match fields in this frame; then, because the tangential component of electric field must be continuous in any reference frame, we must have

$$\mathbf{E}_t^V + (\frac{\mathbf{V}}{c} \times B_o^V)_t = 0$$

where the subscript t denotes the tangential component. This is the second boundary condition. However it can be put in a more convenient form by adding the normal components of each term to the equation and taking the curl. With the aid of Maxwell's equations and a little vector algebra we obtain

$$\hat{\mathbf{n}} \cdot \frac{\partial \mathbf{B}^V}{\partial t} = \hat{\mathbf{n}} \cdot \nabla \times (\mathbf{V} \times \mathbf{B}_o^V)$$

where $\hat{n}$ is the normal to the plasma surface. Since $\frac{\partial \mathbf{B}}{\partial t}$ and $\mathbf{V}$ are zero in equilibrium, we can replace n by the unperturbed normal i_r. Using $\mathbf{V} = \frac{\partial}{\partial t} \xi$, we obtain

$$B_{ir}^V = \left\{ \nabla \times (\xi \times \mathbf{B}_o^V) \right\}_{r-a}. \tag{IV-17}$$

The final form of the second boundary condition now becomes

$$B_{ir}^V = i \left(\frac{m}{r} B_{o\theta}^V + k B_{oz}^V \right) \xi_r. \tag{IV-18}$$

We are now in a position to obtain the dispersion relation for the problem. Equations (IV-10) and (IV-13) give the result

$$\xi_r = - \frac{A k I_m'(kr)}{\rho_o(\gamma^2 + k^2 V_A^2)} \tag{IV-19}$$

where prime denotes derivative with respect to argument. Calculating the perturbed field in the vacuum from Eq. (IV-4) and substituting Eq. (IV-10 and 19) into Eq. (IV-16), we find

$$\left\{ I_m(ka) - \frac{k I_m'(ka)}{\rho_o(\gamma^2 + k^2 V_A^2)} \frac{B_{o\theta}(a)}{4\pi} \frac{\partial B_{o\theta}}{\partial r}\bigg|_{r-a} \right\} A$$

$$- \frac{i\mathbf{k} \cdot \mathbf{B}_o^V(a)}{4\pi} K_m(ka) C = 0 \tag{VI-20}$$

where $\mathbf{k} \cdot \mathbf{B}_o^V = \dfrac{m B_{o\theta}^V}{r} + k B_{oz}^V$. Then substituting from Eq. (IV-19) and the expression for B_r^V (from Eq. (IV-14)) into Eq. (IV-18) results

$$\frac{i \mathbf{k} \cdot \mathbf{B}_o^V(a) I_m'(ka)}{\rho_o(\gamma^2 + k^2 V_A^2)} A + k K'(ka) C = 0. \qquad \text{(IV-21)}$$

The condition for nontrivial solution of Eqs. (IV-20 and 21) gives the required dispersion relation

$$\gamma^2 = - k^2 V_A^2 + \frac{k \cdot B_o^V(a))^2}{r \pi \rho_o} \frac{I_m'(ka) K_m(ka)}{I_m(ka) K_m'(ka)}$$

$$+ \frac{k (B_{o\theta}^V(a))^2}{4 \pi \rho_o a} \frac{I_m'(ka)}{I_m(ka)}. \qquad \text{(IV-22)}$$

Since $Im'(ka)/Im(ka) > 0$ and $Km'(ka)/Km(ka) < 0$ it is only the third term on the right hand side of Eq. (IV-22) which is destabilizing. In order to see when this term is larger than the other stabilizing terms, consider long wavelength $ka << 1$. Using the fact that

$$I_m'(ka)/I_m(ka) \approx m/ka$$

and

$$K_m'(ka)/K_m(ka) \approx - m/ka,$$

Eq. (IV-22) can be written

$$-\gamma^2 = - k^2 V_A^2 - \frac{\left[k B_{oz} + \dfrac{m}{a} B_{o\theta}^V(a) \right]^2}{4 \pi \rho_o} + \frac{m (B_{o\theta}^V(a))^2}{4 \pi a^2 \rho_o}. \qquad \text{(IV-23)}$$

The most unstable k value is

$$k = - \frac{m}{a} \frac{B_{o\theta}^V(a)}{2 B_{oz}}. \qquad \text{(IV-24)}$$

Substituting this into Eq. (IV-23), we find that the maximum growth rate is

$$\gamma_{MAX}^2 = \frac{m}{a^2} \frac{B_{o\theta}^2(a)}{4 \pi \rho_o} \left[- \frac{m}{2} + 1 \right] \qquad \text{(IV-25)}$$

so that the $m = 1$ surface mode is unstable, $m = 0$ and 2 are marginally stable and all higher m (long wavelength) are stable.

It is also of interest to write Eq. (IV-23) in the form

$$\gamma^2 = -\frac{2k^2 B_{oz}^2}{4\pi\rho_o} - 2\frac{m}{a}\frac{B_{oz} B_{o\theta}^V (a) k}{4\pi\rho_o} \qquad (\text{IV-26})$$

$$-\frac{m}{a^2}\frac{(B_{o\theta}^V (a))^2}{4\pi\rho_o}(m-1).$$

Since only the $m = 1$ mode is unstable we can immediately obtain the range of unstable wavelengths

$$0 < |k| < \frac{1}{a}\frac{B_{o\theta}^V (a)}{B_{oz}}.$$

For a torus, the minimum value of k is $\frac{1}{R}$, so a toroidal plasma is stable if

$$q(a) = \frac{aB_{oz}}{RB_{o\theta}^V (a)} > 1. \qquad (\text{IV-27})$$

Equation (IV-27) is the celebrated Kruskal-Shafranov limit on the $q(a)$ value of a toroidal discharge.

Let us see what this condition implies for a tokamak plasma. The plasma and metal wall are shown in Fig. (IV-1). The value of q at the plasma edge must be greater than unity. In the vacuum region between $r = a$ and $r = b$, $B_{o\theta}^V (r)$ decreases as $\frac{1}{r}$ so that in the vacuum region $q(r)$ increases as r^2, so that $q(b) > \left(\frac{b}{a}\right)^2$. Thus, depending on where the plasma boundary is, the value of q at the limiter must be somewhat greater than unity in order for the plasma to be stable to gross kink modes. This lower limit on $q(a)$ implies an upper limit on current for stable configuration. Using $B_{oV}^\theta (r = b) = \frac{I}{5r}$ where I is in amps, B in Gauss and r in cm, the maximum current is

$$I < \frac{5a^2 B_{oz}}{R}. \qquad (\text{IV-28})$$

We now turn to a discussion of the other type of free surface mode, that where the plasma has a uniform current up to $r = a$ and vacuum outside. Also we assume $B_{oz} \gg B_o$, $R \gg a$, and treat the case where B_{oz} is constant. In equilibrium

$$0 = \frac{dP_o}{dr} - \frac{1}{c} J_{zo} B_{\theta o} \qquad (\text{IV-29})$$
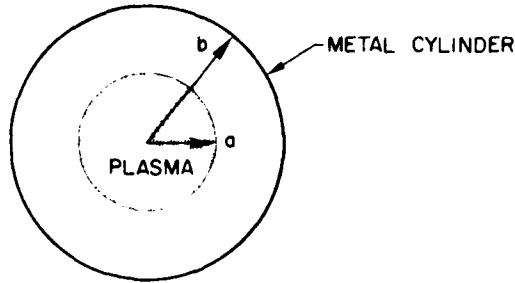
Fig. IV-1 — A cylindrical or toroidal plasma
surrounded by a conducting wall

so the pressure profile is parabolic and vanishes at $r = a$, since $B_{\theta o} \sim r$ and J_{zo} is constant. We will see that this plasma can be unstable for all m instead of just $m = 1$ as was the case for a surface current.

Before calculating the growth rate, let us show physically why this is so. As discussed in the last chapter, a perturbation is most likely to be unstable if $\mathbf{k} \cdot \mathbf{B}_o = 0$ since in this case, it does not couple to stable shear Alfven waves. Right at the surface of the plasma, $\mathbf{k} \cdot \mathbf{B}_o = kB_{oz} + \dfrac{mB_{o\theta}^V (a)}{r}$, and as we just saw, the plasma is unstable when this nearly vanishes. However if $\mathbf{k} \cdot \mathbf{B}_o$ is zero at the plasma edge, it is equal to kB_{zo} inside the plasma. Thus, modes which are flute like (that is perpendicular to $\mathbf{B}_o$) on the plasma surface are not flute like in the plasma interior, and there is a strong coupling to shear Alfven waves there. This is the explanation of the stabilizing first term on the right hand side of Eq. (IV-22). Clearly the thing responsible for this stabilizing effect is the fact that the magnetic field abruptly changes direction as one crosses the plasma boundary. However, if the axial current density is uniform, the poloidal magnetic field is a continuous function of radius so that a perturbation which is flute like on the plasma surface will be flute like in the plasma interior also. Thus we expect the plasma with uniform current to be *less* stable than the plasma with a surface current.

We now proceed to derive the properties of unstable modes in a plasma with a uniform axial current with $B_{zo} \gg B_{\theta o}$ and $\dfrac{r}{R} \ll 1$, the so called tokamak ordering. Since the axial field is very large, one expects that the most unstable motion could not compress this field, implying two dimensional motion in the $r\theta$ plane, i.e., $V_z = B_z = 0$. We will assume this to be true for now and prove it a posteriori. The perturbed magnetic field in the vacuum is unchanged and is given by Eq. (IV-14).

The problem now is to derive an equation for the magnetic field inside the plasma. To do so, take the z component of the curl of the equation of motion. Using the fact the $\mathbf{J}_o$ is constant in the plasma, $\nabla \cdot \mathbf{J} = \nabla \cdot \mathbf{B} = 0$ and B_{oz} is constant, we find

$$\frac{\gamma}{r}\left(\frac{\partial}{\partial r}r\rho_o V_\theta - im\ V_r\right) = \frac{1}{c}\nabla \times (\mathbf{J}\times\mathbf{B}_o + \mathbf{J}_o\times\mathbf{B})\Big|_z \quad \text{(IV-30)}$$

$$= \frac{1}{c}ik\ B_o\ \mathbf{J}_z.$$

Relating J_z to B_z via Maxwells current equation, and using the fact that

$$\nabla\cdot\mathbf{B} = \frac{1}{r}\frac{\partial}{\partial r}r\ B_r + \frac{im}{r}B_\theta = \nabla\cdot V$$

$$= \frac{1}{r}\frac{\partial}{\partial r}rV_r + \frac{im}{r}V_\theta = 0 \quad \text{(IV-31)}$$

we find

$$-\gamma\left(\frac{1}{r}\frac{\partial}{\partial r}r\rho_o\frac{1}{im}\frac{\partial}{\partial r}(rV_r) + \frac{\rho_o im}{r}\right) \quad \text{(IV-32)}$$

$$= \frac{iF}{4\pi}\left(-\frac{1}{r}\frac{\partial}{\partial r}\frac{1}{im}\frac{\partial}{\partial r}(rB_r) - \frac{im}{r}B_r\right)$$

where

$$F = \frac{mB_{\theta o}}{r} - \frac{nB_{zo}}{R} \equiv \mathbf{k}\cdot\mathbf{B}_o. \quad \text{(IV-33)}$$

Note that for the case of constant current density $B_{o\theta}$ is proportional to r so F is constant. The other relation between B_r and V_r comes from Eq. (IV-11). Taking the radial component, we find

$$V_r = \frac{\gamma B_r}{iF}. \quad \text{(IV-34)}$$

Inserting Eq. (IV-34) into Eq. (IV-32), we find the single equation for B_r

$$\left(\frac{4\pi\rho_o\gamma^2 + F^2}{mr}\right)\left[\frac{d}{dr}r\frac{d}{dr}r\ B_r - m^2B_r\right] = 0 \quad \text{(IV-35)}$$

where we have assumed ρ_o constant.

The factor outside is simply the dispersion relation for shear Alfven waves and cannot vanish for positive γ. The quantity in the square brackets must then be zero. Trying a solution $B_r = r^n$ and insisting that B_r be well behaved at the origin, we find

$$B_r = A \, r^{m-1}. \tag{IV-36}$$

Of course A above and C from Eq. (IV-14) can be simply related by requiring that B_r be continuous across the free surface. (Since the unperturbed fields are continuous across the free surface, all we need to is say that the perturbed radial field is continuous across the unperturbed free surface.) Using Eqs. (IV-31 and 34) we also find

$$V_\theta = i \, V_r$$

$$B_\theta = i \, B_r. \tag{IV-37}$$

The dispersion relation then follows from assuming pressure balance across the free surface, or

$$\left. \frac{B_{zo}B_z + B_{\theta 0}B_\theta}{4\pi} \right|_v = \left. \frac{B_{\theta 0}B_\theta}{4\pi} + P \right|_p \tag{IV-38}$$

where we have made use of the fact that $B_Z^V = 0$ and that $|B_o|^2$ is continuous. In the vacuum, one can immediately derive

$$B_z = i \, \frac{K_m(ka)}{K_m'(ka)} \, B_r \qquad \text{(a)}$$

$$B_\theta = \frac{im}{r} \, \frac{K_m(ka)}{kK_m'(ka)} \qquad \text{(b)}. \tag{IV-39}$$

It remains only to calculate p in terms of B_r. This comes from the θ component of the momentum equation

$$\rho_o \gamma V_\theta = - \frac{im}{r} p + \frac{1}{c} [-J_r B_{oz} + B_r J_{oz}]. \tag{IV-40}$$

Now

$$J_r = \left. \frac{c}{4\pi} \, \nabla \times \mathbf{B} \right|_r = \frac{ck}{4\pi} \, B_r \tag{IV-41}$$

where we have used Eqs. (IV-37b and 36). Thus by using Eq. (IV-41) and the expression for V_θ in terms of B_r from Eqs. (IV-37a and 34), Eq. (IV-40) relates p to B_r. Plugging into Eq. (IV-38), we find the dispersion relation

$$\gamma^2 = \left\{ \frac{F}{\rho_o} \frac{B_{\theta o}}{2\pi r} - \frac{F^2}{2\pi \rho_o} \left(1 - \frac{mK_m(ka)}{kr \, K_m'(ka)} \right) \right\}. \tag{IV-42}$$

Since $K_m/K_m' < 0$, the term proportional to F^2 is stabilizing. The term proportional to F can be destabilizing if $F > 0$, or $\dfrac{mB_{\theta o}}{r} > \dfrac{nB_{zo}}{R}$. Clearly the plasma can be unstable in the limit of $F \rightarrow 0$. Since B_{oz} is constant and $B_{o\theta}$ decreases as a function of r in the vacuum region, the

plasma can be unstable if the singular surface, $F = 0$, falls just outside the plasma. If the singular surface falls inside the plasma $F(r = a) < 0$ so the plasma is stable. Also if the singular surface falls too far outside the plasma, the second term on the right of in Eq. (IV-42) dominates the first and the plasma again is stable.

Let us see what this means for the current buildup of a tokamak plasma. As the current rises the value of $q(a)$ decreases. Thus

$$F = \frac{mB_{\theta o}}{r} - \frac{nB_{zo}}{R} = \frac{mB_{\theta o}}{r}\left[1 - \frac{nq(a)}{m}\right]$$

starts out negative but as the current builds up it decreases. When the current reaches the value at which

$$q(a) = \frac{m}{n} \qquad\qquad\qquad\qquad \text{(IV-43)}$$

F changes from negative to positive and the plasma is unstable to modes with values of m/n given in Eq. (IV-43). This instability occurs where Minov oscillations occur in tokamak plasmas, and it may be that the two are related. However as the current increases, the mode becomes stable because of the stabilizing effect of the second term on the right of Eq. (IV-42). Thus only certain values of total current give instability. In building up tokamak current, the idea then is to program its rise so that it passes through the unstable values very quickly. However the maximum plasma current will always still be limited by Eq. (IV-28).

We close by determining the conditions under which the motion is two dimensional, as we have assumed. The velocity in the z direction comes from the z component of the momentum equation. Assuming $B_z = 0$, we find

$$\gamma\rho_o V_z = ikp.$$

Inserting for p from Eq. (IV-40) and taking the maximum value of γ, from Eq. (IV-42), we find

$$\frac{V_z}{V_r} \sim \frac{kr}{2} \qquad\qquad\qquad\qquad \text{(IV-44)}$$

so the motion basically is two dimensional as long as $\frac{kr}{2} \ll 1$.

Two early references on stability of sharp boundary cylindrical plasmas are:

Hydromagnetic Instability in a Stellarator, M.D. Kruskal, J.L. Johnson, M.B. Gottlieb, and L.M. Goldman, Phys. Fluids, 1, 421 (1958).

The Influence of an Axial Magnetic Field on the Stability of a Constricted Gas Discharge, R.J. Taylor, Proc. Roy. Soc. (London), B70, 1049 (1957).

More recent work on stability of a cylindrical plasma with more realistic current profile is:

Hydromagnetic Stability of a Current Carrying Pinch in a Strong Longitudinal Field, V.D. Shafranov, Sov. Phys. Technical Phys., 15, 175 (1970).

Chapter V

GRAVITATIONAL (g) MODES IN
SLAB GEOMERTY

This chapter discusses modes driven by a gravitational force in slab geometry. If gravity is present, the MHD equations for a perfectly conducting, incompressible fluid are

$$\frac{\partial \rho}{\partial t} + \mathbf{V} \cdot \nabla \rho = 0 \qquad \text{(V-1)}$$

$$\rho \frac{\partial x}{\partial t} + \rho \, \mathbf{V} \cdot \nabla \mathbf{V} = -\nabla p + \frac{\mathbf{J}}{c} \times \mathbf{B} - \rho F \qquad \text{(V-2)}$$

$$\frac{\partial \mathbf{B}}{\partial t} = -\nabla \times \mathbf{V} \times \mathbf{B} \qquad \text{(V-3)}$$

$$\nabla \times \mathbf{B} = \frac{4\pi}{c} \mathbf{J} \qquad \text{(V-4)}$$

$$\nabla \cdot \mathbf{V} = 0. \qquad \text{(V-5)}$$

All variation is assumed to be in the x direction.

At this point we will digress briefly to consider what the significance of g is. First, and most obvious, g could correspond to a real physical forces. For instance in the ionosphere, the earths gravity does give rise to Raleigh Taylor instability. Also g could correspond to an inertial force. Consider for instance θ pinch implosion shown in Fig. V-1. Clearly, as the theta pinch implodes, the plasma accelerates inward. In analyzing the local MHD stability of the imploding pinch, one could work in the reference frame in which the fluid is locally at rest. The inward acceleration is then described by an outward inertial force. Also if a θ pinch plasma is rotating with angular velocity Ω, one could analyze its stability by working in a rotating reference frame. Then the inertial force is the sum of the centrifugal, $\Omega^2 r \mathbf{i}_r$ and coriolis, $2\boldsymbol{\omega} \times \mathbf{V}$. The former is outward and acts like a gravitational force. In fact, θ pinches are observed to disrupt due to the onset of rotational instabilities. In ideal MHD, any rotation produces instability. However with finite Larmon radius and other effects included, the rotation speed must be greater than the ion diamagnetic speed $V_o = cT(d \, n/dx)/eBn$ in order for the plasma to be unstable.
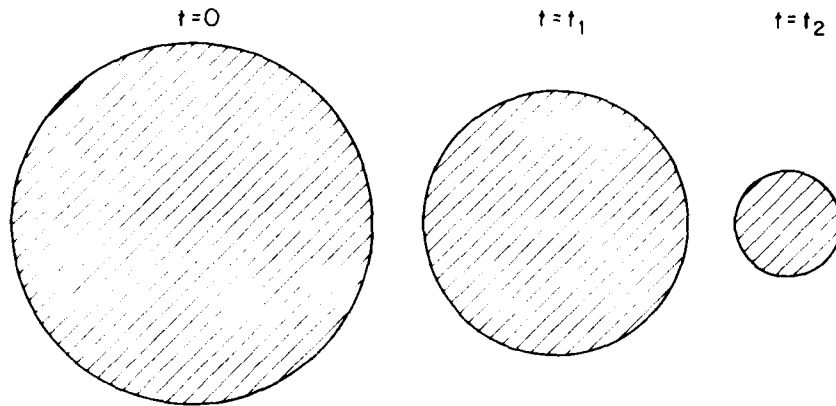
Fig. V-1 — Schematic of stages in the implosion of a θ pinch

Less obvious, certainly less precise, but probably more useful, the acceleration g can be used to model complicated geometric aspects of the magnetic field as was seen in Chapter III where the energy driving a pressure driven mode was compared with the energy driving a gravitational mode. There it was shown that if the radius of the field line points in the direction of increasing pressure, δW can be made negative so the plasma can be unstable. On the other hand, if the radius points away from the plasma, the plasma is stable. Stable and unstable configurations are shown in Figs. (V-2 and 3). The energy was then compared with the energy of a plasma in a gravitational field. For our purposes now, we simply model $\mathbf{g} = \mathbf{i}_R \ V_T^2/R$. where $\mathbf{i}_R$ is a unit vector pointing outward along the radius of curvature of the field line, and V_T is a typical thermal velocity (that is V_T is roughly either the ion thermal velocity or else $(M_e/M_i)^{1/2}$ times the electron thermal velocity).
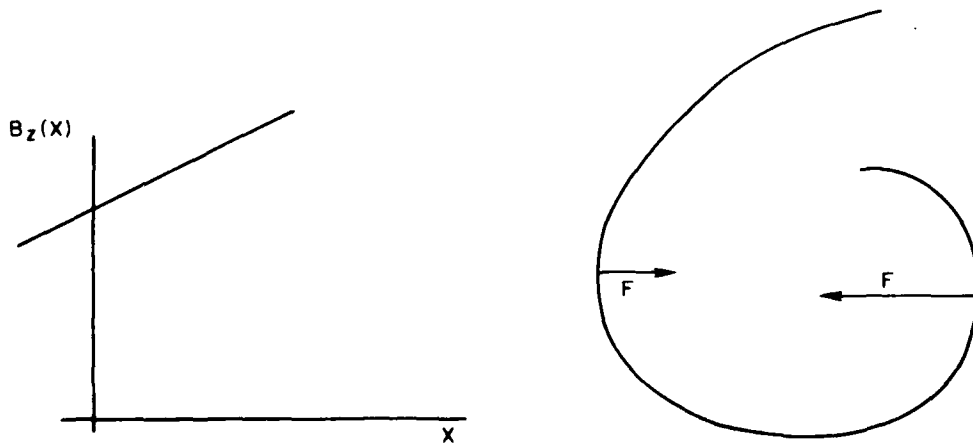

Fig. V-2 — Schematic showing how a gradient in B exerts an average
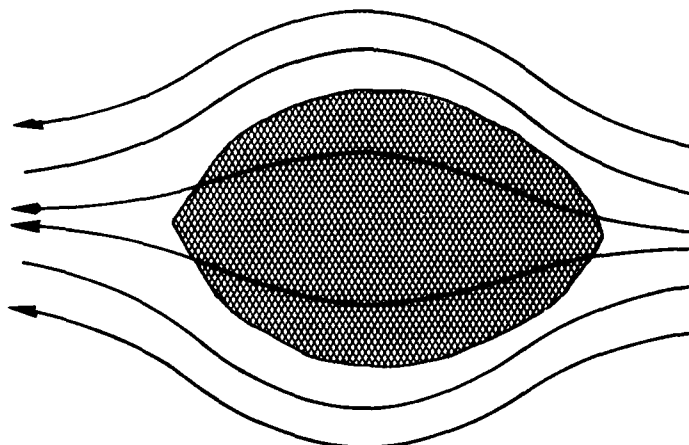force on a charged particle as it traverses its larmor orbit

Fig. V-3 — Picture of a plasma confined in a magnetic
configuration with unfavorable curvature

After this digression on the significance of gravity, we return to a
discussion of g modes as described by the linearized version of Eq. (V-
1). All variation is taken to be in the x direction and g also points in
the x direction. The magnetic field points in the z direction and is
taken to be uniform. The basic g mode is then very easily derived.
Assuming a time dependence exp γt for perturbed quantities the linear-
ized versions of Eqs. (1-5) are

$$\gamma \rho + V_X \frac{\partial \rho_o}{\partial X} = 0 \qquad \text{(a)}$$

$$\gamma \rho_o \mathbf{V} = -\nabla p - \frac{1}{4\pi} \{\nabla (\mathbf{B}_o \cdot \mathbf{B}) - (\mathbf{B}_o \cdot \nabla) \mathbf{B}$$

$$- (\mathbf{B} \cdot \nabla) \mathbf{B}_o + \rho g \mathbf{i}_x\} \qquad \text{(b)}$$

$$\nabla \cdot \mathbf{V} = 0 \qquad \text{(c)} \qquad \text{(V-6)}$$

where now perturbed quantities have no subscript and unperturbed
quantities have a subscript zero. Let us further simplify by assuming a
spatial dependence of exp $i\, ky$ (that is no x or z dependence) for per-
turbed quantities. Then inserting from Eq. (V-6a) into Eq. (V-6b) and
taking the x component, we find

$$\gamma^2 = - g \; \frac{\frac{\partial \rho_o}{\partial x}}{\rho_o}. \qquad \text{(V-7)}$$

Thus, if g and $\partial \rho o/\partial x$ have opposite signs the plasma is unstable.
Notice also that this instability is extremely violent. Assuming that L_n
$$\equiv \left| \rho_o \, \frac{\partial \rho_o}{\partial x} \right|^{-1}$$ is of order of R which is of order of the size of the

plasma R, the growth time is of order R/V_T. That is the time for the mode to grow is roughly the time for the plasma to escape the system from the micro trap traveling at the thermal velocity; in other words, there is no confinement of the plasma at all!

Clearly, in order to confine the plasma, some means must be devised to stabilize these modes. One possibility is to utilize a cusp (like minimum B) type configuration like that shown in Fig. (V-4) so the $g\, \partial\rho_o/\partial x > 0$ either everywhere or else so averaged over a flux tube. This is generally called magnetic well stabilization and it is usually used to stabilize mirror machines. To reverse the sign of $g\rho'$ involves fields with fairly complex structure and we will not emphasize magnetic well stabilization here.
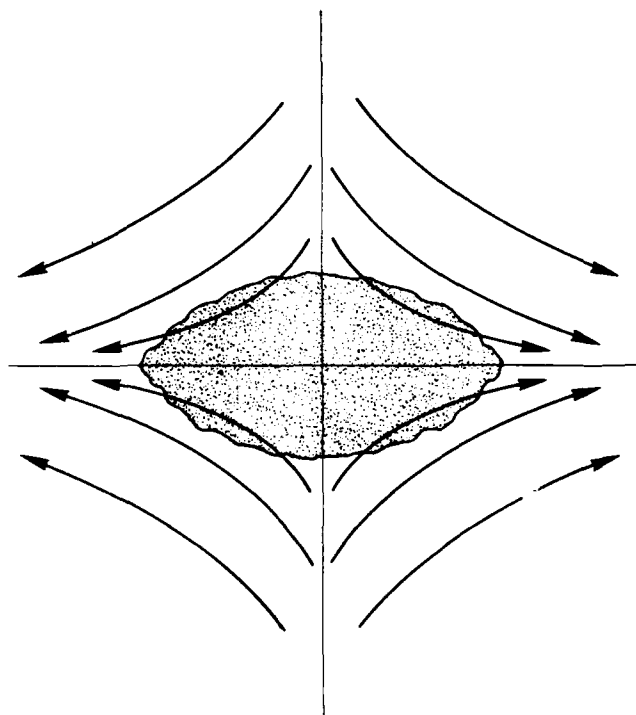
Fig. V-4 — Picture of a plasma confined in a magnetic
configuration with favorable curvature

One other way to stabilize these modes is by magnetic shear. A discussion of this stabilization mechanism will occupy the remainder of this chapter. In order to set the stage for our calculation of shear stabilization of g modes, we begin by considering these modes when $k_z \neq 0$. If perturbed quantities vary as $\exp i\,(k_y y + k_z z)$, then the x component of Eq. (V-6b) becomes

$$\gamma \rho_o V_x = \frac{ik_z B_o}{4\pi} B_x - \frac{V_x}{\gamma} g \frac{\partial \rho_o}{\partial x}. \qquad (V\text{-}8)$$

To obtain B_x in terms of V_x, one uses the x component of Eq. (V-1c). Inserting for B_x in terms of V_x, we find that the dispersion relations is

$$\gamma^2 = - \frac{k_z^2 B_o^2}{4\pi \rho_o} - \frac{g}{\rho_o} \frac{\partial \rho_o}{\partial x}. \qquad (V\text{-}9)$$

Notice that for $k_z^{\ 2} V_A^2 > g \frac{\partial \rho_o}{\partial x}/\rho_o$ the mode is stable. Clearly as k_z increases, the unstable g mode attempts to couple to a stable shear Alfven mode. Postulating a k_z sufficiently large that γ^2 given by Eq. (V-9) is negative is , or course, not equivalent to stabilizing the system. In an unsheared field, the plasma is still free to pick a parallel wave number equal to zero. The basic idea behind shear stabilization is to remove this freedom by imposing an equilibrium variation on the **direction** of $\mathbf{B}_o$.

Let us now say that

$$\mathbf{B}_o(x) = B_o \left(\mathbf{i}_z + \frac{x}{L_s} \mathbf{i}y\right) \qquad (V\text{-}10)$$

where we imagine $x \ll L_s$. Since this additional x variation is imposed on the system, all perturbed quantities have the functional form

$$f(x) \exp(i\,ky + \gamma t)$$

where we have set $k_z = 0$. Notice however that the variation in a perturbed quantity is no longer perpendicular to $\mathbf{B}_o$. Indeed

$$(\mathbf{B}_o \cdot \nabla) f(x) \exp(i\,ky + \gamma t)$$

$$= i\,k\,B_o \frac{x}{L_s} f(x) \exp(i\,ky + \gamma t). \qquad (V\text{-}11)$$

Thus the presence of shear forces any perturbed quantity to vary parallel to $\mathbf{B}_o$ as long as $x \neq 0$. This forced variation parallel to $\mathbf{B}$ will tend to couple to shear Alfven modes and stabilize the plasma. We now proceed to calculate just how much shear is needed for stabilization.

In a sheared field, the equation for the perturbed x velocity is slightly, but not much more difficult to specify. Because of the inherent x dependence of $\mathbf{B}_o$, one can no longer assume that perturbations are independent of x. To begin, take the curl of the perturbed momentum equation

$$\gamma \nabla \times \rho_o \mathbf{V} = \frac{1}{4\pi\gamma} \nabla \times \{ (\mathbf{B}_o \cdot \nabla) (\nabla \times \mathbf{V} \times \mathbf{B}_o)$$

$$+ [(\nabla \times \mathbf{V} \times \mathbf{B}_o) \cdot \nabla] \mathbf{B}_o \}$$

$$- g \nabla \times \left\{ \frac{1}{\gamma} V_x \frac{\partial \rho_o}{\partial x} \mathbf{i}_x \right\} \qquad\qquad (\text{V-12})$$

where we have made use of the fact that $\mathbf{B} = \dfrac{1}{\gamma} \nabla \times \mathbf{V} \times \mathbf{B}_o$. Now

consider the x component of Eq. (V-12). Recalling that $\dfrac{\partial}{\partial z} = 0$, a

short calculation gives the result

$$\left[\rho_o \gamma^2 + \frac{B_o^2}{4\pi} \left(\frac{x}{L_s} \right)^2 k^2 \right] V_z = 0. \qquad (\text{V-13})$$

Equation (V-13) above dictates that either $V_z = 0$, or else the quantity in the square brackets vanishes. The latter case implies shear (stable) Alfven waves at each point x. Since these are not unstable, we assume the former, i.e.,

$$V_z = 0. \qquad\qquad (\text{V-14})$$

From the fact that $V_z = 0$, one can show easily from Eq. (V-1d) that also

$$B_z = 0. \qquad\qquad (\text{V-15})$$

Thus the perturbation is two dimensional in the $x - y$ plane. The incompressibility condition then relates V_x to V_y and B_x to B_y

$$\frac{\partial B_x}{\partial x} - ikB_y = \frac{\partial V_x}{\partial x} + ikV_y = 0. \qquad (\text{V-16})$$

Then, taking the z component of Eq. (V-12) and making use of Eq. (V-16) above, we find the following simple equation for V_x:

$$\frac{\partial}{\partial x} \left[\rho\gamma^2 + k^2 \left(\frac{x}{L_s} \right)^2 \frac{B_o^2}{4\pi} \right] \frac{\partial V_x}{\partial x} - k^2 \left[\rho_o\gamma^2 + k^2 \left(\frac{x}{L_s} \right)^2 \right.$$

$$\left. \frac{B_o^2}{4\pi} + g \frac{\partial \rho_o}{\partial x} \right] V_x = 0. \qquad (\text{V-17})$$

Notice that the term in the parentheses on the right hand side is simply the local dispersion relation, Eq. (V-9), if one assumes $k_z^2 = k^2 (x/L_s)^2$. However, this is no longer the dispersion relation in the sheared system. For instance if Eq. (V-9) were initially satisfied,

disturbances near $x = 0$ would grow while those far from $x = 0$ would not. A strong x dependence would then be induced by the local growth, and eventually the first term of Eq. (V-17) would also be important. The problem then is to find the eigenfunctions and eigenvalues of Eq. (V-17). In the limit of $x \to \infty$, the equation approximately reduced to

$$\frac{\partial^2 V_x}{\partial x^2} \approx k^2 V_x \qquad\qquad\text{(V-18)}$$

with solution

$$V_x \approx \exp \pm kx \qquad\qquad\text{(V-19)}$$

clearly the proper boundary condition is that V_x approaches zero at both $x = \pm \infty$. Since

$$\rho_o \gamma^2 + k^2 \left|\frac{x}{L_s}\right|^2 \frac{B_o^2}{4\pi} \equiv Q > 0 \qquad\qquad\text{(V-20)}$$

as long as $\gamma^2 > 0$, Eq. (V17) has no singular points on the real x axis. Therefore one could easily solve this equation numerically for the eigenvalues γ^2.

We now see what insights may be obtained analytically. One can immediately show that if $g \dfrac{\partial \rho_o}{\partial x} > 0$, no solution with $\gamma^2 > 0$ can satisfy the boundary conditions. To do so, note that $\rho \gamma^2 + k^2 \left|\dfrac{x}{L_s}\right|^2$ $\dfrac{B_o^2}{4\pi} \equiv Q(x)$ is then greater than zero. Assume that at $x \to -\infty$, V_x is well behaved and also that $V_x > 0$. Then

$$\frac{\partial V_x}{\partial x} = \frac{1}{Q(x)} \int_{-\infty}^{x} k^2 \, G(x') \, V_x \, dx' \qquad\qquad\text{(V-21)}$$

where

$$G(x) = Q(x) + g \frac{\partial \rho_o}{\partial x} \qquad\qquad\text{(V-22)}$$

which is greater than zero since $g \partial \rho_o / \partial x$ is. Therefore $\dfrac{\partial V_x}{\partial x} > 0$ for all x so that the solution for V_x is a monotonically increasing function of x. Hence, it does not satisfy the proper boundary condition as $x \to +\infty$. Clearly, in order for V_x to satisfy the proper boundary condition as $x \to +\infty$, there must be some region of x where $G(x) < 0$.

Now let us examine how an unstable eigenfunction can be constructed. If $g \, \partial \rho_o / \partial x$ is greater than zero the function is monotonically increasing, and as $x \rightarrow \infty$ it diverges as $\exp kx$. Now depending upon the sign of $G(x)$ (Eq. V-22), the equation has two fundamentally different types of behavior. If $G(x) > 0$, the solution for V_x is a monotonically increasing function of x as we have just discussed. On the other hand, if $G(x) < 0$, the solution for V_x is generally oscillatory in x. The local wave number is given very roughly by $k(-G(x)/Q(x))^{1/2}$. If $G(x)$ changes sign as x varies, we will denote the regions of $G(x) > 0$ as monotonic regions and the regions where $G(x) < 0$ as oscillatory regions. We have just shown that the regions $x \rightarrow \pm \infty$ are monotonic.

If $g \, \partial \rho_o / \partial x < 0$, there is an oscillatory region specified by

$$x_{os}^2 < \frac{4\pi L_s^2}{k^2 B_o^2} \left[- g \, \frac{\partial \rho_o}{\partial x} - \gamma^2 \right]. \qquad (V\text{-}23)$$

Since the wave number of the oscillation in the oscillatory region is given roughly by $k(-G(x)/Q(x))^{1/2}$, it is clear that increasing γ increases the wavelength in the oscillatory region. Let us imagine that a $\gamma \equiv \gamma_-$ can be found such that $V_x = 0$ at $x = x_{os}$. Then, since $x > x_{os}$ is a monotonic region, the solution for V_x for $x > x_o$ diverges toward minus infinity as $x \rightarrow +\infty$ as shown in curve A in Fig. (V-5). As γ is increased, the wavelength in the oscillatory region increases so that the solution for V_x will not curve downward as much here. Thus for a sufficiently large $\gamma \equiv \gamma_+$, the solution for V_x diverges toward positive infinity as $x \rightarrow \infty$ as shown in Fig. (V-5) curve B. Clearly, there exists some $\gamma \equiv \gamma_o$ where $\gamma_- < \gamma_o < \gamma_+$ for which the solution to Eq. (V-17) asymptotes to zero for through positive values of V_+ as shown in Fig. (V-5) curve C. This then is an unstable eigenfunction with eigenvalue γ_o.

One can now deduce the following criterion for determining whether Eq. (V-17) has unstable eigenvalues. First select a γ and assume V_x is well behaved as $x \rightarrow -\infty$ and integrate the equation towards plus infinity. If there is one zero of V_x before the solution diverges at $x = +\infty$, then there will be one eigenfunction with a growth rate larger than this assumed γ. Similarly, if there are two zeros of V_x before the solution diverges for $x \rightarrow +\infty$, there are two eigenfunctions with growth rate larger than the assumed γ; and so on. Clearly, the more nodes to the eigenfunction, the smaller is γ. The equation, and this technique of determining a sequence of eigenvalues is closely related to the Sturm-Louisville equation described in Morse
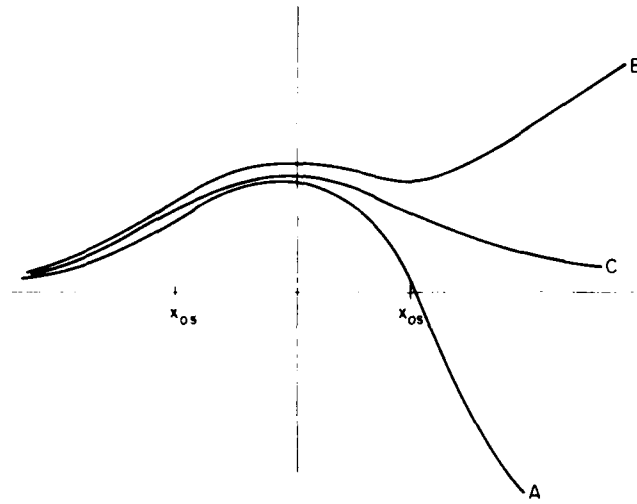
Fig. V-5 — Diagram of how to form the eigenfunction
and calculate the eigenvalue (γ) of Eq. (V-17)

and Feshback, Methods of Theoretical Physics, Vol. I, Chapter VI or
almost any advanced calculus textbook.

Now it is possible to derive very quickly an approximate criterion
for shear stabilization of g modes. In order that $V_x(x_{os}) \approx 0$, it is
necessary that there be roughly one half a wavelength of oscillation in
the oscillatory region. Approximating the wave number of this oscilla-
tion by the square root maximum value of $k^2 G$ divided by the square
root of the maximum value of Q, we find instability if

$$\frac{2}{\pi} x_{os} k\left[-g \frac{\partial \rho_o}{\partial x}/k^2 \frac{x_{os}^2}{L_s^2} \frac{B_o^2}{4\pi}\right]^{1/2}$$

$$= \frac{2}{\pi}\left[-g \frac{\partial \rho_o}{\partial x}\right]^{1/2} \frac{L_s\sqrt{4\pi}}{B_o} > 1. \qquad (V\text{-}24)$$

For L_s much larger than specified by Eq. V-24, the mode grows with
growth rate given roughly by Eq. (V-7). Equation (V-25) is then a
condition for shear stabilization of g modes which have scale length of
order x_{os}. One might think that by localizing the mode very close to
$x = 0$, and by greatly decreasing the growth rate, the wavelength of the
oscillation for V_x in the oscillatory region could be significantly reduced
so that unstable eigenfunctions could be constructed even if Eq. (V-25)
is violated. This possibility will now be examined.

For very small x and γ, the equation for V_x can be written as

$$\frac{\partial}{\partial x}\left[\rho\gamma^2 + k^2\left(\frac{x}{L_s}\right)^2\frac{B_o^2}{4\pi}\right]\frac{\partial V_x}{\partial x} - k^2 g\frac{\partial \rho_o}{\partial x}V_x = 0. \qquad \text{(V-25)}$$

In Eq. (V-25) above, the γ^2 is retained in the left hand term so that the solution is non singular at $x = 0$. However clearly, for

$$x^2 \gg L_s^2\frac{4\pi \rho\gamma^2}{k^2 B_o^2} \qquad \text{(V-26)}$$

the γ term in Eq. (V-25) is not important. Therefore, we can neglect γ, but restrict ourselves to the range of x denoted by Eq. (V-26). By considering the limit $x \to 0$ we can see how the solution behaves for small x and γ, and particularly, we can see whether the solution has a node. (Naturally one cannot connect the solution at positive x to the solution at negative x in this way, because to do so one must also have the solution in the region where Eq. (V-26) is violated.)

If $\gamma = 0$ in Eq. (V25), one can solve in the neighborhood of $x = 0$ by assuming $V_x = x^n$. In this case one can solve for n and find

$$n = -1/2 \pm (1 + 4\psi)^{1/2} \qquad \text{(V-28)}$$

where

$$\psi = 4\pi g\frac{\partial \rho_o}{\partial x}L_s^2/B_o^2. \qquad \text{(V-29)}$$

The condition for the exponent n to be complex is simply

$$\psi < -1/4. \qquad \text{(V-30)}$$

However if n is complex, $n = n_r + in_i$ the behavior of V_x is oscillatory, and the wavelength of oscillation approaches zero as $x \to 0$, that is

$$V_r = x^{n_r}\exp{(in_i \ln x)}.$$

Thus there are an infinity of nodes of V_r in the limit of $x \to 0$. This means that there are an infinity of unstable eigenfunctions. The growth rates of these eigenfunctions approach zero as the number of nodes increase. The condition for such localized unstable modes is given by Eq. (V-30), while the approximate condition for stabilizing modes spread over x_{os} is given by Eq. (V-24). Notice that the equations have roughly the same form except that about three times as much shear (that is L_s smaller by one third) is required to stabilize modes localized over x_{os} than is required to stabilize modes localized right at the position $x = 0$. A condition for the occurrence of unstable modes is then given by Eq. (V-30).

To summarize, pressure driven modes are analogous to gravitationally driven modes in an incompressible plasma. These can be stabilized in one of two ways, first by magnetic well, or by contouring the field so that the radius points away from the plasma; and secondly by shear stabilization.

The Raleigh Taylor Instability has been known for a long time and is discussed in such textbooks as:

   Hydrodynamic and Hydromagnetic Stability, S. Chandrasekhar, (Oxford: Clarendon Press, 1961).

Experimental Stabilization of a Mirror Plasma by removing the destabilizing field line curvature is reported on in:

   Y.T. Baborodov, M.S. Ioffe, V.M. Petrov, and R.L. Sobolev, J. Nuclear Energy, Pt.C, **5**, 409 (1963).

Rotation and rotation driven instabilities have long been observed in θ pinch plasmas. An early reference is:

   Fission of a Hot Plasma, N. Rostoker and A.C. Kolb, Phys. Rev., **124**, 965 (1961).

A more recent reference is:

   Field Reversal Experiments, R.K. Linford, W.T. Armstrong, D.A. Platts, and E.G. Sherwood, Plasma Physics and Controlled Thermonuclear Fusion Research, 1978, Vol. 2, p. 447 (IAEA Vienna, 1979).

A gravitational instability in an accelerated fluid is studied in:

   Raleigh Taylor Instabilities of a Collapsing Cylindrical Shell in a Magnetic Field, E.G. Harris, Phys. Fluids, **5**, 1057 (1962).

Finite Larmor Radius effects can be an important stabilizing effect on g modes, as studied in:

   Finite Larmor Radius Stabilization of "Weakly" Unstable Confined Plasmas, M.N. Rosenbluth, N.A. Krall, and N. Rostoker, Nucl. Fusion, 1962, Supplement, Part 1, 143

Recent theoretical studies of Rotational Instabilities can be found in:

Rotational Instabilities in a Theta Pinch, J.P. Freidberg and L.D. Pearlstein. Phys. Fluids, **21**, 1207 (1978).

Finite Larmor Radius Equations in an Arbitrary Near Theta Pinch Geometry, Phys. Fluids, **21**, 1218 (1978).

Chapter VI

RESISTIVE g MODES

In the previous chapter it was shown how shear in the magnetic field produces a stabilizing effect on instabilities driven by a gravitational field g. In this chapter we shall again consider the stability of a plasma supported against gravity by a sheared magnetic field, but with the addition of a further physical effect, namely resistivity. For the g modes of the previous chapter the ideal MHD model was used for which the field and fluid are frozen together. However, for the instabilities to be described in this chapter, the magnetic field and fluid become decoupled due to the presence of resistivity. It will be found that the instability is again localized at the resonant surface where $\mathbf{k} \cdot \mathbf{B} = 0$, which, as we will see, is the only place where a small resistivity can introduce a significant amount of decoupling in motion of field and fluid. The net effect of resistivity on g modes is to nullify the stabilizing effect of magnetic shear. An ideal g mode which was stabilized by the presence of magnetic shear will be shown to be unstable—albeit at a reduced growth rate—when the presence of a small amount of resistivity is allowed for. Thus, if the effect of magnetic shear is compared to a dyke, then resistivity turns the dyke into a leaky one.

Let us now describe the resistive g mode in slab geometry, as in Chapter V. The magnetic field is taken as

$$\mathbf{B}_o(x) = B_o \, \mathbf{i}_z + B_o \, \frac{x}{L_s} \, \mathbf{i}_y$$

where B_o is a constant. The gravitational acceleration is in the x direction and all equilibrium fluid quantities also vary in only the x direction. We treat the plasma as an incompressible, weakly resistive fluid. The linearized equations of motion are

$$\rho_o \, \frac{\partial \mathbf{V}}{\partial t} = -\nabla p + \frac{1}{4\pi} \, (\nabla \times \mathbf{B}) \times \mathbf{B}_o$$
$$+ \frac{1}{4\pi} \, (\nabla \times \mathbf{B}_o) \times \mathbf{B} + \rho \mathbf{g} \qquad \text{(VI-1)}$$

$$\frac{\partial \mathbf{B}}{\partial t} = \nabla \times (\mathbf{V} \times \mathbf{B}_o) - \frac{\eta c^2}{4\pi} \nabla \times (\nabla \times B) \qquad \text{(VI-2)}$$

$$\frac{\partial \rho}{\partial t} = -(\mathbf{V} \cdot \nabla) \rho_o \qquad \text{(VI-3)}$$

$$\nabla \cdot \mathbf{V} = 0. \qquad \text{(VI-4)}$$

Note that we have treated the resistivity as uniform in obtaining Eq. (VI-2). Since the equilibrium varies only with x, we know that the eigenfunction of all perturbed quantities varies as $f(x) \exp(\gamma t + iky)$. We then find the V_z and B_z decouple from the remaining variable so that only the x and y components of Eqs. (VI-1 and 2) are required. (The variables V_z and B_z describe the properties of shear Alfven waves so that we may put both of these variables equal to zero when analyzing the behavior of linearly independent resistive g modes.)

The x and y components of Eq. (VI-1 and 2) give

$$\gamma \rho_o V_x = -\frac{\partial p}{\partial x} + \frac{B_o}{4\pi} \frac{x}{L_s} ik B_x$$

$$- \frac{1}{4\pi} \frac{\partial}{\partial x} \left[B_o \frac{x}{L_s} B_y \right] + \rho g \qquad \text{(VI-5)}$$

$$\gamma \rho V_y = -ikp + \frac{B_x}{4\pi} \frac{\partial}{\partial x} \left[B_o \frac{x}{L_s} \right] \qquad \text{(VI-6)}$$

$$\gamma B_x = ikB_o \frac{x}{L_s} V_x + \frac{\eta c^2}{4\pi} \left[\frac{\partial^2}{\partial x^2} - k^2 \right] B_x \qquad \text{(VI-7)}$$

$$\gamma B_y = -B_o \frac{\partial}{\partial x} \left[\frac{x}{L_s} V_x \right] + \frac{\eta c^2}{4\pi} \left[\frac{\partial^2}{\partial x^2} - k^2 \right] B_y. \qquad \text{(VI-8)}$$

We now simplify the problem by expressing all variables in terms of either V_x or B_x. Using Eqs. (VI-6 and 4) we find

$$p = \frac{\gamma \rho_o}{k^2} \frac{\partial V_x}{\partial x} - \frac{i B_o}{4\pi k L_s} B_x. \qquad \text{(VI-9)}$$

Substituting Eqs. (VI-3 and 9) into Eq. (VI-5) and using Maxwell's equation $\nabla \cdot \mathbf{B} = 0$, gives

$$- \frac{\partial}{\partial x} \gamma^2 \rho_o \frac{\partial V_x}{\partial x} + k^2 \left[\rho_o \gamma^2 + g \frac{\partial \rho_o}{\partial x} \right] V_x$$

$$= -i\gamma k \frac{B_o}{4\pi} \frac{x}{L_s} \left[\frac{\partial^2}{\partial x^2} - k^2 \right] B_x. \qquad \text{(VI-10)}$$

We must now solve the pair of equations (VI-7) and (VI-10). Notice that with $\eta = 0$ in Eq. (VI-7), the equations describing g modes in ideal MHD results.

Before solving these equations with $\eta \neq 0$, let us consider the effect of resistivity on the stability of the system. As already mentioned, the instability will be localized around the resonant surface $\mathbf{k} \cdot \mathbf{B}_o$. This is also the position where the motion of the fluid and field can most easily decouple. The form of Ohm's law which has been used to give Eq. (VI-2) is

$$\eta \mathbf{J} = \mathbf{E} + \frac{\mathbf{V}}{c} \times \mathbf{B}_o. \qquad \text{(VI-11)}$$

For $\eta = 0$ the condition of frozen in field lines is simply

$$\mathbf{E} = - \frac{\mathbf{V}}{c} \times \mathbf{B}_o. \qquad \text{(VI-12)}$$

On the other hand, the opposite extreme to this is clearly when the fluid moves freely through the field lines, i.e., $V \neq 0$ but $E \approx 0$. In this case, Eq. (VI-11) gives

$$J_z = \frac{\mathbf{V} \times \mathbf{B}_o}{\eta_c} \bigg|_z = \frac{x}{cL_s} B_o \frac{V_x}{\eta}. \qquad \text{(VI-13)}$$

One part of the force exerted on the plasma is then

$$\mathbf{F} = \frac{\mathbf{J}}{c} \times \mathbf{B}_o = - \mathbf{i}_x B_o^2 \left(\frac{x}{L_s} \right)^2 \frac{V_x}{\eta c^2}. \qquad \text{(VI-14)}$$

From the negative sign, we see that the force is a restraining force and furthermore, for $x \neq 0$ and small η, this force is very large. This only means, of course, that the plasma does not slip through the field lines, rather the field remains frozen into the flow. However for $x = 0$ (that is $k \cdot B = 0$), the restraining force becomes small and the plasma can leak through the field. We therefore see the importance of the resonant surface and the reason that resistivity can be important at this point, but unimportant everywhere else in the plasma.

Let us assume that in the vicinity of the resonant surface the plasma flow is decoupled from the field, so that Eq. VI-7 becomes

$$\left(\frac{\partial^2}{\partial x^2} - k^2 \right) B_x = - \frac{4\pi i k}{\eta c^2} B_o \frac{x}{L_s} V_x. \qquad \text{(VI-15)}$$

As we will see shortly, one simplifying feature of resistive g modes, as compared to for instance tearing modes (next chapter), is that resistive g modes are localized about the resonant surface. Therefore, for resistive g modes, Eq. (VI-5) can be taken to apply everywhere.

Substituting Eq. (VI-15) into Eq. (VI-10), we obtain

$$-\frac{\partial}{\partial x}\rho_o \gamma^2 \frac{\partial V_x}{\partial x} + k^2 g \frac{\partial \rho_o}{\partial x} V_x + \frac{\gamma k^2 B_o^2 x^2}{\eta c^2 L_s^2} V_x = 0. \quad \text{(VI-16)}$$

The problem is now reduced to the solution of a single second ordinary differential equation, the quantum mechanical harmonic oscillator in fact. Since we are interested in solutions localized around $x = 0$, we neglect the dependence of ρ_o on x and also neglected $k^2 B_x$ compared to $\frac{\partial^2 B_x}{\partial x^2}$ in Eq. (VI-5). Finally we have assumed that the growth rate γ is much less than the growth rate in an unsheared field $\left[g/\rho_o \frac{\partial \rho_o}{\partial x}\right]^{1/2}$.

Introducing the constants

$$A = \frac{\gamma \eta c^2 \rho_o L_s^2}{k^2 B_o^2} \quad \text{(VI-17a)}$$

and

$$B = -\frac{g}{\gamma} \frac{\partial \rho_o}{\partial x} \eta \frac{L_s^2}{B_o^2}. \quad \text{(VI-17b)}$$

Eq. (VI-16) can be rewritten

$$A \frac{d^2 V_x}{dx^2} + (B - x^2) V_x = 0. \quad \text{(VI-18)}$$

Introducing a change in variables

$$x' = A^{-1/4} x$$

Eq. (VI-8) becomes

$$\frac{d^2 V_x}{dx'^2} + \left[\frac{B}{A^{1/2}} - x'^2\right] V_x = 0. \quad \text{(VI-19)}$$

The solutions to Eq. (VI-19) which vanish at $x = \pm\infty$ are the Hermite functions

$$V_x = H(x') \exp - x'^2/2 \quad \text{(VI-20)}$$

and the eigenvalues are

$$B/A^{1/2} = 2n + 1. \quad \text{(VI-21)}$$

Notice that there can only be a real eigenvalue γ, for $B > 0$. From the definition of B, Eq. (VI-17b), this means $g\rho_o' < 0$; that is density gradient is opposite to g so that the mode in an unsheared field is unstable.

Equation (VI-21) is the dispersion relation for the resistive g mode. Substituting for A and B, we find

$$\gamma = \left\{ \frac{1}{2n+1} \left[-g \frac{\partial \rho_o}{\partial x} \right] \frac{kL_s}{B_o} \right\}^{2/3} \left[\frac{\eta c^2}{\rho_o} \right]^{1/3}. \qquad \text{(VI-22)}$$

This shows the characteristic dependence of the growth rate of the resistive g mode on the one third power of resistivity. Notice also that this mode cannot be stabilized by shear. As L_s decreases (increasing shear), the growth rate is reduced but there is not critical value at which it vanishes. Hence the earlier analogy with a "leaky dyke."

Finally, let us use the above solution to check the validity of the approximation which enabled us to carry out this analysis. This was the neglect of the γB_x compared with $\frac{\eta c^2}{4\pi} \frac{\partial^2 B_x}{\partial x^2}$ in Eq. (VI-7). This approximation is only expected to be valid over a small distance, (say x_c) where x_c is given approximately fromf Eq. (VI-16) by the condition

$$-k^2 g \frac{\partial \rho_o}{\partial x} V_x \approx \gamma \frac{k^2 B_o^2}{\eta} \left[\frac{x_c}{L_s} \right]^2 V_x$$

or

$$x_c \approx \left\{ \frac{-g \dfrac{\partial \rho_o}{\partial x} \eta L_s^2}{\gamma B_o^2} \right\}.$$

Using this to compare the orders of magnitude of the neglected term γB_x with $\frac{\eta c^2}{4\pi} \frac{\partial^2 B_x}{\partial x^2}$, we find

$$\frac{\gamma B_x}{\dfrac{\eta c^2}{4\pi} \dfrac{\partial^2 B_x}{\partial x^2}} \sim 4\pi \gamma x_c^2 \sim \frac{4\pi \gamma}{\eta} \left[-g \frac{\partial \rho_o}{\partial x} \right] \frac{\eta L_s^2}{\gamma B_o^2}.$$

From the expression for g given in the previous chapter

$$g \sim \frac{P_o}{\rho_o R} \sim \frac{P_o B_0^2}{\rho_o r \, (B_z^2 + B_\theta^2)}$$

where R, the radius of the field line is $r(B_z^2 + B_\theta^2)/B_\theta^2$, and $L_s \sim Rq$ (R is the major radius of the torus), the condition for validity becomes

$$\frac{4\pi \, P}{B_{z0}^2 + B_{\theta 0}^2} \ll 1. \tag{VI-23}$$

This condition is well satisfied in all current tokamaks and pinches.

Let us recall that there are two ways of stabilizing pressure (g) modes in ideal MHD, shear and magnetic well stabilization. However the former is not a stabilization mechanism of resistivity is allowed, because the fluid can now slip through the field. The latter is, because it relies on changing the sign of $g\rho'$, or of taking away free energy which drives the mode.

Chapter VII

THE TEARING MODE

In this chapter we turn to a discussion of one of the most important, and interesting modes in all of MHD theory, the tearing mode. This mode is quite different from the resistive g mode. There, resistivity allowed the plasma to slip through the sheared field, rather like (but much slower than) the case where there was no shear. The tearing mode is a totally different type of fluid motion and it is allowed only because of the presence of resistivity. In the resistive g mode, the fastest growing mode had V_x an even function of x. For the tearing mode however, V_x is an odd function of x so that for a particular y, two fluid elements on opposite sides of the singular surface are flowing either towards each other or away from each other.

Before actually discussing the tearing mode, it is worthwhile to examine this type of motion. By doing so, we will show that if magnetic field lines can reconnect, certain restraining forces disappear so that the equilibrium is more likely to be unstable. Let us consider two dimensional incompressible motion in the xy plane where initially

$$\mathbf{B} = B_o \frac{x}{L_s} i_y. \tag{VII-1}$$

Then specify the following velocity profile in the x direction

$$V_x = \begin{cases} - V_o \cos ky & \delta < x \\ - V_o \dfrac{x}{\delta} \cos ky & 0 < x < \delta \end{cases} \tag{VII-2a}$$

$$V_x (-x) = - V_x (x) \tag{VII-2b}$$

where δ is taken to be very small. Using the fact that the flow is two dimensional and incompressible, we find

$$V_y = \begin{cases} 0 & \delta < x \\ \dfrac{V_o}{\delta} \sin ky & 0 < \delta < x \end{cases} \tag{VII-3a}$$

$$V_y (-x) = V_y(x). \tag{VII-3b}$$

81

Thus in the separation layer $|x| < \delta$, there is very rapid flow in the y direction. The velocity stream lines are as shown in Fig. (VII-1). The two fluids on opposite sides of the singular surface $x = 0$ stream towards each other for $y > 0$, recoil near $x = 0$ and then stream away from each other at some $y < \pi/k$. Similarly two fluid elements streaming towards each other at $y < 0$ recoil and stream away somewhere around $y > -\pi/k$. The fluid exactly at $y = 0$ initially, does not stream away toward either positive or negative y, but piles into the stagnation point at $x = y = 0$. We will call this type flow a tearing flow or tearing motion.
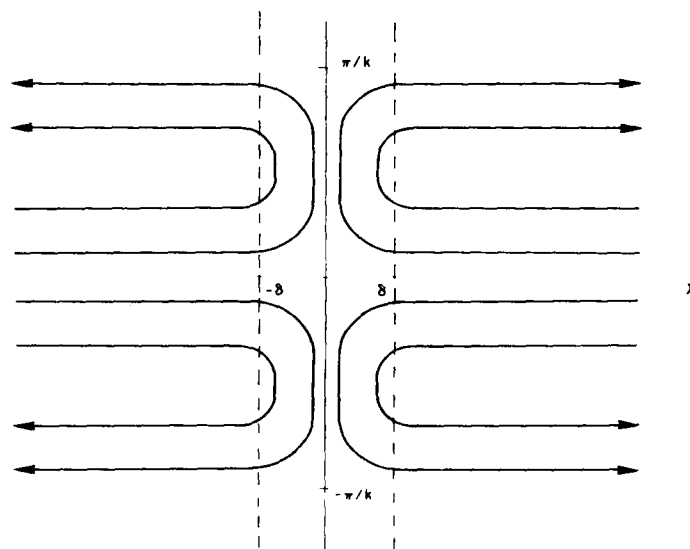
Fig. VII-1 — The velocity streamlines for a tearing motion

Now imagine that the fluid is magnetized with the field given by Eq. (VII-1). In ideal MHD, the magnetic field is frozen into the flow. This allows us to see just how the magnetic field reacts to the flow pattern shown in Fig. (VII-1). In Fig. (VII-2a) is shown a portion of two magnetic field lines $-\pi/2k < y < \pi/2k$ initially at x and $-x$ where $|x| > \delta$ at time $t = 0$. On one of these field lines in Fig. (VII-2a) are a series of dots (A-A'). Since the field is frozen into the flow, it must always pass through these dots no matter where they go. Thus by following the positions of these dots, we can construct the field line at later times. The field line for positive x can of course be drawn in an analogous way. Since $V_x = V_y = 0$ at $y = \pm\pi/2k$, the points A and A' do not move, while the other points B-E move toward $x = -\delta$ with progressively higher velocity. Thus at a later time the field lines bulge as shown in Fig. (VII-2b). Now consider a still later time when points D, E and D' have entered the separation region $-\delta < x < 0$. Point D
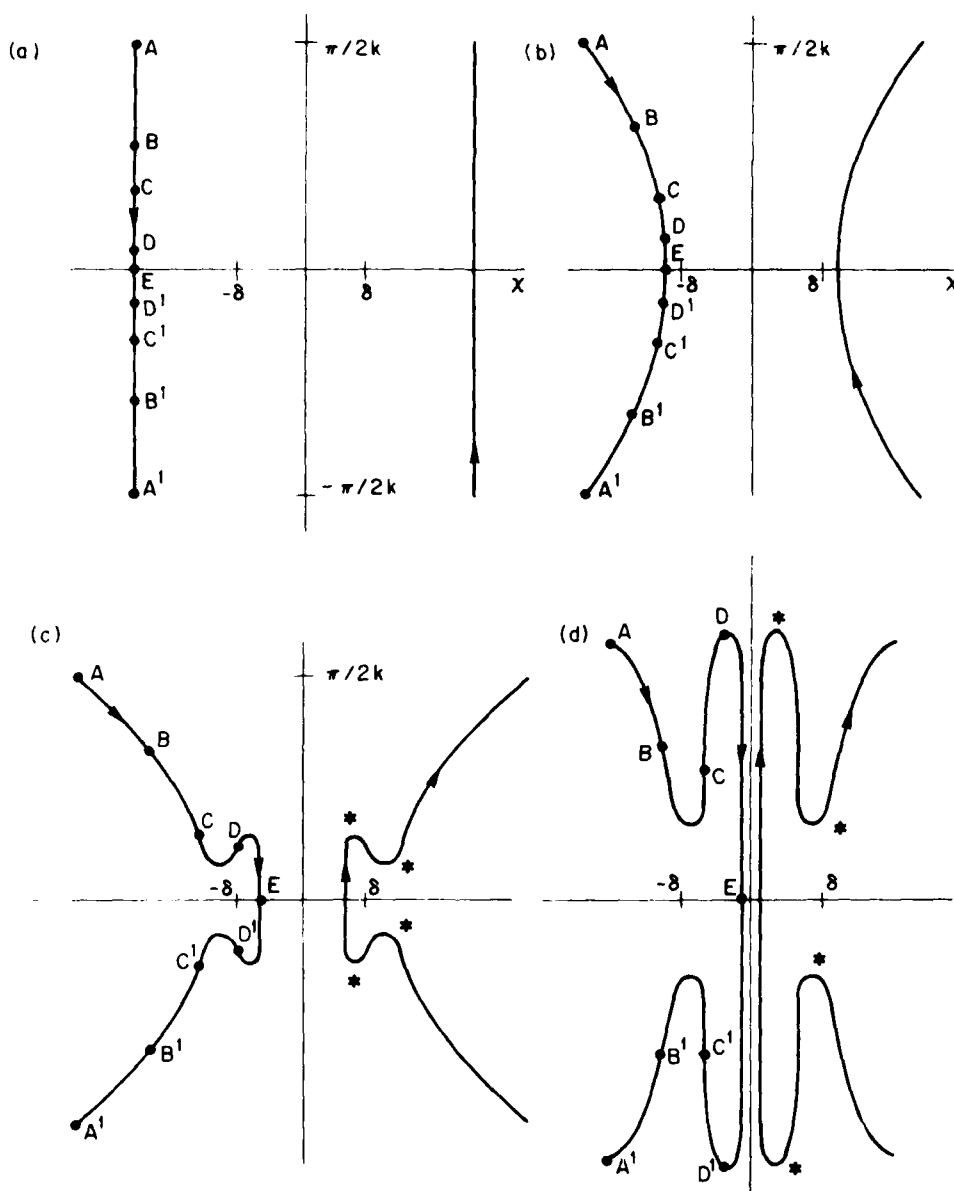
Fig. VII-2 — The magnetic field line, frozen into the
tearing motion a successive times

shoots upward, D' downward and E remains on the line $y = 0$, always
approaching the separation point $x = y = 0$. Thus the field lines are
distorted as shown in Fig. (VII-2c). At a later time this distortion is
further accentuated and the field line looks as shown in Fig. (VII-2d).
Notice that the field lines get very twisted and contorted by this type of
motion.

This contortion of the field line strongly affects the fluid motion. The field line is sharply curved at the points marked with a star on the right hand side of Figs. (VII-2c and d). However, as we have seen in Chapter III, a curved field line exerts a tension along the line rather like a rubber band. Thus the magnetic forces at the starred points in Figs. (VII-2c and d) (and of course at the analogous points on the left hand graph) are trying hard to snap the line back into its original shape. That is, the magnetic forces provide a strong restoring force which tends to prevent the type of fluid motion given by Eq. (VII-2 and 3).

Now, let us examine what effect nonzero resistivity has on this motion. If the plasma has resistivity, the field lines can break and reconnect. Notice also that in addition to the sharp corners induced at the stars in Fig. (VII-2c and d), there are also long lines of weak, oppositely directed fields forced right next to each other near the singular surface $x = 0$. Thus if resistivity, and thereby magnetic diffusion is allowed, the field lines, rather than looking like those in Fig. (VII-2c and d) would look like that shown in Fig. (VII-3).

Notice that the field pattern in Fig. (VII-3) does not have nearly as many sharp corners as that in Fig. (VII-2c or d). Thus, it provides a much weaker restraining force against the tearing motion described by Eq. (VII-2 and 3). Indeed, as we will see in this chapter, configurations which are stable to tearing motion in ideal MHD can be unstable if the resistivity is nonzero.

We now continue by writing out the equations for the linear stability of the system. We assume that $\mathbf{B}_o = B_o \mathbf{i}_z + B_{oy} (x)\mathbf{i}_y$ where $B_{oy} = 0$ at $x = 0$. The procedure is exactly the same as in Chapter V, namely take the x component of the curl of the momentum equation to show that $V_z = 0$. The z component of Eq. (V-1c) then shows that $B_z = 0$. Then take the z component of the curl of the momentum equation, use the fact that V and B are two dimensional and incompressible, and arrive at the result

$$\gamma \left[\frac{\partial}{\partial x} \frac{\rho_o}{ik} \frac{\partial V_x}{\partial x} + ik\rho_o V_x \right] = -\frac{1}{4\pi} \left[-B_{oy} \frac{\partial^2 B_x}{\partial x^2} \right.$$
$$\left. + B_x \frac{\partial^2 B_{oy}}{\partial x^2} + k^2 B_{oy} B_x \right] \qquad \text{(VII-4)}$$

assuming, as usual that perturbed quantities vary as $\exp(\delta t + iky)$. Notice that Eq. (VII-4) combined with the x component of Eq. (V-1c)
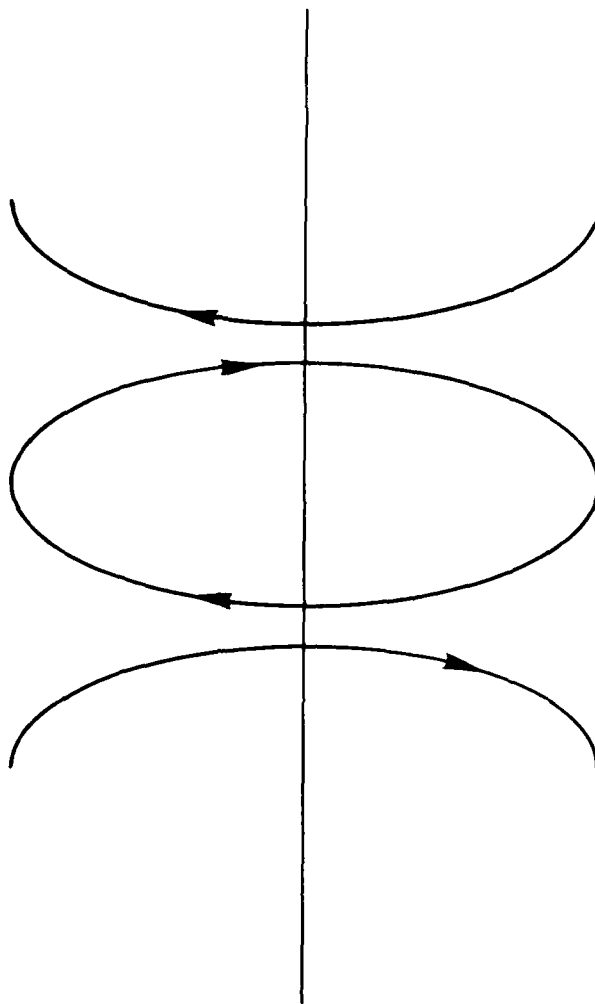
Fig. VII-3 — The field lines from Fig. 2c or d
if reconnection is allowed

would give Eq. (V-17) except that in the former g is assumed to vanish, while in the latter, the second derivative (i.e., the derivative of the current) is assumed zero.

If the resistivity is present, the equation relating B_x to V_x is

$$\gamma B_x = ik\, B_{oy}\, V_x + \frac{\eta c^2}{4\pi}\left[\frac{\partial^2 B_x}{\partial x^2} - k^2 B_x\right]. \qquad \text{(VII-5)}$$

Let us first prove that this configuration is stable in ideal MHD (i.e., if $\eta = 0$). Substituting $B_x = ikB_{yo}\, V_x/\gamma$ into the right hand side of Eq. (VII-4), we find the result

$$\frac{\partial}{\partial x}\left[\frac{\rho_o\gamma^2}{k^2} + \frac{B_{oy}^2}{4\pi}\right]\frac{\partial}{\partial x}\,V_x = \left[\frac{k^2\,B_{oy}^2}{4\pi} + \rho\gamma^2\right]V_x. \qquad \text{(VII-6)}$$

Notice that for real γ, the right hand side of Eq. (VII-6) is positive for all x. Thus, as discussed in Chapter V, V_x is a monotonically increasing function of x for all x as long as V_x and $\dfrac{\partial V_x}{\partial x}$ are both positive in the limit of $x \rightarrow \infty$. Hence there is no way to have a solution for V_x which approaches zero as $z \rightarrow \pm\,\infty$, so the plasma is stable in ideal MHD.

Another way to understand this ideal MHD stability is as follows. According to Maxwells equation an electric field

$$E_z = -\frac{\gamma}{ick}\,B_x \qquad \text{(VII-7)}$$

is induced by th fluid motion. However, we also have

$$E_x = -\frac{1}{c}\,V_x\,B_{oy} \qquad \text{(VII-8)}$$

so that any nonzero E_z induces an infinitely large V_x near the singular point $x = B_{yo} = 0$. The only possible resolution in ideal MHD is of course $\gamma = 0$, or stability for the fluid. If the resistivity is nonzero, then near the singular point the electric field can be balanced not only by fluid flow, but by Ohmic dissipation.

Let us now imagine that the resistivity is very small, but nonvanishing, and that its presence gives rise to instabilities whose growth rate vanishes in some way as $\eta \rightarrow 0$. Then, away from the singular point we expect the plasma to be described by the Ideal MHD equations with zero γ, or setting the right hand side of Eq. (VII-4) equal to zero,

$$\frac{\partial^2 B_x}{\partial x^2} = \left[k^2 + \frac{1}{B_{oy}}\,\frac{d^2 B_{oy}}{dx^2}\right]B_x. \qquad \text{(VII-9)}$$

Let us briefly discuss the significance of the neglect of γ. Neglecting the growth rate in the momentum equation simply means

$$\frac{1}{c}\,(\mathbf{J}\times\mathbf{B}_o) + \frac{1}{c}\,(\mathbf{J}_o\times\mathbf{B}) - \nabla p = 0,$$

or equivalently

$$\nabla\,x\,\{\mathbf{J}\times\mathbf{B}_o + \mathbf{J}_o\times B\} = 0.$$

That is away from the singular region, the perturbed plasma is in a state of ideal MHD pressure balance equilibrium. Imagine that the tearing mode we consider grows with growth rate much less than kV_A where

V_A is a characteristic Alfven speed in the outer region. Then if the plasma configuration is not in pressure balance equilibrium, magnetosonic waves and/or shocks with frequency $\omega \sim kV_A$ will be generated. Once these magnetosonic disturbances damp out, pressure balance will be attained. Our fundamental assumption then is that the time scale for maintaining this pressure balance is much less than the characteristic growth time of the tearing mode. Therefore, in the outer region, pressure balance applies for all time and this outer region is described by Eq. VII-9.

There are two difficulties in describing the entire system with Eq. (VII-9) above. First of all there is no eigenvalue γ, so that a solution which satisfies the proper boundary condition at $x = -\infty$ in general will not satisfy the boundary condition at $x = +\infty$. Stated another way, if the solution satisfies the boundary conditions at both $x = -\infty$ and $x = +\infty$, in general there will be a discontinuity in slope at the position where the two solutions meet (assuming the solutions are normalized so that there is no discontinuity in B_x itself). Secondly, the equation is singular at $x = 0$ where $B_{oy} = 0$. A power series expansion shows that the two linearly independent solutions, denoted ψ_i and ψ_2 behave for small x as.

$$\psi_1 = x$$
$$\psi_2 = C_1 + C_2 x \ln x \qquad \text{(VII-10)}$$

where ψ_2 has a logarithmic dependence because the exponents of x in the two solutions differ by an integer. The idea then is that Eq. (VII-9) applies for all x except a very narrow range around $x = 0$, (the outer region). The solution of Eq. (VII-9) in the outer region has a discontinuity in slope at $x = 0$. In a very narrow range around $x = 0$ (the inner region), inertia and resistivity both come into play and smoothly connect the two outer solutions.

Before actually calculating the growth rate we consider more carefully just what drives instability and calculate qualitative expressions for the growth rate. Let us calculate the power liberated by the fluid in its motion. Imagine the fluid is acted upon by a force density $\mathbf{F}$ and that the fluid velocity is $\mathbf{V}$. Then the power P going into the fluid is

$$P = \int d^3x \; \mathbf{V}^* \cdot \mathbf{F} + c.c. \qquad \text{(VII-11)}$$

However for incompressible motion,

$$\mathbf{V} = \text{curl } \mathbf{R} \qquad \text{(VII-12)}$$

so that the power going into the fluid is

$$P = \int d^3x \, \text{curl} \, \mathbf{R} \cdot \mathbf{F} = \int d^3x \, \mathbf{R} \cdot \text{curl} \, \mathbf{F} \qquad \text{(VII-13)}$$

where we have assumed the solution is well behaved at $x = \pm\infty$ and that the velocities at $x = 0^+$ are somehow smoothly connected to those at $x = 0^-$. For two dimensional incompressible motion

$$\mathbf{R} = \frac{V_x}{ik} \, \mathbf{i}_z$$

so that

$$P = \int d^3x \left[\frac{V_x^*}{-ik} \right] \cdot (\nabla \times \mathbf{F})_z + c.c. \qquad \text{(VII-14)}$$

In ideal MHD, V_x is related to B_x by Eq. (VII-6), with $\eta = 0$, and the right hand side of Eq. (VII-4) is an expression for the z component of the curl of the force density. Putting these together we find

$$P = -\frac{1}{4\pi} \int d^3x \, \frac{\gamma}{k^2} \, B_x \left\{ -\frac{d^2 B_x}{dx^2} + k^2 B_x \right. $$
$$\left. + \frac{\dfrac{d^2 B_{oy}}{dx^2}}{B_{oy}} \, B_x \right\} + c.c. \qquad \text{(VII-15)}$$

where we have assumed that B_x is real. Of course the expression for power liberated is consistent with the δB^2 and $\mathbf{J}_o \cdot (\boldsymbol{\xi} \times \mathbf{B}) \cdot$ term in the energy equation, Eq. (III-24). The quantity in the curly brackets is just Eq. (VII-10) and is zero in the outer region. However, Eq. (VII-10) is not satisfied everyone in the plasma, but only in the outer region. Thus power can be dissipated by the fluid in the inner region.

The outer region solutions for large x generally have a discontinuous derivative at $x = 0$, but as is apparent from Eqs. (VII-11a and b), B_x itself is well behaved and continuous. This means that in the inner region, $\partial^2 B_x/\partial x^2$ is very large so that it is the dominant term in Eq. (VII-5). Hence the power per unit area dissipated in the inner region is given by

$$P = \frac{\gamma}{4\pi k^2} \, B_x^2 \, (x = 0) \, \Delta + c.c. \qquad \text{(VII-16)}$$

where

$$\Delta = \frac{1}{B_x \, (x = 0)} \left\{ \frac{dB_x}{dx} \bigg|_{x=0^+} - \frac{dB_x}{dx} \bigg|_{x=0^-} \right\}. \qquad \text{(VII-17)}$$

Thus if Δ is positive, energy is dissipated by the fluid in the inner region, and we expect that the plasma is unstable. Clearly the potential energy driving this dissipation comes from the outer region. This is obvious because B_{oz} is not involved in the motion and B_{oy} is zero at the singular point, so there is no free energy in the inner region. In Chapters VIII and XI we will discuss other aspects of the free energy which drives the tearing mode.

The basic picture of a tearing mode is then that energy is released in the outer region and dissipated in the inner region. The condition for release of energy in the outer region, and therefore the condition for instability is

$$\Delta > 0. \tag{VII-18}$$

One can show that for the sheet current at $x = \pm a$, and for the magnetic profile

$$B_{oy} = B_{oy} \tanh (x/a), \tag{VII-19}$$

the Δ's are given respectively by

$$\Delta = 2k \left[\frac{1 - ka - ka \tanh ka}{ka - (1 - ka) \tanh ka} \right] \tag{VII-20}$$

$$\Delta = 2 \left[\frac{1}{ka^2} - k \right]. \tag{VII-21}$$

Hence for sufficiently small k, each current distribution is potentially unstable to tearing modes.

One other interesting aspect of the instability criterion $\Delta > 0$ is the following. If $\Delta = 0$, the MHD solutions for $\gamma = 0$ connect smoothly to each other through the singularity. Thus if $\Delta = 0$ there is another MHD equilibrium $(B = B_o + B)$ which can be arrived at from the original equilibrium with no expenditure of energy. Hence the condition for tearing mode instability is that there be a neighboring equilibrium of the magnetic structure which has the same energy as the initial equilibrium. This aspect will be important later on when we discuss the nonlinear theory.

Now that we have the condition for instability, we continue by estimating the size of the inner region and the growth rate. To start, we will eliminate the d^2B_x/dx^2 term in Eq. (VII-4) by using Eq. (VII-5). The result is

$$\frac{\partial}{\partial x} \rho_o \frac{\partial V_x}{\partial x} - k^2 \rho_o V_x - \frac{k^2 B_{oy}^2(x)}{\eta c^2 \gamma} V_x$$

$$= - ik \left[\frac{-B_{oy}}{\eta c^2} + \frac{B_{oy}''}{4\pi\gamma} + \frac{k^2 B_{oy}}{4\pi\gamma^2} \right] B_x \qquad \text{(VII-22)}$$

where we have neglected $k^2 B_x \ll \dfrac{\partial^2 x}{\partial x^2}$ in Eq. (VII-5). Within the inner region, B_x is nearly constant as we have discussed previously, and $B_{oy} \approx B_o \dfrac{x}{L_s}$. Thus Eq. (VII-22) is an inhomogeneous differential equation for V_x in terms of the now constant B_x. Clearly the characteristic length scale on which V_x varies in the inner region is

$$L_c = \left[\frac{\rho_o \, \eta c^2 \, \gamma \, L_s^2}{k^2 \, B_o^2} \right]^{1/4}. \qquad \text{(VII-23)}$$

To derive the growth rate, let us assume that the energy released in the outer region is dissipated by Ohmic heating in the inner region. Recall that $\dfrac{\partial B_x}{\partial x}$ is discontinuous across the inner region. Since $B_y = - \dfrac{1}{ik} \dfrac{\partial B_x}{\partial x}$, B_y is then itself discontinuous across this region. Thus there is a strong current in the z direction which flows in the inner region. A rough estimate of the magnitude of this current is

$$J_z = \frac{c}{4\pi} \frac{B_y^+ - B_y^-}{L_c} \approx \frac{c}{4\pi \, ik} B_x \, (x = 0) \frac{\Delta}{L_c}. \qquad \text{(VII-24)}$$

The power dissipated per unit area is then $\eta J_z^2 L_c$. Equating the Ohmic power dissipated in the inner region with the power released by the fluid in the outer region, we find

$$\frac{\eta c^2 \Delta^2 B_x^2(x = 0) \, L_c}{16\pi^2 \, k^2 \, L_c^2} \approx \frac{\gamma}{4\pi \, k^2} \Delta \, B_x^2(x = 0) \qquad \text{(VII-25a)}$$

or

$$\gamma \approx \left[\frac{1}{4\pi} \right]^{4/5} (\eta c^2)^{3/5} \, \Delta^{4/5} \left[\frac{k^2 B_o^2}{\rho_o \, L_s^2} \right]^{1/5} \qquad \text{(VII-25b)}$$

and

$$L_c \approx \left[\frac{\rho_o L_s^2}{4k^2 \, B_o^2} \right]^{1/5} (\eta c^2)^{2/5} \left[\frac{\Delta}{4\pi} \right]^{1/5}. \qquad \text{(VII-25c)}$$

Notice that once again, as for the case of the resistive g mode, the growth rate is proportional to a fractional power of the resistivity. This means that even if $\nabla \times \eta \nabla \times \mathbf{B}_o \neq 0$, so that the plasma is not initially in equilibrium, the time for the relaxation of the plasma due to tearing modes, $t \sim \eta^{-3/5}$ is quicker than the time scale for relaxation of the assumed equilibrium due to resistive diffusion $t_r \sim \eta^{-1}$.

Let us re-emphasize that even in ideal MHD, there is free energy to drive a tearing mode if only one could ignore the MHD constraint $\mathbf{E} + \mathbf{V}/c \times \mathbf{B} = 0$. One way around this constraint is to introduce resistivity. However there are other ways around this constraint also, and the arguments from Eq. (VII-22)-(VII-25) basically follow. We will consider two examples.

For the first let us consider electron inertia as the nonideal effect. Then Ohms law becomes

$$m \frac{\partial \mathbf{V}}{\partial t} = -\frac{m}{ne} \gamma \, \mathbf{J} = -e \left(\mathbf{E} + \frac{\mathbf{V}}{c} \times \mathbf{B} \right) \qquad \text{(VII-26)}$$

where n is the electron number density. The small parameter now is the electron mass m and the growth rate will be proportional to some power of this quantity. As is apparent from Eq. (VII-26), inertia plays the exact same role as resistivity if one makes the replacement

$$\eta \rightarrow \frac{m\gamma}{ne^2}. \qquad \text{(VII-27)}$$

The singular layer width L_c will still be defined by Eq. (VII-23) if one uses Eq. (VII-27).

The power gain within the singular layer now arises from acceleration of electrons, there rather than from resistive dissipation. The power gain per unit area is $nmV \dfrac{\partial V}{\partial t} L_c = \dfrac{\gamma m}{ne^2} J^2 L_c$ so that the growth rate for an electron inertia driven tearing mode is given by

$$\gamma(m) \approx \Delta^2 \left(\frac{mc^2}{4\pi ne^2} \right)^{3/2} \frac{kB}{L_s \sqrt{4\pi\rho_o}}. \qquad \text{(VII-28)}$$

The second non-ideal effect which we consider is electron shear viscosity so that Ohms law becomes

$$0 = -e \left(\mathbf{E} + \frac{V}{c} \times B \right)\bigg|_z = -m\mu \frac{\partial^2}{\partial x^2} V_{ez} = \frac{m\mu}{ne} \frac{\partial^2 J_z}{\partial x^2} \qquad \text{(VII-29)}$$

where μ is the electron shear viscosity, which has the dimension of a diffusion coefficient. Also we have assumed that the electron density n is nearly constant within the singular layer. Since Eq. (VII-29) now has a higher derivative than for instance Eq. (VII-26), there is no exact mathematical analogy with the resistive tearing mode. However it is clear that the energy deposited in the inner layer will now be dissipated by viscous dissipation. The power dissipated per unit area in the layer is now

$$nm\mu \left[\frac{\partial V_z}{\partial x}\right]^2 L_c = \frac{m\mu}{ne^2} \left[\frac{\partial J}{\partial x}\right]^2 L_c.$$

To get the scaling of L_c replace $\dfrac{\partial^2 J_z}{\partial x^2}$ in Eq. (VII-29) by $- J_z/L_c^2$ so it now has the same form as Eq. (VII-26). The analysis from (VII-22-25) follows as before and we find

$$\gamma(\mu) \sim \left[\frac{m\mu c^2}{4\pi ne^2}\right]^{1/3} \frac{\Delta^{2/3}}{\left[\dfrac{4\pi\rho \, L_s^2}{k^2 B_o^2}\right]^{1/3}}. \qquad (VII\text{-}30)$$

Thus for a tearing mode, energy in the outer region is available to drive an MHD instability. Any process which circumvents the MHD constraint and allows this energy to be dissipated in the inner region, will give rise to a tearing mode. Generally we concentrate on resistivity as the non-ideal effect. However, in practice, it may be other things which causes nonzero growth.

We now conclude this chapter by actually calculating the growth rate and also Ohmic and kinetic power dissipated in the inner region for the case that resistivity is the non-ideal effect. Here the velocity is the solution of Eq. (VII-22). We now make a slight simplification and assume that the current sheet is symmetric so that B_{oy}^* also vanishes at the singular surface. In this case, in the limit of $\eta \rightarrow 0$ the dominant term on the right handside of Eq. (VII-22) is the $-B_{oy}/\eta^{c^2}$ term since it diverges as η^{-1} as $\eta \rightarrow 0$, whereas the other two terms diverge as $\eta^{-3/5}$ according to Eq. (VII-25b).

The idea now is to solve Eq. (VII-22) for V_x in the inner region. The growth rate is then calculated by insisting that the inner region solution matches with the outer region solutions for large x. If the inner region is narrow on the length scale which B_x varies on, then B_x on the right hand side of Eq. (VII-22) can be regarded as constant. This is equivalent to the constant ψ approximation first introduced by

Furth, Kileen and Rosenbluth. Making these approximations, Eq. (VII-22) reduces to

$$\rho_o \frac{\partial^2 V_x}{\partial x^2} - k^2 \rho_o V_x - \frac{k^2 B_o^2 x^2}{\eta c^2 \gamma L_s^2} V_x$$

$$= ik \frac{B_o x}{\eta c^2 L_s} B_x(x = 0) \qquad (\text{VII-31})$$

assuming ρ_o does not vary substantially in the inner region. The solution for V_x from Eq. (VII-31) is that linear combination of homogeneous solutions and the particular solutions which satisfy the appropriate boundary conditions, that is $V_x \rightarrow 0$ as $x \rightarrow \pm \infty$. We first look at the solution to the homogeneous equation

$$\rho_o \frac{\partial^2}{\partial x^2} V_x = \left(k^2 \rho_o + \frac{k^2 B_o^2 x^2}{\eta c^2 \gamma L_s^2} \right) V_x.$$

Since the quantity in parentheses is positive, the solution for V_x which is positive at $x \rightarrow -\infty$ is a monotonically increasing function of x and therefore cannot possibly satisfy the boundary conditions. Therefore the appropriate solution to Eq. (VII-31) is the particular solution alone.

To continue, we re-scale the equation by letting $X = x/L_r$ and $Q = \gamma/Q_r$ where

$$L_r = \left[\frac{\rho_0 \eta^2 L_s^2}{k^2 B_0^2} \right]^{1/6} \qquad (\text{VII-32})$$

$$Q_r = \left[\frac{\eta k^2 B_0^2}{\rho_0 L_s^2} \right]^{1/3} \qquad (\text{VII-33})$$

$$\xi = V_x/\gamma. \qquad (\text{VII-34})$$

Thus Q is a dimensionless growth rate. Later on, these will prove to be convenient scaling parameters. Then, neglecting k in Eq. (VII-33) (that is, the inner region width is much less than k^{-1}), Eq. (VII-33) and (VII-5) become

$$\frac{d^2 \xi}{dX^2} = \frac{X^2}{Q} \xi + \frac{X}{Q} \psi(0) \qquad (\text{VII-35})$$

$$\frac{d^2 \psi}{dX^2} = Q(\psi + x\xi) \qquad (\text{VII-36})$$

where

$$\psi = \frac{-iL_s}{kB_0 L_r} \tilde{B}_x. \qquad (\text{VII-37})$$

The form of Eq. (VII-35) naturally suggests an expansion in terms of Hermite functions, and indeed this is how the problem was first solved. However because the behavior of the homogeneous solution as $x \to \infty$ ($\xi \sim x^{-1}$) is very unlike the form of the Hermite functions as $x \to \infty$, an infinite number of terms and the associated difficult manipulations are required to solve the problem in the x domain. An alternative, and much simpler scheme is to solve the problem in the Fourier (θ) domain where the difficulties at $x \to \infty$ transform themselves into simple delta functions and their derivatives at $\theta = 0$. Here $\hat{f}(\theta) = \int_{-\infty}^{\infty} dX\, f(X)\, e^{i\theta X}$. Multiplying Eq. (VII-35) by $e^{i\theta X}$ and integrating over x, we find

$$-\frac{1}{Q}\frac{d^2\hat{\xi}}{d\theta^2} + \theta^2\hat{\xi} = \frac{2\pi i}{Q}\psi(x=0)\,\delta'(\theta) \qquad \text{(VII-38)}$$

where we have used the fact that the Fourier transform of X is proportional to the derivative of a delta function.

For $\theta > 0$, the solution of Eq. (VII-38) is the parabolic cylinder function which approaches zero as $\theta \to \infty$. In the notation of *Abramowitz and Stegun, Handbook of Mathematical Functions, Chapter 19 (by J.C.P. Miller) Dover Publications (1972)*, the function $U(a,x)$ is the solution of the equation

$$\frac{d^2y}{dx^2} - (\frac{1}{4}x^2 + a)\,y = 0 \qquad \text{(VII-39)}$$

which approaches zero as $x \to +\infty$. Hence for $\theta > 0$,

$$\hat{\xi} = A\ U(0,\ \phi) \qquad \phi > 0 \qquad \text{(VII-40)}$$

where

$$\phi = \sqrt{2}\ Q^{\frac{1}{2}}\ \theta. \qquad \text{(VII-41)}$$

Since the source term on the right hand side of Eq. (VII-38) has odd symmetry in θ, we look for a solution also having odd symmetry. The solution for $\phi < 0$ is then

$$\hat{\xi} = -A\ U(0,\ -\phi). \qquad \phi < 0. \qquad \text{(VII-42)}$$

Integrating Eq. (VII-38) twice across a small region near $\theta = 0$, we find that

$$A = -\pi i\ \psi_0 / U(0,\ 0). \qquad \text{(VII-43)}$$

To get the dispersion relation, we assume, as usual, that the outer ideal magnetohydrodynamic region specifies a value of Δ', the discontinuity in $(d\tilde{B}_r/d\tilde{r})/B_r$, across the singular layer. Matching with its counterpart from the inner region, we obtain, from Eq. (VII-36)

$$L_r\Delta' = \int_{-\infty}^{\infty} dX(Q)(\Psi + X\xi). \qquad \text{(VII-44)}$$

To do the integrals over X note that $\xi(X) = (1/2\pi) \times \int_{-\infty}^{\infty} \hat{\xi}(\theta) e^{-i\theta X} d\theta$ while Ψ (assumed constant) is $\Phi_0 \int_{-\infty}^{\infty} \delta(\theta) e^{-i\theta x} dk$. Note that in doing the ξ integral over X, one will ultimately have a derivative of a delta function in the θ integral. Inserting these forms into Eq. (VII-44) we see that both the Ψ and ξ contributions have a delta function component at $\theta = 0$, but these two divergent contributions cancel. This cancellation is of course the analog of the separate integrals in X space of Ψ and $X\xi$ diverging for $X \to \infty$, while the integral of $\Psi + X\xi$ converges.

The remaining part of the θ integral comes from the derivative of the parabolic cylinder function at $\theta = 0$. The final result is

$$L_r\Delta' = 2\pi \frac{\Gamma\left(\dfrac{3}{4}\right)}{\Gamma\left(\dfrac{1}{4}\right)} Q^{5/4}. \qquad \text{(VII-45)}$$

The $\Gamma(\tfrac{3}{4})$ and $\Gamma(\tfrac{1}{4})$ just come from the expression for $U(0, 0)$ and $U'(0, 0)$ in *Abramowitz and Stegun.* As is apparent from the scaling relation Eqs. (VII-32 and 33), the growth rate γ scales as $\eta^{3/5}$.

To summarize, the tearing mode just becomes unstable when there is a second magnetic equilibrium which is accessible from the first with no expenditure of energy. The instability develops by the fluid releasing magnetic energy in the outer region, and dissipating it principally via Ohmic heating in a narrow inner region near the singular surface. This dissipation near $x = 0$ manifests itself by a change in the magnetic field topology, that is, island formation. If $B_y \ll B_0$, the equations for the field lines in the xy plane is

$$\frac{dx}{B \cos ky} = \frac{dy}{B_o \dfrac{x}{L_s}}$$

where B_x is taken as $B \cos ky$. The equation for the field line is then

$$x = \left[K + \frac{2L_s\, B}{B_o\, k} \sin ky \right]^{1/2} . \qquad \text{(VII-46)}$$

This field line has a separatrix if $K = \dfrac{2L_s B}{kB_o}$ and this separatrix has maximum width (the island width)

$$\Delta X_{is} = 2 \left[\frac{BL_s}{kB_o} \right]^{1/2} . \qquad \text{(VII-47)}$$

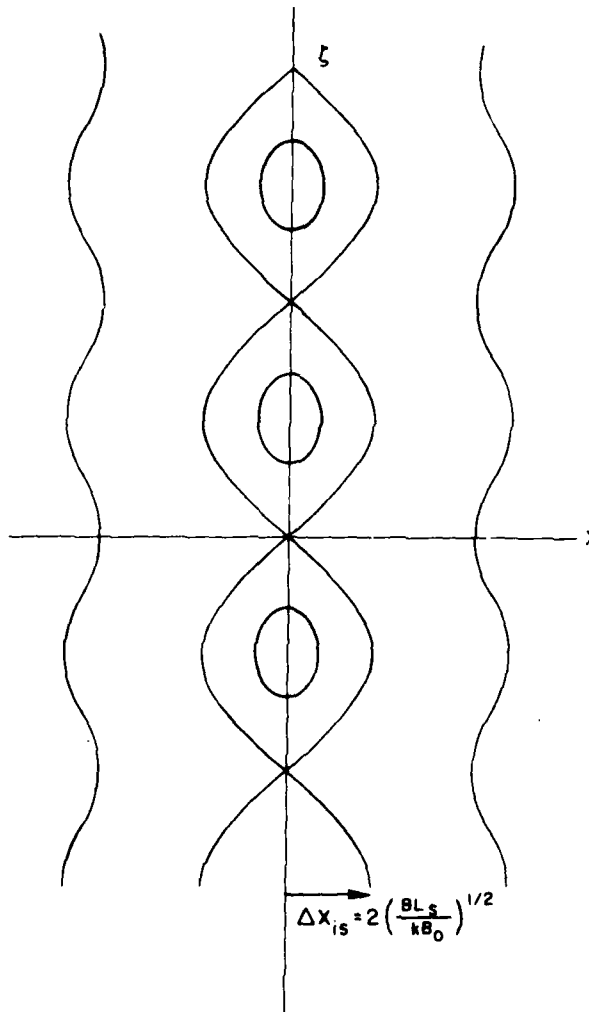The field lines in the xy plane are shown in Fig. (VII-4).

Fig. VII-4 — Magnetic island structure generated
by a tearing mode

The following is for Chapters 6 and 7.

The original paper on resistive instabilities is:

Finite-Resistive Instabilities of a Sheet Pinch, H.P. Furth, J. Kileen, and M.N. Rosenbluth, Phys. Fluids, **6**, 459 (1963).

A clear description of tearing and resistive interchange modes (including a description of matching of the inner and outer (MHD) region for the latter) is in:

Resistive Instabilities in a Diffuse Linear Pinch, B. Coppi, J.M. Greene, and J.L. Johnson, Nuclear Fusion, **6**, 101 (1966).

A description of resistive interchange modes as an eigenfunction along rather than across the field is given in:

Gravitational Resistive Instability for an Incompressible Plasma, K.V. Roberts and J.B. Taylor, Phys. Fluids, **8**, 459 (1965).

Application of tearing modes to tokamaks can be found in:

Tearing Mode in the Cylindrical Tokamak, H.P. Furth, P.H. Rutherford, and H. Selberg, Phys. Fluids, **16**, 1054 (1973).

Stabilization of Resistive Kink Modes in the Tokamak, A.H. Glasser, H.P. Furth, and P.H. Rutherford, Phys. Rev. Lett., **38**, 234 (1977).

A theory of an electron inertia driven tearing mode is given in:

Inertial Magnetic Field Reconnection and Magnetospheric Substorms, G. Van Hoven and M.A. Cross, Phys. Rev. Lett., **30**, 642 (1973).

A full kinetic theory of tearing modes was worked out in:

Kinetic Theory of Tearing Instabilities, J.F. Drake and Y.C. Lee, Phys. Fluids, **20**, 1341 (1977).

Since the tearing mode is relatively subtle, some calculations have solved it essentially by brute force. One possibility is a direct solution

of the fourth order equations with no inner and outer expansion. This can be found in:

Finite Resistive Instabilities in a Sheet Pinch, J.A. Wesson, Nuclear Fusion, **6**, 130 (1966).

Alternatively one can set up a periodic current distribution with long wavelength and analyze the problem by Fourier transformation. Since the instability is quite localized, a large number of harmonics are needed and the matrix must be inverted numerically. This is in:

M.A. Cross and G. Van Hoven, Phys. Rev. A., **4**, 2349 (1971).

Chapter VIII

INTERNAL MHD INSTABILITIES IN
CYLINDRICAL PLASMAS

In this section we discuss MHD instabilities in a cylindrical plasma with no free surface. As we will see shortly, the modes which we have discussed in the previous three chapters have simple analogs in cylindrical geometry. However there are also additional modes in cylindrical geometry which have no analog in slab geometry. Because this chapter is quite long, we subdivide it into six subchapters, VIII.A-VIII.F, which deal respectively with two dimensional MHD modes, ideal MHD modes with $m \geqslant 2$, ideal MHD modes with $m = 1$, resistive MHD modes with $m \geqslant 2$, resistive MHD modes with $m = 1$, and double tearing modes.

VIII.A — MHD Modes With Two Dimensional Structure

Recall from the last three chapters, that in slab geometry, the appropriate modes always had two dimensional structure in the plane perpendicular to B_{zo}. If $B_{zo} >> B_{\theta o}$ and $a << R$, (tokamak ordering) one might expect this to be valid in cylindrical geometry also. This is analogous to the analysis in the second part of Chapter IV where we examined two dimensional unstable modes in a cylindrical plasma with a free surface. Here, as we will see, two dimensional modes in a cylindrical plasma with no free surface are stable. However the analysis here is still useful to set the stage for a study of instabilities resulting from three dimensional or resistive effects.

In cylindrical geometry, all perturbed quantities vary as $\exp i(m\theta + kz)$. To make the transition to toroidal geometry we simply quantize k, that is $k \rightarrow n/R$, but neglect all other complications of the toroidal geometry. The perturbation is perpendicular to the ambient field wherever $mB_{\theta o}/r (r) + nB_{zo}/R = 0$, so we expect unstable perturbations to be in some way localized near this point (we assume here that B_{zo} is independent of r and is $>> B_{\theta o}$). If this is so, $k \approx m/r\, B_{\theta o}/B_{zo} << m/r$ so that the variation in the θ direction is

much more rapid than the variation in the z direction. Therefore, plasma motion will be approximately 2 dimensional in r and θ, quite analogous to the motion in slab geometry. Then $V_z = B_z = 0$, k is taken as a small quantity unless it multiplies B_{zo} and V_r, V_θ, B_r and B_θ are related by the incompressibility condition

$$\frac{1}{r}\frac{\partial}{\partial r}rV_r + \frac{im}{r}V_\theta = \frac{1}{r}\frac{\partial}{\partial r}rB_r + \frac{im}{r}B_\theta = 0. \qquad \text{(VIII-1)}$$

The next step then (analogous to the previous chapters) is to take the z component of the curl of the perturbed momentum equation, or

$$\frac{\gamma}{r}\left[\frac{\partial}{\partial r}r\rho_o V_\theta - \rho_o\, imV_r\right] = \frac{1}{c}\nabla \times (\mathbf{J}\times\mathbf{B}_o + \mathbf{J}_o\times\mathbf{B})\mid_z$$

$$= \frac{1}{c}\{(\mathbf{B}\cdot\nabla)\mathbf{J}_o + (\mathbf{B}_o\cdot\nabla)\mathbf{J} - (\mathbf{J}\cdot\nabla)\mathbf{B}_o - (\mathbf{J}_o\cdot\nabla)\mathbf{B}\}_z. \qquad \text{(VIII-2)}$$

First look at the third and fourth terms on the right hand side of Eq. (VIII-2). Since B_{oz} is assumed to be constant, $(\mathbf{J}\cdot\nabla)\mathbf{B}_o = 0$. The fourth term is $-\,ikj_oB_z$ which is small since both k and B_z are assumed small. The first term on the right is $\frac{1}{c}B_r\frac{dJ_{oz}}{dr}$ while the second is $\left(\frac{im}{r}B_{\theta o} + ikB_{zo}\right)J_z$. However $J_z = \frac{c}{4\pi}\nabla\times\mathbf{B}\mid_z$. Making use of Eq. (VIII-1), Eq. (VIII-2) reduces to

$$-\gamma\left[\frac{1}{r}\frac{\partial}{\partial r}r\rho_o\frac{1}{im}\frac{\partial}{\partial r}(rV_r) + \frac{\rho_o im}{r}V_r\right] =$$

$$\frac{1}{c}\left\{B_r\frac{dJ_{oz}}{\partial r} + \frac{ic}{4\pi}F\left[\frac{-1}{r}\frac{\partial}{\partial r}\frac{r}{im}\frac{\partial}{\partial r}rB_r - \frac{im}{r}B_r\right]\right\} \qquad \text{(VIII-3)}$$

where

$$F = \frac{mB_{\theta o}}{r} + kB_{zo}. \qquad \text{(VIII-4)}$$

Here, unlike the second part of Chapter IV, F depends on r in general. To complete the description of linear modes in a cylindrical plasma in the tokamak ordering, an additional relation between V_r and B_r is required. This comes from Maxwell's equation

$$\gamma\mathbf{B} = -\nabla\times\mathbf{V}\times\mathbf{B} - \frac{\eta c^2}{4\pi}\nabla\times\nabla\times\mathbf{B}. \qquad \text{(VIII-5)}$$

To start we consider only ideal modes, so $\eta = 0$ in Eq. (VIII-5) above. In this case

$$\gamma B_r = iFV_r. \tag{VIII-6}$$

Then inserting for B_r on the right hand side of Eq. (VIII-3), we find after a bit of straight forward manipulation

$$\frac{1}{r}\frac{\partial}{\partial r}r^3\left[\frac{F^2}{4\pi}+\rho_0\gamma^2\right]\frac{\partial}{\partial r}V_r=(m^2-1)\left[\rho_0\gamma^2+\frac{F^2}{4\pi}\right]$$

$$V_r+\gamma^2 r\frac{\partial\rho_0}{\partial r}V_r. \tag{VIII-7}$$

Equation (VIII-7) above must be solved subject to the boundary condition that $V_r = 0$ at $r = a$ and V_r is well behaved for $r = 0$.

Near $r = 0$, Eq. (VII-7) reduces to

$$\frac{\partial}{\partial r}r^3\frac{\partial V_r}{\partial r}=-r(1-m^2)\,V_r \tag{VIII-8}$$

so that the solutions have the form $V_r = r^n$. Solving for n, we find

$$n=-1\pm m. \tag{VIII-9}$$

For $m \geqslant 2$, one root is well behaved at $r = 0$ and one is not. The solution which is well behaved at zero goes as r^{m-1} so that $V_r = 0$ there. Hence the center of the plasma does not move.

On the other hand, if $m = 1$, the well behaved solution for V_r is constant at $r = 0$. Let us now see what this implies for the motion of the plasma center. If $\dfrac{\mathbf{i}_r}{\pi}$ is a unit vector in the r direction $V_r = \mathbf{V} \cdot \mathbf{i}r$. Near $r = 0$, V_r is a constant times $\cos{(\theta + kz)}$ and $\mathbf{i}_r = \mathbf{i}_x \cos\theta + \mathbf{i}y \sin\theta$. Therefore at $z = 0$, the velocity $\mathbf{V}$ is in the positive x direction, and at for instance $z = \pi/2k$, the velocity $\mathbf{V}$ is in the negative y direction. Clearly then, an $m = 1$ mode corresponds to a helical displacement of the center of the plasma.

Since modes with $m \geqslant 2$ do not displace the center of the plasma, the cylindrical geometry is not crucial and modes with $m \geqslant 2$ are not very different from analogous modes in slab geometry. On the other hand modes with $m = 1$ represent a rigid helical displacement of the center of the plasma. Since there is no analogous motion in a slab, we find that $m = 1$ modes in a cylinder can be very different from anything occurring in a slab. We now examine whether Eq. (VIII-7) predicts instability.

If $m \geqslant 2$, the coefficient of V_r on the right hand side of Eq.
(VIII-7) is positive for $p_o' < o$, so that if V_r is a monotonically increasing function of r as long as it is positive in the vicinity of $r = 0$. Thus there is no solution to Eq. (VIII-7) which satisfies the boundary condition at the wall, V_r $(r = a) = 0$; hence there are no unstable modes with $m \geqslant 2$.

If $m = 1$, the solution to Eq. (VIII-7) which is well behaved at the origin is V_r is constant. Since V_r is constant. Since V_r must vanish at the wall, it vanishes everywhere, so there are no unstable modes with $m = 1$ either.

Hence the conclusion is that in a cylinder, there are no unstable modes in ideal MHD which have two dimensional structure and no free surface. The reason is that the coefficient of V_r on the right hand side of Eq. (VIII-7) is always nonnegative, so that, as discussed in Chapter V, there can be no instability. However while this coefficient is not negative, it can be nearly zero wherever $F = 0$, that is wherever the perturbation is perpendicular to the ambient field. Thus small correction to either the two dimensional structure of the mode, or to ideal MHD (that is resistive effects might give rise to instabilities which are somehow centered near the positions where $F = 0$. In the next five subsections, we will see that this is indeed the case.

VIII.B — Ideal MHD Modes With $m \geqslant 2$

In this subsection we consider ideal MHD modes with $m > 2$. We deal with the full three dimensional mode structure and make no approximation concerning either B_θ/B_z of kr/m. The starting point is the linearized fluid equation and Maxwell's equation:

$$\gamma \rho_o \mathbf{V} = - \nabla \left[p + \frac{\mathbf{B}_o \cdot \mathbf{B}}{8\pi} \right] + \frac{(\mathbf{B} \cdot \nabla) \mathbf{B}_o}{4\pi} + \frac{(\mathbf{B}_o \cdot \nabla) \mathbf{B}}{4\pi} \quad \text{(VIII-10)}$$

$$\gamma \mathbf{B} = - \nabla \times \mathbf{V} \times \mathbf{B}_o \quad \text{(VIII-11)}$$

for the two vector quantities $\mathbf{V}$ and $\mathbf{B}$. Consistent with our usual notation, a quantity without a subscript is a perturbed quantity and a quantity with a zero subscript is an equilibrium quantity. The perturbed pressure is eliminated by the incompressibility condition

$$\nabla \cdot \mathbf{V} = 0.$$

The idea now is to reduce this set of equations to a single equation for V_r. The manipulations involved in this are tedious and are set out in the Appendix. The final result is

$$\frac{d}{dr} f \frac{dV_r}{dr} - hV_r = 0 \qquad \text{(VIII-12a)}$$

where

$$f = \frac{r^3 (\rho_o \gamma^2 + F^2/4\pi)}{k^2 r^2 + m^2} \qquad \text{(VIII-12b)}$$

$$h = \frac{2k^2 r^2}{k^2 r^2 + m^2} \frac{dP_o}{dr} + r \frac{k^2 r^2 + m^2 - 1}{k^2 r^2 + m^2} F^2$$

$$+ \frac{2k^2 r^3}{(k^2 r^2 + m^2)^2} \left[(kB_z)^2 - \left[\frac{mB_\theta}{r} \right]^2 \right]$$

$$+ \gamma^2 \left[\frac{\rho_o r k^2 B_{\theta o}^2}{4\pi (k^2 r^2 + m^2) \left[\frac{F^2}{4\pi} + \rho \gamma_o^2 \right]} - r^2 \frac{d}{dr} \left[\frac{\rho_o}{k^2 r^2 + m^2} \right] \right.$$

$$\left. + \rho_o r \frac{k^2 r^2 + m^2 - 1}{k^2 r^2 + m^2} \right] \qquad \text{(VIII-12c)}$$

and where F is given by Eq. (VII-4).

Notice that as long as $\gamma^2 > 0$, Eq. (VIII-12a) is nonsingular and one could simply solve it numerically for γ. This is the approach taken by Friedberg. However there are many insights that can easily be obtained analytically. Specifically, notice that Eq. (VIII-12a) is very similar in structure to Eq. (V-17), derived in our discussion of gravitational modes in a sheared field. That is, regions of negative h are unstable and regions of positive h are stabilizing. As long as $\frac{dP_o}{dr} < 0$, h will always be negative (for small γ) at least at the singular surface where $F = 0$ (of course $k^2 B_z^2 - \frac{m^2 B_\theta^2}{r^2} = 0$ where $F = 0$).

As in the case of g modes in a slab, for fixed $\gamma (\equiv \gamma_o)$ there will always be an unstable mode with $\gamma > \gamma_o$ as long as the eigenfunction $V_r(r)$ has a node between $r = 0$ and $r = a$. The first possibility then is that $V_r(r)$ has a node near $F = 0$ in the limit of $\gamma \to 0$. A calculation identical to that leading up to Eq. (V-30) shows that such a localized mode will be unstable as long as

$$-\frac{dP_o}{dr} \left\{ \frac{rB_{zo}^2}{8\pi} \left[\frac{1}{q} \frac{dq}{dr} \right]^2 \right\}^{-1} < \frac{1}{4} \qquad \text{(VIII-13)}$$

where we have used the fact that $q = \dfrac{r B_{zo}}{R B_{\theta o}}$ and $k = n/R$ for a toroidal plasma. Also, at the singular surface $q = -m/n$. This is the Suydam condition for instability.

A large q' can stabilize this mode, as shown in Eq. (VIII-13). To see that this is a shear stabilization, let us calculate the shear length in cylindrical geometry. Recall that in slab geometry, $k_{||} = k_y\, x/L_s$. In cylindrical geometry, then $k_{||} = \dfrac{(\mathbf{B}_o \cdot \nabla)}{|B_o|} = \dfrac{m/r\, B_{\theta o} + n/R\, B_{zo}}{(B_{\theta o}^2 + B_{zo}^2)^{1/2}}.$

Near the position r_s where $F = 0$, $k_{||} = \left[\dfrac{m}{r}\, \dfrac{B_{\theta o}}{[B_{\theta o}^2 + B_{zo}^2]^2}\, \dfrac{1}{q}\, \dfrac{dq}{dr} \right]$

$(r - r_s)$ so that if m/r is taken to correspond to k_y, then

$$L_s^{-1} = \frac{B_{\theta o}}{(B_{\theta o}^2 + B_{zo}^2)^{1/2}}\, \frac{1}{q}\, \frac{dq}{dr}. \qquad \text{(VIII-14)}$$

Now let us relate these pressure driven modes to the gravitational modes discussed in Chapter V. Setting $d/dr = F = 0$ in Eq. (VIII-12a) and taking the limit $m^2 \gg k^2 r^2$, it reduces to

$$\gamma^2 \rho_o r + \frac{\left[2\dfrac{dP}{dr} + \dfrac{B_{\theta o}^2}{4\pi r} \right] k^2 r^2}{m^2} = 0. \qquad \text{(VIII-15)}$$

Clearly, a negative pressure a gradient causes an instability whose growth rate is roughly

$$\gamma \sim \left[\frac{-P_o'}{\rho_o r} \right]^{1/2} \frac{kr}{m}. \qquad \text{(VIII-16)}$$

However since $F = 0$, $kr/m = B_{\theta o}/B_{zo}$. The radius of curvature of the field line is given by

$$\frac{1}{\mathbf{R}} = -\frac{(\mathbf{B}_o \cdot \nabla)\, \mathbf{B}_o}{|B_o|^2} = \frac{1}{r}\, \frac{B_{\theta o}^2}{B_{zo}^2 + B_{\theta o}^2}\, \mathbf{i}_r$$

and is directed outward. Thus the unstable mode is like a gravitational mode with $g\, \dfrac{\partial \rho_o}{\partial x}$ given roughly by $\dfrac{1}{\rho_o R}\, \dfrac{dP_o}{dx}$ where R is the radius of curvature of the field line. This is very similar to that derived in Chapters III and V.

To summarize, we have shown that modes very similar to gravitational modes can be driven unstable by a negative pressure gradient. These can be stabilized by shear as shown in Eq. (VIII-13). However the plasma is not necessarily stable if Eq. (VIII-13) is violated at every point. Equation (VIII-13) is only the condition for unstable modes localized about a particular singular surface. There also may be gross modes which are not localized. This possibility has been investigated by Newcomb. He examined when the solution of Eq. (VIII-12a) can have a node in the limit of small γ. One can of course also simply solve Eq. (VIII-12a) numerically, the approach taken by Freidberg.

VIII. C — Ideal MHD Modes With $m = 1$

For a cylindrical plasma in ideal MHD, one can always determine mode structure and growth rates by solving Eq. (VIII-12a) subject to proper boundary conditions at $r = 0$ and $r = a$. If $B_{\theta o} \sim B_{zo}$ and $kr \sim m$, as in for instance a reversed field pinch, there is no particular distinction between modes with $m = 1$ and modes with all other m. However in tokamak ordering, $B_{\theta o} \ll B_{zo}$, $kr \ll m$, the behavior of modes with $m = 1$ is strikingly different from the behavior of modes with all other m.

Recall from Chapter V that only those regions of the plasma having $h < 0$ (h is defined in Eq. (VIII-12c)) can drive instability. In tokamak ordering for $m \geq 2$, the second term in h is so large that h can only be negative in a small region around the singular surface. However for $m = 1$, this term nearly vanishes. If k is equal to $-n/R$, then in general, for $m = 1$ and $q(r)$ a monotonically increasing function of r, h will be negative from $r = 0$ to the radial position at which $q = 1/\eta$. Henceforth we specialize to the case of $n = 1$, so that the unstable region is within the $q = 1$ surface.

It was shown in Chapter VIII.A that motions with $m = 1$ are unique in another way, namely these are the only motions which displace the plasma center. Therefore these modes are expected to displace the entire central region of the plasma. We continue by calculating the growth rates and eigenfunctions for these modes and conclude by discussing physically what is happening.

ιι the limit of low growth rate, we neglect the γ^2 terms in h. Thus the equation describing the motion is still given by Eq. (VIII-12a) with

$$f = r^3 \left[\rho_o \gamma^2 + \frac{B_{\theta_o}^2}{4\pi r^2} (q-1)^2 \right] \qquad \text{(VIII-12b')}$$

$$h = \left[\frac{r}{R}\right]^2 \left[2 \frac{dP_o}{dr} + \frac{B_{\theta_o}^2}{r} (q-1)^2 + 2 \frac{B_\theta^2}{r} (1-q^2) \right]. \quad \text{(VIII-12c')}$$

Notice that h is multiplied by $(r/R)^2$ which is a small term. Therefore, V_r is given approximately by the solution to the equation

$$\frac{d}{dr} r^3 \left[\rho_o \gamma^2 + \frac{B_{\theta_o}^2}{4\pi r^2} (q-1)^2 \right] \frac{dV_r}{dr} = 0. \qquad \text{(VIII-18)}$$

As we will see shortly, V_r is nearly constant for r within the singular surface, and is nearly zero for r outside. Thus dVr/dr is nearly zero everywhere except in the vicinity of the singular surface $r \approx r_s$. Anticipating this result, and setting $q - 1 = q'(r - r_s)$, we find from Eq. (VIII-18)

$$\frac{dV_r}{dr} = \frac{\text{constant}}{r_s^3 \left[\rho_o \gamma^2 + \frac{B_{\theta_o}^2 (r=r_s)}{4\pi r_s} [q'(r-r_s)]^2 \right]}. \qquad \text{(VIII-19)}$$

Integrating once more,

$$V_r = K, \arctan \left[(r-r_s)/\left\{ \frac{4\pi \rho_o \gamma^2 r_s^2}{B_{\theta_o}^2 (r=r_s)(q')^2} \right\}^{1/2} \right] + K_2. \quad \text{(VIII-20)}$$

Thus, as long as $\gamma_o^2 \ll \frac{B_{\theta_o}^2 (q')^2}{4\pi \rho_o}$, V_r approaches a constant for $r - r_s \to \pm \infty$ and the two different values are smoothly connected in a narrow region of width $\left[\frac{4\pi \rho_o \gamma^2 r_s^2}{B_{\theta_o}^2 (r_s) q'^2} \right]^{1/2}$ about $r = r_s$. The proper boundary condition of course is $V_r (r = a) = 0$, which dictates the relation between K_1 and K_2

$$K_2 = - \pi/2 K_1. \qquad \text{(VIII-21)}$$

Also, we find

$$K_1 = - \frac{1}{\pi} V_r(r = 0). \qquad \text{(VIII-22)}$$

The eigenfunction $V_r(r)$ is shown in Fig. VIII-1.

Now we must solve for γ. Of course γ must result from the h term which drives the instability. Assuming that V_r is constant between $r = 0$ and $r = r_s$, we find that another relation for $\frac{dVr}{dr}$ is

Fig. VIII-1 — A plot of $V_r(r)$ for an $m = 1$ mode
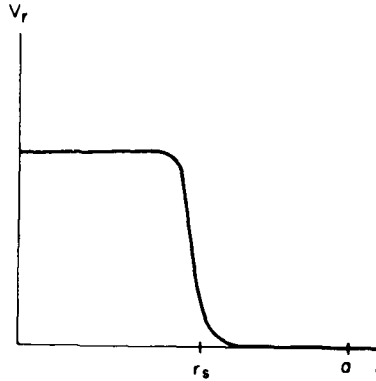
$$\frac{dV_r}{dr} = \frac{1}{\rho_o \gamma^2 r_s^3 + \dfrac{B_{\theta o}^2 (r = r_s) r_s}{4\pi} (q^1)^2 (r - r_s)^2}$$

$$\int_0^r h(r) V_r (r = 0). \qquad \text{(VIII-23)}$$

Now the $\dfrac{dVr}{dr}$ from Eq. (VIII-23) must be consistent with that derived in Eq. (VIII-19 or 20) in the limit as $r \rightarrow r_s$. This allows us to solve for γ the result being

$$\gamma = -2(\pi)^{3/2} \frac{1}{B_{\theta o} (r = r_s) r_s^2 q^1 \sqrt{\rho_o}} \int_0^{r_s} h(r) dr. \qquad \text{(VIII-24)}$$

Thus, as long as $\int_o^{r_s} h(r) < 0$, the mode is unstable.

We now discuss briefly the physical mechanism of this instability. As emphasized many times, the most unstable perturbations are always those which bend the field lines least. In slab geometry, with boundary conditions imposed at $\pm \infty$, this means that the perturbation is somehow localized near the singular surface. In cylindrical geometry however there is another possibility. A rigid displacement of a cylinder certainly does not bend any field lines. The problem is that a rigid displacement cannot satisfy the boundary condition $V_r (r = a) = 0$. The question then is, can only the inner part of the cylinder be rigidly displaced but still not bend the field lines?

To investigate this question, we first examine the fluid motion. The motions $V_r =$ constant for $r < r_s$ is of course something of an over-simplification. Clearly such motion cannot be incompressible. To describe more precisely this incompressible motion, imagine that in a

narrow layer of width δ about $r = r_s$, V_r decreases linearly to zero. In this case

$$V_\theta = \left\{ \begin{array}{l} 0, \\ -\dfrac{ir_s}{\delta} V_r \\ 0, \end{array} \left| \begin{array}{l} r < r_s, \\ r_s < r < r_s + \delta, \\ r_s + \delta < r, \end{array} \right| \begin{array}{l} V_r \\ V_r \dfrac{r_s + \delta - r}{\delta} \\ 0 \end{array} \right\} = V_r. \text{ (VIII-25)}$$

This motion is reminiscent of the tearing motion described in the last chapter. Assuming that the radial velocity goes as $\cos\left(m\theta + \dfrac{z}{R}\right)$, the velocity streamlines are shown in Fig. (VIII-2) at four different axial positions, $Z = 0$, $\pi R/2$, πR and $3\pi R/2$. The streamlines are solid lines, while the two circles $r = r_s$ and $r = r_s + \delta$ are dashed. Also shown on each plot are three dots labeled 1, 2 and 3. Dot number one corresponds to an initial position just inside the singular layer, where $q = 1$. Since the pitch of the field line is the same as the pitch of the perturbation, the same field line passes through all dots labeled 1. As the flow proceeds, for a time Δ_2 and Δ_3, the fluid element passes to positions 2 and 3, while the field line, of course, continues to interlace these points. In each of the four curves shown, the displacement between positions 1 and 2 and between 2 and 3 is the same except for a 90° rotation. Thus the field line is not bent or stretched as the fluid races around, from front to back, near the singular surface. For $r < r_s$ the fluid motions is a rigid displacement in the $(r\theta)$ plane which does not bend field lines. For $r_s < r < r_s + \delta$, the pitch of the field line is the same as the pitch of the perturbation, allowing the field line to be rigidly displaced around the singular layer. Therefore the type of motion shown in Fig. (VIII-2) does not initially bend field lines and is likely to be unstable.

Now examine the motion for a field line which at $\Delta = 0$ is not near the singular surface. In the standard tokamak configuration, $q < 1$ for $r < r_s$, so this field line winds a tighter helix at $\Delta = 0$. The cylinder which the field line is initially on is dotted in Fig. (VIII-2) and at the various Z's the field line passes through the points A. However, the field line does not enter the singular region at the same time anymore, since at some axial points it is initially closer, along a stream line, to the singular region. Thus some points of the field line whip around the singular region before other points do. Clearly, this involves considerable bending and stretching of the field line and is a stabilizing effect. Therefore as the motion proceeds, there is an opposing force, which increases with the displacement, rather like compressing a spring. The distortions of a field lines with $q = 1$ and $q < 1$ are
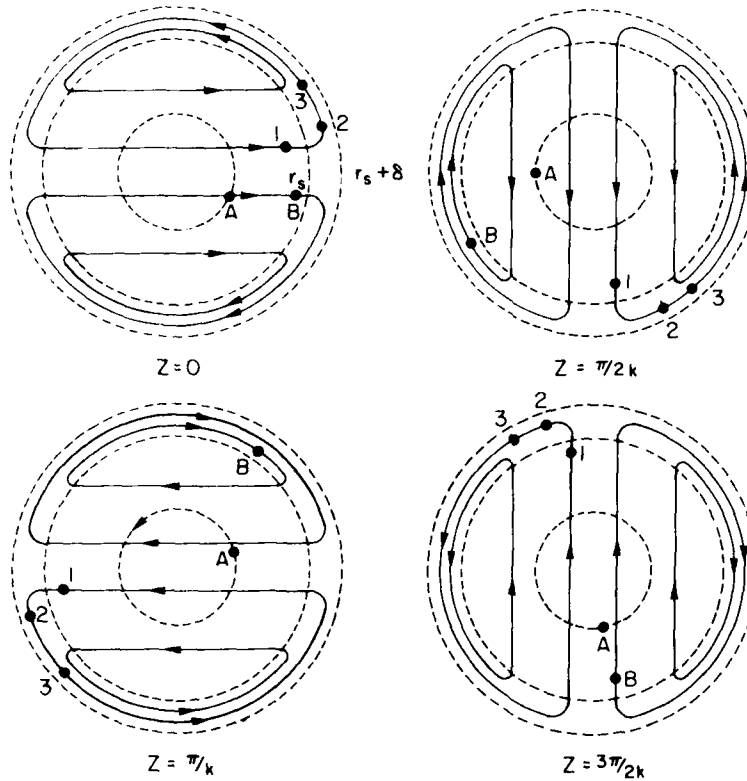
Fig. VIII-2 — The flow pattern at four axial positions. The dots labeled 1, 2, and 3 are intersections of a field line, having the same pitch as the flow, with these four planes at three different times. The points labeled A are intersections of a field line having $q < 1$ with these four planes. At $Z = 0$, point A is closer along a stream line to the separation region. Therefore it will enter this region first and will race around the cylinder before it does so at other axial positions. This will lead to considerable bending and stretching of the field line.

shown in Figs. (VIII-3 and 4). This lets us interpret somewhat the various effects which contribute to γ in Eq. (VIII-24). The integral h simply represents the average force which displaces the plasma, while the q' in the denominator represents the restraining force from the bending of the field lines. Of course if $q' = 0$, the analysis leading up to Eq. (VIII-24) is invalid. For $q' = 0$, however, the analysis leading up to Eq. (VIII-16) is still valid and we find that for zero shear, the growth rate is given by

$$\gamma^2 = 2P_o'/R^2\rho_0'\qquad\qquad\text{(VIII-26)}$$

so that there is instability if P_o' and ρ_o' have the same sign. The growth rate in Eq. (VIII-26) is much greater than that in Eq. (VIII-24), so the presence of shear slows down these modes but does not stabilize them.
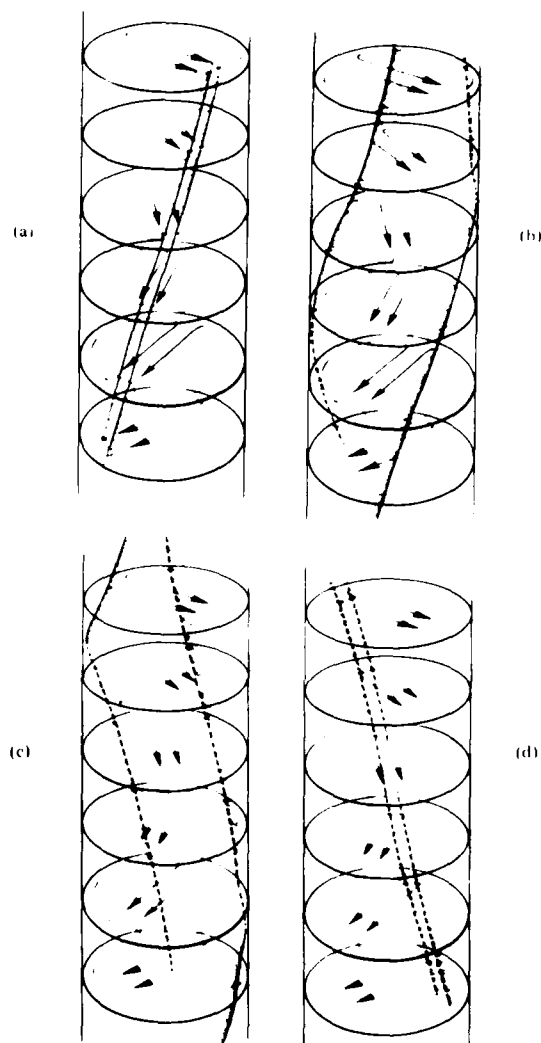
Fig. VIII-3 — A three dimensional view of the
motion of two neighboring field lines having $q =$
1 (same pitch as the flow). A solid field line
means it is near the front of the cylinder, dotted
means near the back. At $t = 0$ (a) the field lines
in front of the cylinder are convected towards the
separation region. At t_1, (b) they both enter the
separation region and whip around the cylinder in
opposite directions. At t_2 (c) they are continuing
around the edge. Finally at t_3 (d) they have both
re-entered the main rigid body flow, and now are
in back of the cylinder.
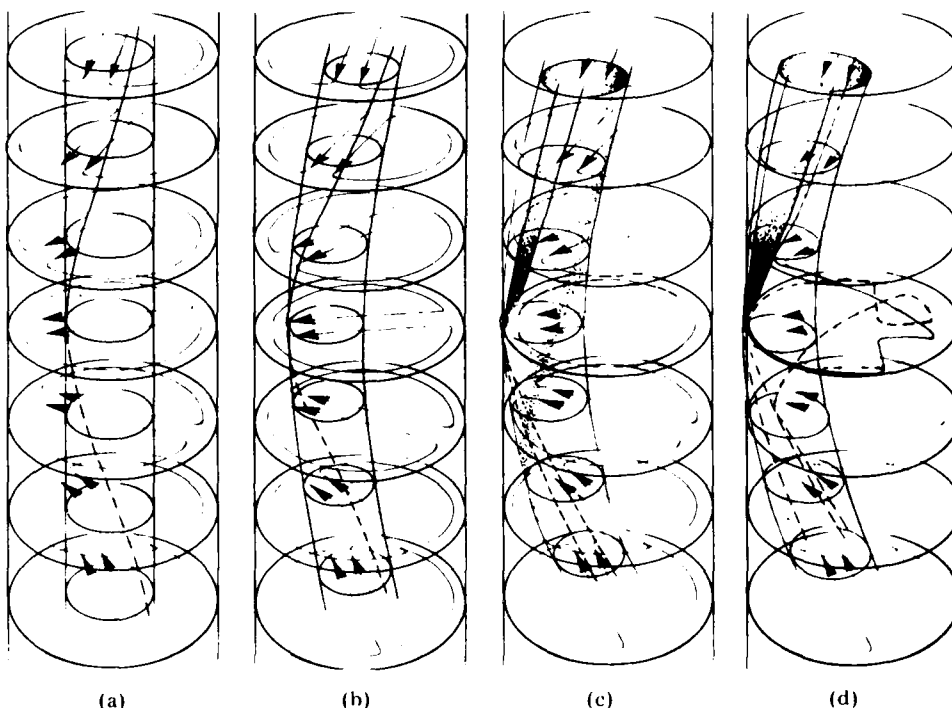
Fig. VIII-4 — A three dimensional plot of a field line having higher pitch ($q > 1$) than the flow pattern. At $t = 0$, the field line wraps around the inner cylinder shown in (a). At $t = t_1$, (b) this cylinder convects like a rigid body (in the $r\theta$ plane) with the main flow and the field line continues to wrap around it. At $t = t_2$ (c), the field line enters the separation region at one point and begins to whip around, while most of the field line just continues to move as a rigid body. At $t = t_3$, (d) most of the field line has entered separation region and the first part of the field line to enter the separation region has re-emerged out the other side of the cylinder. Clearly the field line is contorted much more than in Fig. VIII-3.

VIII. D — Resistive Instabilities for $m \geqslant 2$

In this section we discuss resistive instabilities in a plasma with $m \geqslant 2$. The two types of instabilities are resistive g modes and tearing modes. In Section VIII.B, it was shown that in a cylindrical plasma, there are simple analogous to g modes where $g \dfrac{\partial \rho_o}{\partial x} \approx \dfrac{1}{\rho_o R} \dfrac{dP_o}{dr}$.

Here R is the radius of curvature of the field lines and the sign is such that a negative pressure gradient gives rise to instability. In ideal MHD, these pressure driven modes could be stabilized by sufficient shear, as indicated in Eq. (VIII-13). However, in slab geometry, it was shown in Chapter VI that finite resistivity could destabilize these modes by allowing the plasma to leak through the sheared field. Clearly, in cylindrical geometry, we expect the same result to apply, namely that,

analogous to Eq. (VI-22), finite resistivity allows pressure driven modes to go unstable with a growth rate given by

$$\gamma \approx \left\{ \frac{1}{\rho_o R} \frac{dP_o}{dr} \left[\frac{mL_s}{r\, B_{\theta o}} \right] \right\}^{2/3} \left[\frac{c^2 \eta}{\rho_o} \right]^{1/3} \qquad \text{(VIII-27)}$$

where R is given in Eq. (VIII-17) and L_s in Eq. (VIII-14).

The tearing mode for $m > 2$ in tokamak ordering ($B_{\theta o} \ll B_{zo}$, $kr \ll 1$) also follows in a straight forward way from analogous results in slab geometry discussed in Section VII. That is if the inertial terms in Eq. (VIII-3) are set equal to zero, the equation for the perturbed field gives

$$\frac{1}{r} \frac{\partial}{\partial r} r \frac{\partial}{\partial r} r\, B_r = \left[\frac{m^2}{r} + \frac{4\pi m}{cF} \frac{dJ_{oz}}{dr} \right] B_r \qquad \text{(VIII-28)}$$

if $k = -n/R$, the quantity $F = B_\theta/r\, (m - nq)$ vanishes at the singular surface $r = r_s$ where $q = m/n$. The procedure now is exactly as it was for the slab (Chapter VII). First calculate solutions for Eq. (VIII-28) for $r < r_s$ and $r > r_s$ which satisfy the proper boundary conditions at $r = 0$ and $r = a$. If these solutions are normalized to have the same value of B_r at $r = r_s$, in general there will be a discontinuity in slope as one crosses r_s. Then if Δ (defined in Eq. (VII-17)) is positive the plasma is unstable to tearing modes. Since the width of the tearing layer is very small compared to r_s the connection between the two MHD solutions can proceed exactly as in slab geometry. Thus to see whether a cylindrical equilibrium in the tokamak ordering, is stable to tearing modes, one simply solves Eq. (VIII-28) numerically and investigates the condition for $\Delta > 0$. Calculations such as these have been made by a variety of authors. Stated very qualitatively, the conclusion is that for sufficiently smooth current profiles, tearing modes are stable if $m \geq 4$. For $m = 2$ or 3, the profile is typically unstable. However by tailoring the current profile, it is possible to stabilize these modes also.

We conclude this subsection with a simple physical picture illustrating the free energy which drives a tearing mode in an incompressible plasma. To begin, take Eq. (VIII-3), multiply by $\dfrac{iV_r^{\bullet} r}{m}$ and integrate over the plasma volume. Integrating the second derivative terms by parts and neglecting the end point contributions, we find the result:

$$2\pi\gamma\int_{o}^{a}rdr\,[\rho_{o}(|V_{r}|^{2}+|V_{\theta}|^{2})+\frac{1}{4\pi}\,(|B_{r}|^{2}+|B_{\theta}|^{2})]=$$

$$-2\pi\int_{o}^{a}rdr\,\frac{\gamma}{mcF}\,\frac{dJ_{oz}}{dr}\,|B_{r}|^{2}. \qquad \text{(VIII-29)}$$

In calculating Eq. (VIII-29) we have made use of the incompressibility condition to relate V_{θ} and B_{θ} to V_{r} and B_{r}. Notice that the left hand side of Eq. (VIII-29) is simply the rate of change of kinetic plus magnetic energy. The term on the right hand side then represents a driving term. This term can only drive instability in those regions of the plasma where $\frac{dJ_{o}}{dr}$ and F have opposite signs. If $\frac{1}{F}\,\frac{dJ}{dr}$ is everywhere positive, then one can easily show from Eq. (VIII-28), that for boundary conditions $B_{r}=0$ at $r=0$ and $r=a$, B_{r} is a monotonically increasing function of r for $r < r_{s}$ and a monotonically decreasing function of r for $r > r_{s}$. Thus $\Delta < 0$ and the plasma is stable. Hence $\Delta' > 0$ can only arise if $\frac{1}{F}\,\frac{dJ}{dr} < 0$, somewhere in the plasma.

In the standard tokamak configuration $\frac{dJ_{o}}{dr}$ is negative and $q(r)$ is a monotonically increasing function of r. Therefore since $F = B_{\theta}/r\,(m - nq)$, these terms have opposite signs for $m > nq$, or for radii less than the radius of the singular surface. Thus for a tearing mode in cylinder, the region inside the singular surface releases free energy; the region outside soaks some of it up. What is left over is deposited as Ohmic hearing near the singular layer.

It is instructive to examine physically the nature of this driving energy. Since the plasma motion is incompressible, the motion of each fluid element can be expressed as a displacement plus a rotation. We will consider for now the rotational part of the motion. The power input into rotation is the torque times the angular velocity. In Fig. (VIII-5) is shown a fluid element in polar coordinates between r and $r + dr$ and θ and $\theta + d\theta$. To calculate the torque, we calculate the difference between the θ components of the force on the two edges at r and $r + dr$. Clearly one element of this torque $\tau = \mathbf{r} \times \textbf{Force}$ is

$$\tau = \frac{\mathbf{i}_{z}}{2c}\left(\frac{dJ_{oz}}{dr}\,dr\right)-B_{r}dr. \qquad \text{(VIII-30)}$$

The problem now is to calculate the angular velocity of the fluid element about its own axis. To calculate the angular velocity about the axis, first subtract out the displacement of the axis. Then any variation

$$\Omega = \frac{1}{\Delta r} \frac{dV_r}{d\theta} \Delta\theta$$
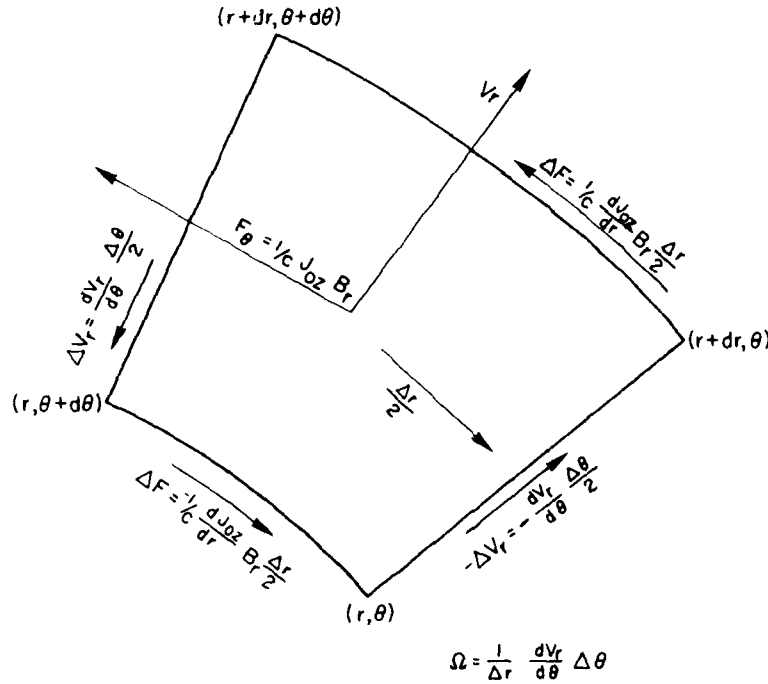
Fig. VIII-5 — A fluid element in cylindrical co-ordinates illustrating
how $\partial J_{oz}/\partial r$ can given rise to a torque which enhances the rotation

of radial velocity with polar angle θ must be a rigid rotation about the
axis. Thus this angular velocity, Ω is simply

$$\Omega = - \frac{iz}{dr} \frac{\partial V_r}{\partial \theta} d\theta \qquad\qquad \text{(VIII-31)}$$

where negative $\dfrac{\partial V_r}{\partial \theta}$ implies Ω is in the positive Z. In real notation,
the relation between B_r and V_r in ideal MHD is

$$\gamma B_r = \frac{1}{m} F \frac{\partial V_r}{\partial \theta}. \qquad\qquad \text{(VIII-32)}$$

Therefore

$$P = \tau \cdot \Omega = \frac{\gamma B_r^2}{2r \, F} \frac{d J_{oz}}{dr} \, rdrd\theta \qquad\qquad \text{(VIII-33)}$$

so that F and $\dfrac{dJ_{oz}}{dr}$ having opposite sign means that P is positive. Now
the interpretation is clear; when F and dJ_{oz}/dr have opposite signs, the
torque on a fluid element is in the same direction as the rotation,
thereby tending to increase the rotation.

VIII.E — Internal $m = 1$ Tearing Modes

As we have seen in Chapter VIII.C for tokamak ordering, modes with $m = 1$ can be driven unstable in ideal MHD by the three dimensional nature of the motion. However, as noted in VIII.C the basic motion is two dimensional and it consists of a rigid displacement in the $r\theta$ plane for $r < r_s$, coupled to a rapid flow around the edge of the cylinder defined by $r \sim r_s$. This motion is illustrated in Fig. (VIII-2). It is instructive to compare Fig. (VIII-2) with Fig. (VIII-1). Clearly these two types of motion are quite similar; in the former, a magnetized fluid collides and bounces off a stationary fluid, while in the latter, two fluids with equal and opposite velocity collide and bounce off each other. Since the fluid motions are so similar, we might expect that this $m = 1$ motion in a cylindrical plasma is also unstable if finite resistivity (and therefore magnetic reconnection) is allowed. Indeed, as is apparent from Fig. (VIII-4), if there is shear, the frozen in magnetic field lines have sharp turns which provide strong restraining forces. The presence of resistivity allows the lines to break and reconnect, so that they would appear as in Fig. (VIII-6). The field in Fig. (VIII-6) (analogous to that in Fig. (VIII-3)) has fewer sharp turns and thus provides weaker restraining forces. Thus for nonzero resistivity, there is more free energy to drive the instability.

Simpler diagrams illustrating the same point are shown in Figs. (VIII-7 and 8). For purely two dimensional $m = 1$ motion in a cylindrical plasma with $B_z = 0$, the frozen in field lines in the $(r\theta)$ plane are shown at four times in Fig. (VIII-7) (which is analogous to Fig. (VIII-2)). Clearly sharp corners develop where the field has to stretch to follow the fluid motion. However if nonzero resistivity is allowed, the fields here will break and reconnect so that the field pattern at $t = t_4$ appears as in Fig. (VIII-8) (analogous to Fig. (VIII-3)). In these figures, the dots are the magnetic 0 point singularities (nulls); the two dimensional field lines circle these points. For the case of ideal MHD, no new null point can be produced and as complicated as the field line gets, it circles the dot only once. However if resistivity is present, the topological constraint is relaxed and new nulls (also called islands) can be produced. In this case an island is produced near the cylinder wall **opposite** from the direction of flow.

If $B_z \neq 0$, the field surfaces are three dimensional. Figures (VIII-7 and 8) can be regarded as projections of the field lines back into the $Z = 0$ plane for ideal and resistive MHD. The dots then correspond not to nulls, but now to magnetic axes. In ideal MHD in
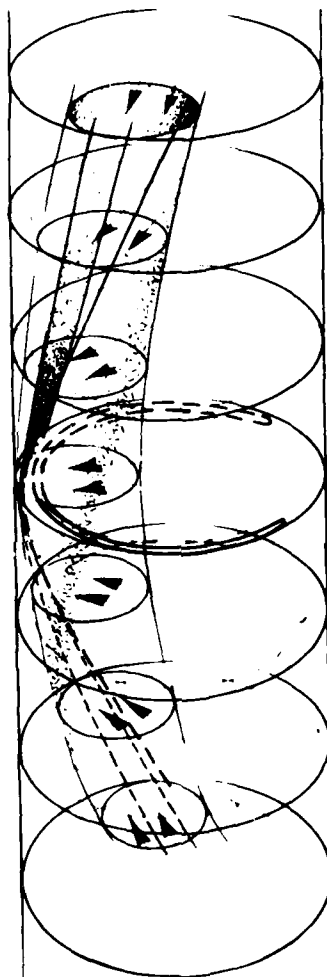
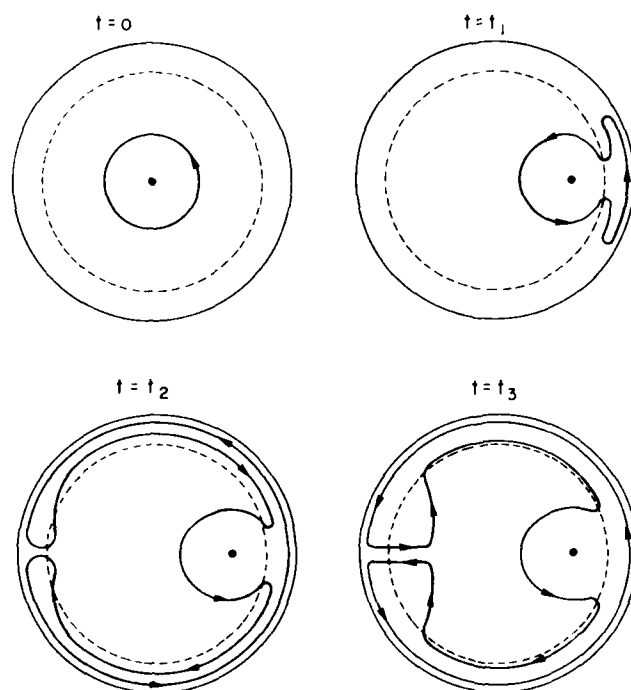Fig. VIII-6 — The field pattern, analogous to Fig. VIII-4c if magnetic reconnection is allowed

Fig. VIII-7 — A two dimensional field line in the r, θ plane which is frozen into the flow given by Eq. VIII-25. The field line is shown at four different times. Notice that it is rapidly convected around the separation layer and re-emerges into the main flow on the other side of the circle. At $t = t_3$ fields of opposite sign are forced next to each other in the separation layer and along a horizontal diameter on the left side of the circle.

Fig. VIII-8 — If the resistivity is non zero the nearby field of opposite sign can diffuse into each other and annihilate each other leaving the field pattern shown here. Notice a magnetic island is formed in the circle on the side opposite to the direction of flow.
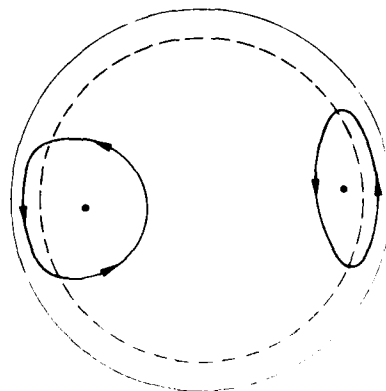
three dimensions the topological constraint preserves the number of times one field line winds about another. However if resistivity is present, new magnetic axes can be formed and the field lines can start to wind around new axes.

Now let us qualitatively discuss resistive $m = 1$ instabilities. As shown in Section (VIII.C), the velocity is constant for $r > r_s$. Thus, for ideal MHD, the expression for B_r has the functional form

$$B_r = \begin{cases} F = \dfrac{B_\theta}{r}\,(q - 1) & r < r_s \\ 0 & r > r_s. \end{cases} \qquad \text{(VIII-34)}$$

Since B_r vanishes at $r = r_s$, the quantity Δ from Chapter VII is infinite and the theory of tearing modes described there does not apply. The growth rate must be calculated by solving the coupled equations

$$i\gamma \left[\frac{1}{r} \frac{\partial}{\partial r} r\rho_o \frac{\partial}{\partial r}(rV_r) - \frac{\rho_o V_r}{r} \right] \frac{1}{c} \left\{ B_r \frac{\partial J_{oz}}{dr} + \frac{cF}{4\pi} \right.$$

$$\left. \left(-\frac{1}{r}\frac{\partial}{\partial r} r \frac{\partial}{\partial r}(rB_r) + \frac{B_r}{r} \right) \right\} \qquad \text{(VIII-35a)}$$

$$\gamma\, B_r = iFV_r + \frac{\eta c^2}{4\pi} \frac{\partial^2}{\partial r^2}\, B_r \qquad \text{(VIII-35b)}$$

subject to proper boundary conditions.

We will not follow this route, but instead will derive a qualitative expression for the growth rate by balancing power released in the outer MHD region with Ohmic power dissipated in the inner region near the singular surface. Since the motion is two dimensional and incompressible, the velocity is the curl of a vector potential $\mathbf{Q}$ where

$$\mathbf{Q} = -\, i\, rV_r\, \mathbf{i}_z. \qquad \text{(VIII-36)}$$

Then, as calculated in Chapter VII, the power liberated per unit length is:

$$P_F = \int (iV_r^*) \cdot \nabla \times \mathbf{F}|_z\, d_r^2. \qquad \text{(VIII-37)}$$

The Z component of $\nabla \times \mathbf{F}$ was calculated in Section VIII.A and the result is

$$P_F = -2\pi \int r dr \, \frac{\gamma r B^*}{F} \left\{ \frac{1}{c} B_r \frac{dJ_{oz}}{dr} + \frac{F}{4\pi} \right.$$

$$\left. \left[-\frac{1}{r} \frac{\cdot d}{dr} r \frac{d}{dr} r B_r + \frac{B_r}{r} \right] \right\}. \tag{VIII-38}$$

The quantity in the curly brackets vanishes in the outer MHD region, exactly as in Chapter VII. However near the singularity, the bracket is no longer zero, since ideal MHD with $\gamma = 0$ is no longer an accurate description of the plasma. In a narrow region of width x_c the slope of B_r goes from zero to some constant value. Thus $d^2 B_r / dr^2$ is the dominant term in the bracket. The functional form of $B_r(r)$ is shown in Fig. (VIII-9) as the solid curve, while the ideal MHD solution is shown as the dotted curve. Clearly, B_r and $\dfrac{d^2 B}{dr^2}$ have the same sign, so that P_F is positive and energy is available to drive instability. If the value of B_r at $r = r_s - x_c$ is denoted B_{rc}, Eq. (VIII-38) yields the approximate expression,

$$P_F \approx \frac{\gamma \, r_s^3 \, |B_{rc}|^2}{2x_c}. \tag{VIII-39}$$

The Ohmic power per unit length dissipated in the singular layer is given roughly by

$$2\pi r_s \, x_c \, \eta J_z^2 \tag{VIII-40}$$

where J_z is the current flowing in the singular layer. However

$$J_z \approx \frac{c}{4\pi} \frac{B_{\theta c}}{x_c} \approx \frac{cr_s}{4\pi} \frac{B_{rc}}{x_c^2} \tag{VIII-41}$$

where the first relation in Eq. (VIII-41) comes from Maxwell's current equation and the second from $\nabla \cdot \mathbf{B} = 0$. Then combining Eq. (VIII-39 and 40) we find

$$\gamma \approx \frac{\eta c^2}{4\pi \, x_c^2}. \tag{VIII-42}$$

The only problem now is to determine x_c in terms of γ and η. The procedure here is exactly the same as in Chapter VII. Namely, substitute for the $\dfrac{d^2 B_r}{dr^2}$ term in Eq. (VIII-35a) from Eq. (VIII-35b). Then, exactly as in Eq. (VII-23),

$$x_c \approx \left\{ \frac{\rho \, \gamma \eta c^2}{(F')^2} \right\}^{1/4}. \tag{VIII-43}$$
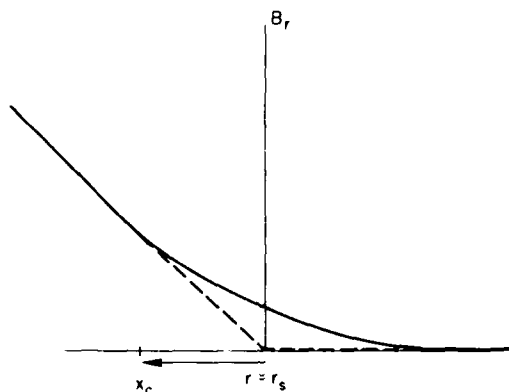
Fig. VIII-9 — A plot of B_r as a function of r
for an $m = 1$ tearing mode

This then gives the results

$$\gamma \approx \frac{(\eta c^2)^{1/3}}{(4\pi)^{2/3}} \left\{ \frac{(F')^2}{\rho_o} \Big|_{r=r_s} \right\}^{1/3} \qquad \text{(VIII-44)}$$

and

$$x_c \approx (\eta c^2)^{1/3} \left\{ \frac{\rho}{4\pi \ (F')^2} \Big|_{r=r_s} \right\}^{1/6}. \qquad \text{(VIII-45)}$$

Thus, one can derive in a fairly simple way the basic results of $m = 1$ tearing modes.

VIII.F — Double Tearing Modes

We conclude this chapter with a study of double tearing modes; that is tearing modes which are excited when there are two zeros of F near each other. For tokamak ordering, this generally means a current density which is not a monotonically decreasing function of radius, but which peaks at some radius, in other words a skin effect. This can be seen from Fig. VIII-10a and b. The solid curves are normal current density and poloidal field as a function of radius. The dotted curves show the effect of a narrow skin layer on both J and B_θ. Since $F = B_{\theta o}/r - kB_z$, F clearly has basically the same behavior near r_c as the dotted curve in Fig. (VIII-10b).

To investigate the stability of such a configuration, first look at the regions of the plasma where ideal MHD is valid. Using the definition of F and Maxwells current equation, Eq. (VIII-28) can be reduced to
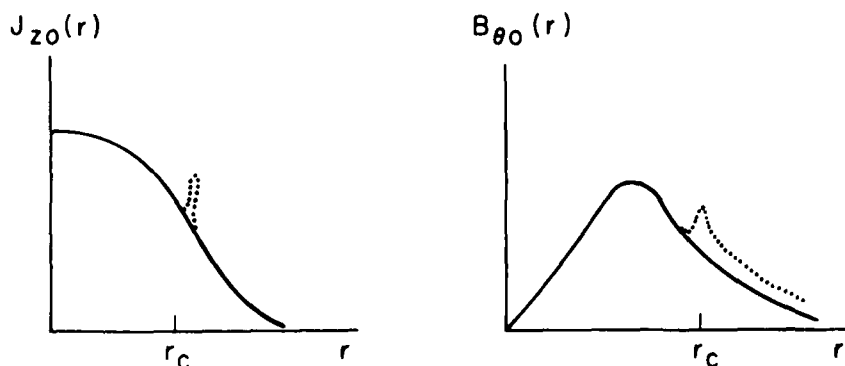
Fig. VIII-10 — Schematic diagram showing how the skin effect
can give rise to non-monotonic $q(r)$ profile

$$\frac{F}{r^2}\frac{d}{dr}r^3\frac{dB_r}{dr} = \frac{B_r}{r^2}\frac{d}{dr}r^3\frac{dF}{dr} + F\frac{m^2-1}{r}\cdot B_r. \quad \text{(VIII-46)}$$

This equation is to be solved subject to appropriate boundary conditions
at $r = 0$ and $r = a$.

If r_{c1} and r_{c2} are the positions where F vanish, and if
$r_{c1} - r_{c2} \ll r_c$, then $r \sim r_c$, the second term on the right hand side of
Eq. (VIII-46) is much smaller than the first, and can be neglected.
Making this approximation, one can easily construct a solution to Eq.
(VIII-46) which satisfies boundary conditions at $r = 0$ and $r = a$ and is
everywhere continuous. The solution is

$$B_r = \begin{cases} 0 & r < r_{c2} \\ F & r_{c2} < r < r_{c1}. \\ 0 & r_{c1} < r \end{cases} \quad \text{(VIII-47)}$$

This is analogous to the solution for B_r for $m = 1$ tearing modes.
If ρ_o, η and F' have the same value at $r = r_{c1}$ and r_{c2}, an analysis like
that in the previous section gives Eq. (VIII-44 and 48) for growth rate
and size of singular region. (Of course $x_c \ll r_{c1} - r_{c2}$ is also
assumed.) Notice that the growth rate for a skin current goes as $\eta^{1/3}$,
whereas for a normal tearing mode it goes as $\eta^{3/5}$. Since η is a small
quantity, a double tearing mode grows much faster than a conventional
tearing mode.

Since the ideal MHD relation between V_r and B_r is $\gamma B_r = iFV_r$,
the solution for B_r in Eq. (VIII-47) gives

$$V_r = \begin{cases} 0 & r < r_{c2} \\ \text{constant} & r_{c2} < r < r_{c1} \\ 0 & r_{c1} < r \end{cases} \qquad \text{(VIII-48)}$$

The flow pattern is then that which is characteristic of tearing modes, namely a fluid collides with and recoils off a stationary fluid. Such a flow pattern is illustrated in Fig. (VIII-11) for the case of $m = 4$.
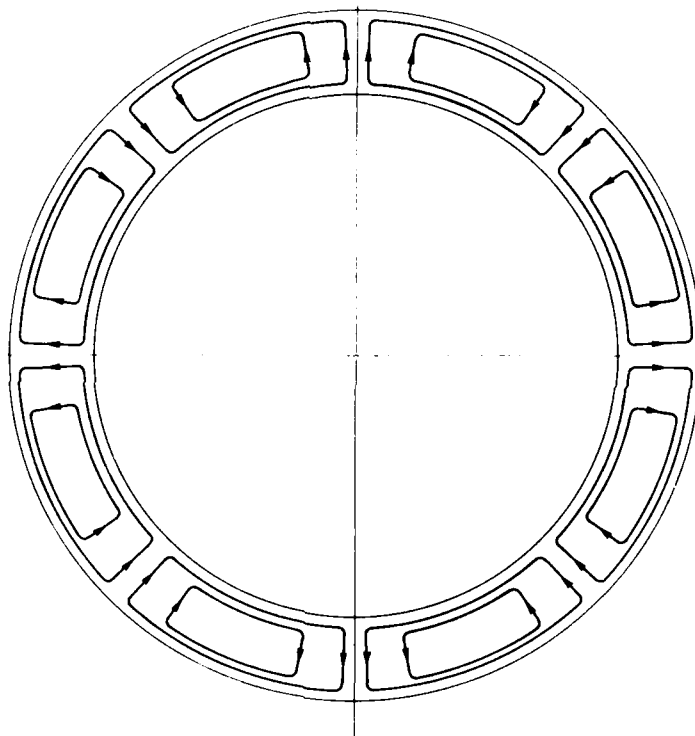
Fig. VIII-11 — The flow pattern for an $m = 4$ double tearing mode

An early work on the MHD stability in cylindrical geometry is:

Hydromagnetic Stability of a Diffuse Linear Pinch, William Newcomb, Ann. Phys., **10**, 232 (1960).

Other results from ideal MHD analysis are in:

Magnetohydrodynamic Stability of a Diffuse Linear Pinch, J.P. Freidberg, Phys. Fluids, **13**, 1810 (1970).

High Beta Diffuse Pinch Configurations, D.C. Robinson, Plasma Phys., **13**, 439 (1971).

The MHD Stability of the $m = 1$ mode in cylindrical geometry is taken from:

Nonlinear Properties of the $m = 1$ Kink Instability in the Cylindrical Tokamak, M.N. Rosenbluth, R.Y. Dagazian, and P.H. Rutherford, Phys. Fluids, **16**, 1894 (1973).

The tearing mode in cylindrical geometry is studied in:

Tearing Mode Stable Diffuse Pinch Configurations, D.C. Robinson, Nuclear Fusion, **18**, (1978).

The $m = 1$ kink tearing mode was studied in:

Resistive Internal Kink Modes, B. Coppi, R. Galvão, R. Pellat, M.N. Rosenbluth, and P.H. Rutherford, Sov. Phys. Plasma Phys., **2**, 533 (1977).

The theory of a double tearing mode can be found in:

Linear Analysis of the Double Tearing Mode, P.L. Prickett, Y.C. Lee, and J.F. Drake, Phys. Fluids, **23**, 1368 (1980).

Tearing and Resistive Interchange Modes in a cylinder including compressibility, Hall terms in the momentum equation and field curvature and pressure gradient instead of gravity and density gradient have been studied in:

B. Coppi, Phys. Fluids, **7**, 1501 (1964).

P.J. Tayler, J. Nucl. Energy PLC, **5**, 345 (1963).

B. Coppi, Phys. Rev. Lett., **15**, 417 (1964).

B. Coppi, Phys. Fluids, **8**, 2273 (1965).

J.M. Finn and W.M. Manheimer, Phys. Fluids, **25**, 697 (1982).

J.M. Finn, W. Manheimer and T.M. Antonsen, Phys. Fluids, **26**, 962 (1983).

R. Dagazian, Nucl. Fusion, **21**, 1599 (1981).

Chapter IX

INSTABILITIES IN A TOROIDAL PLASMA

In this chapter, we just touch upon the question of MHD instabilities in toroidal geometry. The actual calculations of relevant instabilities has many more mathematical complications than the equivalent calculations in slab or cylindrical geometry because toroidal plasmas are inherently two dimensional. For instance if the toroidal co-ordinates are as shown in Fig. (IX-1), the equilibrium is symmetric in toroidal angle ζ, but depends on the two variables r and θ. Thus calculating the stability involves a two dimensional eigenvalue equation in r and θ, rather than one dimensional calculations (in r for cylindrical geometry, or in x for slab geometry) as done in the preceding chapters.
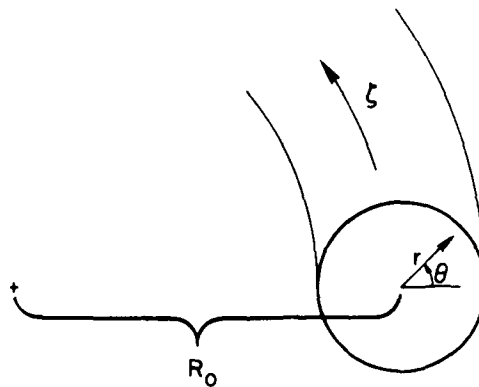
Fig. IX-1 — The toroidal co-ordinate
r, θ, and ζ

We will not attempt such a two dimensional calculation here; rather will examine first how modes in cylindrical plasmas are affected by toroidicity, and second will show that there are instabilities in a toroidal plasma which have no analog in cylindrical geometry. In tokamak ordering, the results are that free surface modes and tearing modes exist as in cylindrical geometry. The pressure driven modes, described in Chapter VIII.B, are stabilized of $q > 1$. Finally a new

125

mode, usually called a ballooning mode, can exist in the regions of locally bad curvature. These ballooning modes give rise to a pressure limit for tokamak plasmas.

We now examine these points more thoroughly. In the tokamak ordering, $a \ll R$, $B_\theta \ll B_z$, and all toroidal effects will be small by a factor of at least a/R. However in deriving the equations for modes with two dimensional structure in cylindrical geometry (Eqs. (IV-35) or (VIII-7)), all terms of order a/R were neglected. Therefore, any instabilities which exist in this approximation for a cylindrical plasma should also exist in toroidal geometry if a/R. The relevant instabilities are then the free surface modes described in Chapter IV and the tearing modes described in Chapter VIII.A-F. However, as pointed out in Chapter VIII.A, a plasma with no free surface and with zero resistivity is stable to modes with two dimensional structure. Now let us examine the pressure driven modes discussed in Chapter VIII.B. These modes were driven by a pressure gradient, and as is apparent from Eq. (VIII-12c), the driving term is multiplied by $k^2 r^2 \sim (r/R)^2$. However toroidal effects are also of this order, so that these pressure driven modes can be strongly affected. Calculation of the exact stability condition is mathematically involved and was first given by Mercier and also by Shafranov, and others.

These analyses are almost always done in flux co-ordinates, where one co-ordinate component in taken to be constant along a field line or flux surface. The simplest result for sheer stabilization of pressure driven modes in a torus is for a high aspect ratio torus with low beta and circular flux surfaces. The result is that the condition for shear stabilization of pressure driven modes is given by

$$- (1 - q^2) \frac{dp_o}{dr} \left\{ \frac{r B_{z0}^2}{8\pi} \left[\frac{1}{q} \frac{dq}{dr} \right]^2 \right\}^{-1} < 1/4. \qquad \text{(IX-1)}$$

It is different from the analogous cylindrical geometry result only by the factor $(1 - q^2)$. Although this seems like a very simple result, this does not appear to be so. Shafranov, who makes all approximations with regard to flux surfaces, etc., at the outset, must still use a fairly complex co-ordinate system. He finds the $1 - q^2$ factor in Eq. (IX-1) is the result of a combination of three effects; the radius of curvature of the toroidal field, which is stabilizing at small major radius and destabilizing at large major radius; the outward shift of the flux surfaces, which results from the toroidal nature of the equilibrium, and the poloidal variation in the pitch of the field lines.
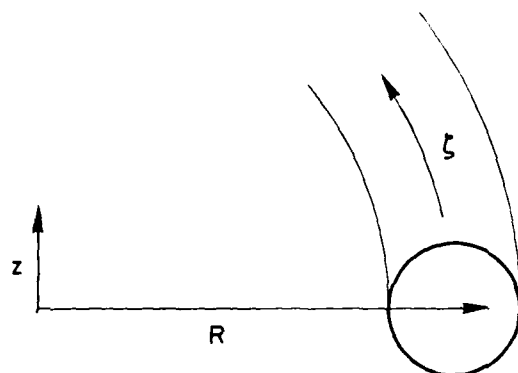
Fig. IX-2 — The toroidal co-ordinate R, z and ζ

However this toroidal effect plays quite an important role. It *implies* that tokamaks, which are characterized by $q > 1$, are stable to pressure driven modes. Reversed field pinches, however, which have $q < 1$, are potentially unstable to pressure driven modes in ideal MHD if the shear is not great enough, and are also potentially unstable to resistive g modes no matter what the shear is.

We close this chapter by qualitatively examining the problem of ballooning modes in tokamaks. Recall that any pressure driven mode is ultimately driven by a pressure gradient which has a component in the direction of the radius of curvature of the field line (see for instance Eq. (III-41). In a toroidal plasma there two components of the field line curvature. First there is the curvature of the poloidal field $\kappa_p \approx (B_{\theta o}^2/B_{zo}^2 \, r)\mathbf{i}_r$ which drives pressure modes in cylindrical geometry as the previous chapter. Secondly there is the curvature of the toroidal field line $\kappa_T \approx \mathbf{i}_R/R$ which has no analog in cylindrical geometry. Generally $\kappa_T \gg \kappa_p$. However $\kappa_T \cdot \nabla p$ nearly averages to zero along the field line. For instance at $\theta = 0$, $\nabla p \sim -\mathbf{i}_r = -\mathbf{i}_R$, while at $\theta = \pi$, $\nabla p \sim -\mathbf{i}_r = +\mathbf{i}_R$. Thus if the mode structure is uniform along the field line, as for a flute mode, the effect of the curvature of the toroidal field should not be dominant. This naturally brings up the following question: Can a mode be localized along a field line so that it only sees the positive, destabilizing, values of $\kappa_T \cdot \nabla p$ (around $\theta \approx 0$) and not the negative, stabilizing, values? We will see that such instabilities can indeed by generated if the plasma pressure is too high. These are usually called ballooning modes, probably in comparison to the behavior of a balloon of varying thickness. Imagine a balloon whose thickness varies around its surface, also imagine a second balloon of uniform thickness equal to the average thickness of the first. Say that someone is too weak to blow up and pop the second balloon; he might still be

able to blow up and pop the first, because it blows out much more easily where the surface is thin.

This is then analogous to an MHD instability in a tokamak picking out the most unstable (outer) region and localizing itself there. Of course, it is not so simple for a mode to localize itself along a field line. Any disturbance which is localized along a field line is also setting up shear. Alfven waves, which tend to give a positive frequency V_A^2/L^2 where L is the characteristic length of the disturbance along the field line and V_A is the Alfven speed. The distance L is given roughly by the characteristic distance along a field line, Rq. The maximum growth rate is given roughly by the maximum value of g divided by the gradient scale length, taken here as $1/r$. The plasma can only be stable if the outward motion forced by the pressure gradient does not overcome the resistance to field line bending, or if

$$\frac{V_i^2}{Rr} < k_{11}^2 V_A^2 \sim \frac{V_A^2}{R^2 q^2}$$

where V_i in the ion thermal velocity. This gives rise to an approximate limit on the total β of a tokamak of

$$\beta = \frac{V_i^2}{V_A^2} \lesssim \frac{r}{Rq^2} \cdot \qquad (IX\text{-}2)$$

Now let us show how this basic result can be obtained more rigorously by modeling the system with a slab in a gravitational field which is spatially dependent. If we assume slab geometry with all perturbed quantities varying as $f(z) \exp i ky$, $\mathbf{B}_o$ uniform and in the z direction, the density gradient in the x direction, and g varying with z, an analysis similar to that which led to Eq. (V-17) gives the result

$$\left[-\gamma \rho_o - \frac{B_o^2}{4\pi\gamma} \frac{\partial^2}{\partial z^2} \right] V_x + \frac{1}{\gamma} \frac{\partial \rho_o}{\partial x} g(z) V_x = 0 . \qquad (IX\text{-}3)$$

Specializing to a tokamak, where $\dfrac{\partial}{\partial z} = \dfrac{1}{Rq} \dfrac{\partial}{\partial \theta}$ and $g(z) = \dfrac{V_i^2 \cos\theta}{R}$, we find that Eq. (IX-3) reduces to

$$\left\{ -\frac{V_A^2}{R^2 q^2} \frac{d^2}{d\theta^2} + \gamma^2 - \frac{V_i^2 \cos\theta}{RL_n} \right\} V_x(\theta) = 0 \qquad (IX\text{-}4)$$

where L_n is the gradient scale length. Notice that the last term in the parentheses is periodic in θ with period 2π. However the solution for $V_x(\theta)$ must also be periodic with the same periodicity, since V_x must be a single valued function of θ. Thus γ is determined by the condition

that solutions to Eq. (IX-4) exist which are periodic in θ with period 2π. An approximate criterion for unstable roots can be derived as follows. If $\gamma = 0$, the solutions to Eq. (IX) are oscillatory between $-\pi/2 < \theta < \pi/2$ and are exponentially growing and damping for $\pi/2 < |\theta| < \pi$. Imagine a solution for V localized between $-\pi/2$ and $\pi/2$ and which damps to a very small value between say $\pi/2 < \theta < \pi$. Then the solution for V_x between $-\pi/2$ and $\pi/2$ does not affect the solution for V_x between say $3\pi/2$ and $5\pi/2$. The condition for a solution to Eq. (IX-4) with zero γ is simply the condition for localized roots between the turning points, or according to WKB theory,

$$\int_{-\pi/2}^{\pi/2} d\theta \ \frac{V_i}{V_A} \ q \left[\frac{R}{L_n} \cos \theta \right]^{1/2} = \pi/2 . \qquad \text{(IX-5)}$$

The eigenfunction is as shown in Fig. (IX-3). Notice that between $\pi/2 < \theta < \pi$, V_x gets so small that it does not affect the value of V_x

Fig. IX-3 — The eigenfunction (dotted curve) and local wave number squared (solid curve) for ballooning modes in a tokamak

in $3\pi/2 < \theta < 5\pi/2$, where V_x gets large again. Using the fact that

$$\int_{-\pi/2}^{\pi/2} \sqrt{\cos}\, d\theta = \frac{\pi\, \Gamma\left[\frac{3}{2}\right]}{\sqrt{2}\left[\Gamma\left[\frac{5}{4}\right]\right]^2}$$ we find that the plasma is unstable if

$$\frac{V_i^2}{V_A^2} > 0.42\, \frac{L_n}{Rq^2}. \qquad \text{(IX-6)}$$

This condition then puts a limit on the maximum pressure which can be stably confined in a tokamak. If the plasma is unstable, growth rates can be calculated in an analogous way by setting

$$\oint d\theta \left[\frac{2V_i^2 q^2 \cos\theta}{R\, L_n\, V_A^2} - \gamma^2\right]^{1/2} = \pi. \qquad \text{(IX-7)}$$

The problem of ballooning modes in sheared fields, and with nonzero resistivity is much more complicated and is still under active investigation.

The first calculation of both interchange and ballooning modes in a plasma with no shear is in:

I. Bernstein, et al., Proc. Roy. Soc. (London), **A224**, 17 (1958).

The Mercier condition for stability of interchange modes in a torus is given in:

C. Mercier, Nuclear Fusion, **1**, 47 (1960).

Stability Criteria for Arbitrary Hydromagnetic Equilibria, J.M. Greene and J.L. Johnson, Phys. Fluids, **5**, 510 (1962).

Conditions for Flute Instability of a Toroidal Geometry Plasma, V.D. Shafranov and E.I. Yurchenko, Sov. P,hys. JETP **26**, 682 (1968).

As of this time, ballooning modes in tokamaks are under active investigation because of their relevance to pressure limits in tokamaks. Some recent work includes:

Topology of Ballooning Modes, B. Coppi, Phys. Rev. Lett., **39**, 939 (1977).

Theory of Ballooning Modes in Tokamak with Finite Shear, D. Dobrott, D.B. Nelson, J.M. Greene, A.H. Glasser, M.S. Chance, and E.A. Frieman, Phys. Rev. Lett., **39**, (1977).

Stability Limitations on High Beta Tokamaks, A.M. Todd, M.S. Chance, J.M. Green, R.C. Grimm, J.L. Johnson, and J. Manickam, Phys. Rev. Lett., **38**, 826 (1977).

A very ingenious way to reduce the ballooning mode problem for high mode number to a one dimensional problem is given in

Shear, Periodicity and Plasma Ballooning Modes, J.W. Connor, R.J. Hastie, and J.B. Taylor, Phys. Rev. Lett., **40** 396 (1978).

A study of resistive modes in a toroidal plasma is in:

Resistive Instabilities in General Toroidal Configurations, A.H. Glasser, J.M. Greene, and J.L. Johnson, Phys. Fluids, **19**, 567 (1976).

A study of ballooning modes in a reversed field plasma is given in:

Ballooning and Interchange Stability in Anisymmetric Field Reversed Equilibria, John Finn, Phys. Fluids, **24**, 274 (1981).

Chapter X

QUASI-LINEAR THEORY OF MHD INSTABILITIES

This chapter begins the second part of this book, that concerning the nonlinear theory of MHD instabilities. Before commencing it is necessary to point out that the nonlinear theory of MHD instabilities is not nearly as well developed as the linear theory and much of what will be discussed here is necessarily more speculative than the material discussed in the preceding chapters, which treated the linear theory.

We begin by examining the quasi-linear theory of MHD instabilities in which the perturbed velocities are non-singular. This applies potentially to $m = 1$ kink tearing modes and double tearing modes (Chapters VIII E and F) as well as to ideal MHD modes. In this and the next chapter we change the notation slightly from that in the previous chapters. Now any quantity (say A) will be denoted by $<A> + \tilde{A}$ where $<A>$ is the ensemble average and $\tilde{A}$ is the perturbation about the ensemble average. Ensemble averaging will be denoted by angular brackets.

For instance, if we restrict ourself to cylindrical geometry, A is a function of radius only, and

$$\tilde{A} = \sum_{m-k \neq 0} A(r,m,k) \exp i(kz + m\theta) + c.c. \qquad (X\text{-}1)$$

the $\neq 0$ under the summation indicating m and k are not both $= 0$. Since any physical quantity must be real, the complex conjugate is added on in Eq. (X-1). The process of taking the ensemble average can then be defined as an average over θ from zero to 2π and an average over z from 0 to L, where L is either a periodicity length if such a length exists or else is some very large length. Clearly $<\tilde{A}> = 0$, but

$$<\tilde{A}\tilde{B}> = \sum_{k,m \neq 0} A(r,m,k) B^*(r,m,k) + c.c. \qquad (X\text{-}2)$$

Expressing the fluid quantities in this way, the four fluid equations for ρ, $\mathbf{V}$, $\mathbf{B}$ and p become

$$\frac{\partial}{\partial t} (<\rho> + \tilde{\rho}) + \nabla \cdot (<\rho> + \tilde{\rho})(<V> + \tilde{V}) = 0 \qquad \text{(X-3a)}$$

$$(<\rho> + \tilde{\rho}) \frac{\partial}{\partial t} (<V> + \tilde{V}) + (<\rho> + \tilde{\rho})(<V> + \tilde{V})$$

$$\cdot \nabla (<V> + \tilde{V}) = - \nabla (p + \tilde{p})$$

$$+ \frac{1}{4\pi} \{\nabla \times (<B> + \tilde{B})\} \times (<B> + \tilde{B}) \qquad \text{(X-3b)}$$

$$\frac{\partial}{\partial t} (<B> + \tilde{B}) = \nabla \times (<V> + \tilde{V}) \times (<B> + \tilde{B}) \qquad \text{(X-3c)}$$

$$\frac{\partial}{\partial t} (<p> + \tilde{p}) + (<V> + \tilde{V}) \cdot \nabla (<p> + \tilde{p})$$

$$+ \frac{5}{3} (<p> + \tilde{p}) \nabla \cdot (<V> + \tilde{V}) = 0 \qquad \text{(X-3d)}$$

where we have assumed $\gamma = 5/3$ to avoid confusion between the adiabatic γ and the growth rate.

The first step is to take the ensemble average of (Eqs. X-3). The result is

$$\frac{\partial <\rho>}{\partial t} + \nabla \cdot <\rho><\tilde{V}> = - \nabla <\tilde{\rho}\tilde{V}> \qquad \text{(X-4a)}$$

$$<\rho>\frac{\partial <V>}{\partial t} + <\rho><V> \cdot \nabla <V> + \nabla <p>$$

$$- \frac{1}{4\pi} (\nabla \times <B>) \times <B> = - <\tilde{\rho}\frac{\partial}{\partial t}\tilde{V}>$$

$$- <\tilde{\rho}\tilde{V}> \cdot \nabla <V> - <\tilde{\rho} <V> \cdot \nabla \tilde{V}>$$

$$- <\rho> <\tilde{V} \cdot \nabla \tilde{V}> - <\tilde{\rho}\tilde{V} \cdot \nabla \tilde{V}>$$

$$+ \frac{1}{4\pi} <(\nabla \times \tilde{B}) \times \tilde{B}> \qquad \text{(X-4b)}$$

$$\frac{\partial <B>}{\partial t} + \nabla \times <V> \times <B> = \nabla \times <\tilde{V} \times \tilde{B}> \qquad \text{(X-4c)}$$

$$\frac{\partial <p>}{\partial t} \times <V> \cdot \nabla <p> + \frac{5}{3}<p>\nabla \cdot <V>$$

$$= - <\tilde{V} \cdot \nabla \tilde{p}> - \frac{5}{3}<\tilde{p}\nabla \cdot \tilde{V}>. \qquad \text{(X-4d)}$$

Then subtracting Eqs. (X-4) from Eqs. (X-3) gives the equations

$$\frac{\partial \tilde{\rho}}{\partial t} + \nabla \cdot (\tilde{\rho} <V> + <\rho> \tilde{V}) = - (\nabla \cdot \tilde{\rho} \tilde{V} - \nabla < \tilde{\rho} \tilde{V} >) \qquad (X\text{-}5a)$$

$$<\rho> \frac{\partial \tilde{V}}{\partial t} + \tilde{\rho} \frac{\partial <V>}{\partial t} + \tilde{\rho} <V> \cdot \nabla <V> + \rho \tilde{V} \cdot \nabla <V>$$

$$+ <\rho> <V> \cdot \nabla \tilde{V} + \nabla \tilde{p}$$

$$- \frac{1}{4\pi} \{ (\nabla \times \tilde{B}) \times <B> + (\nabla \times <B>) \times \tilde{B} \}$$

$$= \frac{\partial \tilde{V}}{\partial t} + <\tilde{\rho} \frac{\partial \tilde{V}}{\partial t}>$$

$$- \tilde{\rho} \tilde{V} \cdot \nabla <V> + <\tilde{\rho} \tilde{V}> \cdot \nabla <V> - \tilde{\rho} <V> \cdot \nabla \tilde{V}$$

$$+ <\tilde{\rho} <V> \cdot \nabla \tilde{V}>$$

$$- <\rho> \tilde{V} \cdot \nabla \tilde{V} + <\rho> <\tilde{V} \cdot \nabla \tilde{V}> - \tilde{\rho} \tilde{V} \cdot \nabla \tilde{V} + <\tilde{\rho} \tilde{V} \cdot \nabla \tilde{V}>$$

$$+ \frac{1}{4\pi} (\nabla \times \tilde{B}) \times \tilde{B} - \frac{1}{4\pi} <(\nabla \times \tilde{B}) \times \tilde{B}> \qquad (X\text{-}5b)$$

$$\frac{\partial \tilde{B}}{\partial t} - \nabla \times \tilde{V} \times <B> - \nabla \times <V> \times \tilde{B}$$

$$= \nabla \times \tilde{V} \times \tilde{B} - \nabla \times <\tilde{V} \times \tilde{B}> \qquad (X\text{-}5c)$$

$$\frac{\partial \tilde{p}}{\partial t} + \tilde{V} \cdot \nabla <p> + <V> \cdot \nabla \tilde{p} + \frac{5}{3} \tilde{p} \nabla \cdot <V> + \frac{5}{3} <p> \nabla \cdot \tilde{V} =$$

$$- \tilde{V} \cdot \nabla \tilde{p} + <\tilde{V} \cdot \nabla \tilde{p}> - \frac{5}{3} \tilde{p} \nabla \cdot \tilde{V} + \frac{5}{3} <\tilde{p} \nabla \cdot \tilde{V}>. \qquad (X\text{-}5d)$$

Equations (X-4a-d) and Eq. (X-5a-d) are now a complete set of nonlinear equations for $<\rho>$, $\tilde{\rho}$, $<V>$, $\tilde{V}$, $<B>$, $\tilde{B}$, $<p>$ and $\tilde{p}$, and so far no approximations have been made.

The quasi-linear approximation to these equations consists of neglecting the $<\tilde{\rho} \tilde{V} \cdot \nabla \tilde{V}>$ term (that is the term cubic in fluctuating quantities from the right hand side of Eq. (X-4b) and in neglecting the entire right hand side of Eqs. (X-5a-d). We will briefly discuss these approximations now. The fluctuating quantities are assumed to be small so that a term like $<\tilde{\rho} \tilde{V} \cdot \nabla \tilde{V}>$ is expected to be much smaller than a term like $\rho <\tilde{V} \cdot \nabla \tilde{V}>$ since $\tilde{\rho} << \rho$. This is the basic justification for neglecting the cubic nonlinear terms on the right hand side of Eq. (X-4b).

Notice that all terms on the right hand side of Eqs. (X-5a-d) are various quantities minus their ensemble averages. This ensures that for our cylindrical case of azimuthal and axial averaging, there is no quantity on the right hand side of Eqs. (X-5a-d) which is a function of only r. That is every driving term on the right hand side has oscillatory structure in θ and/or z. For instance if there are two fluctuations at (k_1, m_1) and (k_2, m_2), the quadratic terms on the right hand side will drive additional fluctuations at $(2k_1, 2m_1)$, $(2k_2, 2m_2)$ and $(k_1 \pm k_2, m_1 \pm m_2)$. However no fluctuation will be driven at $k = m = 0$ since the ensemble (i.e., azimuthal and axial) average of the right hand side is subtracted out. These terms then describe the coupling of fluctuations at different wave lengths directly with each other. It is worth noting that the terms we have neglected are mode coupling terms. That is they couple modes nonlinearly to each other, rather than nonlinearly to the ensemble average background.

Thus the quasi-linear approximation neglects coupling of the fluctuations among themselves, but includes the coupling (correct to second order) of the fluctuating to ensemble average quantities. Therefore the basic idea behind the quasi-linear approximation is that coupling of the waves to the background is more important than the coupling of the waves to each other.

With the right hand side of Eqs. (X-5a-d) set equal to zero, the equations for the tildad quantities are very similar to the linearized fluid equations of earlier chapters, but with two important complications. First of all the background velocity is not equal to zero in Eqs. (X-5a-d) and secondly, the background quantities are functions of time as well as radius. To proceed, we now restrict ourselves to the lowest order tokamak ordering and to systems not far above stability threshold. As we will now show, these complications can then be eliminated. In lowest order tokamak ordering, recall $B_z >> B_\theta$, $R >> a$ and the mode structure is two dimensional in the $r\theta$ plane (that is $\tilde{V}_z = \tilde{B}_z = 0$). Also $\nabla \cdot \tilde{V} = 0$, that is, the perturbation is incompressible. The equation for B_z, from Eq. (X-4c) then becomes

$$\frac{\partial B_z}{\partial t} = -\frac{1}{r} \frac{\partial}{\partial r} r V_r B_z. \qquad (X-6)$$

Since B_z is very large, it cannot change very much without drastically altering the systems energy density. However for B_z to remain unchanged, it must be that

$$V_r \approx 0. \qquad (X-7)$$

Thus to lowest order in tokamak ordering, the ensemble average radial velocity vanishes. Now let us consider the azimuthal and axial component of velocity. Making use of the fact that the fluctuating flow and magnetic field are incompressible in two dimensions, it is a straight forward matter to show that the θ and z components of the terms on the right hand side of Eq. (X-4b) are proportional to V_θ, $\dfrac{\partial V_z}{\partial r}$ and $\dfrac{\partial V_\theta}{\partial r}$. Thus there is no term which acts as a source term for an acceleration in θ and z (one can also show that this is true in cylindrical geometry without an expansion in tokamak ordering). Therefore, if V_θ and V_z are initially zero, they will be zero at all subsequent time. Hence, to lowest order in tokamak ordering, there is no induced fluid velocity, or

$$V = 0. \tag{X-8}$$

(In general in cylindrical geometry $V_z = V_\theta = 0$, but $V_r \neq 0$.)

In this case the equation for the perturbed quantities (Eqs. (X-5a-d) with the right hand side $= 0$) are different from the linearized equations in previous chapters only in that the background quantities are functions of time. Therefore the perturbed quantities cannot be assumed to have a time dependence like $\exp \gamma t$. However if the time scale for the change of equilibrium quantities, τ_{eq} satisfies the condition

$$\gamma \, \tau_{eq} >> 1 \tag{X-9}$$

where γ is the linear growth rate (assuming the ensemble average quantities are time invariant), then one can solve Eqs. (X-5a-d) by making a WKB approximation. This is, fluctuating quantities are proportional to $\exp \int \gamma (t) \, dt$. The zero order WKB approximation to Eqs. (X-5a-d) then give the conventional result

$$\gamma \tilde{\rho} + V \cdot \nabla <\rho> (t) = 0 \tag{X-10a}$$

$$\gamma <\rho(t)> V = -\nabla \tilde{p} + \frac{1}{4\pi} \{(\nabla \times B) \times <B(t)> \tag{X-10b}$$

$$+ (\nabla \times <B(t)> \times$$

$$\gamma B = \nabla \times V \times <B(t)> \tag{X-10c}$$

$$\nabla \cdot V = 0 \tag{X-10d}$$

where we have assumed the flow is incompressible in Eq. (X-10d). These are just the conventional equations for perturbed quantities which we have studied in previous sections. Using them to express $\tilde{\rho}$,

$\tilde{B}$ and $\tilde{p}$ in terms of $\tilde{V}$, it is a simple matter to show that the equations for ρ, p, and B_θ are

$$\frac{\partial <\rho>}{\partial t} = \frac{1}{r}\frac{\partial}{\partial r} r \sum_{mk} \gamma <\tilde{\xi}_r^2 (r,m,k)> \frac{\partial <\rho>}{\partial r} \qquad \text{(X-11a)}$$

$$\frac{\partial <\rho>}{\partial t} = \frac{1}{r}\frac{\partial}{\partial r} r \sum_{mk} \gamma <\xi_r^2 (r,m,k)> \frac{\partial <\rho>}{\partial r} \qquad \text{(X-11b)}$$

$$\frac{\partial <B_\theta>}{\partial t} = \frac{\partial}{\partial r}\frac{1}{r}\frac{\partial}{\partial r} \sum_{mk} \frac{\gamma}{m} \{ <\xi_r^2 (r,m,k)> r^2$$

$$(\frac{m<B_\theta>}{r} + k<B_z>)\} \qquad \text{(X-11c)}$$

where $\tilde{\xi}_r$ is the radial displacement, $\tilde{\xi}_r = \tilde{V}_r/\gamma$ and where as usual the perturbation is assumed to be a summation of individual fluctuations proportional to $\exp (im\,\theta + ikz)$. It only remains to check a posteriori that Eq. (X-9) is satisfied. If r_n is the radial scale length for say the density variation, and if one makes the simple assumption that $\frac{\partial}{\partial r} \sim r_n^{-1}$, then Eq. (X-9) reduces to

$$\xi_r << r_n. \qquad \text{(X-12)}$$

Thus Eq. (X-9) is satisfied as long as the radial displacement is small compared to the radial scale length.

Equations (X-11a-c) then describe the evolution of the background density, pressure and poloidal field in response to the instability. These equations in themselves do not guarantee pressure balance. However pressure balance can easily be maintained through very small changes in B_z. Thus we expect that V_r will not exactly vanish, but rather that there will be a very small V_r which will modify very slightly, B_z (according to Eq. (X-6)) so as to maintain pressure balance at all times.

Now let us examine the behavior of the Quasi-linear equations as expressed in Eqs. (X-10 and 11). The first thing to note is that the right hand side is non zero only because γ is nonzero. Thus the plasma responds to the growth of the fluctuation; once the growth ceases, for whatever reason, the plasma ceases to evolve. Thus the quasi-linear theory, as expressed in Eqs. (X-10 and 11) cannot describe a situation of steady state turbulence, but rather the evolution of an initially unstable configuration to a final stable one.

To describe this evolution, note that Eqs. (X-10) are just the linear equations for the fluctuation at the local equilibrium. Thus they can all be replaced by

$$\frac{d}{dt}\, \tilde{\xi}_x = \gamma\, \xi_x, \qquad\qquad (X-13)$$

so that Eq. (X-11a), for instance can be replaced by

$$\frac{\partial <\rho>}{\partial t} = \frac{1}{2}\, \frac{1}{r}\, \frac{\partial}{\partial r}\, r \sum_{m,k} \frac{d}{dt} <\xi_r^2\,(r,m,k)>\, \frac{\partial <\rho>}{\partial r}. \qquad (X-11a')$$

Assuming that the plasma is near marginal stability, so that the background density changes only slightly, the time dependence of $<\rho>$ can be neglected on the right hand side of Eq. (X-11a'). Then Eqs. (X-13 and 11a) can be integrated in time to give

$$\xi_r(r,m,k) = \xi_x(r,m,k,t=0)\ \exp \int^{t} \gamma(t')\, dt' \qquad (X-14a)$$

$$<\rho> = <\rho\,(t=0)> + \frac{1}{2}\, \frac{1}{r}\, \frac{\partial}{\partial r}\, r \sum_{m,k} <\xi_r^2(r,m,k)>$$

$$\frac{\partial <\rho\,(t=0)>}{\partial r}. \qquad\qquad (X-14b)$$

The time dependence of $\gamma(t)$ is unspecified here. It is the eigenvalue of the temporally local equations for the fluctuation, Eq. (X-10). The solutions expressed in (X-14) are meaningful only if $\int_0^\infty \gamma(t)\, dt$ is finite. Thus quasi-linear theory can only be valid if the plasma evolves from an initial unstable state to a final stable one.

Let us now briefly discuss the effect of mode coupling. This effects the time dependence of fluctuating quantities through the interaction of the fluctuations with each other. By neglecting mode coupling we assume that its effect on the integrated growth of $\tilde{\xi}$, expressed by Eq. (X-14a) is small.

There is one aspect of Eqs. (X-11a and c) which might at first appear paradoxical. That is the ensemble average magnetic field is no longer frozen into the ensemble average flow. This can most easily be seen in slab geometry. If the perturbation is two dimensional and incompressible in the xy plane, a simple calculation shows that the slab geometry analogs to Eqs. (X-11a and c) are

$$\frac{\partial <\rho>}{\partial t} = \frac{\partial}{\partial x}\, \gamma <\tilde{\xi}_x^2>\, \frac{\partial <\rho>}{\partial x} \qquad (X-15a)$$

$$\frac{\partial < B_y >}{\partial t} = \gamma \frac{\partial^2}{\partial x^2} <\tilde{\xi}_x^2> <B_y>. \qquad (X-15b)$$

Since $V_x = 0$, frozen in field means ρ/B_y is constant which clearly is not the case if ρ and B_y obey Eqs. (X-15).

The resolution of this apparent paradox comes from the fact that the MHD constraint does not require the average field to be frozen into the average density; rather it requires that the exact field be frozen into the exact flow. The two requirements are not the same as we will now show. To show this imagine a fluid with initial density $\rho_0(x)$ and field $B_0(x)\, \mathbf{i}_y$. Then give each element of the fluid a displacement ξ sin $ky\, \mathbf{i}_x$ where ξ is constant. Let us now calculate the new density and magnetic field. To this do consider 3 neighboring points initially at (x,y), $(x + dx, y)$ and $(x, y + dy)$. After displacement, these points go to $(x + \xi$ sin $ky, y)$, $(x + dx + \xi$ sin $ky, y)$, and $(x + \xi$ sin $ky + \xi\, kdy$ cos $ky, y + dy)$. The two difference vectors before and after the displacement are $dx\mathbf{i}_x$ and $dy\, \mathbf{i}y$ before; and $dx\mathbf{i}_x$ and $\xi\, dy\, k$ cos $ky\, \mathbf{i}_x + dy\, \mathbf{i}_y$ after. The original and final area is $dxdy$, as can be seen by taking cross products of the two sets of difference vectors. This confirms the incompressible character of the displacement. Thus if the initial position of a point (i.e., (x,y)) is denoted $\mathbf{r}_0$, and the final position $(x + \xi$ sin $ky,y)$ is denoted $\mathbf{r}$, then

$$\rho_0(\mathbf{r}_0) = \rho(\mathbf{r}).$$

Solving for $\mathbf{r}_0$ in terms of $\mathbf{r}$, we have

$$\rho(\mathbf{r}) = \rho_0(x - \xi\text{ sin }ky).$$

Assuming that the variation of ρ_0 is small in a distance ξ, we find that the density averaged over y is given approximately by

$$<\rho(x)> = \rho_0(x) + \frac{1}{4}\,\xi^2\frac{\partial^2\rho_0}{\partial x^2}. \qquad (X\text{-}16)$$

We will now continue by calculating the field, exploiting the fact that it is frozen into the flow. In the undisplaced fluid, the field is parallel to the first difference vector $dy\, \mathbf{i}_y$. This difference vector is displaced to $dy\, (\xi\, k$ cos $ky\, \mathbf{i}_x + \mathbf{i}_y)$ and this must be parallel to the 'displaced' field. Thus a unit vector parallel to B is

$$\mathbf{i}_B = \frac{\xi\, k\text{ cos }ky\, \mathbf{i}_x + \mathbf{i}_y}{(1 + \xi^2 k^2\text{ cos}^2\, ky)^{1/2}}. \qquad (X\text{-}17)$$

Now calculate the magnitude of B. The initial flux through the line $\{(x + dx,y) - (x,y)\}$ is $(B_0(x)\mathbf{i}_y) \cdot (dx\mathbf{i}_y) = B_0(x_0)\, dx$. After displacement flux is frozen in, so

$$B\,(r)\mathbf{i}_B \cdot i_y\,dx \;=\; B_0(x_0)\,dx_0, \quad \text{or} \tag{X-18}$$

$$B\,(r) = B_0(x_0)\,((\xi k \cos ky)^2 + 1)^{1/2}$$

$$= B_0(x - \xi \sin ky)\,((\xi\,k \cos ky)^2 + 1)^{1/2}.$$

The y component of B in the displaced fluid is

$$B_y = B\,(r)\,\mathbf{i}_B \cdot i_y = B_0(x - \xi \cos ky). \tag{X-19}$$

Again, assuming that B_0 varies only slightly in a distance ξ, we find

$$<B_y> \;=\; B_0(x) + \frac{1}{4}\,\xi^2\frac{\partial^2 B_0}{\partial x^2}. \tag{X-20}$$

As is apparent from Eqs. (X-16 and 20), $<\rho>/<B_y> \neq \rho/B$ so the average field is not frozen into the average density. Yet the field was calculated by making explicit use of the fact that the exact field is frozen into the exact density. Therefore ensemble averaging destroys the 'frozen in' nature of magnetic fields in ideal MHD.

In a sense, this is not a surprising result. As we have seen in Chapter VII and VIII, fluid flow with frozen in field can lead to very complicated, small scale magnetic structures which may well be completely washed out with any kind of ensemble averaging. However, this complicated structure was a direct consequence of frozen in fields, so averaging field and density will in all likelihood destroy this link.

An analogous situation is an incompressible fluid with variable density $\rho\,(x)$ filling the square $-L < x, y, < L$. Imagine stirring up this fluid for a long time. Even though the flow is incompressible, low and high density parts are forced near each other in an almost random way. Hence any kind of coarse grain averaging of the fluid will give rise to nearly uniform density, even though this might at first sight appear to be impossible due to the incompressibility condition. Therefore, in all cases, 'microscopic' constraints can become unglued upon ensemble averaging.

Let us now apply the quasi-linear theory to an internal $m = 1$ kink tearing mode. The theory is greatly simplified because $\xi_r \approx$ constant (that is independent of r) within the $q = 1$ surface, and only the $m = n = 1$ mode is assumed to exist. As it can easily be shown that for $B_z =$ constant and $\tilde{\xi}_r =$ constant, there is no contribution to $\dfrac{\partial B_\theta}{\partial t}$ from B_z, the equation for B_θ is

$$\frac{\partial B_\theta}{\partial t} = \gamma \frac{\partial}{\partial r}\frac{1}{r}\frac{\partial}{\partial r}\, r <\xi^2> B_\theta \tag{X-21}$$

which is very much like a diffusion equation. Another way of writing Eq. (X-21) is to take the curl and write it as an equation for the plasma current in the z direction. The result

$$\frac{\partial}{\partial t} J_z = \gamma \frac{1}{r} \frac{\partial}{\partial r} r \frac{\partial}{\partial r} <\xi^2(t)> J_z \qquad \text{(X-22)}$$

which is a diffusion equation for J_z.

We now examine what sort of an interpretation for $m = n = 1$ sawtooth oscillations can be made by using quasi-linear theory. Imagine that at time $t = 0$, an Ohmically heated tokamak discharge has $q(r = 0) < 1$; and, as is usually the case, monotonically decreasing profiles of $\rho(r)$, $p(r)$ and $J_z(r)$ (but monotonically increasing profile of $q(r)$) as shown is Fig. (X-1a). This configuration is unstable to the $m = n = 1$ kink tearing mode. According to quasi-linear theory, this mode will grow at its local growth rate and ρ, p and J_z all obey diffusion equations. Thus current, density and pressure all diffuse outward, and tend to evolve the plasma to a final state where J_z (and thereby q), ρ and p all have no radial gradient within the singular region, as shown in Fig. (X-1b). Now let us postulate that the steep gradient near the singular surface in Fig. (X-1b) rapidly diffuses away, either by classical diffusion, or more likely by exciting some sort of micro-instability. (Actually we will see in Chapter XV that Kadomtsev proposes a non-linear scheme for the effect to be felt beyond the singular surface. After this, the profile has smoothed out and looks like that shown in Fig. (X-1c), where the interaction between the $m = n = 1$ instability and whatever smoothes out the profile, will insure that in the final state, $q(r = 0) \geqslant 1$, so the plasma is stable. However the plasma is heated by Ohmic heating, so that the hotter central region tends to be preferentially heated. This lowers the resistivity, and channels the current into the center thereby lowering $q(r = 0)$ until it is less than unity. Thus the current channeling tends to force the plasma back into an unstable state. This channeling plus the quasi-linear reaction of the plasma have the property of forming a relaxation oscillation.

The time of the down stroke, according to quasi-linear theory, would be the time for the fluctuation to exponentiate to a level large enough to affect the background. This could be a time of order five or ten linear growth times. For a large size (singular surface radius ~ 10 cm) hot $(T_e \sim 2 \, Kev)$ plasma characteristic of say TFR, the linear growth time is about $100 \, \mu$ sec, so one might expect that quasi-linear theory would predict a down-stroke time of something less than a millisecond. This appears consistent with experimental data from TFR.
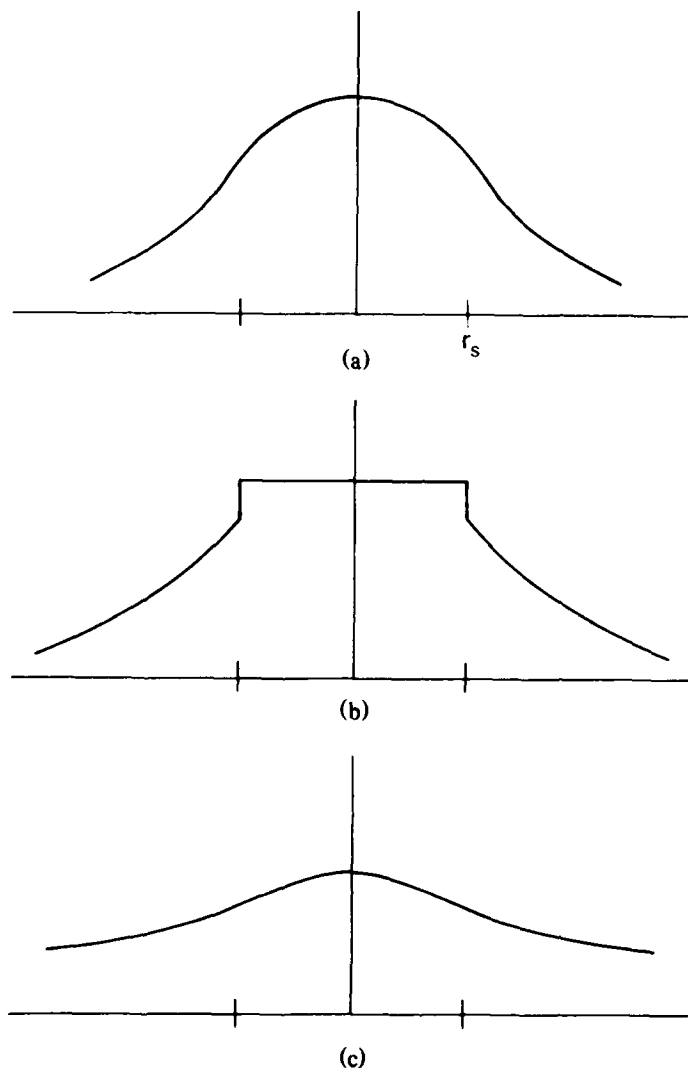
Fig. X-1 — The quasi-linear evolution of the toroidal current for
an $m = n = 1$ internal kink tearing mode. (a) The initial
current, (b) the current on completion of the MHD instability
phase, (c) The current after the resulting steep gradients diffuse
away.

Another possible application of the quasi-linear theory to tokamak
plasmas is current penetration due to excitation of double tearing
modes. As discussed in VIII F, if a skin current forms as the current
builds up in for instance a tokamak, there will be two nearby rational
surfaces and double tearing modes can be excited. According to Eq.
X-22, the double tearing mode will cause diffusion of the current
between the two rational surfaces and will tend to reduce the skin effect
and help the current penetrate to the interior of the tokamak plasma.

Since the edge plasma is cooler and more resistive and the rational sur-
faces are closer together, the growth rate of the double tearing mode
will be larger than that of an $m = n = 1$ internal kink. The growth
time is about 10 μsec, so that quasi-linear theory might predict current
penetration between the two rational surfaces in a time of about 50 to
100 μsec. The current penetration time for the entire plasma would of
course be much longer.

Chapter XI

QUASI-LINEAR THEORY AND SIMPLIFIED NONLINEAR THEORY OF TEARING MODES

Since the tearing mode is driven by magnetic energy in the outer region, it is tempting to describe its nonlinear evolution in terms of a quasi-linear theory of only the outer region. In this way, one might be able to follow the growth of the tearing mode coupled to the depletion of free energy which drives it. Then, when all of the free energy is used up, linear growth should stop. Another attractive feature of an outer region quasi-linear theory is that it works the same way no matter what the dissipation mechanism in the inner region is. The problem is that the MHD equation for the outer region is singular, so that one still has to treat the singularity. For instance if $\tilde{B}_x(x,y,t) = \tilde{B}_x(x)$ exp i $(ky + \gamma t) + c.c.$, then Eq. (X-13b) reduces to

$$\frac{\partial <B_y>}{\partial t} = \frac{2\gamma}{k^2} \frac{\partial^2}{\partial x^2} \frac{|\tilde{B}_x|^2}{<B_y>} = \frac{\gamma}{k} \frac{\partial^2}{\partial x^2} i \tilde{\xi}_x^* \tilde{B}_x + c.c. \qquad (\text{XI-1})$$

where we have related $\tilde{B}_x$ to the displacement by the ideal MHD relation $\tilde{B}_x = i k <B_y> \xi$. Also, as in Chapter X, we have assumed the presence of a large, uniform B_z. Clearly, Eq. (XI-1) is singular at $x = 0$, the position where $<B_y> = 0$. For $<B_y(x)>$ as shown in Fig. (XI-1a), it is possible to show that in the outer region, the ambient magnetic field loses energy and thereby drives the mode. To do so, make use of the fact that around $x = 0$, because of the nonzero resistivity $\xi(x)$ is actually a well behaved function of x over the entire domain $-\infty < x < \infty$. Therefore, the last form of Eq. XI-1 can be integrated by parts so that

$$\frac{d}{dt} \int_{-\infty}^{\infty} dx \frac{<B_y^2>}{2} = \int_{-\infty}^{\infty} \frac{\gamma}{k} <B_y> \frac{\partial^2}{\partial x^2} i \tilde{\xi}_x^* \tilde{B}_x + c.c.$$

$$= \int_{-\infty}^{\infty} dx \frac{\gamma}{k} i \tilde{\xi}_x^* \tilde{B}_x \frac{\partial^2}{\partial x^2} <B_y> + c.c.$$

$$= \int \frac{2\gamma}{k^2} \frac{|\tilde{B}_x|^2}{<B_y>} \frac{\partial^2}{\partial x^2} <B_y>. \qquad (\text{XI-2})$$
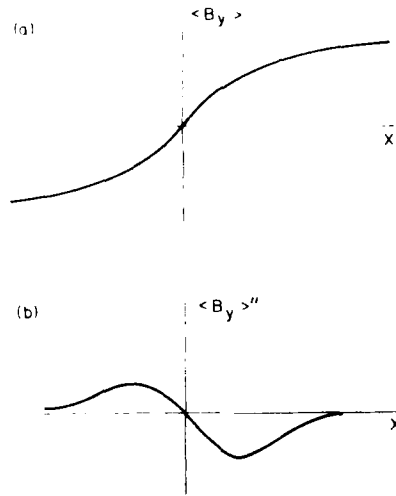
Fig. XI-1 — The initial profiles of $<B_y>$ and $<B_y>''$ for a slab plasma unstable to tearing modes

Since $<B_y> = 0$ and $\dfrac{d^2}{dx^2}<B_y> = 0$ at $x = 0$, the last integral in Eq. X-2 is not singular. Also B_y and its second derivative everywhere have opposite signs (see Fig. (X-1a and b), so it is clear that energy is released from initial magnetic field. This energy goes to drive the tearing mode. Clearly the energy released within the inner region is not accurately calculated; however, this should be unimportant, very little magnetic energy is there in the first place.

We now examine how the quasi-linear evolution of the plasma in the outer region can be carried out. There are two relevant widths in the inner region, first there is the resistive layer size L_c given by Eq. (VII-25c) and secondly there is the island width Δx_{is}. It is clear that Eq. (XI-1) is not valid for $x < L_c$ because all information concerning resistivity was left out. However, it is also true that Eq. (XI-1) cannot be valid for $x < \Delta x_{is}$ either. The reason is that it is a partial differential equation relating the change in $<B_y>$ to the spatial structure of $<B_y>$ in the immediate neighborhood. However, during reconnection, the magnetic field line is suddenly affected by the other field line it reconnects with; a field line which is generally very far away. Thus the behavior of the ambient field during reconnection cannot be described by a single partial differential equation. This can also be seen in the derivation leading up to Eq. (X-20). From this it is clear that Eq. (XI-1) described the response of the average frozen in field to small displacements of the fluid.

Therefore, Eq. (XI-1) can only be valid both outside the singular layer *and* outside the island. In the linear regime, where $\tilde{B}$ is infinitesimal, the island width is smaller than the resistive layer width. However since L_c is small, as $\tilde{B}$ grows, soon $\Delta x_{is} > L_c$ so the island width becomes the relevant inner layer width. Equation (XI-1) then is only valid for $x > \Delta x_{is}$.

We now show how the quasi-linear evolution of a single tearing mode may be carried out. If the variables are renormalized in dimensionless form as

$$\rho = kx \qquad\qquad\qquad \text{(XI-3a)}$$

$$\tau = \int \gamma \, dt \qquad\qquad \text{(XI-3b)}$$

the equations for $\tilde{B}_x$ and B_y are

$$\frac{\partial^2 \tilde{B}_x}{\partial \rho^2} = \left[1 + \frac{\dfrac{\partial^2 <B_y>}{\partial \rho^2}}{<B_y>} \right] \tilde{B}_x \qquad\qquad \text{(XI-4a)}$$

$$\frac{\partial \tilde{B}_x (\rho = \rho_{is}, \tau)}{\partial \tau} = \tilde{B}_x(\rho = \rho_{is}, \tau) \qquad \text{(XI-4b)}$$

$$\frac{\partial}{\partial t} <B_y> = 2 \frac{\partial^2}{\partial \rho^2} \frac{|\tilde{B}_x|^2}{<B_y>} = 4 \frac{\tilde{B}_x^2}{<B_y>} + \frac{4}{<B_y>} \left(\frac{\partial \tilde{B}_x}{\partial \rho} \right)^2$$

$$- \frac{8 \tilde{B}_x}{<B_y>^2} \frac{\partial \tilde{B}_x}{\partial \rho} \frac{\partial <B_y>}{\partial \rho} + \frac{4 \tilde{B}_x^2}{<B_y>^3} \left(\frac{\partial <B_y>}{\partial \rho} \right)^2 \qquad \text{(XI-4c)}$$

$$+ \frac{\tilde{B}_x^2}{<B_y>^2} \frac{\partial^2 <B_y>}{\partial x^2} .$$

To get the second form of Eq. (XI-4c), we have expanded the derivatives and used Eq. (XI-4a) to express $\dfrac{\partial^2 \tilde{B}_x}{\partial x^2}$. Despite the apparent complexity, the second form in Eq. (XI-4c) is much simpler to work with because the diffusion term now has a positive diffusion constant. Also, we have assumed $\tilde{B}_x$ is real. Equation (XI-4a) is the equation for $\tilde{B}_x$ in the outer region (the same as Eq. VII-9) except that now

$$|\rho| > \rho_{is} \text{ where } \rho_{is} = 2 \left[2 \frac{\dfrac{\tilde{B}_x}{\partial <B_y>}}{\dfrac{\partial <B_y>}{\partial \rho}} \Big|\rho = 0 \right]^{1/2} . \text{ (The additional factor}$$

of $\sqrt{2}$ between this and Eq. (VII-41) comes from the difference between sin cos and exponential notation.) Equation (XI-4b) simply

says that the fluctuation at $\rho = \rho_{is}$ grows as the linear growth rate. Equation (XI-4c) is the quasi-linear equation for $<B_y>$, which is valid only outside the island, that is $|\rho| > \rho_{is}$.

The question now is how to calculate the island width, which depends upon the slope of $<B_y>$ at $x = 0$, that is, inside the singular region. Clearly it is necessary to make some assumption concerning the current and field distribution inside the singular layer. We make the reasonable assumption that $<B_y>$ is linear in x within the island. Then Eqs. (XI-4) must be solved numerically in space and time, coupled with a calculation of the island width. The procedure is as follows.

At $\tau = 0$ start with a field profile, which we will specify as $<B_y> = B_0 \tanh (\rho/L_s)$ and $\tilde{B}_x$ outside the island given by the solution of Eq. (XI-4a) with some assumed small amplitude. Here L_s is the scale length in units of k^{-1}. To advance from τ to $\tau + \Delta\tau$, first solve Eq. (XI-4a) for $\tilde{B}_x$ subject to the boundary condition that $\tilde{B}_x$ approaches zero at both $X = \pm\infty$. If the solution is normalized so that $\tilde{B}_x(x = 0)$ is the same on each side of the island, then there will be a discontinuity in derivative across it. From $\tilde{B}_x$, calculate

$$\Delta = \frac{1}{\tilde{B}_x(\rho = \rho_{is})} \left\{ \frac{\partial \tilde{B}_x}{\partial \rho}\bigg|_{\rho_{is}} - \frac{\partial \tilde{B}_x}{\partial \rho}\bigg|_{-\rho\,is} \right\}$$

$$= \frac{2}{\tilde{B}_x(\rho = \rho_{is})} \frac{\partial \tilde{B}_x}{\partial x}\bigg|_{\rho_{is}} \qquad (XI-5)$$

due to the symmetry. Note that now Δ is calculated across the island rather than as a discontinuity at $x = 0$. This means the Δ in Eq. (XI-5) is proportional to the field energy liberated outside the island. If $\Delta < 0$, the plasma has become stable and the calculation is finished with the $<B_y> = <B_y(\tau)>$. If $\Delta > 0$ the plasma is still unstable so that $B_y(\rho = \rho_{is}, \tau)$ is advanced according to Eq. (XI-4b) and $<B_y>$ is advanced according to Eq. (XI-4c). To calculate the island width first calculate the quantity

$$L_{is}(\rho, \tau + \Delta\tau) = 2[2\rho \,\tilde{B}(\rho = \rho_{is}, \tau + \Delta\tau)/$$

$$<B_y(\rho, \tau + \Delta\tau)>]^{1/2}. \qquad (XI-6)$$

This is the island width, determined at each ρ, assuming the field inside the island is linear up to that ρ and equal to $<B_y(\rho)>$ at ρ. The actual island width is then determined at each time step by solving

$$L_{is}(\rho, \tau + \Delta\tau) = \rho \qquad (XI-7)$$

and the solution of Eqs. (XI-4a and c) is invoked only outside the island. The field inside the island then is linear in ρ, and Eq. (XI-7) insures that $<B_y>$ is continuous at $\rho = L_{is}(\rho, \tau + \Delta\tau)$.

Equations (XI-4a-c) were solved numerically by Dr. Barbara Mellander using this assumption for the field inside the island. The initial and final magnetic fields for four choices of L_s are shown in Fig. (XI-2a-d). For weakly unstable plasma (larger L_s), the asymptotic field is a very smooth function of space. However, as L_s gets smaller there is a larger and larger discontinuity in derivative at the island edge. Most likely this means that the quasi-linear theory becomes less accurate as the plasma becomes more unstable. The arrow on the horizontal axis of the four graphs is the position of the maximum of $\tilde{B}$ at $\tau = 0$. For weakly unstable plasmas, the final island width turns out to be smaller than this, for strongly unstable plasmas, larger. In Fig. (XI-3) is shown both the final island width and final island width divided by L_s as a function of L_s. In Fig. XI-4 is shown the liberated magnetic energy per unit area and the liberated magnetic energy per unit area divided by $L_s B_0^2/8\pi$ as a function of scale size. To summarize, the quasi-linear evolution of the outer region always drives a tearing mode to a final stable state with $\Delta = 0$ if one assumes $<B_y>$ is linear in x within the inner region. Also, this state will be the same no matter what is the dissipation mechanism in the inner region. However, the quasi-linear theory almost certainly gets less and less accurate as the mode gets more and more unstable.

The next question is whether there are nonlinear effects within the island itself that either stabilize the mode or strongly affect its behavior. This problem was analyzed by Rutherford (P. Rutherford, Phys. Fluids *16*, 1903 (1973)). He found that nonlinear effects in the island did not stabilize the mode, but did significantly reduce its growth rate. Here we give a very much simplified version of his theory. To start, recall that Eq. (VII-16) gives the power liberated per unit area in the outer region as

$$p = \frac{\gamma\Delta}{\pi k^2} \tilde{B}_x \frac{d\tilde{B}_x}{dt} \tag{XI-8}$$

assuming $\tilde{B}_x$ is real. This power is dissipated by Ohmic heating within the inner region of width L_c. That is, the current associated with the discontinuity in B_y is assumed to flow essentially uniformly within L_c, so that this current is given by Eq. (VII-24), $\tilde{J}_z = \frac{c}{4\pi ik} \tilde{B}_x(x = 0)\frac{\Delta}{L_c}$. Balancing the Ohmic heating with this power liberated yielded the approximate expression for the growth rate, Eq. (VII-25b).
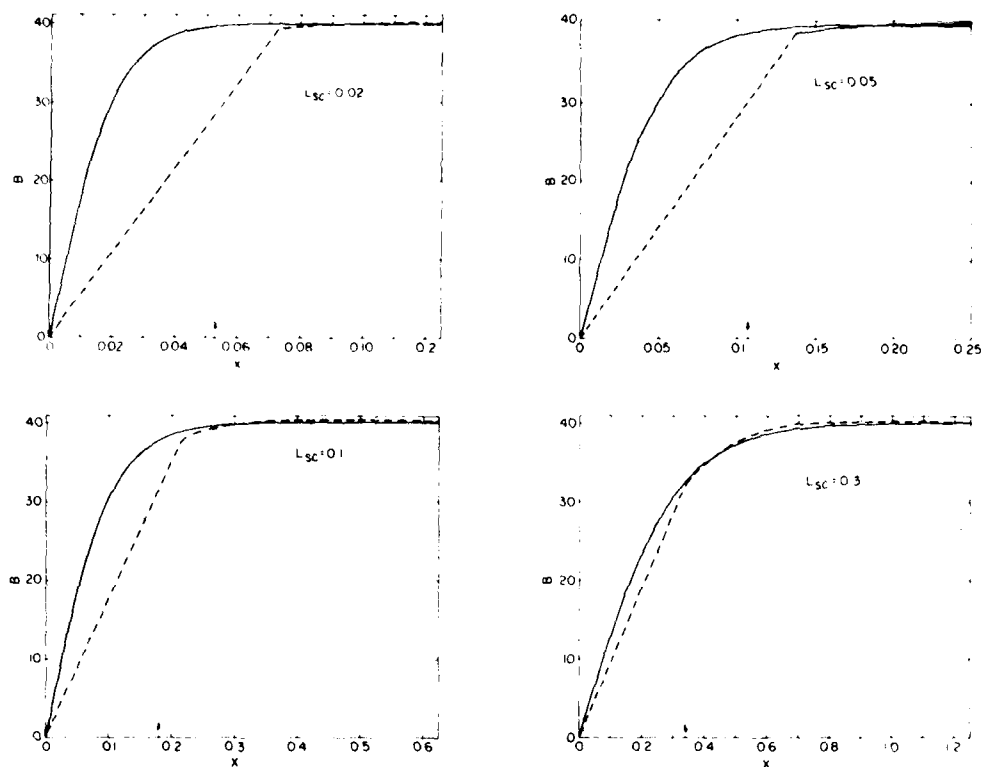
Fig. XI-2 — The initial (solid) and final (dotted) magnetic field
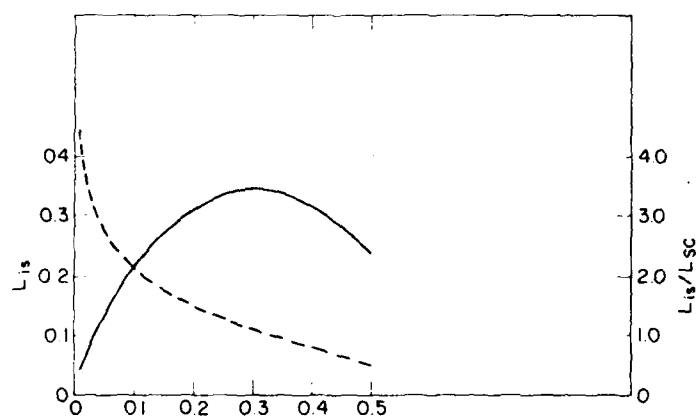for four scale lengths (scale length normalized to k_y^{-1})

Fig. XI-3 — The final island width (solid) and final island width
divided by initial scale length (dotted) as a function of initial
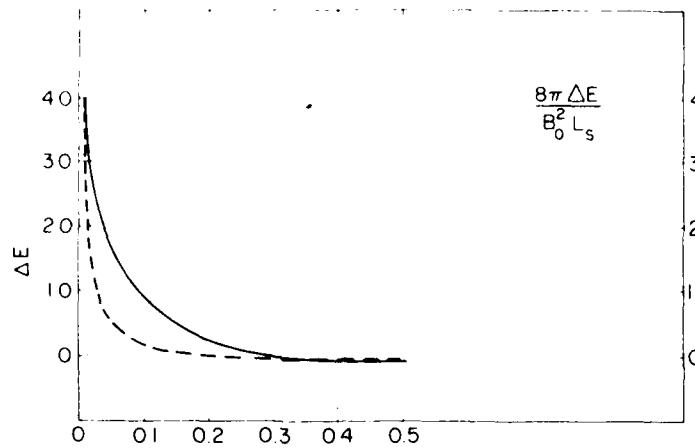scale length

Fig. XI-4 — Liberated magnetic energy per unit area (solid) and liberated magnetic divided by magnetic energy in a scale length as a function of initial scale length

If one now makes the reasonable assumption that Δx_{is}

$$= 2 \left(k \frac{2\tilde{B}_x}{\dfrac{\partial <B_y>}{\partial x}} \right)^{1/2} > L_c,$$ the current flows throughout the island, the

simple analysis leading up to Eq. VII-25b, is replaced with

$$\frac{d\tilde{B}_x(\rho = \rho_{is})}{dt} = \frac{1}{8} \frac{\eta c^2}{4\pi} \Delta \left(\frac{\partial <B_y>}{\partial x} k \tilde{B}_x \right)^{1/2}, \qquad \text{(XI-9)}$$

or for long time

$$\Delta x_{is} = \frac{1}{4} \frac{\eta c^2}{4\pi} \Delta t. \qquad \text{(XI-10)}$$

Thus the island growth becomes linear, rather than exponential in time, and the growth rate goes as first power of resistivity, rather than some fractional power. Thus once $\Delta x_{is} > L_s$, the island growth rate does not stop, but it does drastically slow up, even if Δ does not change. Hence there are two complimentary aspects to the nonlinear evolution of tearing modes. First, as the background evolves, Δ is reduced and eventually brought to zero by the quasi-linear evolution of the outer region magnetic field structure. Second, because of the change in the character of the inner region for $\Delta x_{is} > L_c$, the growth of the island width is drastically reduced and it proceeds on the much slower resistive diffusion time scale, the same time scale as for changes in equilibrium quantities.

Now let us discuss the implication of this for minor and major disruptions in tokamak plasmas. As was discussed in Chapter I, a minor disruption is a sudden burst of x-ray activity generally associated with a measurable disturbance at some m number, which can be 2 or 3. The time scale for this x-ray activity in PLT was typically 100 μsec. One possible interpretation is that tearing modes of the associated helicity are excited. The plasma is not in an absolutely steady state but is continuously evolving due to for instance changes in the external circuit. These changes propagate to the interior of the plasma in a resistive skin time, about 100 milliseconds or more. As the interior of the plasma changes, it might evolve to an unstable state with $\Delta > 0$. Then a tearing mode will be excited. Its growth time will be very small compared to the time for plasma evolution. For PLT, Eq. VII-25b gives a growth time of between about 100 usec and 1 millisec depending on which parameters one chooses. The theory developed in this chapter would predict that the plasma then evolves to a stable state at which either $\Delta = 0$ for complete stability, or $\Delta x_{is} \geq L_c$ for drastic reduction in growth rate. The time scale would be several growth times. This would be manifest by the plasma very suddenly changing its equilibrium, accompanied by an x-ray burst and the onset of island structure.

Now let us discuss whether a single tearing mode could lead to a major disruption. Imagine that at some radius a tearing mode is excited. At this radius an island or chain of islands is formed. While the tearing mode evolves quickly compared to the magnetic diffusion time, it evolves slowly compared to the Alfven time. Therefore each of the magnetic surfaces within the island is an MHD equilibrium. Hence as the tearing mode evolves new MHD equilibria form, each flux surface in the island having some average of the pressure of the two or more original flux surfaces which reconnected to form it.

If the island grows to a sufficient size that it touches the limiter, the hot plasma from the interior can flow freely along the field to the limiter and this will cool the plasma. In all likelihood large numbers of metal impurity ions from the limiter will also. Radiation from these impurities will further cool the plasma. If the plasma cannot adjust to this sudden cooling of the interior, it may be that a major disruption will result. Thus it is likely that a tearing mode can produce a major disruption in a tokamak if the island can grow until it reaches the limiter. This hypothesis seems to be confirmed by the results on Pulsator discussed in the introduction. Here an island is artificially induced by external coils, and when the island touches the limiter, a major disruption did result.

This chapter discussed so far how an initially tearing mode unstable plasma in slab geometry evolves toward a final state having a periodic chain of islands. We will close the chapter with a discussion of the subsequent evolution of this island chain. If the original equilibrium variation was in the x direction, this time asymptotic periodic chain of islands extends in the y(horizontal) direction. Each island, of course, represents a current filament in the z direction. Since these currents are all in the same direction, they attract each other. The plasma is in equilibrium because an island feels equal and opposite attractive forces from the island to the right and the island to the left.

Now consider what happens if the island is given a rightward displacement. First of all the attractive force of the two nearby islands is greater than the attractive force to their now more distant neighbors. Thus the nearby islands tend to attract each other and ultimately coalesce so if this effect is dominant, the island chain is unstable. This attractive force, however, may be balanced by a repulsive force. As the two islands move toward each other, the flux, which is frozen into the flow, must be compressed between the two islands. Thus the magnetic pressure increases there and this forces the two islands apart. If this latter effect dominates, the plasma is stable, at least to this type of displacement. The calculation of the stability of this plasma is very complicated due to the two dimensional nature of the equilibrium. One calculation has been made by J. Finn and P. Kaw (Phys. Fluids 20, 72 (1977)) and they found that the attractive force generally dominates so that the island chain is unstable to coalescence of the individual islands.

A numerical simulation of the evolution of this equilibrium was done by P. Prichett and C. Wu (Phys. Fluids 22, 2140 (1979)). At $t = 0$ an MHD equilibrium of a periodic chain of islands was set up, the flux surfaces of which are shown in Fig. (XI-5). The simulation had periodic boundary conditions in the horizontal (y) direction, each periodicity length containing two islands. If the plasma had zero resistivity, the islands displaced toward each other, but ultimately stopped when the magnetic field compressed between them became large enough to repel their coalescing motion. The flux surfaces at two later times are shown in Fig. (XI-6). However, if resistivity is present, the field structure can change its topology and the islands can coalesce. The flux surfaces for a simulation with $\eta \neq 0$ are shown in Fig. (XI-7). Clearly the magnetic reconnection proceeds to completion and the two initial islands merge to form a single island.
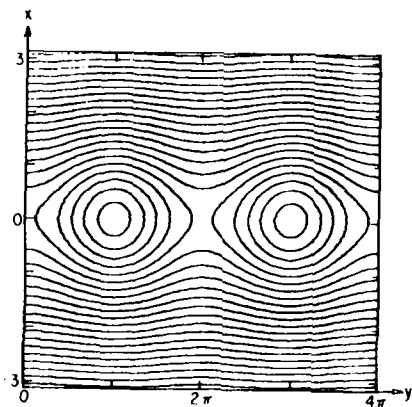
Fig. XI-5 — The initial island structure
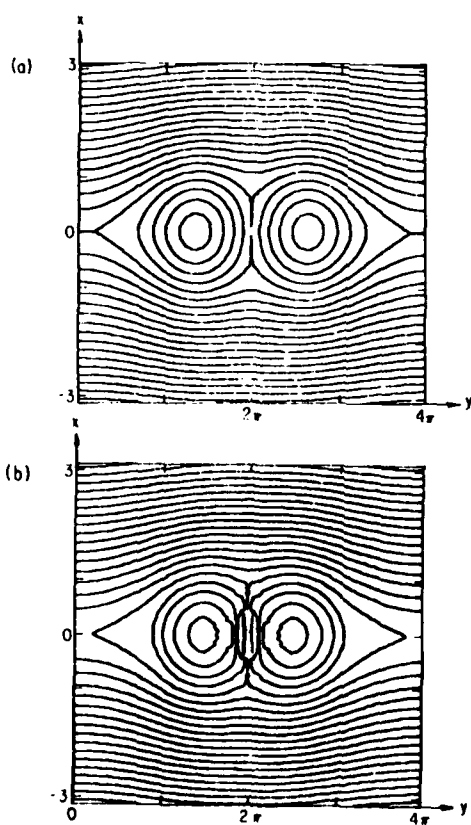examined by Prichett and Wu

Fig. XI-6 — The evolution of this island structure
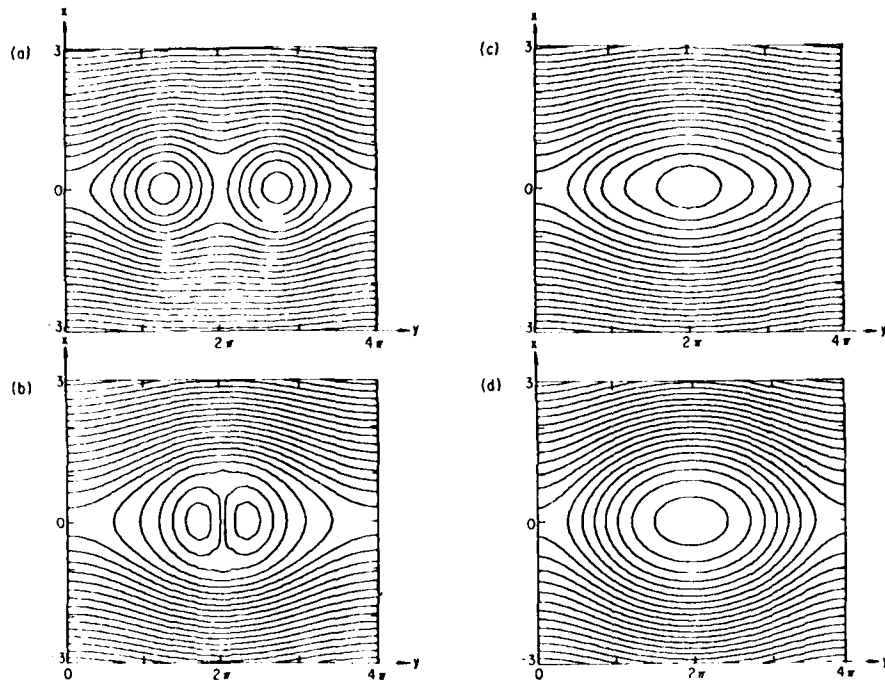for a plasma with $\eta = 0$

Fig. XI-7 — The evolution of this island structure
for a plasma with $\eta \neq 0$

Thus the nonlinear evolution of a tearing mode unstable plasma can be quite complex. There are at least three processes which can play a role, quasi-linear evolution of the plasma in the outer region, reduction in growth due to the dynamics of the plasma in the island, and ultimately coalescence of the resulting island chain.

Chapter XII

STEADY STATE QUASI-LINEAR THEORY OF RESISTIVE g MODES

The previous two chapters emphasized that for ideal MHD instabilities as well as tearing instabilities away from the singular surface, the background plasma responded to the fluctuation only if $\gamma \neq 0$. That is the background responds directly to the growth of the mode. In this chapter we will show that there are some cases in which quasi—linear theory has the background plasma responding even if $\gamma = 0$. To motivate this, we first examine a little more closely just when the background plasma responds to the presence of a fluctuation.

This is easiest to do for an ordinary g mode in an incompressible fluid which has growth rate $\gamma^2 = -g \frac{\partial <\rho>}{\partial x} / <\rho>$. Note the if g and $<\rho'>$ have opposite signs, γ is real and a fluctuation grows exponentially in time. That is, a fluctuating quantity has a spatial and temporal dependence going as $\exp \gamma t \cos ky$. On the other hand, if g and $<\rho'>$ have the same sign, the mode oscillates in time with frequency $\omega = \left[g <\rho'>/\rho \right]^{1/2}$. That is, a fluctuating quantity now has a spatial and temporal dependence going as $\cos(ky - \omega t)$.

Now consider the response of the background density to the presence of such a fluctuation. Quasi—linear theory gives the result

$$\frac{\partial <\rho>}{\partial t} = \frac{\partial}{\partial x} \tilde{V}_x \tilde{\rho}. \qquad \text{(XII-1)}$$

The density fluctuation $\tilde{\rho}$ is obtained from the fluid displacement, ξ by integrating the density equation in time,

$$\tilde{\rho} = \tilde{\xi}_x \frac{\partial <\tilde{\rho}>}{\partial x} \tilde{\rho}. \qquad \text{(XII-2)}$$

157

The remaining calculation is to relate $\tilde{\xi}_x$ to $\tilde{V}_x$ and here is where the difference between oscillation and exponential growth plays a crucial role. If the fluctuation grows exponentially, then $V_x = \gamma\xi_x e^{\gamma t} \cos ky = \gamma\xi_x$ and we get the ordinary quasi-linear equation for the density evolution as expressed in for instance Eq. (X-15a). However, if g and ρ' have the same sign, the fluctuation oscillates so $V_x = \omega\xi_x \sin (ky - \omega t)$. Now there is no simple relation between V_x and ξ_x since one varies as $\sin(ky - \omega t)$ while the other varies as $\cos(ky - \omega t)$. Even more important, $\langle\xi_x V_x\rangle = 0$ since ξ_x and V_x are exactly 90° out of phase with each other.

Thus the crucial requirement for quasi—linear relaxation of the background plasma is that the two involved fluctuating quantities are not 90° out of phase. For the density response, the involved quantities are $\tilde{\rho}$ and $\tilde{V}$; for magnetic field response they are $\tilde{B}$ and $\tilde{V}$; and for pressure response they are $\tilde{V}$ and $\tilde{p}$. Note that $\tilde{\rho}$ and $\tilde{V}$ do not have to be in phase for density response, they just cannot be exactly 90° out of phase. If say $\tilde{\rho}$ has a component in phase with $\tilde{V}$ which is much smaller than its out of phase component, $\langle\tilde{\rho}\tilde{V}\rangle \, |\neq 0$, so there can be a quasi—linear response of the background density.

In everything we have considered up to now, the in phase component has resulted from the linear growth of the fluctuation. However this is not the only effect which can cause an in phase component. Dissipation can cause it also. To show this let us consider a very simple dissipation mechanism for the gravitational oscillation. Say that some dissipative effect tends to relax a perturbed density to the ambient density with decay rate ν. Then the equation for perturbed density is

$$\frac{\partial\tilde{\rho}}{\partial t} + \nu\tilde{\rho} + \tilde{V}_x\frac{\partial\langle\rho\rangle}{\partial x} = 0. \tag{XII-3}$$

We further assume that g and $\tilde{\rho}'$ have the same sign so all quantities vary in time and space as Re exp $i(ky - \omega t)$ where ω is real. Thus

$$\tilde{\rho} = -\frac{\tilde{V}_x}{\nu - i\omega}\frac{\partial\langle\rho\rangle}{\partial x}. \tag{XII-4}$$

Note that for zero ν, $\tilde{\rho}$ and $\tilde{V}$ are 90° out of phase. However, the presence of ν introduces an in phase component. Inserting $\tilde{\rho}$ from Eq. XII-4 into Eq. (XII-1), the quasi-linear ensemble average equation for the time average of $\langle\rho\rangle$ becomes

$$\frac{\partial\langle\rho\rangle}{\partial t} = \frac{\partial}{\partial x}\frac{|V_x|^2\nu}{\nu^2 + \omega^2}\frac{\partial\langle\rho\rangle}{\partial x}. \tag{XII-5}$$

Thus, to conclude, we note that either the growth of the fluctuation, or else the presence of dissipation can give rise to a quasi—linear evolution of ensemble average quantities.

Let us now examine the quasi—linear theory of a resistive g mode. The only dissipation involved here is resistivity. That is, ohms law is

$$\frac{\mathbf{V}}{C} x <\mathbf{B}> = \eta \tilde{\mathbf{J}} \tag{XII-6}$$

where as discussed in Chapter 6, we have assumed $\tilde{\mathbf{E}} = 0$. Thus, we expect $\mathbf{B}$ will have a component in phase with $\mathbf{V}$ which is driven by dissipation rather than growth. This should give rise to magnetic diffusion. Thus the quantity we wish to compute an induced ensemble average electric field in the z direction,

$$E_z = -\frac{1}{c}\left(\tilde{V}_x \tilde{B}_y^* - \tilde{V}_y \tilde{B}_x^*\right). \tag{XII-7}$$

The problem now is to calculate these quantities on the right for a resistive g mode. We take the configuration specified in Chapter 6 so $V_z = B_z = \frac{\partial}{\partial z} = \nabla\, \mathbf{B} = 0$. Then, as shown in Eq. VI-20

$$\tilde{V}_x = \tilde{V}_0 \exp - 1/2\left(x/l\right)^2 \tag{XII-8}$$

where $\tilde{V}_0$ is the mode amplitude and l is the width

$$l = (\eta c^2)^{1/3} k^{-1/3} \left(\frac{B_0}{L_s}\right)^{-2/3} \left(-g\frac{\partial <\rho>}{\partial x} <\rho>\right)^{1/6}. \tag{XII-9}$$

By using $\nabla\cdot\mathbf{B} = 0$ and assuming $\frac{\partial}{\partial x} >> k$, Eq. (VI-15) can easily be solved for $\tilde{B}_y$ in terms of $\tilde{V}_x$. The result is

$$\tilde{B}_y = \frac{-4\pi l^2}{\eta c^2} \frac{\partial <B_y>}{\partial x} \tilde{V}_0 \exp-\frac{1}{2}\left(x/l\right)^2. \tag{XII-10}$$

Then using the fact that $\nabla \cdot \tilde{\mathbf{V}} = \nabla\cdot\tilde{\mathbf{B}} = 0$ we find for the other two components

$$\tilde{V}_y = \frac{x}{ikl^2} \tilde{V}_0 \exp -1/2\left(x/l\right)^2 \tag{XII-11}$$

and

$$\tilde{B}_x = -ik\frac{4\pi}{\eta c^2} l^3 \sqrt{\frac{\pi}{2}} \frac{\partial <B_y>}{\partial x} \tilde{V}_0 \,\mathrm{erf}\left(\frac{x}{\sqrt{2}l}\right). \tag{XII-12}$$

Inserting from Eqs. (8, 10, 11 and 12) into Eq XII- 7, we find

$$\frac{\partial <B_y>}{\partial t} = c\frac{\partial}{\partial x}E_z = 2\frac{\partial}{\partial x}\sum_i \frac{4\pi}{\eta c^2}|\tilde{V}_{oi}|^2\left\{l_i^2 \exp-\left(\frac{x-x_i}{l_i}\right)^2\right.$$

$$+\sqrt{\frac{\pi}{2}}l_i(x-x_i)\,\text{erf}\left(\frac{x-x_i}{\sqrt{2}l_i}\right)$$

$$\left.\exp-\frac{1}{2}\left(\frac{x-x_i}{l_i}\right)^2\right\}\frac{\partial <B_y>}{\partial x} \qquad\qquad \text{(XII-13)}$$

where in Eq (XII-13), we have made a slight change of notation. Specifically we have summed over i where x_i denotes the position of the center of the ith mode. In Chapter VI, we have assumed the mode had $k_z = 0$ and was centered at $x = 0$. However nothing is sacred about $x = 0$; if a k_z were included, one could simply center the mode at the position where $k_z B_0 + kB_0\frac{x}{L_s} = 0$. Thus Eq (XII-13) sums the magnetic diffusion over each mode center.

Note that there is no γ in front of the right hand side of Eq. (XII-13). However since we have used linear theory to calculate the functional form of $\tilde{V}_x$, $\tilde{V}_0$ is growing with the linear growth rate γ. Thus the magnetic diffusion, as expressed in Eq. (XII-13) is not actually steady state diffusion. However, if some nonlinear effect limits the fluctuating velocity, but does not greatly perturb the spatial structure of V_x, then Eq. (XII-13) does describe a steady state quasi-linear magnetic diffusion driven by resistivity. Since reversed field pinches have $q < 1$ everywhere, they are expected to be unstable to resistive interchange modes if any pressure gradient is present. Thus these devices may well exist in a steady state, but with small scale fluid turbulence and the associated anomalous magnetic diffusion. This may be one possible reason that in the quiescent state, the lifetime of a reversed field pinch is much less than what one expects from classical magnetic diffusion.

The following is for Chapters 10, 11 and 12.

The quasi-linear theory is not often discussed in MHD. Two textbooks which discusses it for collisionless infinite homogeneous plasma instabilities are:

Nonlinear Plasma Theory, Chapter II, Sagdeev and Galeev, W.A. Bengamin, N.Y., 1969.

Methods in Nonlinear Plasma Theory, Chapters 9-12, R.C. Davidson, Academic Press, N.Y., 1972.

One nonlinear tearing mode calculation which does find saturation, possibly similar to the quasi-linear calculation here is:

Energy Release by Magnetic Tearing, Nonlinear Limit, G. Van Hoven and M.A. Cross, Phys. Rev. A., 7 1347 (1973).

Rutherfords work on nonlinear theory is:

Nonlinear Growth of the Tearing Mode, P.H. Rutherford, Phys. Fluids, 16, 1903 (1973).

A study of the linear stability of a string of islands, and an analogous numerical simulation are given in:

Coalescence Instability of Magnetic Islands, J.M. Finn and P.K. Kaw, Phys. Fluids, 20, 72 (1977).

Coalescence of Magnetic Islands, P.L. Prichett and C.C. Wu, Phys. Fluids, 22, 2140 (1979).

Quasi-linear theory of resistive interchange modes is in:

Steady State Magnetic Diffusion from Resistive Interchange Modes in a Plasma, W.M. Manheimer, Phys. Rev. Lett., 45, 1249 (1980).

Experimental results for reversed field pinches in the quiescent state can be found in:

Factors Influencing the Period of Improved Stability in Zeta, D.C. Robinson and R.E. King, Plasma Physics and Controlled Thermonuclear Fusion Research, 1968, Vol. 1, p. 263 (IAEA Vienna, 1969).

Optimization and Properties of Reversed Field Pinches in the Eta Beta II Experiment, A. Buffa, et al., in Proceedings of Reversed Field Pinch Workshop, Los Alamos, N.M., 1980.

Chapter XIII

ISLAND OVERLAP AND THE ONSET
OF STOCHASTICITY

In Chapter XI we discussed the response of the plasma to a single tearing mode in slab geometry. Although the magnetic topology is changed by a tearing mode, magnetic surfaces *still* do exist. In this section we investigate under what circumstances unstable MHD fluctuations can destroy magnetic surfaces. For simplicity we considered cylindrical geometry to lowest order in tokamak ordering, so that $\tilde{\mathbf{B}}$ is two dimensional in r and θ and B_z is constant and very large.

Hence **B** follows from

$$B_r = \frac{1}{r} \frac{\partial}{\partial \theta} A \, (r,\theta,z) \qquad\qquad \text{(XIII-1a)}$$

$$B_\theta = -\frac{\partial}{\partial r} A \, (r,\theta,z) \qquad\qquad \text{(XIII-1b)}$$

where A is the z component of the vector potential. The equation for the field line is

$$\frac{dr}{dz} = \frac{B_r}{B_z}, \quad \frac{\partial \theta}{\partial z} = \frac{1}{r} \frac{B_\theta}{B_z}. \qquad\qquad \text{(XIII-2)}$$

There are at least two possible ways to display the solution of Eqs. (XIII-2). First of all, the solutions could be projected to $z = 0$, the result being a curve in the $r\theta$ plane. Secondly, if the system is periodic in z with period $2\pi R$ (obviously like a tokamak with radius R), the intersection of the field line with the planes $z = 2\pi nR$ could be displayed on the $z = 0$ plane. The result now is not a curve, but a series of points which may either lie on a curve, or else fill an area.

Making use of Eq. (XIII-1), it is clear that Eqs. (XIII-2) are Hamiltonian in form, with z playing the role of t, and A the role of the Hamiltonian. Since A depends on z, the Hamiltonian is not a constant of the motion. However since the motion of the field line does follow

from a Hamiltonian, the transformation from $r(z = 0)$, $\theta(z = 0)$ to $r(z)$, $\theta(z)$ is an area preserving transformation. There has been a tremendous amount of recent work on whether such area preserving transformations have an ordered or stochastic nature. (A good introduction and review can be found in J. Ford, Fundamental Problems in Statistical Mechanics III, E. Cohen ed 1974). The basic motivation behind this work is to see when statistical mechanics is valid for an isolated Hamiltonian system. This work can be quite mathematically abstract. For instance, it has only recently been proven rigorously that a hard sphere gas obeys the ergodic theorem. To quote Ford, this proof occupies "about one hundred journal pages and will involve such concepts as discontinuous transverse foliations, completely positive Kolmogorov entropy, and the like." Of course it is far beyond the scope of this work to more than scratch the surface of the mathematical theory of ergodic behavior. Principally we are interested in whether the intersection of field with $z = 2\pi nR$ (or what we will call the equivalent $z = 0$ plane) fill this plane, or some region of it ergodically, or whether the intersections lie on a well defined curve.

One thing is very easy to show. Namely if there does exist a constant of motion say $\chi(r, \theta, z) =$ constant, then the intersections of field lines with the equivalent $z = 0$ plane lie on a well defined curve; in other words the motion of the field line is not ergodic. To show this, first note that since the system is periodic in z,

$$\chi(r,\theta,z) = \chi(r,\theta, z + 2\pi nR).$$

(XIII-3)

Therefore on the equivalent $z = 0$ plane,

$$\chi(r,\theta,z = 0) = \text{constant}$$

(XIII-4)

so that the intersections of a field line with this plane lie on the curve defined by Eq. (XIII-4).

We will now prove that if the perturbed magnetic field has helical symmetry, that is the dependence on θ and z is through the combination $\tau = m\theta + kz$, then a constant of motion exists. To do so, note that $\nabla \cdot \mathbf{B} = 0$,

$$\frac{\partial}{\partial r} r B_r + m\frac{\partial B_\theta}{\partial \tau} + rk\frac{\partial B_z}{\partial \tau} = 0.$$

(XIII-5)

Therefore B can be expressed in terms of a "helical flux function" ψ as

$$B_r = -\frac{1}{r}\frac{\partial \psi(r,\tau)}{\partial \tau}$$

(XIII-6a)

$$mB_\theta + krB_z = \frac{\partial \psi(r,\tau)}{\partial r}.$$

(XIII-6b)

The condition that Eqs. (XIII-6) have a solution for ψ, if **B** is given, is simply that the divergence of **B** is equal to zero. Notice that in general, Eq. (XIII-6) cannot be used to solve for **B** in terms of ψ since it consists of only two equations for the three components of **B**. (If tokamak ordering, or B_z = constant, is valid, then Eqs. (XIII-6a and b) also solve for B if ψ is given.) However the information in Eq. (XIII-6) is sufficient to show that a constant of motion exists. It follows directly from Eqs. (XIII-6) that

$$\mathbf{B} \cdot \nabla \psi = 0 \qquad \qquad \text{(XIII-7)}$$

so that **B** lies in the surfaces of constant ψ. In other words ψ is constant along the line of force.

Now consider a magnetic field with a helical perturbation specified by

$$\psi(r, \tau) = \psi_0(r) + \epsilon\,(r)\cos\tau \qquad \qquad \text{(XIII-8)}$$

and for simplicity, take also $k = -1/R$. Note that the derivation of the ψ_0 term vanishes at radial position r_s given by

$$q(r_s) = m. \qquad \qquad \text{(XIII-9)}$$

Near this singular surface the surfaces of constant ψ are given by

$$r - r_s = \left[\frac{K - \epsilon(r_s)\cos\tau}{1/2\psi_0''(r_s)} \right]^{1/2} \qquad \qquad \text{(XIII-10)}$$

so that the surfaces of constant ψ look as shown in Fig. (XIII-1). The maximum radial island (i.e., when $K = \epsilon$) widti from center to boundary, is given by

$$\Delta r_{is} = 2\left[\frac{\epsilon(r_s)}{\psi_0''} \right]^{1/2}. \qquad \qquad \text{(XIII-11)}$$

Returning to standard cylindrical geometry, the surfaces of constant ψ are shown in Fig. (XIII-2) for the case of $m = 3$. The projection onto the equivalent $z = 0$ plane is shown in Fig. (XIII-3). Thus for the case of a single perturbation, the helical symmetry allows us to prove the existence of constant of motion. Therefore the field line is not ergodic.

The obvious question is what happens if the helical symmetry is broken, for instance by the presence of an additional perturbation with k still equal to $-1/R$ but a different azimuthal wave number m'. Now there is no single helical symmetry, and no obvious constant of motion.
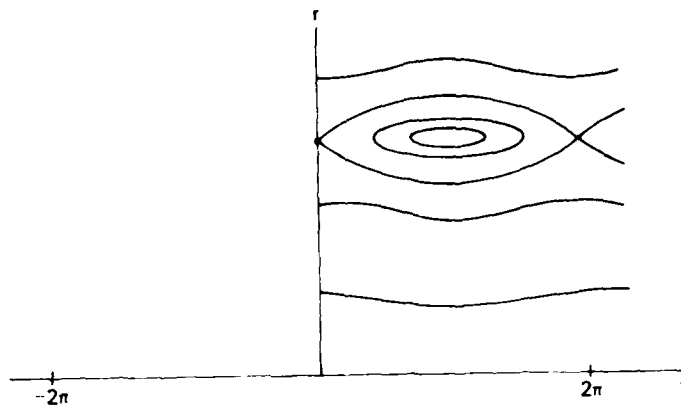
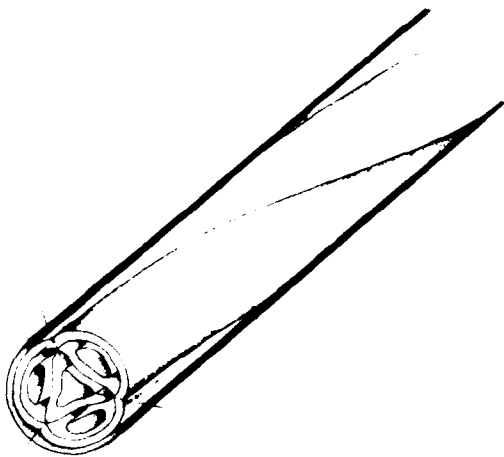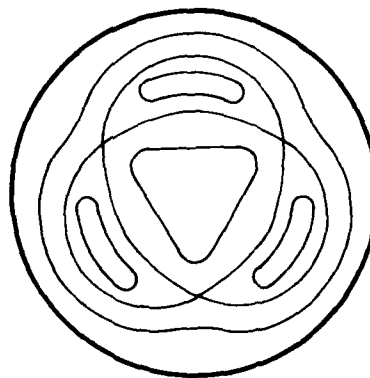Fig. XIII-1 — A plot of ϕ as a function of τ

Fig. XIII-2 — The island structure in cylindrical geometry for $m = 3$

Fig. XIII-3 — The projection of the island structure onto the equivalent $Z = 0$ plane for $m = 3$

This problem has been investigated extensively by numerical simulation. While a fact of ergodicity still eludes a rigorous mathematical proof, the results of many numerical simulations and analytic theories does point toward a very reasonable hypothesis. Namely, if the island widths of the m and m' perturbation are small compared to the inter-island separation, well defined islands exist around the $q = m$ and $q = m'$ points. However the separatrices may not be distinct lines but rather thin ergodic regions.

Thus a more complicated constant of the motion exists in some regions of space where the field lines lie on closed curves. However in other regions where the field lines ergdig, there is no constant of motion. The lines separating these regions of space are called KAM (Kolmogorov, Ainold, Moser) surface and the calculation of these surfaces is one of the fundamental problems in this area of research.

Between the $q = m$ and $q = m'$ points, the field line projections are mostly as in Fig. (XIII-3) except there may be small regions of ergodicity and small chains of secondary islands, as indicated in Fig. (XIII-4a) for an $m = 2$ and $m = 3$ perturbation with all islands having the same width. As the island width increases, the ergodic regions increase around the separatrix as shown in Fig. (XIII-4b). Finally, when the island edges overlap, most of the region between the $q = 2$ and $q = 3$ surface is ergodic, except for perhaps a small region in the center of each island, as shown in Fig. (XIII-4c). Thus the condition of island overlap is almost universally accepted to be the condition for ergodic behavior between the relevant rational surfaces.

Let us see what this implies for the case of an $m = 2$ and $m = 3$ perturbation. The distance between the two rational surfaces $q = 2$ and $q = 3$ is given roughly by

$$\Delta r_{\text{rat}} \approx \left| \frac{\partial q}{\partial r} \right|^{-1} \qquad \text{(XIII-12)}$$

while the island width is given by Eq. (XIII-11). Expressing ψ_0'' in terms of $\frac{\partial q}{\partial r}$, we find

$$\Delta r_{is} \approx 2 \left| \frac{\epsilon}{B_\theta q'} \right|^{1/2} \qquad \text{(XIII-13)}$$

assuming $\epsilon(m = 2) = \epsilon(m = 3)$. Hence an approximate condition for island overlap is

Fig. XIII-4 — The projection of the island structure onto the equivalent $Z = 0$ plane for the case of equal $m = 2$ and $m = 3$ perturbations. The dotted regions represent the region of stochastic field lines. As the amplitude of the perturbations increase, more of the region is stochastic.
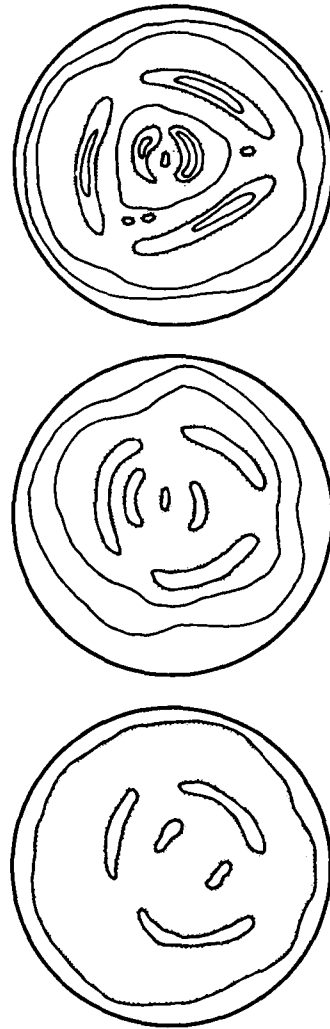
$$\epsilon > \frac{1}{16} B_\theta / \left| \frac{\partial q}{\partial r} \right| .$$ (XIII-14)

Thus in a system with strong shear (large q'), island overlap is accomplished with smaller perturbed field. Each island is smaller, but the distance between neighboring rational surfaces is also less.

Consider now the implication of this for a tokamak plasma. Imagine that the plasma is initially unstable to both an $m = 2$ and $m = 3$ tearing mode. In the early stages, when the island width is small compared to island separation, the equilibrium must readjust to the presence of the fluctuations, but since magnetic surfaces exist, equilibrium

also at least exists. However, when the perturbations grow to such an amplitude that these islands overlap MHD equilibrium is suddenly (i.e. within a growth time) lost in a very large region of the plasma, and the only possible pressure profile is $p =$ constant in this extensive ergodic region. The sudden and violent re-arrangement of the pressure profile as a result of island overlap is a possible cause of major disruptions.

Ford's review of the modern theory of stochastic process can be found in:

> The Statistical Mechanics of Classical Analytic Dynamics, Joseph Ford in Fundamental Problems in Statistical Mechanics III, p. 215, E. Cohen, Ed., 1974, North Holland Publishing Co., Amsterdam.

Another series of articles in this area can be found in:

> Intrinsic Stochasticity in Plasmas, G. Laval and G. Gresillon, Ed., Les Editions de Physique Costaboeuf, B.P., 112 91402 Orsay France, June 1979

Other papers on the problems of overlapping resonances and the stochastic transition are:

> A Method for Determining a Stochastic Transition, J.M. Greene, Princeton University Matt. Report PPPL-1489, Nov. 1978, Princeton, N.J.

> Destruction of Magnetic Surfaces in Tokamaks by Current Perturbations, J.M. Finn, Nuclear Fusion, **15**, 845 (1975).

> Stochastic Instability of a Nonlinear Oscillator, A.B. Rechester and T.H. Stix, Phys. Rev. A., **19**, 1656 (1979).

Some authors have calculated analytically the turbulent diffusion as a function of island overlap.

> Calculation of Turbulent Diffusion for the Chirikov - Taylor Model, A.B. Rechester and R.B. White, Phys. Rev. Lett., **44**, 1586 (1980).

> Fourier Space Paths Applied to Calculation of Diffusion for the Chirikov - Taylor Model, A.B. Rechester, M.N. Rosenbluth and R.B. White, Phys. Rev., **A23**, 2664 (1981).

There has also been recent work concerning anomalous transport in tokamaks due to destruction of magnetic surfaces. Some references are:

Destruction of Magnetic Surfaces by Magnetic Field Irregularities, M.N. Rosenbluth, R.Z. Sagdeev, J.B. Taylor, and G.M. Zaslavsky, Nuclear Fusion, **6**, 297 (1966).

Drift Wave Turbulence Effects on Magnetic Structure and Plasma Transport in Tokamaks, J.D. Callen, Phys. Rev. Lett., **39**, 1540 (1977).

Electron Heat Transport in a Tokamak with Destroyed Magnetic Surfaces, A.B. Rechester and M.N. Rosenbluth, Phys. Rev. Lett., **40**, 38 (1978),

Diffusion from Magnetic Flutter, Gordian Knot or Granny?, W.M. Manheimer and I. Cook, Comments on Plasma Phys., **5**, 9 (1979).

Electron Heat Conductivity of the Plasma Across a "Braided" Magnetic Field, B.B. Kadomtsev and O.P. Pogutse, Plasma Physics and Controlled Thermonuclear Fusion Research, 1978, Vol. 1, p. 649 (IAEA Vienna, 1979).

Magnetic Islandography in Tokamaks, J.D. Callen, et al., Plasma Physics and Controlled Thermonuclear Fusion Research, 1978, Vol. 1, p. 145 (IAEA Vienna, 1979).

Disruptions and Turbulence in Tokamaks, M. Dubois and A. Samain, Plasma Physics and Controlled Thermonuclear Fusion Research, 1978, Vol. 1, p. 615 (IAEA Vienna, 1979).

Magnetic Turbulence in Tokamaks, A. Samain, Journal de Physique, Colloque C6 Supplément, **12**, 103 (1977).

Chapter XIV

THE TAYLOR-WOLTJER THEORY OF SPONTANEOUS FIELD REVERSAL AND CURRENT LIMITATION

The past four chapters have discussed nonlinear theory with reference to some particular instability. Other authors, however, have looked at the nonlinear motion of an unstable plasmas, but without specific reference to a particular instability. In this chapter and the next, we survey some of this work. This chapter discusses the theory of Woltjer (Proc. Natl. Acad. Sci. U.S. **44**, 489 (1958)) and Taylor (Phys. Rev. Lett. **33**, 1139 (1974)), for spontaneous reversal of the axial field and of current limitation in a reversed field pinch. The fundamental assumption in this work is this work is that a plasma will relax to its lowest energy state cpnsistent with all the constraints on it. Taylor's main initial assumption is that the thermal and flow energy of the plasma is much less than the magnetic energy, $\int d^3r \, B^2/8\pi$. This (unfortunately) is true in current tokamaks and pinches, although the ultimate hope is certainly to attain a high beta plasma. The fact that the pressure is vanishingly small, of course, imposes severe constraints on the MHD equilibrium. Consider for a moment the MHD equilibrium of a high aspect ratio $(R/a \gg 1)$ torus; that is the topology is that of a torus, but all vector equations can be expressed in cylindrical co-ordinates. This equilibrium now becomes

$$\frac{1}{4\pi}\left(\nabla \times \mathbf{B}\right) \times \mathbf{B} - \nabla p = 0. \tag{XIV-1}$$

Equation (XIV-1) simply says that $\mathbf{J}$ is everywhere parallel to $\mathbf{B}$, or

$$\nabla \times \mathbf{B} = \lambda(\mathbf{r})\mathbf{B} \tag{XIV-2}$$

where λ is some scalar function of position. Taking the divergence of both sides of Eq. (XVI-2) and making use of the fact that $\nabla \cdot \mathbf{B} = 0$, we find

$$\mathbf{B} \cdot \nabla \lambda = 0 \tag{XIV-3}$$

so that λ is constant along every flux tube, flux surface, or flux volume; whichever is appropriate.

Taylor's theory then gives a prescription for finding λ and also determining the resulting boundary conditions for Eq. (XIV-2). It does this by minimizing the magnetic energy subject to appropriate constraints. The first order of business then is to find these constraints; minimizing magnetic energy subject to no constraints gives only the trivial solution $\mathbf{B} = 0$.

The configuration is a toroidal pinch bounded by a conductor. However, as shown in Fig. (XIV-1), there is a poloidal slit with a voltage source across it. At $t = 0$, $\mathbf{J} = 0$ and there is only a toroidal field specified by

$$\mathbf{B} = B_i \mathbf{i}_z \qquad A = \frac{rB_i}{2}\mathbf{i}_\theta. \qquad \text{(XIV-4)}$$

Then at $t = 0$, a voltage V_0 is pulsed across the gap for a time δt. For later times, the gap is shorted out (crowbarred). The plasma then responds to this induced voltage, and relaxes, presumably due to instabilities, to some final minimum energy state. Since the plasma is surrounded by a perfect conductor, no toroidal flux can get in or out, so the toroidal flux is conserved and has value $\psi = \pi B_i a^2$. However because of the poloidal slit, poloidal flux can go in or out during the time δt, so it is not conserved. Thus the first constraint is that ψ is constant. As we will see, this determines the boundary conditions.
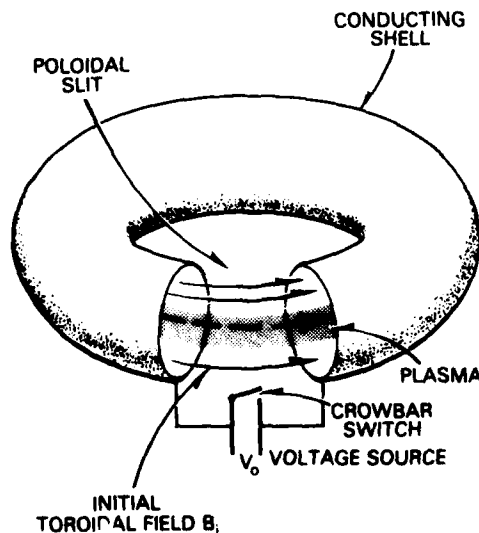

Fig. XIV-1 — A schematic of a reverse field pinch

A second constraint follows from the fact that the magnetic flux is frozen into the fluid flow. We will now show that this implies that as the fluid relaxes, $K = \int \mathbf{A} \cdot \mathbf{B} d^3 r$ is constant after the voltage pulse is shut off. Here the integral is defined as being over the entire volume of the plasma. Since $\mathbf{B} = \nabla \times \mathbf{A}$, Maxwell's equation for $\frac{\partial \mathbf{B}}{\partial t}$ (Eq. II-8) can be integrated once to give

$$\frac{\partial \mathbf{A}}{\partial t} - \mathbf{V} \times \mathbf{B} = \nabla \phi \qquad \text{(XIV-5)}$$

where ϕ is any scalar function. The presence of ϕ on the right-hand side of Eq. (XIV-5) of course accounts for the gauge. Taking the dot product of Eq. (XIV-5) with $\mathbf{B}$ and integrating over space gives the result

$$\int \int \int d^3 r \, \mathbf{B} \cdot \frac{\partial \mathbf{A}}{\partial t} = \int \int \int d^3 r \, \mathbf{B} \cdot \nabla \phi$$

$$= \int \oint d\mathbf{S} \cdot \mathbf{B} \phi = 0. \qquad \text{(XIV-6)}$$

The surface integral arises because $\nabla \cdot \mathbf{B} = 0$; it vanishes because $\mathbf{B}$ is everywhere parallel to the bounding surface. Thus

$$\frac{d}{dt} \int \int \int d^3 r \mathbf{B} \cdot \mathbf{A} = \int \int \int d^3 r \mathbf{A} \cdot \frac{\partial \mathbf{B}}{\partial t} = -c \int \int \int d^3 r \mathbf{A} \cdot \nabla \times \mathbf{E}$$

$$= -c \left\{ \int \int \int \mathbf{E} \cdot \mathbf{B} d^3 r - \int \oint d\mathbf{S} \cdot (\mathbf{A} \times \mathbf{E}) \right\}. \qquad \text{(XIV-7)}$$

Now examine the two terms on the extreme right hand side of Eq. (XIV-7). In a perfectly conducting plasma $\mathbf{E}$ is perpendicular to $\mathbf{B}$, so the first term vanishes. To evaluate the second, we need the components of $\mathbf{E}$ and $\mathbf{A}$ only in the plane of the bounding surface. After the system is crowbarred, $\mathbf{E}$ is zero in the plane of the surface (since the surface is a perfect conductor), so that $\int \int \int d^3 r \, \mathbf{A} \cdot \mathbf{B}$ is constant.

For the time δt, during which the system is pulsed, $E_z = V_0 / \delta$ where δ is the width of the slit, so that

$$c \int \oint (boldA \times \mathbf{E}) \cdot d\mathbf{S} = c \int_0^{2\pi} a \, d\theta \int_0^\delta dZ \frac{-V_0}{.\delta} A_\theta. \qquad \text{(XIV-8)}$$

Thus the rate of change of K is simply proportional to the product of voltage times toroidal flux. Since $K(t = 0) = 0$, as is obvious from Eq. (XIV-4), then

$$K = \int\int\int \mathbf{A} \cdot \mathbf{B} d^3 r = -cV_0 \delta t \Psi \qquad \text{(XIV-9)}$$

so that after time δt, K is proportional to the Volt-seconds stored in the external circuit.

The problem now is to determine the state that the plasma relaxes to after the voltage source is turned off. The basic assumption is that the plasma relaxes (presumably by instability) to a state which minimizes the magnetic energy, subject to the constraint that K is constant. Using the method of Lagrange multipliers, this means minimizing

$$\int\int\int \left[B^2 - \mu \mathbf{A} \cdot \mathbf{B} \right] d^3 r \qquad \text{(XIV-10)}$$

where μ is the Lagrange multiplier. It is a simple matter to show that the right hand term in Eq. (XIV-10) is guage invariant by letting $\mathbf{A} \rightarrow \mathbf{A} + \nabla \phi$, integrating by parts, and making use of the fact that $\mathbf{B}$ is parallel to the surrounding conducting wall. To minimize the expression in Eq. (XIV-10), let $\mathbf{B} \rightarrow \mathbf{B} + \delta\mathbf{B}$, $\mathbf{A} \rightarrow \mathbf{A} + \delta\mathbf{A}$ (of course $\delta\mathbf{B} = \nabla \times \delta\mathbf{A}$), and set terms linear in $\delta\mathbf{A}$ and $\delta\mathbf{B}$ equal to zero, so that

$$\int\int\int d^3 r \left[2\mathbf{B} \cdot \delta\mathbf{B} - \mu (\delta\mathbf{A} \cdot \mathbf{B} + \mathbf{A} \cdot \delta\mathbf{B}) \right] = 0. \qquad \text{(XIV-11)}$$

Writing $\mathbf{B}$ and $\delta\mathbf{B}$ in terms of $\mathbf{A}$ and $\delta\mathbf{A}$ and performing various partial integrations, it is not difficult to show that Eq. (XIV-11) reduces to

$$2\int\int\int d^3 r \delta\mathbf{A} \cdot \left[\nabla \times \mathbf{B} - \mu\mathbf{B} \right]$$
$$- \int \oint \{2\mathbf{B} - \mu\mathbf{A}\} \times \delta\mathbf{A} = 0 \qquad \text{(XIV-12)}$$

where the second integral in Eq. (XIV-12) is over the bounding conducting surface. The next step is to prove that this surface integral vanishes.

To start, consider the integral $\oint \mathbf{A} \cdot d\mathbf{l}$ around any closed curve on the surface. This integral is just the magnetic flux linking the closed curve. There are two possibilities. If the curve links the torus in the poloidal direction, the integral is ψ, the toroidal flux. Otherwise the integral vanishes. Since all variations in $\mathbf{B}$ leave the flux invariant,

$$\oint \delta\mathbf{A} \cdot d\mathbf{l} = 0. \qquad \text{(XIV-13)}$$

Therefore on the bounding surface $\delta\mathbf{A} = \nabla_s g$ where ∇_s is a two dimensional gradient within the surface, and g is a scalar function defined on the surface. Since $\delta\mathbf{A}$ normal to the surface gives no contribution to the second term in Eq. (XIV-12), it can be written as

$$\int \oint \left\{ (2\mathbf{B} - \mu\mathbf{A}) \times \nabla_s g \right\} \cdot d\mathbf{S} = \int \oint g \nabla \times (2\mathbf{B} - \mu\mathbf{A}) \cdot d\mathbf{S}$$

$$- \int \oint \nabla \times g(2\mathbf{B} - \mu\mathbf{A}) \cdot d\mathbf{S}. \qquad \text{(XIV-14)}$$

The second term on the right of Eq. (XIV-14) vanishes since the integral over a closed surface of the curl of any vector vanishes. The first term can be expressed as

$$\int \oint g \nabla \times (2\mathbf{B} - \mu\mathbf{A}) \cdot d\mathbf{S}$$

$$= \int \oint g \left[\frac{8\pi}{c} \mathbf{J} - \mu\mathbf{B} \right] \cdot d\mathbf{S}. \qquad \text{(XIV-15)}$$

Because the normal component of both $\mathbf{J}$ and $\mathbf{B}$ are equal to zero on the conducting surface, the right hand side of Eq. (XIII-15) is zero. Hence setting the constrained variation of energy equal to zero, Eq. (XIV-12) reduces to the simple result

$$\nabla \times \mathbf{B} = \mu\mathbf{B}. \qquad \text{(XIV-16)}$$

Since this equation is invariant to the transformation $\mu \rightarrow -\mu$, $B_\theta \rightarrow -B_\theta$, $m \rightarrow -m$ (because of the cylindrical symmetry, $B \sim e^{im\theta}$), μ, can be chosen to be positive without loss of generality.

Comparing Eq. (XIV-16) to Eq. (XIV-2) we see that the only difference is that μ is a constant, whereas λ is constant over a flux tube or surface, but otherwise can vary in space. Thus minimizing the energy subject to the constraint $K =$ constant, picks out a particular MHD equilibrium out of all those which are possible according to Eq. (XIII-2). Let us now examine how this selection comes about.

In deriving Eq. (XIV-16), the only boundary conditions used were that the components of $\mathbf{B}$ and $\mathbf{J}$ normal to the conducting surface both vanish. In ideal MHD, this is not only true at the conducting wall, but is also true of each flux surface, as shown in Chapter II. Therefore, one could equally well minimize the magnetic energy between two flux surfaces, subject to the constraint that K is constant, between them, and derive Eq. (XIV-2) in a way similar to the way Eq. (XIV-16) was derived. Imagine that at $t = 0$ the flux surfaces are circular, as shown in Fig. (XIV-2a), but $\nabla \times \mathbf{B} \neq \lambda(\psi)\mathbf{B}$ (ψ denotes the flux). As the plasma releases its excess magnetic energy and violently evolves toward a final state described by Eq. (XIV-2), these flux surfaces will naturally become very contorted, but must maintain their topological structure because the flux is frozen into the flow, as discussed in Chapter II. For

Fig. XIV-2 — Schematics of initial flux surface and final flux surfaces having $\nabla \times B = \mu B$. Note that because of the ideal MHD constraint, the topology is preserved.
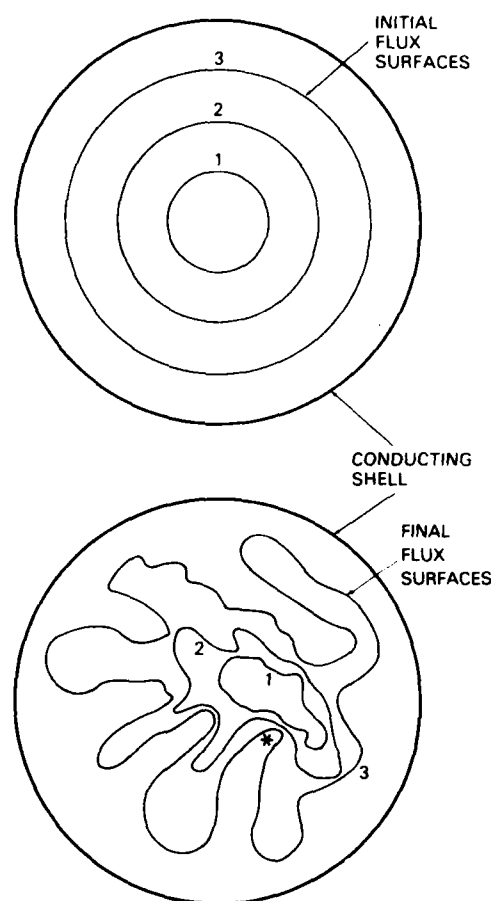
instance at $t = \infty$ infinity, these three flux surfaces might evolve toward that shown in Fig. (XIV-2b). In this final state $\nabla \times \mathbf{B} = \lambda(\psi)\mathbf{B}$ on each flux surface, but λ can vary from one flux surface to another. Notice that there are places in Fig. (XIV-2b) where flux surfaces are forced together. For instance at the star, all three flux surfaces are forced together. Of course all flux surfaces initially between 1 and 3 are forced together at this point also.

Now imagine that there is a very small plasma resistivity, so that the field lines can reconnect. For instance if resistivity were suddenly turned on for the configuration in Fig. (XIV-2b), surely all flux surfaces between 1 and 3 would reconnect with one another near the star, and reconnection would also occur at other places. Of course reconnection changes topology of $\mathbf{B}$, but only has a small effect on the magnitude of B in most places.

Therefore, is this reconnection is allowed, it makes no sense to talk about magnetic energy or constraints between two flux surfaces since they are no longer defined! However all relevant boundary conditions can still be applied on the conducting wall which always remains a flux surface on the time scale of the relaxation. Hence minimizing the total plasma energy, subject to the constraint that K is constant, is still valid for the entire plasma even if not for each initial flux surface. Thus inherent in the reduction of Eq. (XIV-2) (which could have also been derived by minimizing the energy on each flux surface) to Eq. (XIV-16) is the assumption that in the violent relaxation of the plasma to its final state, a small amount of resistivity is allowed, so that topology of the field is destroyed inside the plasma.

Now let us find the solution to Eq. (XIV-16). If $\mathbf{B}$ has cylindrical symmetry, it is a simple matter to show that

$$B_z = B_0 J_0(\mu r)$$

$$B_\theta = B_0 J_1(\mu r) \qquad\qquad (XIV-17)$$

is a solution of Eq. (XIV-16), and

$$A_z = \frac{B_0}{\mu}\Big[J_0(\mu r) - J_0(\mu a)\Big].$$

$$A_\theta = \frac{B_0}{\mu} J_1(\mu r). \qquad\qquad (XIV-18)$$

Here a is the minor radius and A_z has an appropriate constant added to it so that the poloidal magnetic flux through the hole in the torus vanishes. The next problem is to relate μ and B_0 to physical parameters. The axial magnetic flux ψ is just the line integral of the poloidal vector potential, so

$$\Psi = \frac{2\pi a}{\mu} J_1(\mu a) B_0. \qquad\qquad (XIV-19)$$

The simplest other relation is that between μ and the pinch ratio $2I/aB_i c$ where B_i is the initial axial bias field at time $t = 0$. Relating B_i to the flux ψ, and the current to $B_\theta(r = a)$, we find

$$\theta = \frac{B_\theta \text{ (wall)}}{B_i} = \frac{2I}{aB_i c} = \frac{\mu a}{2} \qquad\qquad (XIV-20)$$

where I is the current in CGS units. The quantity K is related to the stored Volt seconds by Eq. (XIV-9). Using the expression for the fields given in Eq. (XIV-17 and 18), one can show that

$$\frac{K}{\Psi^2} = \frac{R}{a} \left[\frac{\mu a (J_0^2 (\mu a) + J_1^2 (\mu a)) - 2 J_0(\mu a) J_1(\mu a)}{J_1^2 (\mu a)} \right] \quad \text{(XIV-21)}$$

which defines μ in terms of initial flux and stored Volt seconds.

The remarkable thing about Eq. (XIV-17) is that it predicts that the toroidal field reverses direction whenever $\mu a > 2.4$, the position of the first zero of J_0, or for pinch parameters

$$\theta > 1.2. \quad \text{(XIV-22)}$$

In Fig. XIV-3 is shown the theoretical prediction of $F = B_2(\text{wall})/B_i$ as a function of θ along with experimental points from HBTX and zeta taken from Fig. (I-14). Clearly the agreement is quite good.
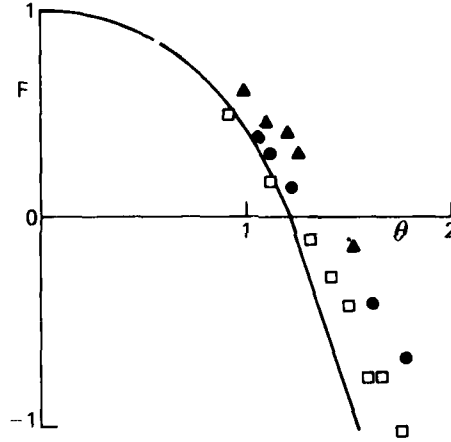

Fig. XIV-3 — Plot of F versus θ,
theory and experiment

So far, we have only considered solutions of Eq. (XIV-16) which have cylindrical symmetry. There are also solutions which are not symmetric. Expressing the azimuthal and axial dependence of the non-symmetric solution to Eq. (XIV-16) as $\exp i(kz + m\theta)$, and using $\nabla \cdot \mathbf{B} = 0$, it is not difficult to show that B_z satisfies Bessels equation, so that the solutions are

$$B_z = J_m (y) \cos(m\theta + kz)$$

$$B_r = \frac{-1}{(\mu^2 - k^2)^{1/2}} \left\{ k J_m'(y) + \frac{m\mu}{y} J_m(y) \right\} \sin(m\theta + kz) \quad \text{(XIV-23)}$$

$$B_\theta = \frac{-1}{(\mu^2 - k^2)^{1/2}} \left\{ \mu J_m'(y) + \frac{mk}{y} J_m(y) \right\} \cos(m\theta + kz)$$

with $y^2 = (\mu^2 - k^2)r^2$. Of course Eq. (XIV-23) is only a valid solution to the equation if

$$B_r(r = a) = 0. \qquad (XIV-24)$$

This then imposes a relation between μ and k which must be satisfied. (However let us note that for the symmetric solution $B_r = 0$ everywhere, so the boundary condition is automatically satisfied) Since Eq. (XIV-16) is linear, the magnetic field can be the symmetric state, Eq. (XIV-17), plus any linear combination of individual solutions in Eq. (XIV-23). The condition this solution must satisfy is that the total K and toroidal flux is given and that $B_r(r = a) = 0$. Since the solutions given in Eq. (XIV-23) have zero toroidal flux, this toroidal flux is determined entirely by the symmetirc state. The quantity K then is a summation over contributions from each solution in Eq. (XIV-23) plus the contribution from the symmetric state.

The question now is which state the plasma picks out. Of course the state is that having minimum magnetic energy. Imagine now that there are two solutions to Eq. (XIV-16) having two different values of μ and which satisfy all of the appropriate boundary conditions. We now show that the minimum energy state is the state having minimum μ. The energy is given by

$$W = \iiint d^3r \, r\mathbf{B} \cdot \mathbf{B} = \iiint d^3r \, \mathbf{B} \cdot \nabla \times \mathbf{A}. \qquad (XIV-25)$$

Writing $\mathbf{B}$ in terms of $\mathbf{A}$ in Eq. (XIV-16) and integrating once, it is easy to show that

$$\nabla \times \mathbf{A} = \mu\mathbf{A} + \nabla\phi \qquad (XIV-26)$$

where ϕ is any scalar function. Thus

$$W = \iiint \mathbf{B} \cdot \left[\nabla\phi + \mu \mathbf{A}\right]d^3r = \mu K. \qquad (XIV-27)$$

The ϕ term vanishes, as one can show by integrating it by parts. Therefore, since K is constant, the minimum energy state is the state with minimum μ.

One possible state for the plasma is simply the symmetric state of Eq. (XIV-17). However if a helically perturbed state with smaller μ can be found, the plasma should relax to it. Taylor (J.B. Taylor, Plasma Physics and Controlled Fusion Research, 1975, IAEA Vienna) has performed a detailed investigation and found that the smallest μ for

which Eq. (XIV-24) can be satisfied is $\mu a = 3.11$ for a helical perturbation having $m = 1$ and $ka = 1.25$. Since all other helical states have higher μ, and higher energy, we need only consider this one.

Now review how the plasma state is set up. At $t = 0$, there is some toroidal flux and the system is pulsed with a certain number of volt-seconds (i.e., K). A current (proportional to μ) is thereby induced in the plasma. The natural expectation is that I (or equivalently μ), is a monotonically increasing function of K (the volt seconds). However for a sufficiently large K, μ will be equal to 3.11. As K is further increased the current will no longer increase. The reason is that a lower energy state exists which is a linear combination of the cylindrically symmetric state and helical state with $\mu = 3.11$. The toroidal flux is determined by the cylindrical state, and the relative amplitudes of the cylindrical and helical state are specified by K. Thus after $\mu = 3.11$, increasing the Volt seconds does not increase the current, but rather increases the amplitude of the helical displacement. The current limitation predicted here,

$$\theta = 1.56 \qquad\qquad (\text{XIV-28})$$

is also in reasonable agreement with what is measured in pinch experiments as shown in Fig. (I-15). Thus this relatively simple theory gives quite good agreement with experiment on the two really amazing features of reverse field pinches, spontaneous field reversal and current limitation.

Let us now discuss the MHD stability of these force free states. As we will see shortly, there are strong and profound conclusions concerning the stability of these states which are attainable with very little effort. In the first part of this chapter we considered first variation of $\int d^3x (B^2 - \mu A \cdot B)$ and showed that it was equal to Eq (XIV-12) where the surface integral was shown to vanish. Since it was a quadratic form which we considered, it is even simpler to calculate the second variation, which is

$$\delta W^* = \int d^3x (\delta B^2 - \mu \delta A \cdot \delta B). \qquad\qquad (\text{XIV-29})$$

It is also a simple matter to show that for the equilibrium described by Eq. (XIV-16), δW^* is equal the potential energy δW, but with the added constraint that the vector potential must be expressed in the form of a plasma displacement ξ as $\delta A = \xi \times B$. That is, with the added constraint that a gauge transformation can make δA everywhere perpendicular to B. (In deriving the energy principle we worked only with ξ so the constraint is trivially satisfied by integrating in time

Maxwells equation for $\frac{\partial B\mathbf{B}}{\partial t}$. Here however, we work only with $\delta\mathbf{A}$'s and $\delta\mathbf{B}$'s and not with ξ's. Thus it is not apparent that we can go backwards and express the now arbitrary trial functions $\delta\mathbf{A}$ and $\delta\mathbf{B}$ in terms of a displacement ξ) Since δW is always bounded from below with an appropriate normalization for the trial function, the presence of an additional constraint implies $\delta W \geqslant \delta W.^*$ Thus the condition $\delta W > 0$ for any trial function is sufficient for MHD stability.

From this, it is possible to show that the solution of Eq. (XIV-16) with minimum eigenvalue μ_0 is MHD stable. Assume for contradiction that this minimum μ state is unstable. Then it follows that there exists a trial function (specified by $\delta\mathbf{A}$ and $\delta\mathbf{B} = \nabla \times \delta\mathbf{A}$) for which δW^* is negative. If this trial function is normalized at a particular value of $\int d^3x |\delta B|^2$, we can minimize δW^* subject to this constraint. That is we can minimize $\lambda = \delta W^* / \int \delta B^2 dx$, where $\lambda < 0$ since the plasma assumed to be MHD unstable. The minimization follows as in the first part of this chapter and we find that

$$\nabla \times \delta\mathbf{B} = \frac{\mu_o}{1 - \lambda}\delta\mathbf{B}. \qquad \text{(XIV-30)}$$

However since $\lambda < 0$, the eigenvalue is less than μ_0 which contradicts our original assumption. Thus the only consistent assumption is that $\lambda > 0$ for the equilibrium with the minimum value of μ. Thus the solution of Eq. XIV-16 with the minimum μ is MHD stable.

The linear combination of the helically perturbed state, Eq. (XIV-23), and the symmetric state, Eq. (XIV-17) which can co exist for a sufficiently large voltage, is the state with the minimum value of μ and it is therefore MHD stable. This then, is quite an amazing result. With virtually no effort we have shown that a fairly complicated, inherently two dimensional helical equilibrium is MHD stable. Generally the MHD stability of a two dimensional equilibrium can only be resolved by very complex simulation of one, kind or another.

To conclude, it is worth noting that Gibson and Whiteman (Plasma Phys. *10*, 1101 (1968)) have examined the stability of the cylindrically symmetric state to tearing modes. They have shown that this transition from a cylindrically symmetric state to a helically perturbed state corresponds to the marginally stable point. Of course this is to be expected, since as was shown in Chapter VII, the tearing mode first goes unstable when the magnetic structure has a neighboring equilibrium at the same energy. The theory in this chapter however is

quite different from linear stability theory in that growth rates are not calculated, but the amplitude of the helical perturbation is.

The original work on evolution toward a force free state is:

> Theorem on Force Free Magnetic Fields, L. Woltjer, Proc. Natl. Acad. Sci. U.S., **44**, 489 (1958).

This was applied to a reversed field pinch in:

> Relaxation of Toroidal Plasma and Generation of Reverse Magnetic Fields, J.B. Taylor, Phys. Rev. Lett., **33**, 1139 (1974).

> Relaxation of Toroidal Discharges to Stable States and Generation of Reverse Magnetic Fields, J.B. Taylor, Plasma Physics and Controlled Thermonuclear Fusion Research, 1974, Vol. 1, 161 (IAEA Vienna, 1975).

Additional Subtleties in this method have been discussed in:

> Minimum Energy State of a Toroidal Discharge, A. Reiman, Phys. Fluids, **23**, 230 (1980).

> Relaxation toward States of Minimum Energy in a Compact Torus, S. Riyopoulos, A. Bondeson and D. Montgomery, Phys. Fluids, **25**, 107 (1982).

The Stability of cylindrically symmetric force free configurations can be found in:

> Tearing Mode Instability in the Bessel Function Model, Gibson and Whiteman, Plasma Phys., **10**, 1101 (1968).

The stability of helical configurations is in:

> General Stability Analysis of Force Free Fields, J. Kruger, J. Plasma Phys., **15**, 15 (1956).

Experimental Results on Field Reversal and Current Limitation in a reversed field pinch are in:

> Recent Results on HBTXI Confinement and Stability of High-Beta Plasma in Reversed Field Pinch, E. Butt, et al., Plasma Physics

and Controlled Thermonuclear Fusion Research, 1974, Vol. 3, p. 417 (IAEA Vienna, 1975).

The Woltjer-Taylor Theory has also been applied to spheromak plasmas. The theory, which predicts tilting instability for oblate shaped plasmas can be found in:

MHD Stability of Spheromak, M.N. Rosenbluth and M.N. Bussac, Nuclear Fusion, **19**, 489 (1979).

J.M. Finn, W.M. Manheimer, and E. Ott, Phys. Fluids, **24**, 1336 (1981).

Tilting Instability of a Cylindrical Spheromak, A. Bondeson, et al., Phys. Fluids, **24**, 1682 (1981).

Experimental results on tilting modes can be found in:

Motion of a Compact Torus Inside a Cylindrical Flux Conserver, T. Jarboe, et al., Phys. Rev. Lett., **45**, 1264 (1980).

Chapter XV

KADOMTSEV'S THEORY OF INTERNAL DISRUPTIONS AND INTRODUCTION TO NUMERICAL SIMULATIONS

This final chapter begins with Kadomtsev's theory for $m = 1$ internal disruptions in a tokamak. Amazingly enough, he is able to develop this theory without ever getting involved in the complications of the $m = n = 1$ internal kink-tearing mode. Preliminary to discussing this theory, it is necessary to review the toroidal flux ψ first introduced in Chapter XIII. Since all dependence on θ occurs in the combination $\tau = m\theta + kz$, it was shown that the fields could be derived from Eq. (XIII-6). In lowest order tokamak ordering where B_z = constant, this is sufficient to solve for B_r and B_θ. (We consider only lowest order tokamak ordering here.) It was also shown that ψ actually is a flux, it is simplest to relate it to the vector potential. By making use of the fact that $\mathbf{B} = \nabla \times \mathbf{A}$, it is not difficult to show that Eqs. (XIII-6) follow if

$$\psi = krA_\theta - mA_z. \qquad \text{(XV-1)}$$

To continue, we will relate ψ to the flux through a helical ribbon at radius r and pitch defined $\tau = kz + m\theta$ = constant. The flux through it is of course just the line integral of $\mathbf{A}$ around it. A unit vector parallel to the edge of the ribbon is

$$\frac{\mathbf{i}_z - \dfrac{kr}{m}\mathbf{i}_\theta}{[1 + \left[\dfrac{kr}{m}\right]^2]^{1/2}} \approx \mathbf{i}_z - \frac{kr}{m}i_\theta$$

making use of lowest order tokamak ordering. Therefore the magnetic flux through the ribbon is given by $2\pi R\psi$, where R is, as usual, the major radius of the torus. Hence ψ is indeed the helical flux.

We now further specialize to the case of $k = -\dfrac{1}{R}$, $m = 1$ and examine the form of $\psi(r)$. As shown in Chapter XIII, $\psi' = 0$ at the

185

resonant surface where $q = \dfrac{rB_z}{RB_\theta} = 1$. The second derivative of ψ at the resonant surface is

$$\frac{d^2\psi}{dr^2} = \frac{dB_\theta}{dr} - \frac{B_z}{R} = -B_\theta \frac{dq}{dr} < 0 \qquad \text{(XV-2)}$$

where we have assumed the normal tokamak profile having $q' > 0$. Thus ψ has a maximum at resonant surface and has the r dependence shown in Fig. (XV-1a).
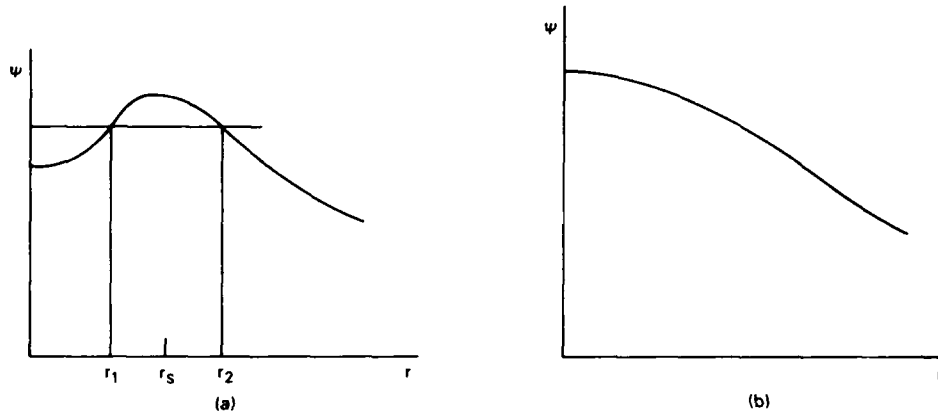

Fig. XV-1 — Initial and final plots of $\psi(r)$
according to Kadomtsev's theory

Let us now examine how magnetic reconnection could proceed in an $m = 1$ internal disruption. The magnetic flux through a ribbon of width dr is $\dfrac{d\psi}{dr}\,dr$. Thus the helical fields, on each side of the singular surface, oppose each other. As the fluid inside the singular surface convects toward one side, regions of plasma with opposing helical fluxes are forced together. If the helical flux surfaces maintain their topological structure, as they would in ideal MHD, then Rosenbluth, Dagazian and Rutherford (Phys. Fluids 16, 1894 (1973)) worked out a nonlinear theory for the asymptotic displacement of the plasma. They did this by balancing the driving force against the additional restraining force of the compressed field. They found that the plasma interior is displaced only slightly, for instance if the initial constant ψ surfaces are shown in Fig. (XV-2a), the final constant ψ surfaces might appear as in Fig. (XV-2b).

Notice however that in this final state, regions of opposite helical field (along a-b) are forced together. If reconnection is allowed in this
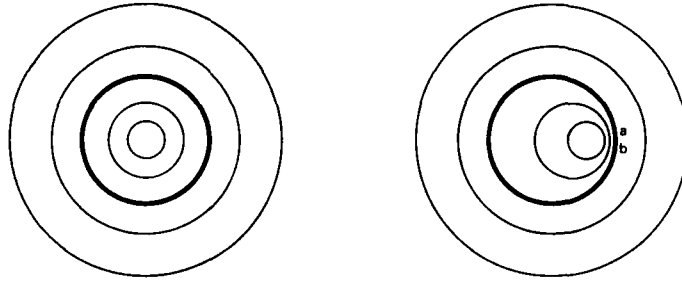
Fig. XV-2 — Initial and final plots of flux surfaces in ideal
MHD according to Rosenbluth, Dagazian and Rutherford

region, the large flux compression will not occur and the plasmas side-
ways displacement can proceed. Now we look into this reconnection
more carefully. Since the magnetic field always has zero divergence,
two different regions can reconnect only if they have equal helical flux.
Thus, as illustrated in Fig. (XV-1a), the field at r_1 can connect with the
field at r_2. If the layers at r_1 and r_2 have widths dr_1 and dr_2, the fact
that the fluxes which reconnect are equal means

$$\frac{d\psi}{dr}\Big|_{r_1} dr_1 = -\frac{d\psi}{dr}\Big|_{r_2} dr_2. \qquad (XV-3)$$

These two flux elements will, at $t = \infty$, come to rest at a position r
having width dr such that $-\dfrac{d\psi_\infty}{dr}dr = \dfrac{d\psi}{dr}\Big|_1 dr_1$. Since the fluid motion
is incompressible

$$rdr = r_1 dr_1 + r_2 dr_2. \qquad (XV-4)$$

Also, since the reconnection occurs only at one point, (around a-b), the
flux is undisturbed in most of the flux tube so

$$d\psi = d\psi_2. \qquad (XV-5)$$

Thus as the field reconnects, the total helical flux in the reconnecting
fluid elements is conserved.

It is not difficult to follow this reconnection process. Initially flux
tubes 1 and 2 connect as shown in Fig. (XV-3a and b) and an island
labeled I is formed opposite to the direction of the kink. In this island,
the helical field is clockwise, as it is outside of the original $q = 1$ sur-
face. Therefore the island has $q > 1$. After tubes 1 and 2 reconnect,
tubes 3 and 4, which have opposite flux, are forced together. Then
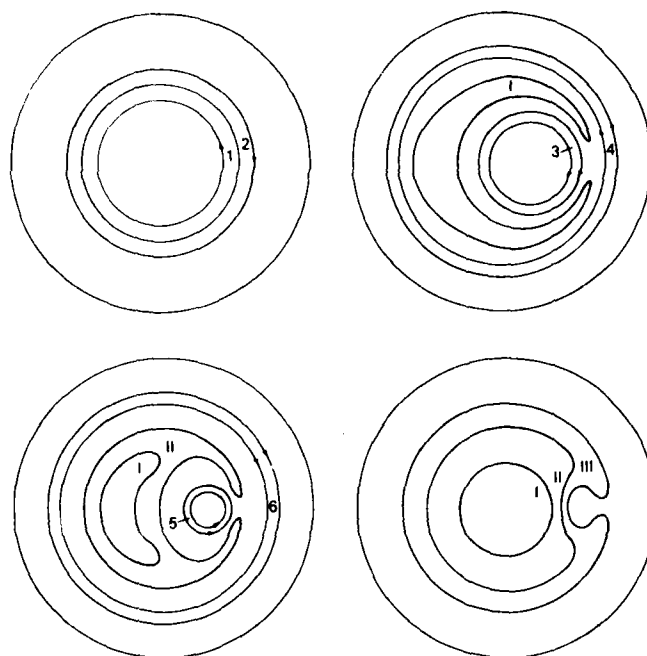these flux tubes reconnect and island II is formed outside of I as shown

Fig. XV-3 — The reconnection process
as envisioned by Kadomtsev

in Fig. (XV-3c). The reconnection process completes itself when flux elements 5 and 6 connect to form island III (Fig. (XV-3d)) at the position where $\psi(r) = \psi(o)$. Since all field lines are now clockwise, q is everywhere greater than unity and the plasma has returned to a stable state. Thus the flux near the original $q = 1$ surface has moved to the center and the flux initially at the center has moved to the outside. The $\psi(r)$ curve then evolves to a monotonically decreasing function of r in which the area between two values of ψ is the same at $t = \infty$ as at $t = 0$. This is illustrated in Fig. (XV-1b) where the helical flux at $t = \infty$ is shown.

Let us re-emphasize that the simplifying feature of this analysis is that each flux tube only breaks and reconnects once. In this reconnection, each flux tube is undisturbed over most of its length. However in this reconnection, an outer flux tube which winds clockwise reconnects with an inner flux tube which winds counter clockwise to form a single, longer flux tube which winds in the same sense as the original outer flux tube.

Thus, without invoking any details of a particular $m = n = 1$ instability Kadomtsev is able to derive the field configuration of a final stable state from an initial unstable state. Once the plasma reaches a

stable state, the channeling of the current into the hotter regions will drive the plasma unstable, as discussed in Chapter X. Therefore a relaxation oscillation will ensue.

It is worthwhile to briefly compare Kadomtsev's theory of $m = n = 1$ instability with the quasi-linear theory of Chapter X. The latter derived a diffusion equation and ultimately flattened the current profile within the $q = 1$ surface. Then some other mechanism was invoked to spread the current beyond the original $q = 1$ surface to produce a plasma with $q > 1$ everywhere. Kadomtsev's theory however suggests a coupling between the plasma inside and outside of the $q = 1$ surface so that only his mechanism is needed to produce a plasma with $q > 1$ everywhere.

We now turn our attention to a very brief survey of numerical simulations of MHD unstable plasmas. There has been a great world wide effort in such simulations recently and many people now feel that this offers the best hope for learning about the nonlinear theory of MHD instabilities. Generally speaking, these simulations are of two types. The first type, pioneered by Rosenbluth and his co-workers at Princeton, assumes helical symmetry, incompressible flow, tokamak ordering and constant density. The full set of three dimensional MHD equations then reduce to two equations for ψ and the z component of the velocity vector potential in the two dimensional r, τ space. The second approach is to simply solve the full set of MHD equations in three dimensions. Here the plasma is generally assumed to fill either a rectangular solid, or else a torus with rectangular cross section. The first method allows much greater resolution, principally because the helical symmetry reduces the dimensionality from three to two. The second method, of course, has much greater flexibility. There are other types of reduced MHD equations, as proposed for instance by Strauss.

The $m = 1$ internal kink-tearing mode has been simulated both ways. In each case, care must be taken to allow sufficient resolution in the singular layer. This has necessitated the use of resistivity much larger than that existing in tokamak plasmas.

A two dimensional simulation of the kink tearing mode was performed by Waddell, Rosenbluth, Monticello and White (Nuclear Fusion 16, 528 (1978)). A current density

$$J_z(r) = \frac{J_0}{\left[1 + \left[\frac{r}{r_0}\right]^2\right]^2} \qquad \text{(XV-6)}$$

is set up at $t = 0$. J_o is chosen so that $q(r = 0) = 0.9$ and $r_0 = 0.6a$ where a is the radius of the conducting wall. For this current profile, the radius of the $q = 1$ surface is at $r_s = 0.2a$ and the radius at which the helical flux ψ has the sme value as it does at $r = 0$ is r_ψ $0.3a$. Island formation is observed, but the helical flux surfaces become quite complicated very quickly, with multiple island structure developing. What is simpler are the flow patterns, shown at four times in Fig. (XV-4). This shows that the basic flow pattern of an $m = 1$ mode persists well into the nonlinear regime. Kadomtsev's theory indicates there should be reconnection out to $r_\psi = 0.3a$. The perturbed flow and perturbed field seem to be limited to radii somewhat smaller than this, but accurate resolution is difficult. Also, Waddell et al., show the total current as a function of radius, and this is shown in Fig. (XV-5). Clearly, the simple quasi-linear theory, which predicts current diffusion within the singular surface, is reasonably accurate.
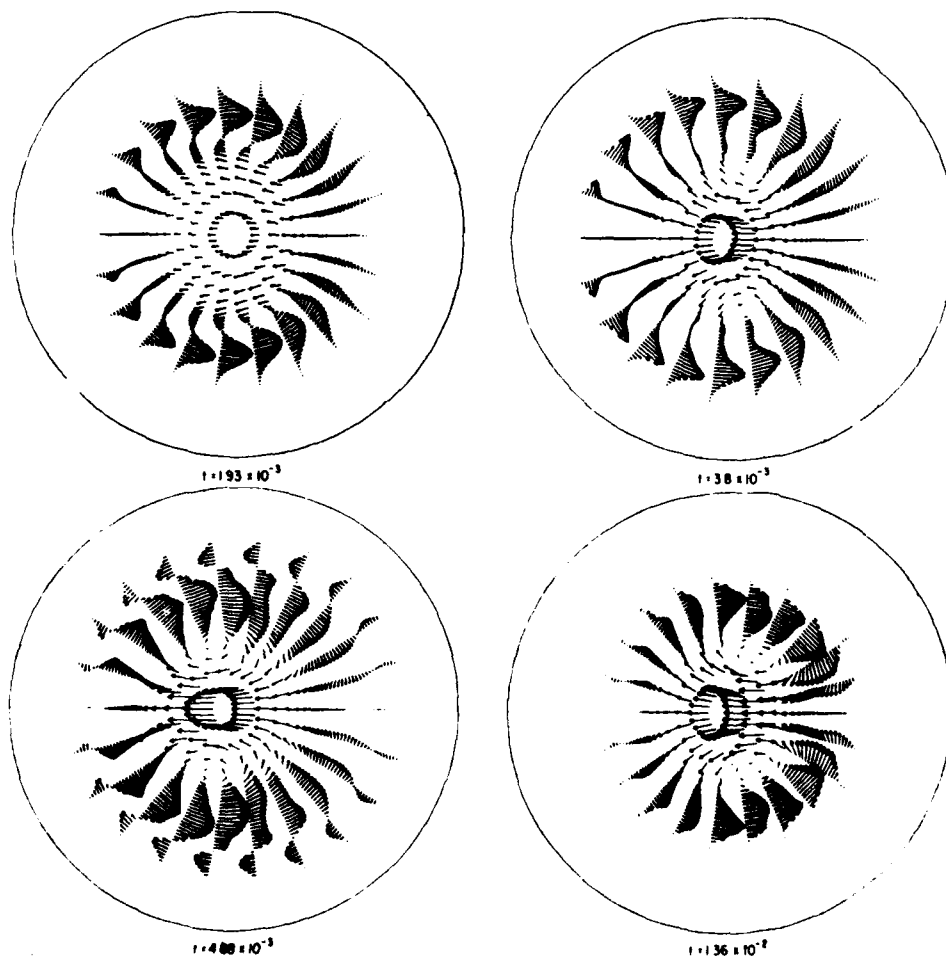

Fig. XV-4 — The time evolution of the flow pattern
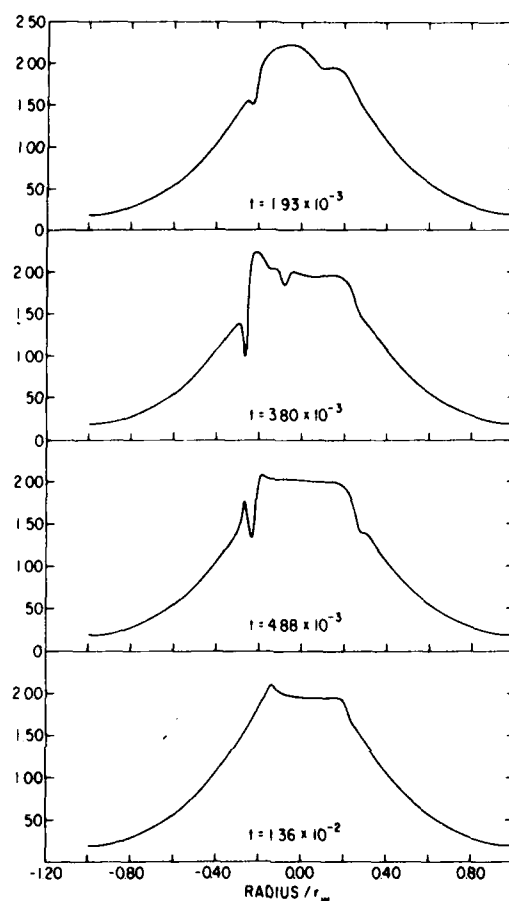for this instability as computed by Waddell et al.

Fig. XV-5 — The time evolution of the
toroidal current profile as computed by Wad-
dell et al.

A full three dimensional simulation of this instability was done
by Sykes and Wesson (Phys. Rev. Lett., **37**, 140, (1976)). By assuming
a resistivity with the functional form $\eta^- T^{-3/2}$, they were able to simu-
late several cycles of the relaxation oscillation. In Fig. (XV-6) are
shown various curves of constant ψ surfaces. Here it can be seen that
an island with $q > 1$ grows and ultimately displaces the orginal flux
surfaces having $q < 1$. However different cycles of the relaxation
oscillation are not all alike. On other cycles, the original island may
return and displace the newly formed island. In this case the original
island relaxes to a state having $q > 1$.

It is clear that numerical simulation can be a very powerful tech-
nique for the study of the nonlinear behavior of MHD instabilities.
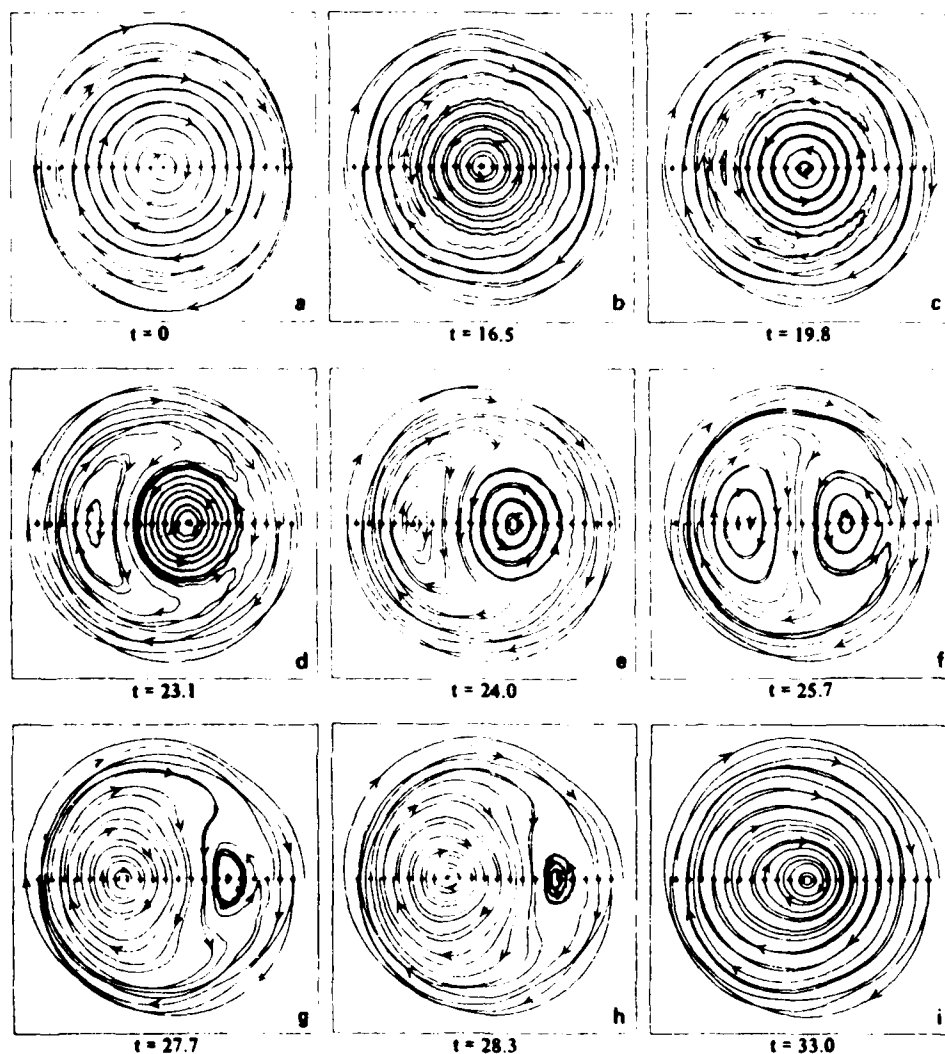
Fig. XV-6 — The time evolution of the magnetic surfaces
as computed by Sykes and Wesson

However, as these two simulations illustrate, different types of simulations of the same process do not necessarily give exactly the same result. Undoubtedly there will be many more such simulations in the future. In fact, many different instabilities have already been studied by simulations, including tearing modes, internal kinks and free boundary kinks.

Kadomtsev's work on the $m = 1$ internal disruptions is in:

Disruptive Instability in a Tokamak, B.B. Kadomtsev, Sov. J. Plasma Phys., 1, 389 (1975).

Reconnection of Field Lines and Disruptive Instability in Tokamaks, B.B. Kadomtsev, Plasma Physics and Controlled Thermonuclear Fusion Research, (1976), Vol. 1, p. 555 (IAEA Vienna, 1977).

A partial list of the numerical simulation approach to the nonlinear (and even linear) theory can be found in:

MHD-Instabilities as an initial value problem for Elongated Cross Sections, W. Schneider and G. Bateman, Plasma Physics and Controlled Thermonuclear Fusion Research, (1974), Vol. 1, 429 (IAEA Vienna, 1975).

Toroidal Calculations of Tokamak Stability, J.A. Wesson and A. Sykes, Ibid, p. 449.

Study of Magnetohydrodynamic Modes in Tokamak Configurations with Non-Circular Cross Sections, M.S. Chance, et al., Ibid, p. 463.

Numerical Studies of Nonlinear Evolution of Kink and Tearing Modes in Tokamaks, R. White, et al., Ibid, p. 495.

Nonlinear, Three Dimensional Magnetohydrodynamics of Non-Circular Tokamaks, H.R. Strauss, Phys. Fluids, 19, 134 (1976).

Dynamics of High Beta Tokamaks, H.R. Strauss, Phys. Fluids, 20, 1354 (1977).

Nonlinear Growth of the $m = 1$ Tearing Mode, B.V. Waddell, M.N. Rosenbluth, D.A. Monticello, and R.B. White, Nuclear Fusion, 16, 538 (1976).

Numerical Studies of Nonlinear Evolution of Kink Modes in Tokamaks, M.N. Rosenbluth, D.A. Monticello, H.R. Strauss, and R.B. White, Phys. Fluids, 19, 1987 (1976).

Relaxation Instability in Tokamaks, A. Sykes and J.A. Wesson, Phys. Rev. Lett., 37, 140 (1976).

Formation and Evolution of Magnetic Islands in a Tokamak Plasma, A.F. Danilov, Yu. N. Dnestrovskii, D.P. Kostomarov, and A.M. Popov, Sov. J. Plasma Phys., 3, 117 (1977).

Nonlinear Tearing Model in Tokamaks, R.B. White, D.A. Monticello, M.N. Rosenbluth, and B.V. Waddell, Plasma Physics and Controlled Thermonuclear Fusion Research, (1976), Vol. 1, p. 569 (IAEA Vienna, 1977).

Numerical Studies of Resistive Instabilities, D. Biskamp and H. Welter, Ibid, p. 579.

Numerical Simulation of MHD Processes in Tokamaks, A.F. Danilov, D.P. Kostomarov, A.M. Popov, and Yu.N. Dnestrovskii, Ibid, p. 591.

Interpretation of Tokamak Sawtooth Oscillations, B.V. Waddell, G.L. Johns, J.D. Callen, and H.R. Hicks, Nuclear Fusion, 18, 735 (1978).

Internal Disruptions in Tokamaks, G.L. Johns, M. Soler, B.V. Waddell, J.D. Callen, and H.R. Hicks, Nuclear Fusion, 18, 609 (1978).

Feedback Stabilization of Magnetic Islands in Tokamaks, D.A. Monticello, R.B. White, and M.N. Rosenbluth, Plasma Physics and Controlled Thermonuclear Fusion Research, 1978, Vol. 1, p. 605 (IAEA Vienna, 1979).

Coalescence of Magnetic Islands, D. Biskamp and H. Welter, Phys. Rev. Lett., 44, 1069 (1980)

Effect of Toroidal Coupling on the Stability of Tearing Modes, B. Carreras, H.R. Hicks and D.K. Lee, Phys. Fluids, 24, 66 (1981)

Finite β Effects on the Nonlinear Evolution of the $(m=1, n=1)$ Mode in:

Tokamaks, J.A. Holmes, B.A. Correras, H.R. Hicks, V.E. Lynch and K.E. Rothe, Phys. Fluids, 25, 800 (1982).

Nonlinear Evolution of Resistive Interchange Modes in a Reversed Field Pinch, D.D. Schnack, J. Killeen and R.A. Gerwin, Nucl. Fusion, 21, 1447 (1981).

MHD Instabilities and flows have even been studied via electromagnetic particle simulation:

Simulation Studies of the Collisionless Tearing Instabilities, I. Katanuma and T. Kamimura, Phys. Fluids, **23**, 2500 (1980).

Dynamic Magnetic X Points, J.N. Leboeuf, T. Tajima and J.M. Dawson, Phys. Fluids, **25**, 785 (1982).

Appendix

In this appendix, we derive an equation for the ideal MHD stability of a cylindrical plasma. We start from the linearized MHD equations in component form

$$\gamma \rho_0 V_{1r} = - \frac{\partial}{\partial r} \left[P_1 + \frac{\mathbf{B}_0 \cdot \mathbf{B}_1}{8\pi} \right] + i \left(\frac{\mathbf{k} \cdot \mathbf{B}_0}{4\pi} \right) B_{1r} \qquad (A1)$$

$$- \frac{B_{0\theta}}{2\pi r} B_{1\theta}$$

$$\gamma \rho_0 V_{1\theta} = - i \frac{m}{r} \left[P_1 + \frac{\mathbf{B}_0 \cdot \mathbf{B}_1}{8\pi} \right] + i \left(\frac{\mathbf{k} \cdot \mathbf{B}_0}{4\pi} \right) B_{1\theta} + \frac{1}{r} \frac{\partial}{\partial r} (rB_{0\theta}) \frac{B_{1r}}{4\pi}$$

$$(A2)$$

$$\gamma \rho_0 V_{1z} = - ik \left[P_1 + \frac{\mathbf{B}_0 \cdot \mathbf{B}_1}{8\pi} \right] + i \left(\frac{\mathbf{k} \cdot \mathbf{B}_0}{4\pi} \right) B_{1z} + \frac{dB_{0z}}{dr} \frac{B_{1r}}{4\pi} \quad (A3)$$

$$\gamma B_{1r} = i(\mathbf{k} \cdot \mathbf{B}_0) V_{1r} \qquad (A4)$$

$$\gamma B_{1\theta} = - \frac{\partial}{\partial r} (B_{0\theta} V_{1r}) + ik (B_{0z} V_{1\theta} - B_{0\theta} V_{1z}) \qquad (A5)$$

$$\gamma B_{1z} = - \frac{1}{r} \frac{\partial}{\partial r} (B_{0z} r V_{1r}) + i \frac{m}{r} (B_{0\theta} V_{1z} - B_{0z} V_{1\theta}) \qquad (A6)$$

$$\frac{1}{r} \frac{\partial}{\partial r} (r V_{1r}) + i \frac{m}{r} V_{1\theta} + ik V_{1z} = 0. \qquad (A7)$$

Now introduce

$$F \equiv \mathbf{k} \cdot \mathbf{B}_0$$

and also introduce the new variable

$$X \equiv P_1 + \frac{\mathbf{B}_0 \cdot \mathbf{B}_1}{8\pi}.$$

This is the scalar part of the perturbed fluid plus magnetic pressure.

197

Substituting for B_{1r}, $B_{1\theta}$ and B_{1z} from Eqs. (A4)-(A6) into Eq. (A2) we have

$$\gamma \rho_0 V_{1\theta} = - i \frac{m}{r} X + i \frac{F}{4\pi} \left\{ k \frac{B_{0\theta}}{i\gamma} V_{1z} - k \frac{B_{0z}}{i\gamma} V_{1\theta} \right.$$

$$\left. - \frac{1}{i\gamma} \frac{\partial}{\partial r} \left(\frac{B_{0\theta}}{r} rV_{1r} \right) \right\} - \frac{1}{r} \frac{\partial}{\partial r} (rB_{0\theta}) \frac{F}{4\pi i\gamma} V_{1r}.$$

Then further manipulation yields

$$i\gamma \rho V_{1\theta} - \frac{F^2}{4\pi_0} \frac{V_{1\theta}}{i\gamma} = \frac{m}{r} X$$

$$- \frac{F}{4\pi} \left\{ \frac{B_{0\theta}}{i\gamma} \left[\frac{m}{r} V_{1\theta} + kV_{1z} - \frac{i}{r} \frac{\partial}{\partial r} (rV_{1r}) \right] \right\}$$

$$+ \frac{F}{4\pi} \frac{1}{\gamma} \frac{\partial}{\partial r} \left(\frac{B_{0\theta}}{r} \right) rV_{1r} - \frac{1}{\gamma} \frac{F}{4\pi} \frac{1}{r} \frac{\partial}{\partial r} (rB_{0\theta}) V_{1r}.$$

Using Eq. (A7) we obtain

$$\left(-\gamma^2 \rho_0 - \frac{F^2}{4\pi} \right) \frac{V_{1\theta}}{i\gamma} = \frac{m}{r} X - 2 \frac{FB_{0\theta}}{4\pi r^2} \frac{rV_{1r}}{\gamma}. \qquad (A8)$$

Substituting Eqs. (A4) and (A6), into (A3) gives

$$i\gamma \rho_0 V_{1z} = kX - \frac{F}{4\pi} \left\{ \frac{m}{i\gamma r} B_{0z} V_{1\theta} - \frac{m}{i\gamma r} B_{0\theta} V_{1z} \right.$$

$$\left. - \frac{1}{\gamma r} \frac{\partial}{\partial r} (B_{0z} rV_{1r}) \right\} - \frac{dB_{0z}}{dr} \frac{F}{4\pi\gamma} V_{1r}.$$

Proceeding as for $V_{1\theta}$ we obtain

$$\left(-\gamma^2 \rho_0 - \frac{F^2}{4\pi} \right) \frac{V_{1z}}{i\gamma} = kX. \qquad (A9)$$

Next, substitute Eqs. (A4) and (A5) into Eq. (A1) to obtain

$$\left(-\gamma^2 \rho_0 - \frac{F^2}{\mu_0} \right) \frac{V_{1r}}{i\gamma} = - i \frac{\partial}{\partial r} X - \frac{2iB_{0\theta}}{4\pi r} \left\{ \frac{kB_{0\theta}}{i\gamma} V_{1z} \right.$$

$$\left. - \frac{kB_{0z}}{i\gamma} V_{1\theta} - \frac{1}{\gamma} \frac{\partial}{\partial r} \left(\frac{B_{0\theta}}{r} rV_{1r} \right) \right\}.$$

Substituting for $V_{1\theta}$ and V_{1z} from Eqs. (A8) and (A9), the above equation becomes

$$\left[-\gamma^2\rho_0 - \frac{F^2}{4\pi}\right] \frac{V_{1r}}{i\gamma} - 4\frac{kB_{0z}}{4\pi r} \frac{FB_{0\theta}^2}{4\pi r^2} \left[-\gamma^2\rho_0 - \frac{F^2}{4\pi}\right] \frac{rV_{1r}}{i\gamma}$$

$$+ 2\frac{B_{0\theta}}{4\pi r} \frac{\partial}{\partial r} \left[\frac{B_{0\theta}}{r} \frac{rV_{1r}}{i\gamma}\right]$$

$$= -i\frac{\partial}{\partial r} X - 2\frac{iB_{0\theta}}{4\pi r} \frac{\left[k^2 B_{0\theta} - k\frac{m}{r}B_{0z}\right]}{\left[-\gamma^2\rho_0 - \frac{F^2}{4\pi}\right]} X. \qquad (A10)$$

Now substitute Eqs. (A8) and (A9) into Eq. (A7) to give

$$\frac{1}{r} \frac{\partial}{\partial r}(rV_{1r}) + i\frac{m}{r}\left\{\frac{m}{r} \frac{i\gamma X}{(-\gamma^2\rho_0 - F^2/4\pi)}\right.$$

$$\left. - \frac{2FB_{0\theta}}{4\pi r^2} \frac{rV_{1r}}{\gamma} \frac{i\gamma}{(-\gamma^2\rho_0 - F^2/4\pi)}\right\}$$

$$- \frac{k\gamma kX}{(-\gamma^2\rho_0 - F^2/4\pi)} = 0.$$

This equation can now be solved for X to give

$$X = ir \frac{(-\gamma^2\rho_0 - F^2/4\pi)}{(k^2 r^2 + m^2)} \frac{\partial}{\partial r} \frac{(rV_{1r})}{i\gamma}$$

$$+ \frac{2FB_{0\theta}}{4\pi} \frac{m}{r} (k^2 r^2 + m^2)^{-1} \frac{rV_{1r}}{\gamma}.$$

Substituting Eq. (A11) into Eq. (A10) yields

$$\frac{\partial}{\partial r}\left\{\frac{r(-\gamma^2\rho_0 - F^2/4\pi)}{(k^2 r^2 + m^2)} \frac{\partial}{\partial r} \frac{(rV_{1r})}{i\gamma}\right\} + \frac{\partial}{\partial r}\left\{\frac{2FB_{0\theta}}{4\pi} \frac{m}{r} \frac{1}{(k^2 r^2 + m^2)} \frac{rV_{1r}}{i\gamma}\right\}$$

$$+ \frac{2B_{0\theta}}{4\pi}\left[k^2 B_{0\theta} - k\frac{m}{r} B_{0z}\right](k^2 r^2 + m^2)^{-1} \frac{\partial}{\partial r}\left[\frac{rV_{1r}}{i\gamma}\right]$$

$$+ \frac{2B_{0\theta}}{\mu_0 r} \frac{\left[k^2 B_{0\theta} - k\frac{m}{r} B_{0z}\right]}{(-\rho_0\gamma^2 - F^2/\mu_0)} \frac{2FB_{0\theta}}{4\pi} \frac{m}{r} \frac{1}{(k^2 r^2 + m^2)} \frac{rV_{1r}}{i\gamma}$$

$$= \left[-\rho_0\gamma^2 - \frac{F^2}{4\pi}\right] \frac{V_{1r}}{i\gamma} - \frac{4kB_{0z}}{4\pi r} \frac{FB_{0\theta}^2}{\mu_0 r^2(i\gamma\rho_0 - F^2/\mu_0)} \frac{rV_{1r}}{i\gamma}$$

$$+ \frac{2B_{0\theta}}{4\pi r} \frac{\partial}{\partial r}\left[\frac{B_{0\theta}}{r} \frac{rV_{1r}}{i\gamma}\right].$$

The coefficient of the $\dfrac{\partial}{\partial r}\dfrac{(rV_{1r})}{i\gamma}$ term is zero. The equation can be written in the form

$$\frac{\partial}{\partial r}\left\{r\frac{(\gamma^2\rho_0 + F^2/4\pi)}{(k^2r^2 + m^2)}\frac{\partial}{\partial r}(rV_{1r})\right\}$$

$$-\left\{\gamma^2\rho_0 + \frac{F^2}{4\pi} - \frac{2B_{0\theta}}{4\pi}\left(\frac{B_{0\theta}}{r}\right)' + \frac{2mr}{\mu_0}\left[\frac{FB_{0\theta}}{r(k^2r^2 + m^2)}\right]'\right.$$

$$\left.\frac{-4k^2F^2B_{0\theta}^2}{16\pi^2(k^2r^2 + m^2)(\gamma^2\rho_0 + F^2/4\pi)}\right\}V_{1r} = 0.$$

Which is the form of Eq. VIII 12.